Evaluación de la actividad antitumoral de nuevos compuestos metálicos y estudio de la reprogramación metabólica en cáncer de pulmón: búsqueda de nuevas dianas terapéuticas y biomarcadores diagnósticos

Roldán Cortés Giráldez

Programa de Doctorado en Biotecnología
Departament de Bioquímica i Biologia Molecular
Facultat de Biologia

Evaluación de la actividad antitumoral de nuevos compuestos metálicos y estudio de la reprogramación metabólica en cáncer de pulmón: búsqueda de nuevas dianas terapéuticas y biomarcadores diagnósticos

Memoria presentada por **Roldán Cortés Giráldez** para optar al grado de Doctor por la Universitat de Barcelona

Marta Cascante Serratosa
Directora

Roldán Cortés Giráldez
Doctorando

EVALUACIÓN DE LA ACTIVIDAD ANTITUMORAL DE NUEVOS COMPUESTOS METÁLICOS Y ESTUDIO DE LA REPROGRAMACIÓN METABÓLICA EN CÁNCER DE PULMÓN: BÚSQUEDA DE NUEVAS DIANAS TERAPÉUTICAS Y BIOMARCADORES DIAGNÓSTICOS.

ROLDÁN CORTÉS GIRÁLDEZ

Hacer una Tesis parece fácil, pero hay que estar ahí.
Friedrich Nietzsche

00. ÍNDICE

1. INTRODUCCIÓN GENERAL **08**

1.1. El cáncer **09**
1.2. El cáncer de pulmón **12**
1.3. KRAS y cáncer de pulmón **16**
1.4. El ciclo celular **18**
1.5. La apoptosis **21**
1.6. Métodos para la evaluación del ciclo celular y la apoptosis **24**
1.7. Factores de transcripción FOXO y su relación con el cáncer **26**
1.8. Evaluación de la localización intracelular de FOXO **29**
1.9. Metalofármacos en quimioterapia **30**
1.09.1. Compuestos cicloplatinados de 7 miembros **33**
1.09.2. Compuestos de platino con iminas polifuncionalizadas **33**
1.09.3. Compuestos de platino y paladio derivados del pirazol **34**
1.09.4. Compuestos derivados del ferroceno **34**
1.10. El metabolismo tumoral **35**
1.10.1. La glucólisis y el efecto Warburg **37**
1.10.2. La glutaminólisis **40**
1.10.3. La síntesis de ácidos grasos **41**
1.10.4. La ruta de las pentosas fosfato **43**
1.11. La metabolómica y la flujómica **45**
1.11.1. La flujómica basada en trazadores **46**
1.11.2. Análisis de la distribución isotopomérica **48**
1.12. Explotación de las alteraciones metabólicas del cáncer de pulmón en el diagnóstico mediante el análisis del aire exhalado **50**
1.13. Métodos de análisis metabolómico **52**

2. OBJETIVOS **54**

3. INFORME DEL DIRECTOR **56**

4. RESUMEN DE RESULTADOS, DISCUSIÓN GLOBAL Y CONCLUSIONES **60**

4.1. Resumen de resultados **62**
4.2. Discusión global **73**
4.3. Conclusiones **79**

5. BIBLIOGRAFIA **82**

6. PUBLICACIONES **94**

6.1. Capítulo 1 ..... **95**
6.1.1. Capítulo 1a **97**
6.1.2. Capítulo 1b **109**
6.1.3. Capítulo 1c **119**
6.1.4. Capítulo 1d **131**
6.1.5. Capítulo 1e **141**
6.2. Capítulo 2 ..... **155**
6.3. Capítulo 3 ..... **171**
5.4. Capítulo 4 ..... **203**

01.
INTRODUCCIÓN GENERAL

1.1. EL CÁNCER

El cáncer es un concepto genérico que designa a un gran número de patologías diferentes. Todas ellas, sin embargo, comparten como característica común la división acelerada y descontrolada de las células del organismo, que son capaces no solo de aumentar su número más allá de los límites fisiológicos normales, sino también de invadir otros tejidos de manera local o a distancia, propagándose a través de los vasos sanguíneos y linfáticos. Con cerca de 14.1 millones de diagnósticos y más de 8 millones de muertes a nivel global en 2008 (Bray, Jemal et al. 2012) y una incidencia en aumento, el cáncer constituye una de las principales causas de mortalidad no solo en los países desarrollados, sino también en aquellos en vías de desarrollo.

En los tejidos sanos la proliferación celular está estrictamente controlada mediante diferentes vías de señalización, y una vez superada la etapa de crecimiento la gran mayoría de las células del organismo únicamente se dividen para reemplazar a otras células dañadas o muertas. En el cáncer, por el contrario, los mecanismos de control de la proliferación celular dejan de funcionar correctamente, lo que provoca que las células se multipliquen sin control de manera autónoma provocando la aparición de un tumor.

Para que el tumor se desarrolle, en cualquier caso, no basta con una desregulación de las señales que controlan el crecimiento celular. También es necesario superar diferentes programas biológicos que controlan la proliferación mediante mecanismos muy diversos, como la muerte celular programada o la respuesta inmunológica. Así, tanto el desarrollo inicial como la posterior progresión y expansión del cáncer requieren de múltiples adaptaciones que permitan a las células mantener un potencial proliferativo descontrolado y acelerado a pesar de los distintos mecanismos de control directos e indirectos existentes en el organismo. Aunque hay una gran variabilidad intertumoral (e incluso intratumoral) entre las células tumorales, existen ciertas características comunes a las células de cáncer que han sido definidas por Douglas Hanahan y Robert A. Weinberg (Hanahan and Weinberg 2011) y que se recogen en la **figura 1**.

La adquisición de todas las características necesarias para el desarrollo del cáncer se realiza de manera secuencial. La teoría monoclonal, ampliamente aceptada en la actualidad, sostiene que el cáncer se genera a partir de una única célula sana, que genera un tumor canceroso a través de las tres etapas que conforman el proceso carcinogénico. Esta transformación resulta de la interacción entre los factores genéticos propios de cada individuo con factores externos llamados carcinógenos, que pueden ser físicos (como distintas radiaciones, entre las que se encuentra la luz ultravioleta), químicos (como el humo del tabaco o diversos

productos contaminantes) o biológicos (como distintas infecciones, que pueden ser víricas, bacterianas o parasitarias).

Observaciones empíricas, inicialmente realizadas en modelos experimentales de melanoma, apuntan a que la carcinogénesis es un proceso dividido en tres pasos diferenciados: La iniciación, la promoción y la progresión (Hennings, Glick et al. 1993). En la primera etapa de iniciación, un agente iniciador (el carcinógeno) provoca un daño en el material genético celular, lo que resulta en una mutación. La exposición continuada a agentes iniciadores acaba provocando una acumulación de diferentes mutaciones en la célula, que se convierte así en lo que se denomina una célula iniciada. Esta célula iniciada, aunque aún no presenta cambios detectables en su tasa de proliferación, sí ha incrementado exponencialmente su susceptibilidad para dar origen a un tumor.

La segunda etapa de la carcinogénesis, la promoción, requiere la acción de promotores: agentes carcinógenos que no son mutagénicos por sí mismos pero que provocan, en el tejido en el que se encuentra la célula iniciada, un trastorno capaz de propiciar una proliferación descontrolada a partir de la misma. La acción de los promotores facilita la aparición de tumores benignos, que resultarían fácilmente reversibles en ausencia de nuevos promotores pero que pueden generar un tumor con un crecimiento acelerado consistente si su efecto se mantiene en el tiempo (Rubin 2003).

Tras la promoción, se forma un tumor con células que ya son capaces de mantener de manera autónoma un crecimiento acelerado. La mortalidad del cáncer, sin embargo, recae en la capacidad de las células tumorales para extenderse a otros tejidos del organismo mediante la adquisición de capacidad invasiva en la última etapa carcinogénica: la progresión. En esta etapa intervienen diferentes mecanismos que regulan la invasión local, la angiogénesis (generación de nuevos vasos sanguíneos a partir de los preexistentes), la intravasación a vasos sanguíneos y linfáticos, la extravasación en otros tejidos diferentes y la aparición de tumores metastáticos a distancia.

En las células tumorales aparecen, durante la progresión tumoral, múltiples mutaciones distintas. De acuerdo a las leyes darwinianas de la evolución, las mutaciones que confieren a las células una mayor viabilidad son seleccionadas, viéndose aumentada su proporción en el tumor (Greaves and Maley 2012). Las mutaciones que más ventajas aportan para la progresión tumoral no son únicamente las que aumentan la velocidad de crecimiento celular, sino también las que proporcionan a la célula los mecanismos para sobrevivir en el entorno tumoral, captar nutrientes y oxígeno o evadir las señales supresoras del crecimiento o las defensas del sistema inmune del organismo. Como norma general, una única mutación no es sufi-

ciente para provocar la transformación de una célula sana en una célula tumoral, pero en cualquier caso algunas de las mutaciones aparecidas deben afectar a genes relacionados directa o indirectamente con el control del crecimiento tumoral. Estos genes reciben el nombre de proto-onocogenes y genes supresores de tumores.

FIGURA 01. Características del cáncer. La figura refleja las capacidades que la célula debe adquirir para iniciar y mantener la progresión tumoral. Figura adaptada con permiso Elsevier de *Hallmarks of cancer: the next generation*, Cell 144(5): 646-674.

Los proto-oncogenes están relacionados con funciones promotoras de la proliferación celular. Codifican para factores de transducción y moléculas de vías de señalización relacionadas con la división y el crecimiento, así como para factores reguladores del ciclo celular o de la apoptosis (muerte celular programada). Un oncogen es un proto-oncogen que ha sufrido una mutación de ganancia de función, lo que implica que se encuentra activo de manera constitutiva sin necesi-

dad de señales activadoras. Así, la aparición de oncogenes provoca un aumento de la tasa de proliferación celular (Adamson 1987; Weinstein and Joe 2006).

La función de los genes supresores de tumores, por otro lado, es la de limitar el crecimiento tumoral, respondiendo a situaciones de estrés o a daños bioquímicos mediante la activación de mecanismos de reparación celular o, en los casos en los que la reparación ya no es una opción, mediante la activación de programas de muerte celular programada que eliminan las células sobrantes o defectuosas. Cuando uno de estos genes tiene una mutación que hace que pierda su función, se genera un efecto sinérgico al generado por los oncogenes, con lo que el aumento de la proliferación celular se ve potenciado (Weinberg 1991).

En definitiva, mediante el proceso de carcinogénesis la célula adquiere y selecciona una serie de mutaciones que le permiten adquirir las características necesarias para mantener una proliferación acelerada y descontrolada, esquivar los mecanismos inmunológicos y supresores del crecimiento, sobrevivir en el entorno tumoral e invadir otros tejidos localmente y a distancia generando metástasis en otros puntos del organismo.

1.2. EL CÁNCER DE PULMÓN

El cáncer de pulmón es actualmente el tipo de cáncer que más mortalidad provoca a nivel mundial, siendo además el cáncer más diagnosticado en hombres y el cuarto más diagnosticado en mujeres (Bray, Jemal et al. 2012). La causa más común de cáncer de pulmón es el tabaquismo, siendo alrededor del 90% de los pacientes con esta enfermedad fumadores y ex fumadores. El 10% restante de casos de cáncer de pulmón se atribuyen a una combinación de causas genéticas y exposición a agentes carcinógenos como el gas radón, el asbesto, la contaminación atmosférica o el humo de tabaco (fumadores pasivos).

El cáncer de pulmón se clasifica comúnmente en dos grupos: cáncer de pulmón de células pequeñas (SCLC) y cáncer de pulmón de células no pequeñas (NSCLC, del inglés *non-small cell lung cancer*). El NSCLC constituye alrededor del 85% del total de casos de cáncer de pulmón, y a su vez se subdivide en tres grupos: adenocarcinoma, carcinoma pulmonar de células escamosas y carcinoma pulmonar de células grandes. El adenocarcinoma es el tipo de cáncer de pulmón más común tanto en fumadores y exfumadores como en no fumadores. El carcinoma pulmonar de células grandes, por otro lado, suele ser el cáncer de pulmón de crecimiento más rápido.

Dependiendo del tamaño del tumor generado, el grado de afectación linfática y la aparición o no de metástasis distantes, el cáncer de pulmón se puede clasificar en función de su grado de desarrollo según el método de clasificación TNM (Goldstraw 2013).

Categorías T de cáncer de pulmón:

T1, cuando el tumor no mide más de tres centímetros, no ha alcanzado las membranas que rodean los pulmones (pleura visceral), y no afecta las ramas principales de los bronquios. Si el tumor mide 2 cm (alrededor de 4/5 de pulgada) o menos, se le llama T1a. Cuando el tumor mide más de 2 cm, pero no mide más de 3 cm, se le llama T1b.

T2, cuando el tumor presenta al menos una de las siguientes características:

- Mide más de 3 cm, pero no más de 7.
- Involucra a un bronquio principal, pero no está a menos de 2 cm de la carina (el punto donde la tráquea se divide en los bronquios principales izquierdo y derecho).
- Ha crecido hacia el interior de las membranas que rodean a los pulmones (pleura visceral).
- El tumor obstruye parcialmente las vías respiratorias, pero esto no ha causado el colapso de todo el pulmón ni la aparición de neumonía.
- Si el tumor mide 5 cm o menos, se le llama T2a. Si el tumor mide más de 5 cm (pero no mide más de 7 cm), se le llama T2b.

T3, cuando el tumor presenta una o más de las siguientes características:

- Su tamaño es mayor de 7 cm.
- Ha crecido hacia el interior de la pared del tórax, el músculo que separa el tórax del abdomen (diafragma), las membranas que rodean el espacio entre los dos pulmones (pleura mediastinal), o a las membranas del saco que rodea el corazón (pericardio parietal).

· Invade a un bronquio principal, y está más cerca de 2 cm de la carina, pero no afecta la carina en sí.

· Ha crecido hacia el interior de las vías respiratorias lo suficiente para causar el colapso total de un pulmón o neumonía en la totalidad del pulmón.

· Dos o más nódulos tumorales separados se encuentran presentes en el mismo lóbulo de un pulmón.

T4, cuando el cáncer presenta una o más de las siguientes características:

· Un tumor de cualquier tamaño ha crecido hacia el espacio que existe entre los pulmones (mediastino), el corazón, los vasos sanguíneos grandes cercanos al corazón (tal como la aorta), la tráquea, el tubo que conecta la garganta con el estómago (esófago), la columna vertebral o la carina.

· Dos o más nódulos tumorales separados se encuentran en lóbulos diferentes del mismo pulmón.

Categorías N de cáncer de pulmón:

N0, cuando no hay propagación a los ganglios linfáticos adyacentes.

N1, cuando el cáncer se propagó a los ganglios linfáticos dentro del pulmón y/o alrededor del área donde los bronquios entran al pulmón (a los ganglios linfáticos hiliares). Los ganglios linfáticos afectados se encuentran en el mismo lado del tumor primario.

N2, cuando el cáncer se propagó a los ganglios linfáticos que se encuentran alrededor de la carina (el punto donde la tráquea se divide en los bronquios izquierdo y derecho), o en el espacio entre los pulmones (mediastino). Los ganglios linfáticos afectados se encuentran en el mismo lado del tumor primario.

N3, cuando el cáncer se propagó a los ganglios linfáticos que se encuentran cerca de la clavícula en cualquiera de los lados, y/o se propagó a los ganglios linfáticos hiliares o mediastinales que se ubican en el lado opuesto al tumor primario.

Categorías M de cáncer de pulmón:

M0, cuando el cáncer no se ha propagado a áreas u órganos distantes. Esto incluye al otro pulmón, los ganglios linfáticos de ubicación más distante que los mencionados anteriormente en las etapas N, y otros órganos o tejidos tales como el hígado, los huesos o el cerebro.

M1a, cuando se da cualquiera de los siguientes casos:

- El cáncer se propagó al otro pulmón.
- Se detectan células cancerosas en el líquido que rodea el pulmón (llamado derrame pleural maligno).
- Se detectan células cancerosas en el líquido que rodea el corazón (llamado derrame pericárdico maligno).

M1b, cuando el cáncer se propagó a ganglios linfáticos distantes o a otros órganos, como el hígado, los huesos, o el cerebro.

El cáncer de pulmón es uno de los tipos de cáncer más agresivos que existen. El 50% de los pacientes de cáncer de pulmón mueren en el primer año tras el diagnóstico, y menos del 15% sobreviven más de cinco años. La limitada eficacia que en la mayoría de los casos presentan los tratamientos quimioterapéuticos actuales en NSCLC hace que la extirpación quirúrgica del tumor sea la estrategia más utilizada en el tratamiento de la enfermedad (Padda, Burt et al. 2014), y una de las causas fundamentales de la elevada tasa de mortalidad del cáncer de pulmón es que los tumores diagnosticados acostumbran a presentar numeraciones altas según la clasificación TNM, lo que indica que se encuentran en un estado de desarrollo demasiado avanzado que imposibilita su extracción por cirugía.

La quimioterapia se suele usar en NSCLC como tratamiento posterior a la extirpación quirúrgica del tumor, con la intención de minimizar el riesgo de recaída del paciente, así como en los casos en los que la cirugía no es una opción viable. En solitario o en combinación con radioterapia, los tratamientos más habituales implican el uso de quimioterapia basada en compuestos de platino, como cisplatino o carboplatino (Zarogoulidis, Zarogoulidis et al. 2013). A medida que la comprensión de los mecanismos moleculares del NSCLC ha aumentado, a la quimioterapia convencional se ha añadido el uso de inhibidores biológicos dirigidos contra dianas

moleculares específicas. De entre los más usados, podemos destacar los que tienen actividad antiangiogénica, como por ejemplo bevacizumab, y los dirigidos a inhibir el receptor del factor de crecimiento epidérmico (EGFR, del inglés *epidermal growth factor receptor*), como por ejemplo Erlotinib, un inhibidor de la actividad tirosina quinasa del EGFR que resulta especialmente efectivo en pacientes con mutaciones activadoras del gen EGFR (Reungwetwattana and Dy 2013).

Así, para mejorar la prognosis del cáncer de pulmón, y excluyendo estrategias preventivas (de entre las cuales la más exitosa es sin duda la de no fumar), resulta de crucial importancia el desarrollo de nuevos compuestos con actividad antitumoral que resulten efectivos en el tratamiento del cáncer de pulmón, ya sea por sí mismos o formando parte de nuevas terapias combinadas, así como nuevos métodos diagnósticos que permitan detectar la enfermedad en las primeras etapas de su desarrollo.

1.3. KRAS Y CÁNCER DE PULMÓN

KRAS es parte de la familia de proto-oncogenes RAS, que en humanos incluye también a NRAS y HRAS. La proteína codificada por KRAS, la GTPasa KRas, juega un papel esencial en el control de distintas vías de transmisión de señal que regulan procesos como la apoptosis, el progreso en el ciclo celular o la transcripción, y por lo tanto KRas tiene un papel clave en la proliferación, la diferenciación y la supervivencia celulares (Chetty and Govender 2013). En células quiescentes sanas, KRas se encuentra unida a guanosín difosfato (GDP) en un estado inactivo. Tras recibir señales de activación provenientes de receptores de factores de crecimiento, el GDP pasa a su forma activada guanosín trifosfato (GTP), y el complejo KRas-GTP resultante es capaz de activar diversas vías, incluyendo las de proteín quinasas activadas por mitógenos (MAPK, del inglés *mitogen activated protein kinases*) y fosfo-inositol 3 quinasa (PI3K).

KRas juega un papel crítico en la transmisión de señal inducida por diversos receptores de crecimiento, y su activación constitutiva haría innecesaria la señalización mediada por factores de crecimiento, ya que las vías reguladas por KRas se encontrarían activadas independientemente de la presencia de estos (ver **figura 2**). Mutaciones activadoras de KRas son comunes en muchos tipos de cáncer, y mutaciones activadoras en el gen KRAS constituyen la alteración oncogénica más común en cáncer de pulmón de células no pequeñas (Cooper, Lam et al. 2013). Las mutaciones en KRAS son especialmente comunes en adenocarcinomas de países occidentales, y resultan más frecuentes en varones y en fumadores. Por el contrario, son extremadamente raras en cáncer de pulmón de células pequeñas.

Es interesante resaltar que otra de las mutaciones más comunes en cáncer de pulmón, la del oncogen que codifica para el receptor del factor de crecimiento epidérmico (EGFR, del inglés *epidermal growth factor receptor*) nunca se presenta en pacientes con mutaciones en KRAS, por lo que ambas mutaciones se consideran mutuamente excluyentes. La terapia con inhibidores de tirosina quinasa (TKIs, del inglés *tirosine-kinase inhibitors*), como erlotinib, actúan sobre el receptor EGFR y resultan efectivas en el cáncer de pulmón de pacientes con mutaciones en el gen que lo codifica, pero los pacientes con mutaciones en KRAS no responden a estos tratamientos (Cardarella and Johnson 2013). En general, la alta frecuencia de mutaciones en KRAS que presenta el cáncer de pulmón abre la posibilidad de que KRas sea una diana terapéutica útil en el tratamiento de la enfermedad, pero desafortunadamente los ensayos clínicos de productos enfocados a inhibir esta proteína han resultado decepcionantes hasta el día de hoy.

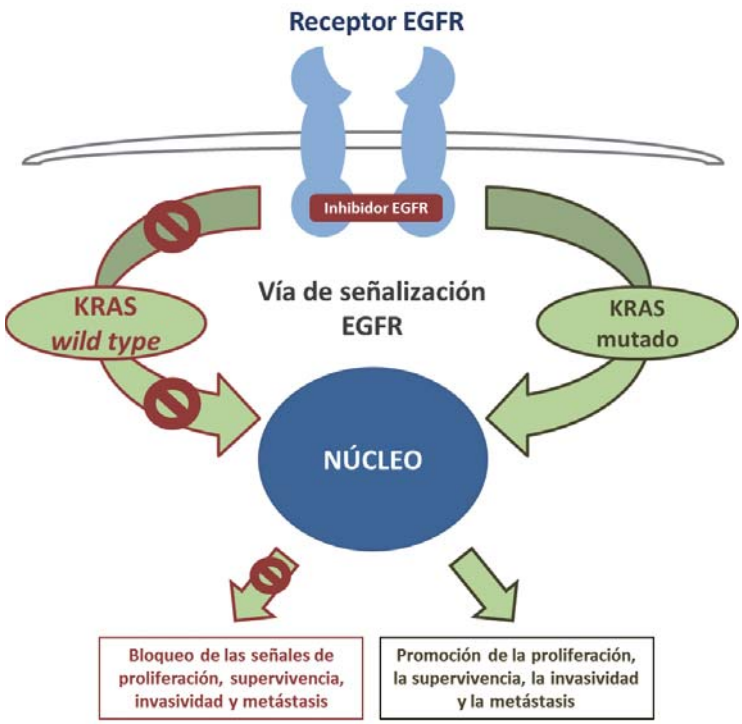

FIGURA 02. Efecto de KRAS. La figura refleja cómo los inhibidores de EGFR no resultan útiles en los casos en los que KRAS cuenta con mutaciones que provocan la activación constitutiva de KRas. KRas se encuentra por debajo de EGFR en la vía de señalización que comparten, y por tanto su activación constitutiva hace que la vía esté activada incluso en ausencia de las señales activadoras mediadas por EGFR.

1.4. EL CICLO CELULAR

Se denomina ciclo celular al conjunto de sucesos altamente regulado por el que una célula origina dos células hijas. Este ciclo, que comprende el periodo entre dos divisiones mitóticas, incluye los procesos durante los cuales la célula aumenta su tamaño, duplica su material genético y finalmente se divide en dos células independientes. El ciclo celular se puede considerar un proceso dividido en las diferentes etapas representadas en la **figura 3**, que conforman la interfase (conjunto de etapas por las que pasa una nueva la célula hasta que está lista para una nueva división) y la fase de división (en la que la célula se divide en dos células hijas).

Concretamente, la interfase se puede subdividir en las siguientes etapas:

- Fase G_1: Periodo comprendido entre el fin de la división anterior y el inicio de la duplicación del material genético celular. Durante esta fase, también llamada primera fase de crecimiento, la célula sintetiza nuevo material citoplasmático, especialmente proteínas y ARN, en preparación para el inicio de la siguiente etapa del ciclo en la que tendrá que sintetizar otra copia de su ADN.

- Fase G_0: En células no proliferantes (la inmensa mayoría de las células sanas de un organismo adulto), las células entran en un estado de quiescencia en el que el ciclo celular no avanza hacia nuevas duplicaciones. Esta fase recibe el nombre de fase G_0, que indica que la célula se encuentra "detenida" ya que no está programada para continuar dividiéndose. Algunas células, como las células madre adultas, entran en fase G_0 de manera reversible, y bajo estímulos fisiológicos normales pueden volver a entrar en la fase G_1, continuando hacia las siguientes fases del ciclo celular y convirtiéndose así de nuevo en una célula proliferante. En células de mamífero completamente diferenciadas, en cambio, así como en células senescentes, la entrada en la fase G_0 se considera prácticamente irreversible, aunque bajo estímulos excepcionales (entre los que se cuentan la inhibición de los supresores de tumores p53 y RB) tanto las células senescentes como las terminalmente diferenciadas son también capaces de reentrar en el ciclo celular (Cheung and Rando 2013).

- Fase S: La fase S (también llamada fase de síntesis) es aquella en la que la célula sintetiza una segunda copia completa de su ADN. Cuando acaba la fase S, la célula cuenta con el doble de cromosomas que al inicio de la misma (4n, ya que las células humanas son diploides y normalmente cuentan con un número de cromosomas igual a 2n, siendo *n* el número de cromosomas aportado por cada uno de los progenitores del organismo).

- Fase G_2: La última etapa de preparación antes de la división celular. También recibe el nombre de segunda fase de crecimiento, y durante la misma continúa la síntesis de ARN y proteínas mientras la célula se prepara para su entrada en la fase de mitosis. A medida que se acerca el final de esta etapa, el ADN empieza a condensarse y los cromosomas se hacen visibles al microscopio.

La fase de división, por otro lado, se divide entre las etapas de Mitosis, durante la cual se produce el reparto equitativo del material genético en la formación de dos núcleos celulares, y Citocinesis, el proceso final de separación física del citoplasma que concluye con la generación de dos células separadas e independientes, cada una de las cuales contendrá una copia idéntica de ADN. La fase de división recibe también el nombre de fase M.

El ciclo celular es un proceso estrechamente controlado mediante señales de diferentes vías reguladoras del crecimiento. En su regulación juegan un papel clave las proteínas quinasas dependientes de ciclinas (CDKs, del inglés *cyclin dependent kinases*) que, como su propio nombre indica, dependen de subunidades reguladoras llamadas ciclinas. Les CDKs actúan de forma secuencial, siendo activadas por sus ciclinas correspondientes en las distintas etapas del ciclo celular a medida que este avanza. Así, durante la fase G_1, se activan los complejos ciclina D-CDK4/6 y ciclina E-CDK2 para conducir a la célula a la fase S a través del punto de restricción R, mientras que la fase S es la ciclina A la que forma complejos con CDK1 y CDK2 para promover la finalización de la fase S y posteriormente son las ciclinas A y B las que se asocian con CDK1 para progresar a través de la fase G_2 y entrar en la fase M (Gallorini, Cataldi et al. 2012). Debido al papel central que juegan en el control del crecimiento y la proliferación celulares, los mecanismos que controlan el ciclo celular se encuentran alterados con mucha frecuencia en el cáncer y constituyen las dianas de diferentes terapias contra la enfermedad (Chan, Koh et al. 2012; Salmela and Kallio 2013; Gorjanacz 2014). Para abandonar la fase de quiescencia del ciclo celular (fase G_0), las células sanas necesitan no solo de una serie de estímulos mitóticos regulados por factores de crecimiento, adhesiones célula-célula o distintos componentes de la matriz extracelular, sino también de la inhibición de distintas señales antiproliferativas que bloquean el crecimiento manteniendo el ciclo celular en un estado continuado de reposo. Dos de las principales características del cáncer descritas por Hanahan y Weinberg, sin embargo, son precisamente la autosuficiencia de señales de crecimiento y la insensibilidad ante señales antiproliferativas que presentan las células tumorales.

La autosuficiencia de señales de crecimiento es adquirida por las células tumorales de maneras diferentes. Hay células tumorales capaces de sintetizar y liberar factores de crecimiento a los que ellas mismas responden, en un proceso denominado autoestimulación autocrina. Otras responden de manera especialmente intensa a señales inductoras de la proliferación que provienen de células de su microentorno, que son capaces de liberar factores de crecimiento como TGF-β, EGF y moléculas como Wnt2(Cheng, Chytil et al. 2008; Ostman and Augsten 2009; Fu, Zhang et al. 2011). La sobreexpresión de receptores de factores de crecimiento en las células tumorales, que las hace hipersensibles a las concentraciones de ligando presentes en su entorno más cercano, contribuye a este fenómeno. Algunos de los receptores de factores de crecimiento presentes en células tumorales son capaces, incluso, de transmitir señales promitóticas en ausencia total de ligando, y en otros casos son las vías intracelulares de transducción de señal, que normalmente sólo se activan al recibir la señal correspondiente de los receptores de membrana, las que están activadas de manera constitutiva en las células tumorales. En este último caso, la mayoría de las veces el punto clave lo constituyen proteínas de la familia Ras, cuya mutación mantiene activadas de forma constante las cascadas de señalización Ras/Raf/MEK/ERK y Ras/PI3K/mTor, que favorecen tanto la proliferación como la supervivencia celular (Miller, Yeager et al. 2009). Como hemos visto, este es el caso en muchos cánceres de pulmón que cuentan con mutaciones activadoras en el gen que codifica para la proteína KRas, con lo que las vías reguladas por esta proteína se encuentran activadas sin necesidad de recibir la señal correspondiente de los receptores de membrana.

Las señales antiproliferativas, por otra parte, suelen englobar distintas proteínas que regulan el ciclo celular induciendo la entrada en fase de quiescencia G_0 o bien impidiendo que se superen los *checkpoints* del mismo. Los *checkpoints* son puntos de control entre las diferentes fases del ciclo celular que sólo pueden ser superados cuando la fase previa al *checkpoint* se ha completado de manera correcta. En general, son mecanismos en los que se detecta si el ADN ha sufrido algún tipo de daño, impidiendo la suplicación de la célula si este no puede ser reparado (Kastan and Bartek 2004). Los checkpoints actúan a través de moléculas inhibidoras de CDKs y de ciclinas, que se engloban en dos grandes grupos: proteínas INK4 (como INK4A, INK4B, INK4C e INK4D) y las familias Cip y Kip (compuestas por los inhibidores de ciclinas y CDKs p21, p27 y p57) (Malumbres and Barbacid 2009). Las moléculas que ejercen este tipo de controles negativos sobre la progresión del ciclo celular tienen una función muy importante en la prevención de la tumorigénesis, y por ello es común que se encuentren desreguladas en el cáncer (Diaz-Moralli, Tarrado-Castellarnau et al. 2013).

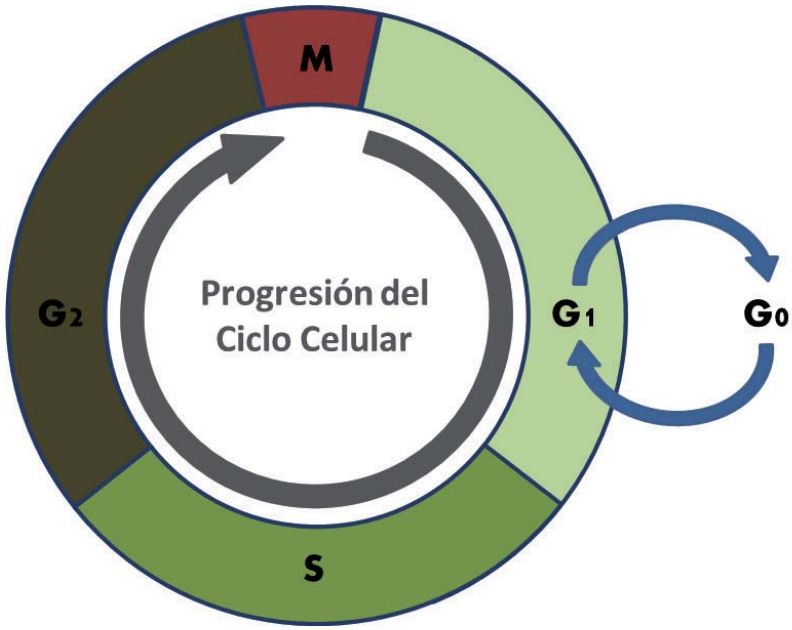

FIGURA 03. El Ciclo Celular. Esquema simplificado del Ciclo Celular. Tras la fase M la célula se divide en dos células hijas que pasan a estar en fase G1. Distintos mecanismos de control, llamados *checkpoints*, controlan el paso de una fase a la siguiente. Las células pueden entrar en un estado quiescente (fase G_0) en el que no se reproducen.

1.5. LA APOPTOSIS

La apoptosis es un mecanismo de muerte celular programada mediante el cual el organismo elimina de manera controlada las células sobrantes, dañadas o que puedan representar un peligro para el organismo. A diferencia de los procesos necróticos, que se caracterizan por una disolución de los orgánulos y una pérdida de la permeabilidad de las membranas celulares con la consiguiente liberación al espacio extracelular de hidrolasas que generan inflamación, la

apoptosis implica el desmantelamiento completo de las principales estructuras celulares de forma controlada, de tal manera que no se producen efectos adversos en células o tejidos contiguos.

Para asegurar el grado de control necesario, la apoptosis es un proceso altamente regulado que consta de diversas fases que se suceden siguiendo un orden establecido. Inicialmente, distintos mediadores genéticos y bioquímicos se activan en un intento de reparar los daños que pueda tener la célula, momento en el que el proceso apoptótico es aún reversible. Si estos mecanismos fallan, sin embargo, se inicia la llamada fase de ejecución, a partir de la cual el proceso es ya irreversible. En la fase de ejecución la célula sufre una serie de cambios estructurales que incluyen la condensación de la cromatina y la formación de los llamados cuerpos apoptóticos, que están constituidos por restos de componentes citoplasmáticos y nucleares rodeados por membrana celular. Estos cuerpos, en los que se acaba descomponiendo la totalidad de la célula, son eliminados del entorno extracelular por células fagocitarias, lo que impide la inflamación del tejido circundante.

La regulación de todos estos pasos está asociada a la activación de un conjunto de proteínas denominadas caspasas, cuya desregulación tiene por tanto una importante influencia en el cáncer (McIlwain, Berger et al. 2013; Yan, Li et al. 2013). Las vías de activación de la apoptosis en las que están involucradas las caspasas representan un paradigma particular en el ámbito de la transducción de señal, ya que esta es transmitida al realizarse cortes específicos en la estructura de las caspasas, que son los que producen la activación de las mismas. Así, las caspasas iniciadoras provocan cortes en las caspasas ejecutoras, activando a estas últimas para que puedan hidrolizar enlaces específicos de sus sustratos diana.

La apoptosis puede ser activada por diversos estímulos, como el cambio en la disponibilidad de hormonas, el estrés oxidativo, el daño en el ADN o la radiación. Como se ve en la **figura 4**, Hay dos vías distintas por las que los estímulos pueden activar la apoptosis: la vía intrínseca y la vía extrínseca. La vía extrínseca está ligada a señales externas transmitidas por receptores transmembrana llamados receptores de muerte (DR, del inglés *death receptors*). La unión a estos receptores de ligandos proapoptóticos provoca la trimerización del receptor y el consiguiente reclutamiento de la proteína adaptadora de dominio de muerte asociada a Fas (FADD, del inglés Fas associated death domain) y de las caspasas 8 y 10, que se unen al dominio citoplasmático del receptor para formar un complejo señalizador inductor de muerte celular (DISC, del inglés death-inducing signal complex). Las caspasas 8 y 10 son llamadas caspasas iniciadoras,

ya que su activación es necesaria para que se inicie el proceso apoptótico. Su activación autocatalítica en el DISC les permite activar a las caspasas 3, 6 y/o 7, llamadas caspasas efectoras, que acaban convergiendo en la vía intrínseca de la apoptosis. La activación de la caspasa 8 también puede provocar la ruptura de la proteína pro-apoptótica BID, cuya forma truncada promueve la formación de oligómeros de las proteínas BAK y BAX, que activan la vía intrínseca en lo que constituye otro punto de convergencia de ambas vías (Khan, Blanco-Codesido et al. 2014). La vía intrínseca, por otro lado, se induce intracelularmente, concretamente desde la mitocondria. Esta vía se activa en respuesta a señales de estrés celular, que se pueden originar por daño en el ADN, hipoxia, fallos en el ciclo celular o pérdida de factores de supervivencia celular. En esta vía, también llamada vía mitocondrial, la permeabilización de la mitocondria hace que se libere Citocromo c, una proteína que forma junto a las proteínas Apaf-1 y pro-caspasa 9 el complejo llamado apoptosoma. Este complejo es capaz, a su vez, de desencadenar la cascada proteolítica apoptótica a través de las caspasas efectoras 3, 6 y 7. La vía intrínseca está estrechamente regulada por un equilibrio de proteínas de la familia Bcl-2, que tienen funciones pro y anti apoptóticas. Las proteínas anti apoptíticas de la familia Bcl-2, como Bcl-XL y MCL-1, tienen como función mantener la integridad de la membrana mitocondrial externa. Las proteínas pro apoptóticas de la familia Bcl-2, como BAD y BMF, además de otras proteínas pro apoptóticas como PUMA o NOXA, se ven activadas por señales de estrés celular de manera que inhiben la acción de las proteínas anti apoptóticas mencionadas (Ren, Tu et al. 2010). Otro subgrupo de proteínas pro-apoptóticas, que incluye a Bid y a BIM, son capaces de activar las proteínas efectoras BAK y BAX (Kuwana, Mackey et al. 2002), que oligomerizan formando poros en la membrana mitocondrial externa, permeabilizándola y provocando que libere al citosol las proteínas citocromo c (que junto con Apaf-1 y pro-caspasa 9 forma el complejo llamado apoptosoma) y Smac/DIABLO (que se une a inhibidores de ptoteínas apoptóticas llamados IAPs, impidiendo que ejerzan su función). El apoptosoma activa por proteólisis la caspasa 9, que a su vez desencadena la cascada proteolítica apoptótica a través de las caspasas efectoras 3, 6 y 7 (Elkholi, Floros et al. 2011; Khan, Blanco-Codesido et al. 2014).

La correcta regulación del proceso apoptótico se ve alterada con mucha frecuencia en las células de cáncer, y de hecho una de las características comunes de las células tumorales, descritas por Hanahan y Weinberg, consiste en la capacidad de evadir la muerte celular. La inmensa mayoría de células tumorales presentan diversas mutaciones de genes o inactivaciones funcionales de proteínas relacionadas con la apoptosis, haciendo que incluso en situaciones de daño en el ADN o estrés celular las células sobrevivan evadiendo todos estos mecanismos de control.

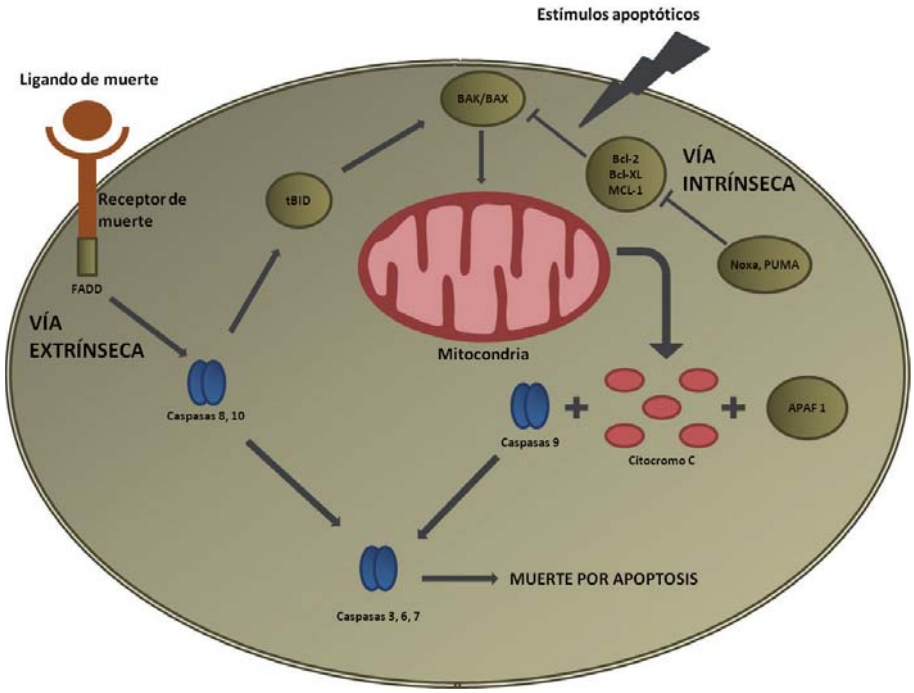

FIGURA 04. La apoptosis. Esquema simplificado del proceso apoptótico, y de las dos vías por las que este puede ser iniciado. La vía extrínseca está mediada por la unión de ligandos de muerte a receptores transmembrana. La vía intrínseca, en cambio, desencadenada habitualmente por estrés celular o daño en el ADN, se induce intracelularmente a partir de la liberación mitocondrial de citocromo C.

1.6. MÉTODOS PARA LA EVALUACIÓN DEL CICLO CELULAR Y LA APOPTOSIS

En su sentido más amplio, la citometría define el análisis de las características de las células. La citometría de flujo, por su parte, es una técnica de análisis celular que mide las características de células en suspensión mediante el paso de las mismas, una a una, por un sistema óptico consistente en láseres que iluminan a las células junto con distintos filtros que dirigen las señales ópticas que estas producen al interaccionar con el láser al detector correspondiente.

La clasificación de células activadas por fluorescencia (FACS, del inglés *fluorescence activated cell sorting*) es un tipo particular de citometría de flujo. Mediante esta técnica, las células en suspensión se hacen pasar por un haz de luz con una determinada longitud de onda, momento en el que un detector mide la dispersión de luz y la intensidad de fluorescencia que presentan cada una de las células que son procesadas en el análisis. Podemos marcar distintas moléculas de la célula de manera que, cuando esta interaccione con el láser emitido por el citómetro, emita fluorescencias determinadas que nos pueden dar información acerca de la presencia y concentración de las moléculas marcadas en las células analizadas. Así, mediante la elección de los marcadores fluorescentes adecuados, se pueden estudiar múltiples características celulares, midiendo así diferentes estados fenotípicos. Algunos ejemplos incluyen la detección de la fase del ciclo celular en la que se encuentra la célula, o si en la misma se está llevando a cabo un proceso apoptótico.

El estudio del ciclo celular mediante FACS se puede realizar previo marcaje de las células con ioduro de propidio. El ioduro de propidio (IP) es un agente intercalante de ácidos nucleicos que se une al ADN celular. Así, tras impermeabilizar las células (para permitir que el IP acceda al núcleo celular) y aplicar este marcaje, la cantidad de IP que contenga una célula, detectable por FACS ya que emite fluorescencia a una longitud de onda de 617 nm, será proporcional a la cantidad de ADN de la misma (Nunez 2001). Como hemos visto anteriormente, en la fase G1 la cantidad de ADN de la célula es de 2n, mientras que en la fase G2 esta cantidad se ha duplicado. Así, midiendo la intensidad de la fluorescencia a 617 nm de células marcadas con ioduro de propidio, podremos deducir si una célula analizada se encuentra en fase G1/G0 (cantidad de ADN: 2n), en fase G2/M (cantidad de ADN: 4n) o en fase S (en la que el ADN está en proceso de duplicación, y por tanto en una cantidad intermedia entre 2n y 4n).

La detección de la apoptosis mediante FACS, por otra parte, se basa en uno de los cambios morfológicos que sufre la célula durante las primeras fases del proceso apoptótico. En la primera etapa de la apoptosis se produce una pérdida de la asimetría de la membrana plasmática, con lo que la fosfatidilserina, que normalmente se encuentra anclada únicamente a la parte interna de la membrana (de manera que queda expuesta al citoplasma celular), se externaliza, entrando así en contacto con el exterior de la célula (Fadok, Voelker et al. 1992). La anexina V es capaz de unirse a la fosfatidilserina, por lo que añadiendo a la suspensión celular un conjugado de anexina V unida a FITC (isotiocianato de fluoresceína, un fluorocromo capaz de emitir fluorescencia tras ser excitado a una determinada longitud de onda) veremos marcaje únicamente en aquellas células que tienen externalizada la fosfatidilserina, que son aquellas en las que se está produciendo un proceso apoptótico (Hammill, Uhr et al. 1999). En el estudio de la apoptosis se suele utilizar

también IP, que solo accede al material genético en los casos en que la célula ha perdido la integridad de sus membranas. Así, como se puede observar en la **figura 5**, se considera que las células que están marcadas con IP se encuentran en un proceso apoptótico tardío (en comparación con las células que solo están marcadas con FITC, que son las que se encuentran en un proceso apoptótico temprano).

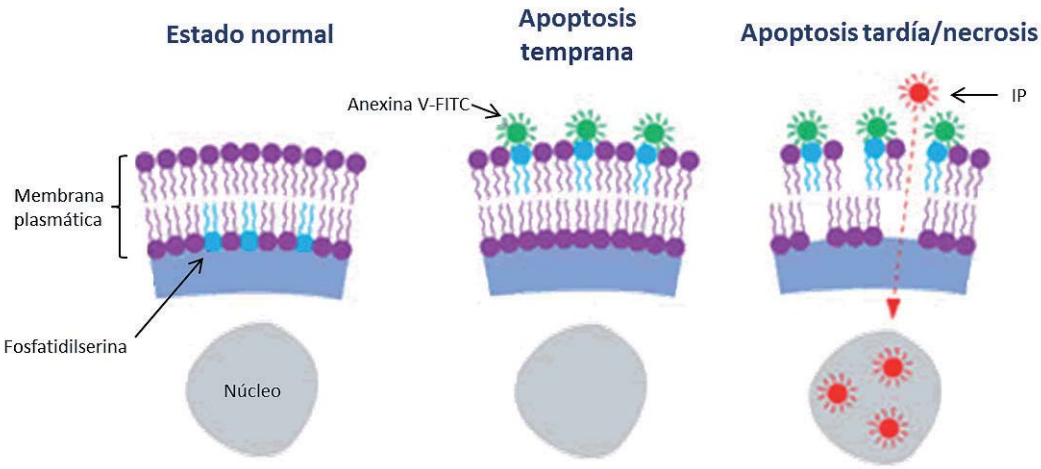

FIGURA 05. Detección de apoptosis por FACS. En una célula normal, la fosfatifdilserina (PS) se encuentra únicamente en la cara interna de la membrana. Al iniciarse el proceso apoptótico, la PS pasa a la cara externa, con lo que se une al complejo Anexina V-FITC, que marca a la célula con fluorescencia verde. En las últimas etapas del proceso apoptótico las membranas celulares pierden su integridad, con lo que el IP accede al núcleo marcando a las células también con fluorescencia roja. Figura adaptada de http://www.imgenex.com

1.7. FACTORES DE TRANSCRIPCIÓN FOXO Y SU RELACIÓN CON EL CÁNCER

La familia de factores de transcripción FOXO (Forkhead Box O) juega un relevante papel en múltiples procesos relacionados con la proliferación y supervivencia celulares (ver **figura 6**). Los factores FOXO, que regulan la transcripción de gran variedad de genes, están implicados en diferentes procesos celulares involucrados en el crecimiento, la diferenciación o la longevidad (Watroba, Maslinska et al. 2012; Eijkelenboom and Burgering 2013).

Se ha demostrado que la deleción de FOXO promueve la aparición de tumores (Zhang, Gan et al. 2011) y que la expresión constitutiva de FOXO promueve la muerte celular en distintos tipos de tejidos mediante inducción de apoptosis (Zhang, Tang et al. 2011; Zhang, Zhao et al. 2013). Además, la expresión de FOXO en células proliferantes es capaz de provocar una parada del ciclo celular en los distintos *checkpoints* que controlan el paso de una fase del ciclo celular a la siguiente, mediante diferentes mecanismos como la promoción de los inhibidores del ciclo celular p21 y p27 (Seoane, Le et al. 2004; Roy, Srivastava et al. 2010), la inhibición de los activadores del ciclo celular ciclina D1 y ciclina D2 (Schmidt, Fernandez de Mattos et al. 2002; Ganapathy, Chen et al. 2010) o la promoción de la expresión de bloqueantes del ciclo celular como la ciclina G2, un tipoparticular de ciclina que, en vez de promover la progresión en el ciclo celular, actúa bloqueando la entrada al mismo (Martinez-Gac, Marques et al. 2004; Fu and Peng 2011). La parada o ralentización del ciclo celular puede hacer que la célula tenga el tiempo que necesita para reparar al ADN dañado, y de manera consecuente los factores FOXO también promocionan la expresión de diversos genes relacionados con la detoxificación de sustancias reactivas de oxígeno (ROS, del inglés *reactive oxygen species*) y la reparación de ADN (Greer and Brunet 2005; Klagge, Weidinger et al. 2011). Por último, los factores de transcripción FOXO también juegan un importante papel en la sobre-expresión de distintos genes que regulan el metabolismo, y especialmente el metabolismo de la glucosa (Gross, Wan et al. 2009; Kousteni 2012; Kim, Zhang et al. 2013).

Todas estas funciones proapoptóticas y antiproliferativas han hecho que los factores FOXO sean considerados supresores de tumores que tienen la función de mantener la homeostasis celular (Paik, Kollipara et al. 2007; Dansen and Burgering 2008; Eijkelenboom and Burgering 2013; Webb and Brunet 2014). Existen múltiples evidencias del papel que estos factores juegan en el cáncer, ya que la expresión de FOXO reduce la proliferación celular y la generación de tumores y su inhibición induce la formación espontánea de los mismos en distintos modelos (Kikuno, Shiina et al. 2007; Cornforth, Davis et al. 2008; Shukla, Bhaskaran et al. 2013). Aunque el efecto de los factores FOXO como supresores de tumores está bien documentado, y aunque existen estudios que indican que existe una deleción de FOXO en adenocarcinomas de pulmón (Blake, Mikse et al. 2010; Mikse, Blake et al. 2010), la inactivación genética de FOXO no es común en las células tumorales. En cambio su inactivación post-transcripcional, normalmente causada por mutaciones en la vía Ras, sí es habitual en distintos tipos de tumores (Dansen and Burgering 2008).

Todas estas evidencias insinúan que la reactivación de FOXO puede ser una estrategia prometedora en la terapia contra el cáncer. Los factores de transcripción de esta familia pueden ser regulados mediante distintas modificaciones post-traduccionales, incluyendo fosforilación, acetilación y ubiquitinación (Daitoku, Sakamaki et

al. 2011; Xie, Chen et al. 2012), aunque la fosforilación por AKT es comúnmente considerada la vía clave de regulación de FOXO. AKT fosforila FOXO permitiendo que este se una a la proteína 14-3-3, formándose un complejo que es traslocado desde el núcleo hasta el citoplasma celular, localización en la que FOXO ya no puede ejercer sus funciones antiproliferativas ni proapoptóticas (Tzivion, Dobson et al. 2011). La defosforliación de FOXO, a su vez, provoca la disociación del complejo, permitiendo la relocalización de FOXO en el núcleo celular en el que sí podrá llevar a cabo su función como supresor de tumores (Zhang, Tang et al. 2011).

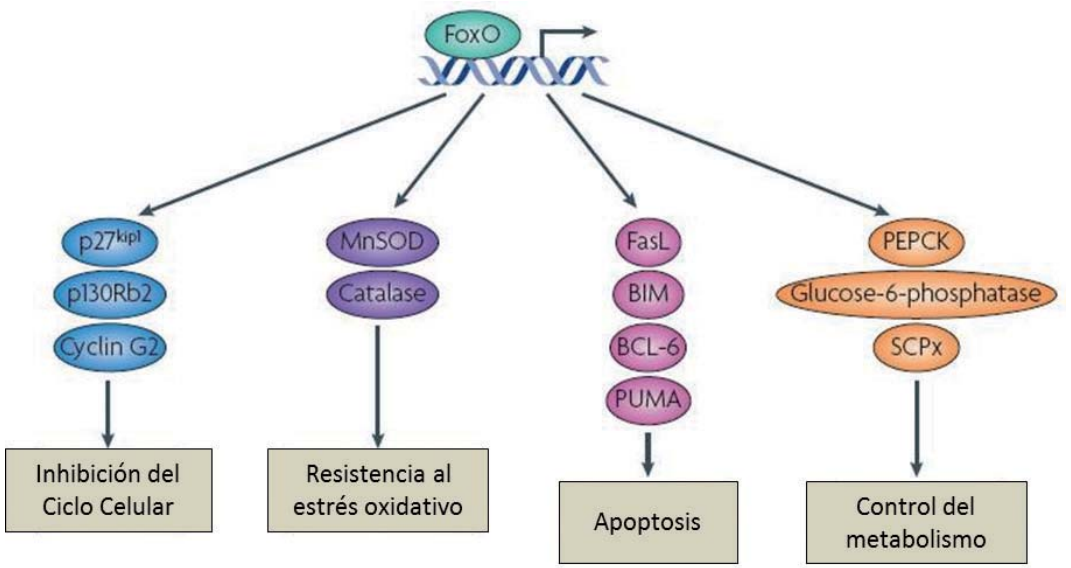

FIGURA 06. Funciones de FOXO. Representación esquemática de algunos de los genes diana de los factores de transcripción de la familia FOXO, y de los procesos en los que estos están implicados. En general, FOXO promueve la transcripción de numerosos genes relacionados con inhibir la proliferación, activar la apoptosis, resistir el estrés celular y controlar el metabolismo, por lo que es considerado un gen supresor de tumores. Figura adaptada con permiso de Elsevier de *Stressing the role of FoxO proteins in lifespan and disease*, Nature Reviews Molecular Cell Biology **8**, 440-450.

Así, es habitual que procesos tumorigénicos impliquen la fosforilación de FOXO y su consiguiente acumulación en el citoplasma, lo que acaba conllevando su degradación y la inhibición general de su actividad transcripcional (Hu, Lee et al. 2004; Huang, Regan et al. 2005; Yang, Zong et al. 2008; Lam, Brosens et al. 2013). La desfosforilación de FOXO y su consiguiente restauración en el núcleo celular, lo que implicaría la activación de sus funciones reguladoras de la apoptosis, el ciclo celular

y la protección contra el estrés oxidativo, puede resultar por tanto una estrategia interesante para combatir la proliferación descontrolada en distintos tipos de tumores.

1.8. EVALUACIÓN DE LA LOCALIZACIÓN INTRACELULAR DE FOXO

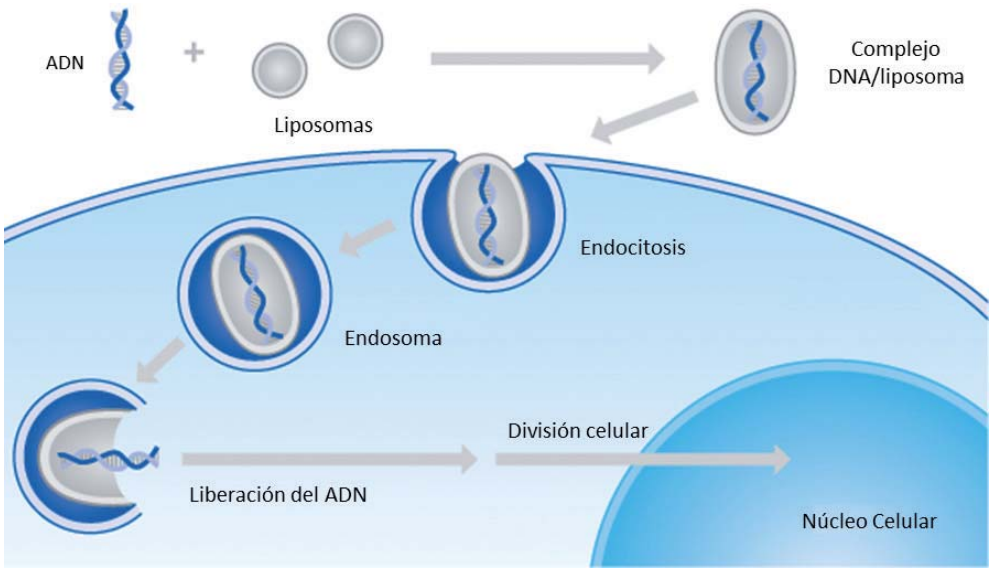

FIGURA 07. Transfección celular. La figura ilustra de manera esquemática en qué consiste la técnica de transfección celular. El ADN de interés es introducido a la célula con la ayuda de liposomas como agentes transfectantes, que atraviesan la membrana celular mediante un proceso de endocitosis. Una vez en el citoplasma, el endosoma se descompone liberando el ADN, que se integrará en el núcleo de las células hijas tras el proceso de división celular. Con ello conseguimos que la célula exprese las proteínas para las que codifica el plásmido introducido. Figura adaptada de http://www.biontex.com

Como se ha descrito anteriormente, FOXO es un factor de transcripción que ejerce su función en el núcleo celular y que se desplaza al citoplasma cuando es inactivado por fosforilación, por lo que el estudio de la localización intracelular de FOXO es un método útil para evaluar su estado de activación. Una manera de estudiar la localización de FOXO consiste en introducir una proteína estable FOXO-proteína verde fluorescente (GFP, del inglés *fluorescent green protein*) en las células a evaluar. Así, mediante un simple análisis por microscopía confocal se puede evaluar si la fluorescencia verde, indicadora de la presencia de FOXO, se

concentra principalmente en el núcleo o en el citoplasma celular. La fluorescencia verde se concentrará en el núcleo cuando FOXO esté activado, mientras que cuando FOXO esté desactivado la fluorescencia verde se concentrará en el citoplasma.

Para generar una línea celular capaz de expresar una proteína quimérica FOXO-GFP hay que someter a la línea modelo a un proceso de transfección con un plásmido de FOXO-GFP. En el proceso de transfección, el material genético contenido en el plásmido (en este caso, ADN que codifica para la proteína quimérica FOXO-GFP) es incorporado al material genético celular gracias a la ayuda de un agente transfectante, normalmente un liposoma, que sea capaz de fusionarse con la membrana celular introduciendo en ella su contenido (ver **figura 7**).

Una vez finalizado el proceso de transfección, la célula incluirá en su material genético ADN que codifica para la proteína quimérica, y por tanto expresará FOXO-GFP cuya localización puede ser detectada fácilmente gracias a la fluorescencia que la GFP emite al ser excitada a una longitud de onda determinada (Zanella, Rosado et al. 2008).

1.9. METALOFÁRMACOS EN QUIMIOTERAPIA

Desde el descubrimiento hace más de 40 años de la actividad biológica del cis-diaminedichloroplatinum(II), [cis-(NH3)2PtCl2], el cisplatino (nombre genérico que recibe el compuesto) ha supuesto un enorme impacto en el tratamiento de muchos tipos de cáncer (Kelland 2007). Aún hoy, el cisplatino y dos de sus derivados (carboplatino y oxaliplatino) se usan en más del 50% de los tratamientos quimioterapéuticos de cáncer existentes (Gasser, Ott et al. 2011). Actualmente sólo estos tres fármacos han sido comercializados a nivel global, mientras que compuestos como el nedaplatino, el heptaplatino y el lobaplatino se comercializan únicamente en Japón, Corea y China, respectivamente (ver **figura 8**).

Sin embargo, y a pesar de la utilidad del cisplatino en el tratamiento de muchos tipos de tumores, el compuesto presenta múltiples desventajas que hacen que su utilidad se vea reducida. De entre estas desventajas destacan, por su importancia, los efectos secundarios del cisplatino y la resistencia al mismo de las células tumorales.

La resistencia al cisplatino es a veces intrínseca de determinados tipos de tumores, como por ejemplo algunos tumores de mama, colon o próstata, que resultan resistentes al compuesto desde el primer tratamiento (Kelland 2007). En cualquier caso, incluso cuando las células cancerosas son inicialmente sensibles al compues-

to, es común que con los sucesivos ciclos de tratamiento se generen resistencias adquiridas (Abu-Surrah and Kettunen 2006). La evidencia experimental acerca del mecanismo de acción del cisplatino indica que este se une covalentemente al ADN celular formando aductos y provocando una distorsión en la estructura del material genético, lo que activa diversas vías de señalización relacionadas con la reparación del daño genético, la proliferación, el ciclo celular y la apoptosis que acaban desembocando en una muerte celular programada (Kelland 2007). Una de las causas más comunes de resistencia al cisplatino se da cuando este no llega a entrar en contacto con el DNA celular en una concentración suficiente, debido principalmente a una baja acumulación del compuesto (Kelland, Mistry et al. 1992) o a su detoxificación por glutatión o metalotioneínas (Mistry, Kelland et al. 1991; Holford, Beale et al. 2000). En ocasiones se presentan resistencias incluso aunque la concentración del cisplatino en contacto con el ADN sea lo suficientemente alta, ya sea porque las células tienen una tolerancia elevada al daño en su ADN o porque cuentan con mecanismos de reparación del mismo lo suficientemente efectivos (Johnson, Swiggard et al. 1994).

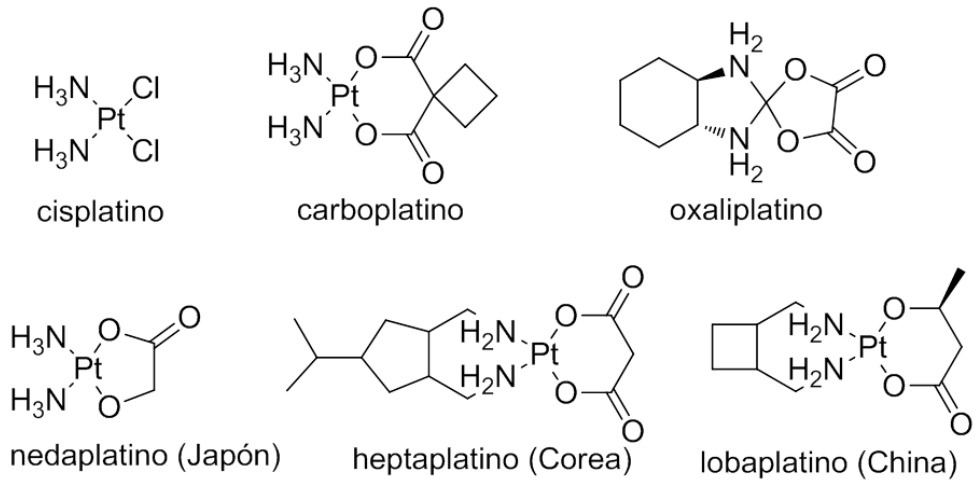

FIGURA 08. Metalofármacos de platino. Estructura química de los complejos de platino que se comercializan en la actualidad como fármacos antitumorales.

Por otra parte, los efectos secundarios del cisplatino son severos y constituyen una importante desventaja de su uso terapéutico. El hecho de que la diana del

cisplatino sea ubicua (todas las células del organismo tienen ADN) hace que la interacción con el mismo no sea específica de las células cancerosas. El efecto secundario más problemático del cisplatino es su elevada nefrotoxicidad, pero también provoca otras alteraciones de gravedad variable como nauseas, vómitos, neuropatía periférica, mielotoxicidad y toxicidad en el tracto gastrointestinal (Abu-Surrah and Kettunen 2006).

Todos estos inconvenientes hacen necesario el descubrimiento de nuevos compuestos mejorados que presenten una mayor actividad biológica y una disminución de los efectos secundarios. Compuestos como el carboplatino, un derivado del cisplatino, han pasado a formar parte de los tratamientos quimioterapéuticos convencionales. Pero aunque en muchos casos presentan toxicidades inferiores y, por tanto, efectos secundarios menos severos, en general no suponen un aumento espectacular de la actividad biológica del cisplatino ni una solución a sus problemas de resistencia, ya sea ésta intrínseca o adquirida durante el tratamiento. Ciertos avances en el área de la resistencia intrínseca se han obtenido con la utilización del oxaliplatino, en el que los ligandos NH_3 se han sustituido por el ligando (1*R*, 2*R*)-cyclohexano-1,2-diamino (*R*,*R*-dach). El oxaliplatino es eficaz en cáncer de colon resistente al cisplatino debido a que forma diferentes aductos con el DNA evitando la unión de proteínas reparadoras del mismo. En cualquier caso, y aunque tras el descubrimiento del cisplatino se sintetizaron y evaluaron gran cantidad de compuestos derivados del mismo con la esperanza de encontrar un tratamiento más efectivo y seguro, en los años posteriores el ritmo de aparición de nuevos avances en este campo disminuyó notablemente. En los últimos años, sin embargo, el interés por la síntesis y evaluación de nuevas generaciones de compuestos de platino se ha revitalizado, debido sobre todo a los descubrimientos acerca de los mecanismos que regulan la resistencia a este tipo de tratamientos.

La investigación de nuevos compuestos metálicos en la búsqueda de terapias más efectivas contra el cáncer no se limita a compuestos con platino, sino que se ha visto ampliada para incluir moléculas con átomos de paladio, hierro, oro, rutenio o iridio, entre otros. Una gran variedad de compuestos organometálicos, definidos como aquellos complejos metálicos que cuentan con al menos un enlace covalente directo carbono-metal, se han revelado recientemente como moléculas con una prometedora acción antitumoral. Los compuestos organometálicos cuentan con una enorme variedad estructural y estequiométrica, son cinéticamente estables, relativamente lipofílicos y a menudo presentan una carga neutra y un bajo estado de oxidación de su átomo metálico. Además, un diseño racional de sus ligandos permite controlar propiedades clave de los compuestos, como por ejemplo su facilidad de hidrólisis.

1.9.1. Compuestos cicloplatinados de siete miembros

Los compuestos ciclometalados con diferentes metales han demostrado en el pasado prometedoras actividades antitumorales (Gasser, Ott et al. 2011). Resulta digno de mención el hecho de que la presencia de un enlace carbono-metal parece incrementar la estabilidad de los complejos, lo que hace que aumente la probabilidad de que los complejos ciclometalados alcancen su diana biológica con su estructura intacta (Edwards, Black et al. 2005).

Los compuestos ciclometalados cuyas actividades biológicas han sido publicadas hasta ahora constan de ciclos planos de cinco miembros. Por otro lado, existen estudios con diaminas queladas en los que los complejos con anillos de siete miembros presentan una mayor actividad antiproliferativa que los complejos de 5 o de 6 miembros (Moradell, Lorenzo et al. 2003).

Por todo ello, la actividad biológica de los compuestos cicloplatinados de siete miembros, así como la comparación de la misma con la de compuestos similares con anillos de cinco miembros, resulta de especial interés en la búsqueda de nuevos compuestos con actividad antitumoral.

1.9.2. Compuestos de platino con iminas polifuncionalizadas

La unión del cisplatino al ADN celular provoca una distorsión de su estructura helicoidal causando la inhibición de su replicación y su transcripción, lo que acaba provocando el arresto del ciclo celular y la activación de la apoptosis de la célula afectada. La alterada estructura del ADN que resulta de la unión del mismo al cisplatino, sin embargo, se convierte en un nuevo sitio de unión de proteínas, como por ejemplo histonas, factores de transcripción, o proteínas reparadoras del ADN. Estas proteínas capaces de unirse al ADN distorsionado tienen la capacidad de modular la efectividad del cisplatino o la resistencia al mismo (Wang and Lippard 2005; Jung and Lippard 2007). Así, una de las estrategias principales para desarrollar nuevos compuestos con capacidad antiproliferativa es la de diseñar compuestos que se unan al ADN celular de manera diferente al cisplatino. Una posible manera de generar estos compuestos consiste en usar ligandos que exhiban átomos de N con capacidad donadora de electrones, como ocurre en las iminas. Estudios sobre la relación estructura-actividad de este tipo de compuestos pueden proporcionar interesante información acerca de cómo la actividad biológica de los mismos se ve alterada por factores como los átomos donadores del ligando, su modo de unión al metal, el tamaño del quelato, la presencia de sustituyentes o la naturaleza de los ligandos auxiliares adicionales.

1.9.3. Compuestos de platino y paladio derivados del pirazol

En la búsqueda de nuevos ligandos N-donadores para la síntesis de compuestos organometálicos optimizados, los azoles suponen una alternativa interesante a las iminas. Los azoles heterociclos son reactivos muy valiosos en la química de coordinación, y se sabe que su unión a un ión metálico afecta a sus propiedades y a su actividad (Budzisz, Lorenz et al. 2008). En la actualidad apenas existe información acerca del potencial antitumoral de compuestos con ligandos de pirazol, con lo que resulta interesante la evaluación de la actividad biológica de nuevos compuestos organometálicos derivados del pirazol, y del efecto que ejercen los sustituyentes del heterociclo, el tipo de enlace del ligando o incluso el tipo de metal del complejo sobre su actividad biológica antiproliferativa.

1.9.4. Compuestos derivados del ferroceno

En la última década, compuestos derivados del ferroceno han adquirido un gran interés debido a su actividad biológica y a sus aplicaciones en biomedicina. Las propiedades únicas del ferroceno, como su aromaticidad, estabilidad en medio acuoso y potencial redox, hacen que resulte especialmente interesante investigar su efecto en la actividad biológica de nuevos compuestos antitumorales, aunque los estudios sobre su actividad antiproliferativa siguen siendo escasos. Además, el uso de derivados del ferroceno en compuestos organometálicos, con distintos átomos donadores de electrones capaces de exhibir diferentes modos de unión al metal o de crear isómeros variados, no ha sido estudiado a fondo. Por ello, los efectos derivados del tipo de enlace al metal o de la orientación espacial de los ligandos sobre la potencial actividad antitumoral de estos productos permanecen relativamente inexplorados, y su investigación resulta de especial interés

Por otro lado, varios fármacos antitumorales, como el paclitaxel, se caracterizan por modular el ensamblaje de microtúbulos mediante la inhibición de la polimerización de la tubulina. Muchos inhibidores de la polimerización de la tubulina se caracterizan por la presencia de un núcleo indólico, y existen estudios sobre derivados del indol que demuestran su capacidad antiproliferativa en líneas celulares humanas de cáncer de mama (Pojarova, Kaufmann et al. 2007). A tenor de todo ello, la caracterización de la actividad de nuevos híbridos ferroceno-indol, y la comparación de la misma con respecto a la de sus análogos puramente orgánicos, resulta también especialmente atractiva en la búsqueda de nuevas estructuras organometálicas con potencial antitumoral.

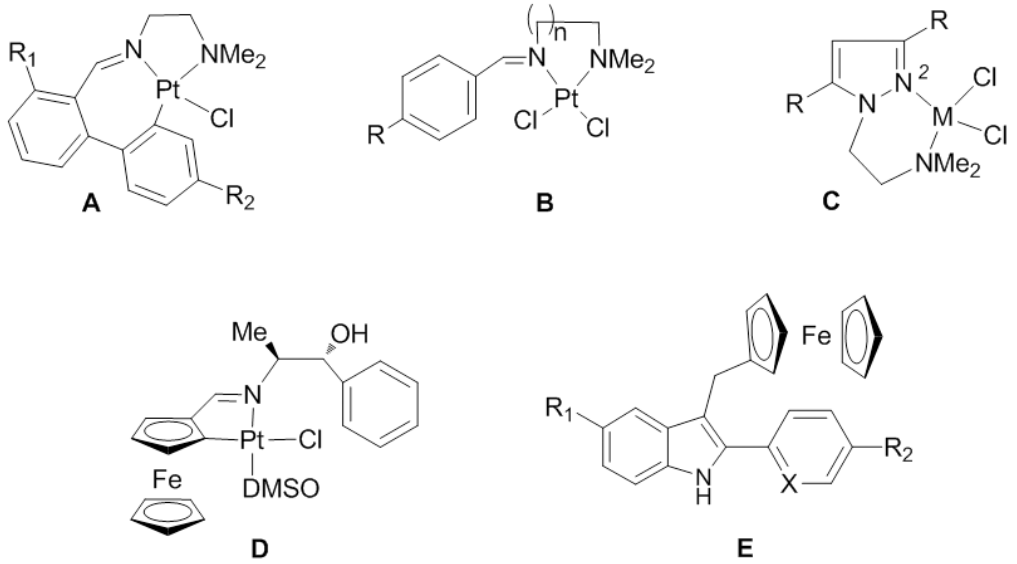

FIGURA 09. Complejos metálicos. Ejemplos de algunas estructuras organometálicas cuya actividad antiproliferativa resulta de interés evaluar. A: Compuestos cicloplatinados de 7 miembros, B: compuestos de platino (II) con ligandos imínicos, C: complejos metálicos derivados del pirazol, D: compuestos ciclometalados de platino (II) y ferroceno, E: complejos híbridos ferroceno-indólicos.

1.10. EL METABOLISMO TUMORAL

El metabolismo es, en su sentido más amplio, el conjunto de transformaciones químicas que ocurren en una célula u organismo. Las reacciones metabólicas son la base de la vida a escala molecular, y gracias a ellas los organismos pueden crecer, reproducirse, construir (y mantener) sus estructuras básicas y adaptarse a las condiciones cambiantes del entorno en el que viven. El metabolismo se suele clasificar en dos procesos opuestos pero complementarios: el anabolismo y el catabolismo. El catabolismo engloba los procesos mediante los que moléculas complejas son degradadas a otras más sencillas para obtener energía, mientras que el anabolismo consiste en la formación de sustancias complejas a partir de otras más simples con la intención de sintetizar diversos componentes celulares, lo que necesita un aporte energético.

El metaboloma, por otra parte, se define como el conjunto de metabolitos o moléculas pequeñas presentes en un organismo como producto final de la actividad proteica. El resto de "omas" (genoma, transcriptoma, proteoma) también definen la función celular, pero es el metaboloma el que refleja de manera más fiel el fenotipo celular en un momento dado, ya que de él depende el estado

fisiológico final de la célula. Históricamente se ha considerado que la relación entre los distintos "omas" era de naturaleza jerárquica: a partir del genoma se generaba el transcriptoma y este definía el proteoma, que a su vez era el encargado de procesar los metabolitos controlando así el estado del metaboloma. En la actualidad, sin embargo, existe la evidencia de que las relaciones entre todos estos niveles de organización celular no son unidireccionales, ya que cada "oma" es capaz de regular a (y susceptible de ser regulado por) todos los demás (ver **figura 10**). Así, el metaboloma no es únicamente un resultado pasivo del estado del proteoma, el transcriptoma o el genoma, sino que también es capaz de controlar recíprocamente estos estados regulatorios (Oltvai and Barabasi 2002).

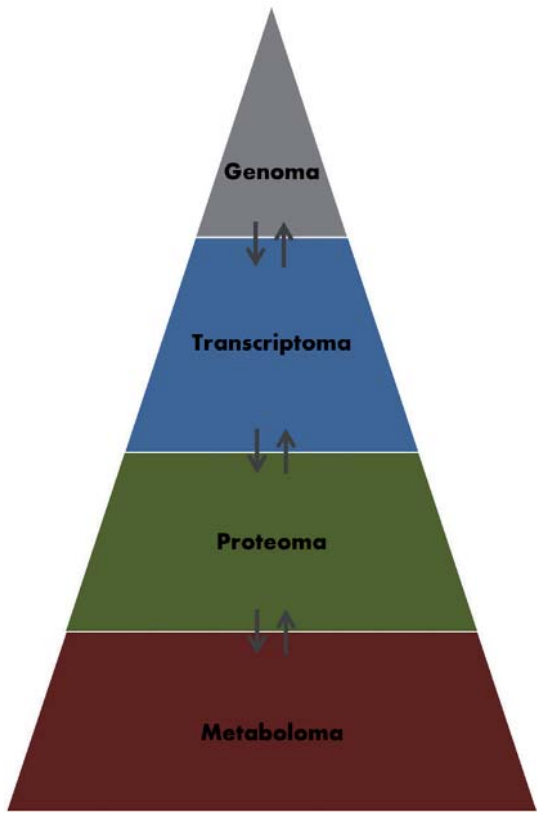

FIGURA 10. Regulación cruzada entre "-omas". El genoma, conjunto de todos los genes del organismo, está formado por secuencias de ADN que al transcribirse generan el transcriptoma. Los tránscritos se traducen dando lugar a las proteínas que conforman el proteoma, y éstas regulan la síntesis y degradación de los metabolitos del organismo, definiendo así el metaboloma. Pero existe una interacción recíproca entre todos los estados del sistema, con lo que cada estrato organizativo es influenciado por el resto de estratos, al tiempo que ejerce su influencia sobre los mismos.

La proliferación cellular descontrolada que acontece en los procesos tumorales necesita una reprogramación del metabolismo energético que permita acelerar el crecimiento y la división celulares. Por ello, la alteración del metabolismo energético es una rasgo tan definitorio del cáncer como la evasión de los mecanismos de muerte celular o la insensibilidad ante señales antiproliferativas, y ha sido definida como una de las características generales del cáncer, necesaria para la proliferación tumoral (Hanahan and Weinberg 2011).

1.10.1. La glucólisis y el efecto Warburg

Las células sanas degradan la glucosa hasta formar piruvato por la vía de la Glucólisis. En condiciones de presencia de oxígeno, el piruvato entra en la mitocondria y se incorpora al ciclo de Krebs, donde será oxidado en un proceso conocido como fosforilación oxidativa para producir energía en forma de ATP. Así, a partir de glucosa y oxígeno, la célula acaba produciendo CO_2 y agua, obteniendo energía, regulando el potencial redox de la célula (a través de la generación de moléculas como NADH y NADPH) y generando además los precursores metabólicos a partir de los cuales la célula sintetizará las moléculas que necesita para su correcto funcionamiento (como ARN y proteínas).

En condiciones anaeróbicas, en cambio, la ausencia de oxígeno imposibilita la obtención de ATP mediante este proceso de fosforilación oxidativa, por lo que las células optan por una vía alternativa en la que el piruvato proveniente de la glucosa es transformado en lactato. Este mecanismo, conocido con el nombre de glucólisis anaeróbica, no sólo es ineficiente como método de obtención de energía (se obtienen únicamente 2 moléculas de ATP por molécula de glucosa, en vez de las 36 generadas en la fosforilación oxidativa), sino que conlleva el problema añadido de la acumulación de lactato, que a diferencia del CO_2 o el agua puede resultar tóxico para las células.

La primera característica metabólica diferencial que fue descrita para las células tumorales, hace ya más de 70 años, recibe el nombre de efecto Warburg. Según este efecto, en las células de cáncer el mecanismo de degradación de la glucosa se encuentra alterado de modo que, incluso en condiciones aeróbicas, la célula favorece la síntesis de lactato por encima de la entrada de piruvato al Ciclo de Krebs, en un proceso conocido como glucólisis aeróbica. El fenómeno resultó inicialmente difícil de explicar, dado que es lógico pensar que las células proliferantes tienen unas necesidades energéticas mayores que las células sanas, y en cambio la degradación de glucosa a lactato tiene, como ya hemos visto, un ren-

dimiento energético muy inferior al de la fosforilación oxidativa. Sin embargo, y a pesar de esta ineficiencia energética, el efecto Warburg concede a las células cancerosas una serie de ventajas que resultan cruciales en el particular microentorno que se genera alrededor de un tumor (Hitosugi and Chen 2013).

En primer lugar hay que considerar que un tumor genera, al crecer y expandirse, una masa celular que cada vez está más alejada de los vasos sanguíneos, con lo que la difusión de oxígeno desde estos hacia las células se ve dificultada. Esto provoca un descenso en la disponibilidad de oxígeno de las células tumorales, situación en la que sólo proliferarán las células con el metabolismo mejor adaptado a una situación hipóxica.

Además, se ha descrito que la cantidad de energía adicional necesaria para producir una nueva célula es, asumiendo que la glucosa es el principal sustrato energético, únicamente el 50% de la energía basal necesaria para mantener la homeostasis celular (Kilburn, Lilly et al. 1969). Esto demuestra que la cantidad de ATP necesaria no es dramáticamente superior en el proceso de proliferación, con lo que la verdadera clave del mismo es la acumulación de biomasa y la replicación de ADN. La síntesis continua de nuevas biomoléculas, además, implica requerimientos adicionales a la energía proporcionada por el ATP. Por ejemplo, una única molécula de glucosa es capaz de proporcionar 5 veces la cantidad de energía necesaria para sintetizar una molécula de palmitato, mientras que el NADPH necesario en esta misma síntesis requiere la metabolización de 7 moléculas de glucosa. De manera análoga, también la síntesis de aminoácidos y nucleótidos requiere de más equivalentes de carbono y NADPH que de ATP. Todo ello implica que, para que una célula prolifere, no puede dedicar toda su glucosa a la producción de ATP, lo que además generaría un desequilibrio en el ratio ATP/ADP que podría inhibir el flujo a través de los intermediarios glucolíticos, limitando aún más la producción de acetil-CoA y NADPH requerida en la síntesis de macromoléculas. Así, se ha propuesto que el efecto Warburg podría suponer un método especialmente efectivo para aumentar las tasas biosintéticas de las células tumorales, lo que a la hora de mantener un ritmo de duplicación acelerado confiere una ventaja más importante que la puramente energética (Vander Heiden, Cantley et al. 2009)Go.

La acidificación resultante de la producción de ácido láctico a partir del lactato, que supone un problema en tejidos sanos, puede resultar beneficiosa para el desarrollo de un tumor (Gillies, Robey et al. 2008; Bailey, Wojtkowiak et al. 2012; Honasoge and Sontheimer 2013). Esto es así porque esta acidificación induce la muerte de las células sanas que rodean el tumor, con lo que las señales inhibidoras de la proliferación que genera el contacto con estas células sanas se ven disminuidas, facilitándose así el crecimiento tumoral. La acidosis también

provoca que fibroblastos y macrófagos liberen enzimas proteolíticas que degradan la matriz extracelular facilitando la invasividad y la metástasis, fenómeno que se ve además potenciado por el hecho de que la acidosis también provoca la secreción de factores activadores de la angiogénesis (como VEGF).

Teniendo en cuenta que la mitocondria juega un importante papel en la generación de especies reactivas de oxígeno (ROS), y dado que está demostrado que estas son capaces de activar la apoptosis, la reducción de la entrada de piruvato en la mitocondria provoca que su actividad metabólica disminuya, con la consiguiente reducción de los niveles de ROS e inhibición de la apoptosis que ello conlleva.

Adicionalmente, se ha descrito que el lactato producido por las células hipóxicas de un tumor puede ser utilizado como sustrato energético por las células aeróbicas que lo rodean, más cercanas a los vasos sanguíneos. Al utilizar el lactato como fuente de energía estas células aeróbicas prescinden de la glucosa, aumentando su disponibilidad para las células hipóxicas tumorales. De este modo se crea una sinergia entre las diferentes subpoblaciones tumorales que beneficia el crecimiento del tumor (Semenza 2008; Kennedy and Dewhirst 2010; Rattigan, Patel et al. 2012). De hecho, la inhibición de la lactato deshidrogenasa A (LDHA) y de los transportadores de lactato se ha propuesto como estrategia terapéutica en distintos tipos de cáncer (Doherty and Cleveland 2013).

Otra característica diferencial de la glucólisis tumoral la constituye la expresión preferencial de PKM2, la isoforma M2 de la piruvato quinasa, frente a PKM1, que es la isoforma predominante en la gran mayoría de tejidos diferenciados. Sorprendentemente, PKM2 tiene menos actividad enzimática que PKM1, y además es, al contrario que esta, sensible a la inhibición por la señalización proveniente de receptores de factores de crecimiento. Al parecer, la actividad reducida de esta isoforma provoca la acumulación de intermediarios glucolíticos, que son derivados a las vías anabólicas de síntesis de biomoléculas que parten de los mismos, como la de la síntesis de bases nitrogenadas a partir de la vía de las pentosas fosfato. Este fenómeno refuerza la idea de que las células proliferantes priorizan las vías anabólicas de síntesis de biomoléculas por encima de las de generación de energía en forma de ATP (Christofk, Vander Heiden et al. 2008; Hitosugi, Kang et al. 2009; Ward and Thompson 2012).

Por último, aunque la eficiencia energética de la glucólisis aeróbica es menor que la de la fosforilación oxidativa, las células tumorales cuentan con un mecanismo compensatorio gracias a la sobreexpresión de transportadores de glucosa que permiten aumentar la tasa de incorporación de la misma (Jones and Thompson 2009; Ortega, Sanchez-Arago et al. 2009; Adekola, Rosen et al. 2012; McCracken and

Edinger 2013; Szablewski 2013). Además, la velocidad de síntesis de ATP por glucólisis aeróbica es mayor que por fosforilación oxidativa, lo que proporciona una ventaja importante en condiciones de competencia por la obtención de glucosa.

Todas estas evidencias señalan que el efecto Warburg confiere importantes ventajas a las células proliferantes de un tumor, lo que refuerza la teoría de que la reprogramación metabólica tumoral no es únicamente una consecuencia pasiva de los cambios genéticos en las células cancerosas, sino que constituye un requerimiento esencial para la progresión de la enfermedad, y por lo tanto una diana terapéutica con una excelente potencialidad para combatirla.

1.10.2. La glutaminólisis

La glucosa es el sustrato energético principal de las células del organismo, pero no es el único. Para mantener su elevada tasa de proliferación, las células tumorales recurren también a la glutamina, el aminoácido más abundante en el plasma. El proceso por el que la glutamina es catabolizada para generar lactato y ATP se conoce como glutaminólisis, una vía metabólica que se encuentra sobreactivada en muchos tipos de tumores.

A día de hoy no existe un consenso científico acerca del destino metabólico final de la glutamina consumida por las células tumorales, probablemente porque dependa del tipo celular en estudio y de sus necesidades en cada momento. En general, la derivación de glutamina a lactato se puede utilizar para generar poder reductor (en forma de NADPH) necesario en procesos anabólicos como la síntesis de nucleótidos o la de ácidos grasos (DeBerardinis, Mancuso et al. 2007; Wise, DeBerardinis et al. 2008), para generar una fuente de nitrógeno con la que sintetizar aminoácidos y proteínas y nucleótidos (Meng, Chen et al. 2010; Hensley, Wasti et al. 2013) o simplemente para obtener energía en forma de ATP y conservar la homeostasis redox celular (Gao, Tchernyshyov et al. 2009), aunque también se ha descrito que la glutamina tiene un papel regulador de distintas vías de señalización que promueven el crecimiento celular (Daye and Wellen 2012; Duran, Oppliger et al. 2012).

El metabolismo de la glutamina comienza por su transformación a glutamato, en una reacción catalizada por la enzima glutaminasa, de la que existen distintas isoformas codificadas por los genes GLS y GLS2. La expresión de las isoformas codificadas por GLS correlaciona con el ratio de proliferación y la malignidad en distintos modelos biológicos (Lobo, Ruiz-Bellido et al. 2000; Gao, Tchernyshyov

et al. 2009; Wang, Erickson et al. 2010; Cheng, Sudderth et al. 2011). El papel de GLS2 en el desarrollo tumoral, en cambio, es mucho menos claro, y aunque se ha descrito que su expresión está aumentada en algunos neuroblastomas, en los que contribuye a la supervivencia celular (Qing, Li et al. 2012), en otros tejidos GL2 se comporta como un supresor de tumores diana de p53 (Suzuki, Tanaka et al. 2010).

En cualquier caso, las células de cáncer consumen una cantidad de glutamina mucho mayor que las células sanas y, como ocurre con los transportadores de glucosa, las células tumorales inducen una activación de los transportadores de glutamina, lo que se ve reflejado en el descenso en los niveles de glutamina circulante que puede ser observado en pacientes de cáncer (Chen, Espat et al. 1993).

1.10.3. La síntesis de ácidos grasos.

Como ya hemos visto, la proliferación acelerada y descontrolada propia de las células tumorales no requiere únicamente una mayor producción de energía, sino que también hace indispensable un mayor aporte de los materiales básicos con los que generar nuevas células de manera continua. Estos materiales incluyen a los fosfolípidos, imprescindibles para formar las membranas de células y orgánulos de nueva síntesis.

Cuando la célula necesita sintetizar nuevos lípidos, el citrato mitocondrial es exportado al citosol y convertido, por acción de la enzima ATP-citrato liasa (ACLY), en oxalacetato y acetil-CoA. El oxalacetato puede ser transformado en piruvato por la enzima málica (ME, del inglés *malic enzyme*) generando además NADPH, que resulta necesario en la síntesis de lípidos. Por otro lado, la enzima acetil-CoA carboxilasa (ACC) transforma el aCoA en malonil-CoA, y la enzima ácido graso sintasa (FAS, del inglés *fatty acid synthase*) acopla un grupo acetilo y 7 grupos malonilo para generar ácido palmítico, a partir del cual se generan el resto de ácidos grasos.

Las enzimas que controlan la lipogénesis, y especialmente la FAS, se encuentran sobreexpresadas en cáncer (Menendez and Lupu 2007), y en general los tumores presentan un metabolismo de ácidos grasos sobreactivado con respecto al de las células normales (Biswas, Lunec et al. 2012). Resulta especialmente interesante resaltar que metabolitos derivados del metabolismo de la glucosa como la misma glucosa, la glucosa-6-fosfato o la xilulosa-5-fosfato, activan la expresión de los genes que codifican para enzimas como ACC o FASN a través de la proteína de unión al elemento de respuesta a carbohidratos (ChREBP, del inglés *carbohydrate response element binding protein*), lo que pone

de relieve la estrecha relación existente entre metabolismo de la glucosa y la síntesis de ácidos grasos (Kabashima, Kawaguchi et al. 2003; Mitro, Mak et al. 2007) . Finalmente, vale la pena señalar que la lipogénesis está regulada por distintas vías de señalización que suelen encontrarse alteradas en el cáncer, como aquellas relacionadas con la proteína de unión al elemento de respuesta a esteroles (SREBP, del inglés *sterol regulatory element binding protein*).

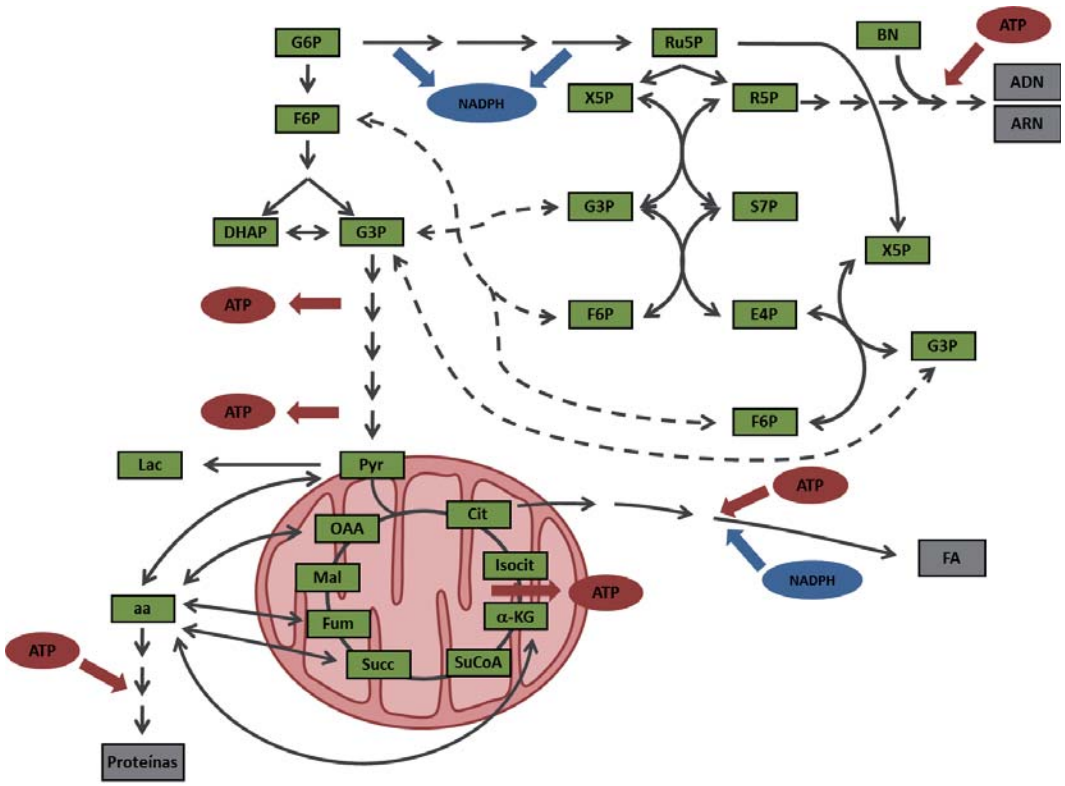

FIGURA 11. Vías del metabolismo central. Representación de las rutas metabólicas del metabolismo central. Las vías señaladas (glucólisis, ruta de las pentosas fosfato, ciclo de Krebs, síntesis de ácidos grasos y síntesis/degradación de aminoácidos) se encuentran con frecuencia alteradas en células tumorales debido a cambios en la expresión de las enzimas que las regulan, a la regulación post-transcripcional de su actividad o a mecanismos de splicing alternativo que generan distintas isoformas de las mismas. Hay metabolitos, relacionados con flechas discontinuas, que forman parte de rutas metabólicas diferentes. G6P: glucosa-6-fosfato, F6P: fructusa-6-fosfato, DHAP: dihidroxiacetona-fosfato, G3P: gliceraldehído-3-fosfato, Ru5P: ribulosa-5-fosfato, X5P: xilulosa-5-fosfato, R5P: ribosa-5-fosfato, S7P: sedoheptulosa-7-fosfato, E4P: eritrosa-4-fosfato, Pyr: piruvato, Lac: Lactato, Cit: citrato, Isocit: isocitrato, α-KG: α-cetoglutarato, SuCoA: succinil-coenzima A, Succ: succinato, Fum: fumarato, Mal: malato, OAA: oxalacetato, BN: bases nitrogenadas, aa: aminoácidos, FA: ácidos grasos, ATP: adenosintrifosfato, NADPH: nicotin-adenin-dinucleótido-fosfato reducido, ARN: ácido ribonucleico, ADN: ácido desoxidibonucleico.

1.10.4. La ruta de las pentosas fosfato.

La formación, a partir de una célula precursora, de dos células hijas que contengan la misma dotación genética que aquella, implica necesariamente la duplicación del ADN celular. Por ello, la ruta biosintética que desemboque en la formación de nucleótidos, los monómeros del material genético, tiene necesariamente una importancia capital para mantener el crecimiento tumoral.

La ribosa-5-fosfato (R5P), sustrato inicial para la síntesis de ADN y ARN, se sintetiza a través de la ruta de las pentosas fosfato (PPP, del inglés *pentose phosphate pathway*). Esta ruta mantiene también una estrecha relación con la síntesis de ácidos grasos, ya que no solo genera xilulosa-5-fosfato (X5P), capaz también de regular la expresión de enzimas lipogénicos a través de ChBREP, sino que además constituye uno de los mecanismos de generación de NADPH, que resulta imprescindible para la lipogénesis.

La ruta de las pentosas fosfato ha sido clásicamente dividida en dos ramas diferentes: la rama oxidativa y la rama no oxidativa. La rama oxidativa, irreversible, transforma la glucosa-6-fosfato (G6P) en ribulosa-5-fosfato (Ru5P) a través de tres reacciones consecutivas que generan dos equivalentes de NADPH. La Ru5P se puede convertir por isomerización en xilulosa-5-fosfato y en ribosa-5-fosfato, que será la unidad usada para la síntesis de ADN y ARN. La enzima G6PDH, que cataliza el primer paso de esta vía oxidativa, es considerada la controladora del flujo metabólico a través de la misma (Boren, Montoya et al. 2002).

La rama no oxidativa de la ruta de las pentosas fosfato es, a diferencia de la oxidativa, reversible. A través de ella, por tanto, es posible no solo generar R5P desde la vía de la glucólisis, sino también reciclar el exceso de pentosas producido en la vía oxidativa hacia esta. En la rama no oxidativa de la PPP, la ribosa-5-fosfato y la xilulosa-5-fosfato generadas en la vía oxidativa se intercambian dos unidades de carbono gracias a la acción de la enzima transcetolasa (TKT), lo que genera Gliceraldehído-3-fosfato (G3P) y sedoheptulosa-7-fosfato (S7P). Estas dos moléculas generan, a su vez, fructosa-6-fosfato (F6P) y eritrosa-4-fosfato (E4P) en una reacción catalizada por la enzima transaldolasa (TA). Finalmente, de nuevo la TKT es capaz de catalizar la transferencia de un fragmento de dos carbonos entre una segunda unidad de xilulosa-5-fosfato y la eritrosa-4-fosfato, generando fructosa-6-fosfato (F6P) y gliceraldehído-3-fosfato (G3P), que serán metabolizados siguiendo la vía glucolítica o bien reintroducidos en la vía de las pentosas fosfato, ya sea a través de su rama oxidativa o a través de la rama no oxidativa en el orden inverso al que acabamos de describir (ver **figura 12**).

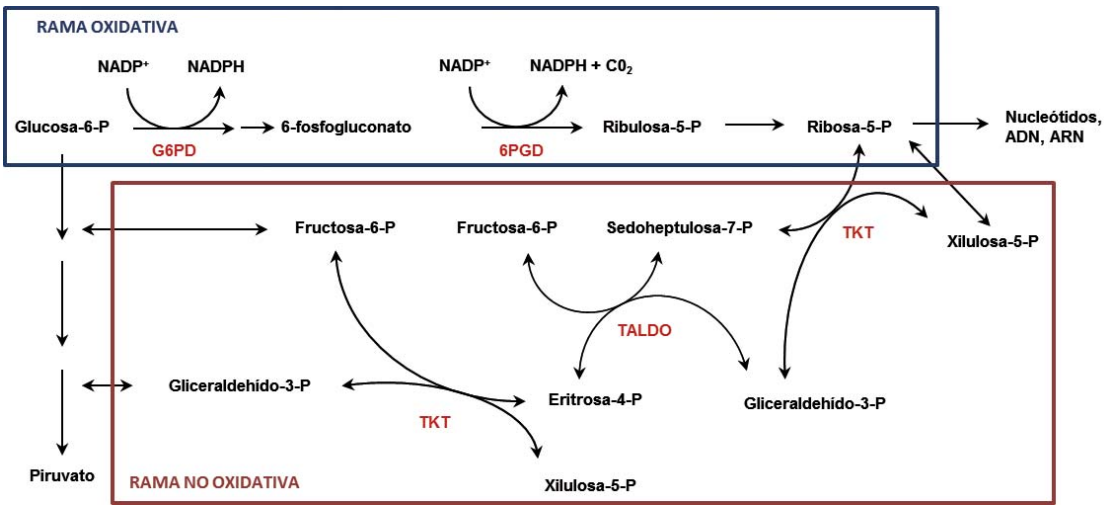

Fig 12. Vía de las Pentosas Fosfato. Representación de las ramas oxidativa y no oxidativa de la vía de las pentosas fosfato. En la rama oxidativa, irreversible, se produce NADPH necesario para la síntesis de ácidos grasos. En la rama oxidativa, reversible, recicla el exceso de pentosas o sintetiza ribosa a partir de intermediarios de la glucólisis. Se indican los enzimas más relevantes en ambos procesos (G6PD: glucosa-6-fosfato deshidrogenasa, 6PGD: 6-fosfogluconato deshidrogenasa, TKT: transcetolasa, TALDO: transaldolasa).

La vía de las pentosas fosfato está regulada por algunos de los más importantes proto-oncogenes y genes supresores de tumores. Se ha descrito que los cánceres con mutaciones en KRAS presentan un incremento simultáneo de los niveles de G6PD, PK y LDH (de Atauri, Benito et al. 2011), lo que hace que tanto la glucólisis como la vía de las pentosas fosfato se encuentren aumentadas. También se ha descrito que KRAS dirige a los intermediarios de la glicólisis a través de la vía no oxidativa de las pentosas fosfato en células de adenocarcinoma (Ying, Kimmelman et al. 2012), y que las células tumorales pueden más prioridad que las no tumorales a la vía no oxidativa de las pentosas fosfato para sintetizar nucleótidos, siendo TKT la enzima clave en este proceso (Cascante, Centelles et al. 2000). Además, la inhibición simultanea de TKT y G6PD ralentiza el crecimiento tumoral en vivo (Mitsuishi, Taguchi et al. 2012), y la proteína TAp73 promueve la proliferación celular a través de G6PD (Jiang, Du et al. 2013).

Todo ello indica de manera fehaciente la existencia de una relación entre la reprogramación metabólica de la vía y el desarrollo tumoral, relación se ve refrendada por el hecho de que el gen supresor de tumores p53 también juegue un papel clave en la regulación de la PPP, siendo capaz de unirse a G6PDH impidiendo la formación

del dímero activo y por tanto inhibiendo su actividad (Jiang, Du et al. 2011; Jiang, Du et al. 2013). Las evidencias sobre el efecto supresor de la apoptosis que implica el aumento de la actividad de G6PD (Riganti, Gazzano et al. 2012) también contribuyen a establecer esta relación entre la vía de las pentosas fosfato y el proceso tumoral.

1.11. LA METABOLÓMICA Y LA FLUJÓMICA

La reprogramación metabólica, una característica que comparten gran cantidad de tumores de distintos tejidos y que es considerada por Hanahan y Weinberg una de las características básicas del cáncer (Hanahan and Weinberg 2011), es imprescindible para que las células tumorales puedan mantener el ritmo de proliferación acelerado que define a la enfermedad. Por ello, el estudio del metabolismo tumoral puede ser una herramienta fundamental para encontrar nuevas dianas terapéuticas que explotar en nuevos tratamientos combinados. Detectando, a través del estudio del metaboloma, cuáles son las vías alteradas en el metabolismo tumoral, y definiendo cuáles son las enzimas clave que controlan esas vías, podremos actuar sobre ellas para impedir la adaptación metabólica en cáncer, ralentizando así la proliferación celular.

Por todo ello, en el pasado reciente la comunidad científica ha abordado el estudio del metabolismo con un renovado interés, en un esfuerzo multidisciplinar para descubrir biomarcadores y desarrollar nuevas terapias para el tratamiento del cáncer. Aun así, la metabolómica es una disciplina que conlleva ciertos desafíos metodológicos que deben ser considerados. Uno de estos desafíos lo constituye el hecho de que, a diferencia de lo que ocurre con el genoma, el transcriptoma o el proteoma, las moléculas que integran el metaboloma presentan una inmensa heterogeneicidad tanto química como estructural. Además, los metabolitos de una muestra biológica se encuentran en un rango de concentraciones amplísimo (algunos metabolitos pueden estar a concentración picomolar, mientras que otros se pueden encuontrar en concentraciones molares). Por último, el entramado metabólico cuenta con infinidad de interconexiones entre especies, y en él se producen transformaciones continuas a gran velocidad y de manera muy difícil de controlar. Así, el estudio de muchos metabolitos se convierte por lo general en una tarea extremadamente compleja, ya sea por su heterogeneicidad general, por su baja concentración o estabilidad o por la dificultad de separar mediante métodos analíticos a aquellos metabolitos que resultan química y estructuralmente muy similares entre sí.

Todas estas dificultades, en resumen, impiden analizar todos los metabolitos presentes en una muestra biológica mediante un único procedimiento. A la hora de llevar a cabo un análisis metabolómico, por tanto, será necesario defi-

nir primero el conjunto concreto de metabolitos que serán objeto del mismo (lípidos, azúcares, intermediarios del ciclo de Krebs…), que son los que determinarán el método analítico a utilizar.

También es necesario considerar que el metabolismo, en su sentido más amplio, es consecuencia de la transformación y el transporte de metabolitos a través de múltiples procesos finamente regulados a distintos niveles y que cuentan con infinidad de interconexiones entre ellos. Para obtener una visión de la dinámica de los procesos metabólicos, que nos permita deducir no sólo la presencia de un metabolito sino la vía metabólica por la que este se ha formado o se está consumiendo, en los últimos años ha surgido una nueva disciplina científica encargada de analizar la distribución de los flujos metabólicos y los cambios que en ellos se producen bajo diferentes estímulos. Esta disciplina, llamada flujómica (Cascante and Marin 2008; Winter and Kromer 2013), es la encargada de estudiar el conjunto de flujos que conforman la red metabólica del sistema en estudio (el flujoma). La flujómica no pretende sustituir a la metabolómica, sino que se complementa con ella permitiendo el estudio del metabolismo desde una perspectiva más dinámica, ofreciendo información que las técnicas clásicas de análisis no permiten obtener.

1.11.1. La flujómica basada en trazadores

El uso de precursores metabólicos marcados con isótopos estables supone una herramienta muy efectiva para estudiar las características de los flujos metabólicos de un sistema biológico. En la mayor parte de los casos se utilizan sustratos metabólicos marcados con isótopos de carbono ^{13}C, también llamados sustratos trazadores, con los que se incuban las células durante un periodo determinado. Con el tiempo, estos sustratos trazadores son consumidos por las células, que los transforman convirtiéndolos, a través de los distintos flujos metabólicos, en otros metabolitos diferentes que incorporarán la marca (los isótopos de ^{13}C) que inicialmente estaba presente en el sustrato trazador original.

Dependiendo de la ruta metabólica seguida por el trazador, los átomos de ^{13}C se ven incorporados a los metabolitos de nueva formación de una manera determinada (tanto en número como en posición), con lo que los metabolitos sintetizados a partir del trazador contarán con una distribución isotopomérica particular que dependerá de la vía metabólica que ha conducido a su formación. En el contexto de esta disciplina, un isotopómero de masa designa a isómeros con un número particular de átomos de ^{13}C, mientras que un isotopómero de posición designa a isómeros con los átomos de ^{13}C en una posición particular (Paul Lee, Wahjudi et al. 2010).

Así, los isotopómeros de masa indican las vías metabólicas por las que, desde el trazador inicial, se han incorporado al metabolito formado cero, uno, dos, etc. átomos de ^{13}C (lo que se indica con m_0, m_1, m_2, etc.). Para un metabolito con un número de carbonos igual a n, el número teórico de isotopómeros de masa que se pueden formar es n+1, mientras que el número de isotopómeros de posición diferentes teóricamente obtenibles es de 2n. El lactato, por ejemplo, que cuenta con 3 átomos de carbono, podría dar lugar potencialmente a 4 isotopómeros de masa (3+1) y 8 isotopómeros posicionales (2^3). Por ello, el isotopómero de masa lactato m_2 (que cuenta con dos átomos de ^{13}C) puede referirse en realidad a tres posibles isotopómeros de posición distintos: $^{13}C_1$-$^{13}C_2$-$^{12}C_3$ (átomos de ^{13}C en las posiciones 1 y 2), $^{13}C_1$-$^{12}C_2$-$^{13}C_3$ (átomos de ^{13}C en las posiciones 1 y 3) y $^{12}C_1$-$^{13}C_2$-$^{13}C_3$ (átomos de ^{13}C en las posiciones 2 y 3).

Debido al gran número teórico de isotopómeros (tanto de masa como de posición) que se pueden obtener tras una incubación con sustratos trazadores, la elección de los mismos resulta de crucial importancia a la hora de diseñar un experimento de este tipo. Existe una amplia variedad de sustratos marcados con ^{13}C, cada uno de los cuales está indicado para el estudio de flujos metabólicos particulares. Tradicionalmente, los sustratos trazadores con ^{13}C han sido empleados en el estudio del metabolismo de microorganismos, que normalmente son incubados en un medio que contiene una única fuente de carbono (Al Zaid Siddiquee, Arauzo-Bravo et al. 2004). La elección del sustrato trazador en células de mamíferos es más complicada, ya que estas son cultivadas en medios que contienen múltiples fuentes de carbono, además de aminoácidos u otros compuestos como nucleótidos o lípidos. En cualquier caso, y aunque se han llegado a utilizar sustratos como acetato, lactato y propionato (Burgess, He et al. 2007; Rodriguez-Prados, Traves et al. 2010; Collins, Neville et al. 2011; Gaglio, Metallo et al. 2011), los sustratos marcados con ^{13}C más utilizados son sin duda la ^{13}C -glucosa y la ^{13}C -glutamina.

De entre los trazadores de glucosa marcada con ^{13}C, uno de los más utilizados, por resultar especialmente informativo acerca de los flujos metabólicos del metabolismo central, es la glucosa marcada con ^{13}C en los carbonos 1 y 2, o [1,2-^{13}C]-glucosa. Este trazador permite estudiar de manera fiable flujos metabólicos como los de la glucólisis, la vía de las pentosas fosfato, o la síntesis de lípidos (Boren, Lee et al. 2003; Marin, Chiang et al. 2003; Vizan, Alcarraz-Vizan et al. 2009), aunque no resulta tan útil para el estudio del flujo en el ciclo de Krebs, ya que la célula excreta la mayoría de átomos de ^{13}C en forma de lactato. Así, para evaluar el flujo en el ciclo de Krebs resulta más conveniente utilizar trazadores de glutamina, como por ejemplo la glutamina marcada con ^{13}C en el tercer átomo de carbono, o [3-^{13}C]-glutamina.

Cuando se lleva a cabo un experimento de metabolómica basado en el uso de sustratos con ^{13}C con más de un trazador (por ejemplo, con [1,2-^{13}C]-glucosa y [3-^{13}C]-glutamina), existen dos aproximaciones experimentales distintas. En la primera de ellas, las células se incuban con ambos trazadores a la vez en el mismo experimento. En la segunda, se realizan experimentos independientes en paralelo, cada uno implica la incubación de las células con un único trazador marcado con ^{13}C (para minimizar la variabilidad, la composición del medio de cultivo suele ser idéntica para todos los experimentos realizados en paralelo). Esta segunda opción permite definir los flujos específicos con más precisión y, en general, conlleva un aumento de la información extraíble a partir de este tipo de experimentos, especialmente cuando el número de medidas es limitado (Crown and Antoniewicz 2013).

1.11.2. Análisis de la distribución isotopomérica

La proporción de los distintos isotopómeros de masa en las moléculas producidas a partir del sustrato marcado inicial, en combinación con medidas extracelulares de consumos y producciones de determinados metabolitos, puede ser usada para determinar de una manera sencilla el estado de determinados flujos metabólicos, o la importancia relativa que flujos distintos han tenido en la síntesis de un determinado metabolito. Esta aproximación, llamada análisis de la distribución de isotopómeros de masa (MIDA, del inglés *mass isotopomer distribution analysis*), utiliza fórmulas sencillas basadas en el conocimiento previo de las reacciones que conforman el entramado metabólico.

Así, por ejemplo, la [1,2-^{13}C]-glucosa se puede transformar en ribosa a través de la vía oxidativa de las pentosas fosfato o a través de la vía no oxidativa de las pentosas fosfato (ver **figura 13**). En el primer caso, se acabará generando ribosa m_1, concretamente [2-^{13}C-ribosa]. En cambio, cuando la glucosa es metabolizada a través de la vía no oxidativa de las pentosas fosfato, la ribosa que se acaba generando es ribosa m_2 (en concreto, [1,2-^{13}C]-ribosa). Así, estudiando la proporción de cada isotopómero de masa de la ribosa generado a partir de [1,2-^{13}C]-glucosa, podremos deducir cuál de las dos ramas de la vía de las pentosas fosfato está priorizando la célula en el momento del análisis. De manera similar, el ratio de los flujos de glucosa a lactato, que pueden discurrir a través de la vía de las pentosas fosfato o a través de la glucólisis directa, puede ser determinado a partir de la distribución isotopomérica del lactato y de la medida del lactato producido. Por otro lado, la contribución de las enzimas piruvato carboxilasa y piruvato deshidrogenasa (PC y PDH) al Ciclo de Krebs se puede estimar estudiando la distribución de ^{13}C en el glutamato producido a partir de la glucosa (Marin, Chiang et al. 2003).

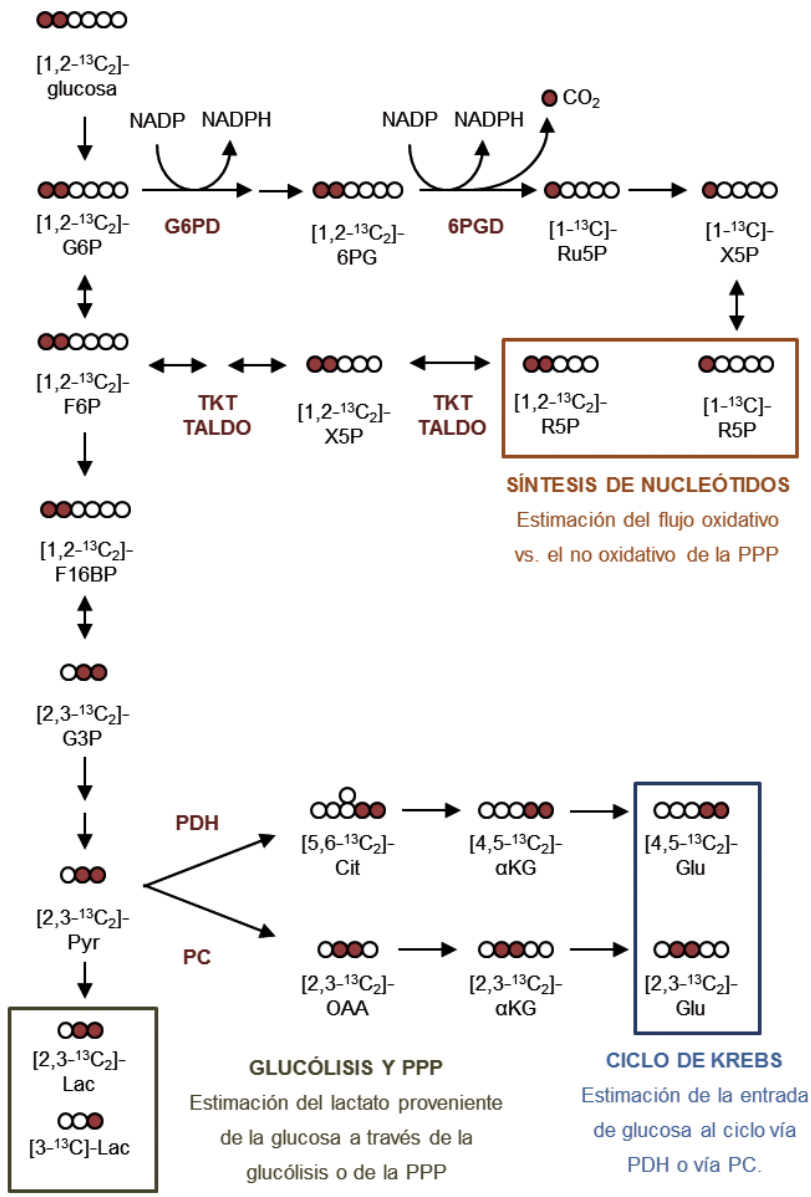

FIGURA 13. Metabolómica basada en el uso de sustratos marcados con ^{13}C. El uso de [1,2-^{13}C]-glucosa permite estimar el estado de actividad relativo de mútiples vías metabólicas, como la vía de las pentosas fisfato, el ciclo de Krebs o la glucólisis. La contribución de las ramas oxidativa y no oxidativa de la PPP a la producción de R5P se puede estimar determinando la proporción de isotopómeros de masa de ribosa que contienen uno o dos átomos de 13C. De manera similar, la distribución isotopomérica del lactato otorga información acerca de la vía metabólica que ha seguido la glucosa (glucólisis o PPP), mientras que la distribución isotopomérica de glutamato indica si la glucosa metabolizada a través del ciclo de Krebs ha entrado al mismo a través de la piruvato deshidrogenasa (PDH) o bien a través de la piruvato carboxilasa (PC).

1.12. EXPLOTACIÓN DE LAS ALTERACIONES METABÓLICAS DEL CÁNCER DE PULMÓN EN EL DIAGNÓSTICO MEDIANTE EL ANÁLISIS DEL AIRE EXHALADO

El descubrimiento de nuevas dianas terapéuticas no es la única aplicación práctica que extraer del estudio de la reprogramación metabólica tumoral. La existencia de un estado metabólico alterado implica cambios en los niveles de distintos metabolitos, que por sí mismos pueden resultar indicativos de la presencia del proceso canceroso. Por ello, el estudio del metaboloma se revela como una herramienta de enorme interés a la hora de definir marcadores biológicos que puedan contribuir a desarrollar mejores métodos en la detección del cáncer, cuyo diagnóstico temprano tiene una importancia vital en la supervivencia de los pacientes.

Esta posibilidad resulta de especial interés en el caso del cáncer de pulmón, ya que uno de los motivos principales de la gran mortalidad asociada a la enfermedad reside en la dificultad de realizar un diagnóstico temprano de la misma. La aparición de síntomas, casi siempre previa al diagnóstico, se produce cuando el tumor ya está extendido, momento en el que los tratamientos disponibles ya no resultan efectivos o viables. Por ello, resultaría de gran utilidad el desarrollo de un método diagnóstico que pudiera detectar la enfermedad en individuos aún asintomáticos. La aplicación de un método diagnóstico de este tipo se llevaría a cabo sobre sujetos que, aunque formaran parte de una población de riesgo, no habrían desarrollado ningún síntoma de la enfermedad, por lo que la no invasividad del método resultaría prácticamente esencial para la viabilidad de su aplicación.

Actualmente se sabe que en los mecanismos fisiopatológicos del cáncer de pulmón, la aparición de sustancias reactivas de oxígeno (ROS) juegan un papel principal (Faux, Tai et al. 2009; Valavanidis, Vlachogianni et al. 2013). El humo de tabaco, considerado el principal factor de riesgo para el desarrollo de la enfermedad, provoca que las células tumorales sufran elevados niveles de estrés oxidativo, lo que a su vez provoca daños en el ADN (Chan, Lewis et al. 2010). El daño en el ADN puede acabar generando mutaciones en proto-oncogenes y en genes supresores de tumores, lo que afecta a la proliferación y la supervivencia celulares iniciando así un proceso tumoral. Una vez generado, el tumor es capaz a su vez de inducir un estado inflamatorio en su entorno, que contribuye a aumentar aún más el estrés oxidativo tumoral. Por ello, la detección del estrés oxidativo es una aproximación que puede resultar útil para la detección temprana del cáncer de pulmón en individuos asintomáticos.

Una de las consecuencias de la presencia de elevados niveles de estrés oxidativo en las células es la generación de un tipo particular de metabolitos llamados

compuestos orgánicos volátiles (VOCs, del inglés *volatile organic compounds*), que se producen mediante reacciones que involucran a distintas ROS. Los VOCs, por su condición de compuestos volátiles, pueden pasar de la sangre al aire exhalado en el intercambio gaseoso que tiene lugar en los alveolos. El hecho de que perros entrenados sean capaces de detectar la presencia de cáncer de pulmón en humanos oliendo la respiración de los pacientes (Lippi and Cervellin 2012; Bijland, Bomers et al. 2013) sugiere que el patrón de VOCs del aire exhalado es distinto en sujetos sanos y enfermos, por lo que el análisis de los metabolitos volátiles presentes en el aire exhalado, que en su conjunto han recibido el nombre de volatoma (Phillips, Cataneo et al. 2013; Das, Bishwal et al. 2014), se perfila como un método prometedor para la detección de biomarcadores asociados con el cáncer de pulmón, con la ventaja añadida de que su desarrollo supondría la creación de un método completamente no invasivo que podría ser usado con gran comodidad en poblaciones de sujetos asintomáticos.

Aunque en la última década el potencial del análisis del aire exhalado como método diagnóstico ha generado un creciente interés (Phillips, Gleeson et al. 1999; Machado, Laskowski et al. 2005; Mazzone, Hammel et al. 2007; Bajtarevic, Ager et al. 2009; Peng, Hakim et al. 2010), hoy en día aún no existe ningún sistema que esté siendo utilizado en la práctica clínica para diagnosticar, a partir de este tipo de muestras, enfermedades como el cáncer. Hay que tener en cuenta que diferentes factores, entre los que se encuentran la edad, la dieta, el género o el ambiente (Phillips, Cataneo et al. 2000; Gordon, Wallace et al. 2002; Calusic, Varnai et al. 2011; Das, Bishwal et al. 2014; Tarnoki, Bikov et al. 2014), tienen el potencial de introducir una gran variabilidad en los patrones de VOCs de las muestras de respiración, complicando severamente el análisis de resultados. En cualquier caso, probablemente la limitación más importante para la existencia de un sistema de este tipo la constituye la falta de un estándar consensuado sobre el método de toma de muestra. En la literatura existen múltiples aproximaciones distintas que otorgan resultados dispares, lo que dificulta la obtención de análisis reproducibles en grupos de investigación diferentes.

Por ello, resulta de especial interés la definición de un sistema de toma de muestra estandarizado, que permita recoger muestras de respiración de manera reproducible y que mitigue, en la medida de lo posible, los factores que introducen mayor variabilidad en los resultados. La aplicación de un sistema de este tipo en el diagnóstico del cáncer de pulmón, especialmente si es capaz de distinguir entre éste y otras enfermedades con afectaciones similares (como la enfermedad pulmonar obstructiva crónica), podría resultar de gran ayuda en el diagnóstico temprano de la enfermedad, lo que resulta clave para el éxito de su tratamiento.

1.13. MÉTODOS DE ANÁLISIS METABOLÓMICO

La espectrometría de masas (MS, del inglés *mass spectrometry*) es una técnica que nos permite identificar analitos por su peso molecular mediante la ionización de los mismos. Al someter a los analitos ionizados a un campo magnético, estos adquieren una determinada velocidad que depende de su relación masa-carga (m/z). Además de su sensibilidad, la principal ventaja de la espectrometría es que permite un análisis rápido con un procesamiento de muestra mínimo. Los espectros obtenidos son, además, fácilmente comparables con espectros almacenados en bases de datos, lo que resulta de gran ayuda para el desarrollo y aplicación de métodos que permitan su identificación automática.

Aunque se puede analizar una muestra por espectrometría de masas introduciendo un extracto de la misma directamente en el espectrómetro (procedimiento conocido como infusión directa), lo habitual es utilizar esta técnica acoplada a otra técnica separativa previa, normalmente una cromatografía de líquidos o de gases (LC/MS o GC/MS, respectivamente). Una técnica cromatográfica previa acoplada a la espectrometría de masas permite reducir diferentes efectos que distorsionan el espectro de masas, con lo que se mejora la sensibilidad del instrumento. Además, el tiempo de retención en la columna cromatográfica es un parámetro nuevo que depende de cada analito, y que por tanto puede ser utilizado para identificar los componentes de la muestra de manera más precisa. En el caso de isómeros (moléculas de idéntico peso molecular pero distinta estructura), esto resulta de especial utilidad ya que pueden tener distintos tiempos de retención y por tanto ser procesados por el MS de manera independiente.

Por sus características, la cromatografía de gases (GC) resulta especialmente útil para realizar análisis metabólicos en experimentos de trazadores marcados con ^{13}C. La GC permite la separación de analitos volátiles en función de su interacción con la fase estacionaria líquida que se encuentra en el interior de una columna capilar, y tiene la resolución suficiente como para identificar isotopómeros de masa, lo que la hace ideal para diferenciar los analitos marcados con ^{13}C cuyo peso molecular aumenta en 1 unidad de masa atómica por cada átomo de ^{13}C que sustituya a un átomo de ^{12}C. Sin embargo, al ser una técnica para el análisis de analitos volátiles, su aplicación para el análisis de moléculas no volátiles hace necesario un proceso de derivatización previo que permita la formación, a partir de las moléculas de interés, de derivados volátiles que serán los finalmente analizados.

A pesar de su precio y del hecho de que requieren de personal cualificado tanto para su operación como para la interpretación de los resultados, los sistemas de GC/MS también resultan ideales para el análisis de los metabolitos volá-

tiles de muestras de respiración. La baja concentración de la mayoría de estos compuestos en el aire exhalado hace necesarias la precisión y sensibilidad que presentan estos sistemas. Además, la información que otorga un análisis de GC/MS (tiempo de retención en la columna cromatográfica y relación m/z de cada compuesto) resulta de gran utilidad para la identificación de cada componente de la muestra. Por último, las medidas de intensidad del espectro de masas generado aportan información cuantitativa que resulta crucial para la comparación de los patrones de compuestos orgánicos volátiles entre diferentes muestras.

02.
OBJETIVOS

El objetivo general de esta Tesis Doctoral es el de explorar nuevas posibilidades de tratamiento y de diagnóstico del cáncer de pulmón, y concretamente del cáncer de pulmón no microcítico de células con mutaciones activadoras de KRAS. Para conseguirlo, las finalidades de esta Tesis incluyen la determinación de la actividad biológica de nuevos compuestos organometálicos con actividad antitumoral, la caracterización de la reprogramación tumoral en líneas de cáncer de pulmón en la búsqueda de nuevas dianas terapéuticas de tipo metabólico y el desarrollo de un método diagnóstico no invasivo con la potencialidad de detectar el cáncer de pulmón en muestras de aire exhalado. Concretamente, se ha fraccionado la Tesis en cuatro objetivos diferentes, que corresponden a los cuatro capítulos que forman la presente memoria:

01. Determinación de la actividad biológica de nuevos complejos metálicos sobre la viabilidad de células tumorales de pulmón.

   a) Caracterización de la actividad antiproliferativa de nuevos compuestos cicloplatinados de siete miembros.
   b) Caracterización de la actividad antiproliferativa de nuevos compuestos de platino con iminas polifuncionalizadas.
   c) Caracterización de la actividad antiproliferativa de nuevos compuestos de platino y paladio derivados del pirazol.
   d) Caracterización de la actividad antiproliferativa de nuevos complejos ferroceno-indol.
   e) Caracterización de la actividad antiproliferativa de nuevos compuestos de platino(II) derivados del ferroceno.

02. Determinación del mecanismo de acción del compuesto de platino(II) derivado del ferroceno **6a** sobre líneas celulares de cáncer de pulmón, y estudio de su potencial como agente antitumoral.

03. Caracterización de las adaptaciones metabólicas asociadas a células de cáncer de pulmón mutadas en KRAS, y explotación de las mismas en el desarrollo de nuevas terapias combinadas.

04. Desarrollo de un nuevo sistema de análisis de aire exhalado con potencial para diagnosticar el cáncer de pulmón y la enfermedad pulmonar obstructiva crónica, que en muchos casos acaba derivando en cáncer de pulmón.

La consecución de estos objetivos permitirá abrir nuevos caminos en la lucha contra la elevada mortalidad del cáncer de pulmón, tanto desde el punto de vista terapéutico como desde el punto de vista diagnóstico.

03.
INFORME DEL DIRECTOR

El trabajo desarrollado por Roldán Cortés Giráldez en el transcurso de su Tesis Doctoral ha dado lugar a 6 artículos publicados y dos más en proceso de publicación en revistas científicas internacionales. El doctorando es el primer autor de 4 de los ocho artículos que componen la presente tesis. Ninguno de los resultados que componen esta Tesis Doctoral ha sido utilizado en la elaboración de otra Tesis anterior.

A continuación se listan todos los artículos incluidos, indicando el factor de impacto de las revistas en las que han sido publicados/enviados a publicar y especificando la participación del doctorando en cada uno de ellos:

---

01. **Roldán Cortés**, Margarita Crespo, Laia Davin, Raquel Martín, Josefina Quirante, Daniel Ruiz, Ramon Messeguer, Carme Calvis, Laura Baldomà, Josefa Badia, Mercè Font-Bardía, Teresa Calvet, Marta Cascante. *Seven-membered cycloplatinated complexes as a new family of anticancer agents. X-ray characterization and preliminary biological studies*. **Publicado** en: European Journal of Medicinal Chemistry (factor de impacto: 3.499).

    Roldán Cortés se encargó de la realización de todos los experimentos sobre la línea tumoral de pulmón A549, así como del análisis de los datos y la interpretación de los resultados obtenidos. También participó en la escritura del artículo.

---

02. Joan Albert, Ramon Bosque, Margarita Crespo, Jaume Granell, Concepción López, **Roldán Cortés**, Asensio Gonzalez, Josefina Quirante, Carme Calvis, Ramon Messeguer, Laura Baldomà, Josefa Badia, Marta Cascante. *Pt(II) complexes with (N,N') or (C,N,E)$^{-}$ (E = N,S) ligands: Cytotoxic studies, effect on DNA tertiary structure and structure–activity relationships*. **Publicado** en Bioorganic & Medicinal Chemistry (factor de impacto: 2.903).

    Roldán Cortés se encargó de la realización de todos los experimentos sobre la línea tumoral de pulmón A549, así como del análisis de los datos y la interpretación de los resultados obtenidos en los mismos. También participó en la escritura del artículo.

03. Josefina Quirante, Daniel Ruiz, Asensio Gonzalez, Concepción López, Marta Cascante, Roldán Cortés, Ramon Messeguer, Carme Calvis, Laura Baldomà, Aurélie Pascual, Yann Guérardel, Bruno Pradines, Mercè Font-Bardía, Teresa Calvet, Christophe Biot. *Platinum(II) and palladium(II) complexes with (N,N') and (C,N,N')$^-$ ligands derived from pyrazole as anticancer and antimalarial agents: Synthesis, characterization and in vitro activities*. **Publicado** en Journal of Inorganic Biochemistry (factor de impacto: 3.197).

Roldán Cortés se encargó de la realización de todos los experimentos sobre la línea tumoral de pulmón A549, así como del análisis de los datos y la interpretación de los resultados obtenidos en los mismos. También participó en la escritura del artículo.

---

04. Josefina Quirante, Faustine Dubar, Asensio González, Concepción Lopez, Marta Cascante, **Roldán Cortés**, Isabelle Forfar, Bruno Pradines, Christophe Biot. *Ferrocene-eindole hybrids for cancer and malaria therapy*. **Publicado** en Journal of Organometallic Chemistry (factor de impacto: 2.000).

Roldán Cortés se encargó de la realización de todos los experimentos sobre la línea tumoral de pulmón A549, así como del análisis de los datos y la interpretación de los resultados obtenidos en los mismos. También participó en la escritura del artículo.

---

05. Daniel Talancón, Concepción López, Mercè Font-Bardía, Teresa Calvet, Josefina Quirante, Carme Calvis, Ramon Messeguer, **Roldán Cortés**, Marta Cascante, Laura Baldomà, Josefa Badia. *Diastereomerically pure platinum(II) complexes as antitumoral agents. The influence of the mode of binding {(N), (N,O)$^-$ or (C,N)}$^-$ of (1S,2R)-[(η^5-C^5H^5)Fe{(η^5-C_5H_4)-CH=N-CH(Me)-CH(OH)-C_6H_5}] and the arrangement of the auxiliary ligands*. **Publicado** en Journal of Inorganic Biochemistry (factor de impacto: 3.197).

Roldán Cortés se encargó de la realización de todos los experimentos sobre la línea tumoral de pulmón A549, así como del análisis de los datos y la interpretación de los resultados obtenidos en los mismos. También participó en la escritura del artículo.

06. Roldán Cortés, Míriam Tarrado-Castellarnau, Daniel Talancón, Concepción López, Wolfgang Link, Daniel Ruiz, Josep Joan Centelles, Josefina Quirante, Marta Cascante. *A novel cyclometallated Pt(II)–ferrocene complex induces nuclear FOXO3a localization and apoptosis and synergizes with cisplatin to inhibit lung cancer cell proliferation*. **Publicado** en Metallomics (factor de impacto: 4.099).

Roldán Cortés se encargó de la realización de todos los experimentos del artículo, así como del análisis de los datos y la interpretación de los resultados obtenidos. También fue el responsable de la escritura del artículo.

---

07. Roldán Cortés, Enric Milà, Vitaly Selivanov, Silvia Marín, Marta Cascante. *Study of lung cancer cells metabolic reprogramming reveals a glutamine dependancy that can be exploited to impair proliferation*. **Enviado** para su publicación en Respiratory Research (factor de impacto: 3.642).

Roldán Cortés se encargó de la realización de todos los experimentos del artículo, además de participar en el análisis de los datos y la interpretación de los resultados obtenidos. También fue el responsable de la escritura del artículo.

---

08. Roldán Cortés, Ana Guaman, Idoya Agudo, Daniel Calvo, Antonio Pardo, Santiago Marco, Yolanda Torralba, Josep Roca, Joan Albert Barberà, Marta Cascante. *Breath analysis by gas chromatpgraphy-mass spectrometry for detection of lung cancer and COPD*. **Enviado** para su publicación en Metabolomics (factor de impacto: 4.433).

Roldán Cortés participó en la puesta a punto del sistema de muestreo y fue el responsable del análisis de todas las muestras generadas y del procesamiento de los espectros generados a partir de las mismas. También participó en el análisis de los datos y la interpretación de los resultados obtenidos, y fue el responsable de la escritura del artículo.

Marta Cascante Serratosa, Directora

04.
RESUMEN DE RESULTADOS, DISCUSIÓN GLOBAL Y CONCLUSIONES

Esta Tesis Doctoral supone una exploración de nuevas alternativas en la lucha contra el cáncer de pulmón con un enfoque multidisciplinar, que engloba desde la evaluación de nuevos compuestos con potencial quimioterapéutico hasta el desarrollo de nuevos métodos diagnósticos no invasivos que permitan detectar la enfermedad de manera temprana, pasando por la definición de nuevas dianas terapéuticas a partir del estudio de la reprogramación metabólica del cáncer de pulmón.

Los complejos metálicos, especialmente los de platino, han sido durante muchos años la punta de lanza del tratamiento farmacológico del cáncer de pulmón de células no pequeñas, que engloba el 87% de casos de cáncer de pulmón. La elevada toxicidad de algunos de estos compuestos, que conlleva multitud de efectos secundarios no deseados, así como la existencia de resistencias intrínsecas o adquiridas a los mismos, limitan la utilidad de muchas de las soluciones actuales. La baja respuesta al tratamiento es un problema especialmente grave en el caso de tumores pulmonares con mutaciones activadoras de KRAS, ya que estos tumores tampoco responden a fármacos inhibidores del receptor del factor de crecimiento epidérmico (EGFR) como *Erlotinib*, un inhibidor de tirosina quinasa que impide la fosforilación intracelular del EGFR. Este tipo de inhibidores específicos se suelen utilizar en conjunción con complejos metálicos como el cisplatino, y aunque pueden resultar eficaces en tumores con mutaciones activadoras en EGFR, no mejoran la prognosis de tumores con mutaciones activadoras en KRAS cuya proliferación es independiente de la señalización mediada por EGFR. Por ello, en el **capítulo 1** de esta Tesis se ha hecho un esfuerzo para evaluar la actividad biológica de nuevos metalofármacos sobre la línea de cáncer de pulmón no microcítico A549, una línea de adenocarcinoma (el tipo más común de NSCLC) mutada en KRAS, con el objetivo de definir nuevos compuestos que sean capaces de afectar la viabilidad de tumores pulmonares con KRAS mutado a concentraciones menores que el cisplatino o mediante mecanismos alternativos al de este, lo que podría reducir los efectos secundarios asociados al tratamiento o permitir el diseño de nuevas terapias combinadas. En el **capítulo 2** de esta Tesis se han evaluado más a fondo los mecanismos de acción de uno de los complejos metálicos ensayados (concretamente, el complejo de Pt(II) derivado del ferroceno **6a**) para explorar sus mecanismos de acción, diferentes a los del cisplatino y que, por lo tanto, pueden suponer una manera de esquivar las resistencias que limitan la efectividad de este. En la evaluación de la actividad antitumoral de este compuesto también se ha utilizado la línea NCIH460, una línea de carcinoma pulmonar de células grandes (LCLC, del inglés *large cell lung cancer*), caracterizado por su elevada velocidad de crecimiento, que también cuenta con una mutación activadora en KRAS.

Por otro lado, cada vez cobra más fuerza la idea de que el estudio de la reprogramación metabólica que se produce en un tumor canceroso puede ofrecer

claves para el diseño de terapias destinadas a inhibir la proliferación celular descontrolada. La sensibilidad y resolución de las nuevas plataformas de análisis químico permiten el estudio detallado de las características moleculares de la reprogramación metabólica tumoral para definir cuáles son las moléculas clave que resultan responsables de este reordenamiento del metabolismo. Estas moléculas constituyen nuevas dianas terapéuticas metabólicas sobre las que actuar para impedir la adaptación metabólica tumoral, afectando así a la viabilidad de las células cancerosas. Por ello, en el **capítulo 3** de esta Tesis se ha caracterizado la reprogramación metabólica característica de las líneas celulares de cáncer de pulmón A549 y NCIH460, con la intención de definir dianas metabólicas explotables en terapias combinadas destinadas a inhibir la proliferación tumoral.

El estudio de las alteraciones metabólicas asociadas al cáncer, sin embargo, no sólo sirve para descubrir nuevas dianas terapéuticas, sino también para descubrir biomarcadores metabólicos que puedan resultar de utilidad en el diagnóstico de la enfermedad. Este punto resulta de especial importancia en cáncer de pulmón, ya que la enfermedad no provoca síntomas hasta encontrarse en una fase avanzada en la que el éxito del tratamiento se ve seriamente comprometido. Con la intención de explorar alternativas diagnósticas que permitan sortear este problema, en el **capítulo 4** de esta Tesis se ha desarrollado un método de análisis de los compuestos orgánicos volátiles presentes en muestras de aire exhalado, con fines diagnósticos enfocados a la detección precoz y completamente no invasiva del cáncer de pulmón.

4.1. RESUMEN DE RESULTADOS

A continuación se exponen, de forma resumida, los resultados obtenidos en los diferentes capítulos en los que se subdivide esta Tesis Doctoral, seguidos de una discusión acerca de los mismos y de una enumeración de las principales conclusiones obtenidas.

4.1.1. *(Capítulo 01)* Estudio del efecto de distintos compuestos organometálicos de nueva síntesis sobre la viabilidad de células de cáncer de pulmón.

Capítulo 1a. **Caracterización de la actividad antiproliferativa de compuestos cicloplatinados de siete miembros.**

Se ha estudiado el efecto de una nueva serie de compuestos ciclometalados de Pt(II) de siete miembros que contienen un ligando tridentado [C, N, N'] (ver **figura 1**). En concreto, se ha estudiado la actividad de 6 nuevos compuestos con

esta estructura (compuestos **1a**-**1c** y **2a**-**2c**) sobre la línea tumoral de pulmón A549. Los compuestos también fueron ensayados sobre las líneas HCT116 y MDA-MB231, de colon y mama respectivamente, para estudiar su efecto sobre líneas tumorales de otro tipo de tejidos.

1a R_1 = Cl R_2 = Me
1b R_1 = H R_2 = Me
1c R_1 = F R_2 = Me
2a R_1 = Cl R_2 = H
2b R_1 = H R_2 = H
2c R_1 = F R_2 = H

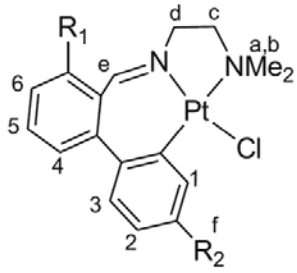

Valores de IC50 (μM)

Compuesto	A549	HCT116	MDA-MB231
1a	2,6 ± 0,1	7,7 ± 0,9	6,3 ± 1,0
1b	3,6 ± 0,1	3,9 ± 0,2	1,3 ± 0,3
1c	2,2 ± 0,5	0,95 ± 0,2	1,1 ± 0,2
2a	5,6 ± 0,1	2,0 ± 0,4	2,0 ± 0,2
2b	4,6 ± 1,4	4,3 ± 0,3	2,2 ± 0,5
2c	4,4 ± 0,1	3,4 ± 0,5	1,1 ± 0,2
Cisplatin	9,3 ± 3,0	40 ± 4,4	6,5 ± 2,4

FIGURA 01. Estructura de los compuestos cicloplatinados de siete miembros sintetizados y tabla con sus valores de IC_{50} sobre las tres líneas tumorales ensayadas.

El estudio del efecto *in vitro* de los compuestos sobre la viabilidad de las líneas tumorales se ha realizado mediante ensayos antiproliferativos consistentes en la incubación de las células durante 72 horas con diferentes concentraciones de los compuestos y la posterior evaluación de la viabilidad celular, mediante una variación (Matito, Mastorakou et al. 2003) del ensayo del MTT (Mosmann 1983). Todos los compuestos ensayados presentan una potente actividad sobre la viabilidad de las células tumorales de pulmón A549. Los valores de IC_{50} indican la concentración necesaria para inhibir la viabilidad de las células en un 50% con respecto a las condiciones control, y en el caso de estos compuestos estos valores se encuentran entre 2.2 y 4.6 micromolar. La IC_{50} del cisplatino obtenida mediante este ensayo fue de 9.3 μM, con lo que los compuestos de nueva síntesis presentan una actividad antiproliferativa mayor que la del cisplatino, que se utiliza clínicamente en el tratamiento del NSCLC.

A concentraciones de 50 y 100 μM, todos los compuestos ensayados provocaron un efecto visible en la movilidad electroforética del ADN, que fue estudiada mediante un ensayo de migración usando un plásmido *pBluescript* de ADN. Esto efecto sugiere que todos los compuestos son capaces de interaccionar con el DNA alterando su estructura terciaria. El cisplatino, aun contando con una IC_{50} más alta que la de los compuestos de nueva síntesis,

fue capaz de afectar la movilidad electroforética del ADN en un grado mayor a estos, incluso a concentraciones más pequeñas.

El compuesto **1c**, que es el que presentó la IC_{50} más baja de todos los compuestos ensayados, se utilizó para realizar ensayos de ciclo celular y apoptosis sobre células A549. El tratamiento de las células con **1c** a su concentración de IC_{50} durante 72 horas provocó un considerable aumento de la proporción de células en las fases S (del 35% al 46%) y G_2/M (del 14% al 20%) del ciclo celular, con la consiguiente disminución de la proporción de células en fase G_0/G_1 (del 50% al 33%). También se estudió el efecto del compuesto 1c sobre la apoptosis de las células A549, y aunque se pudo observar un ligero aumento de la proporción de células en apoptosis temprana tras 72h de tratamiento con el compuesto, el efecto es menos pronunciado que el observado en el ciclo celular.

***Capítulo 1b*. Caracterización de la actividad antiproliferativa de compuestos de platino con iminas polifuncionalizadas.**

Se ha estudiado el efecto sobre la viabilidad celular que ejercen dos grupos de compuestos de Pt(II) en la línea de cáncer de pulmón A549, así como en las líneas de cáncer de colon y mama HCT116 y MDA-MB231 (ver **figura 2**). En concreto, se ha estudiado el efecto de complejos de platino(II) con ligandos bidentados y tridentados, cinco complejos de Pt(II) con ligandos (N,N') bidentados (**4**-**7**) y siete platinaciclos de de cinco miembros con ligandos "pinza" (C,N,E; E = N ó S) (**8**-**11**). A efectos comparativos, se ha estudiado también la actividad antiproliferativa de los ligandos libres.

Los resultados sobre la viabilidad de las líneas estudiadas demuestran que muchos de los compuestos de nueva síntesis tienen valores de IC_{50} en el rango micromolar bajo. En general no resultan más potentes que el cisplatino, cuya actividad fue evaluada por ser el compuesto de referencia en la práctica clínica, aunque la potencia de la actividad biológica de los compuestos es variable. En la línea de pulmón A549, el compuesto **4**, un complejo quelado de 5 miembros, muestra una capacidad antiproliferativa mayor que el compuesto **6a**, un anillo quelado de 6 miembros.

De entre los compuestos ciclometalados con sistemas tricíclicos [6.5.5], el compuesto **8a**, no sustituido, presenta más actividad que el 8b, un 3-, 5- dicloro derivado. El compuesto **8c**, con un ligando metilo, tiene una IC_{50} menor incluso que la de **8a**. Finalmente, tanto los compuestos tricíclicos [6.5.6] **10a** y **10b**

como el compuesto tetracíclico [5.5.5.6] **11** presentan interesantes actividades antiproliferativas sobre todas las líneas tumorales estudiadas, aunque siguen sin ser tan potentes como la del cisplatino. El compuesto **11**, un derivado del ferroceno con un enlace Pt-S, muestra una IC_{50} menor que la del compuesto **9**, otro derivado del ferroceno pero con un enlace Pt-N(amina).

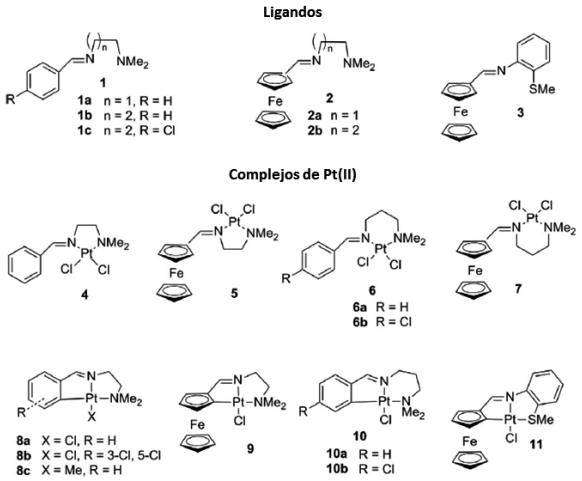

Valores de IC50 (μM)

Compuesto	A549	MDA-MB231	HCT116
1a	>100	>100	>100
1b	>100	>100	>100
1c	>100	>100	>100
3	173 ± 25	nd	44 ± nd
4	26 ± 12	47 ± nd	35 ± 2,2
5	>100	57 ± nd	55 ± 6,8
6a	95 ± 7	14,1 ± 2,4	11,9 ± 9,2
6b	>100	10,7 ± 4,6	10,6 ± 1,7
7	178 ± 32	28 ± 0,3	30 ± 4,2
8a	95 ± 7	10,7 ± 4,6	60 ± 1,7
8b	38 ± 18	42,2 ± 9,5	>100
8c	27 ± 10	30 ± 10,2	44 ± 8,5
9	75 ± 14	87 ± nd	45 ± 7,8
10a	40 ± 14	28 ± 2,4	28 ± 6,7
10b	23 ± 4	17 ± 1,1	18 ± 1,9
11	23 ± 8	32 ± 6,2	20,7 ± 3,8
cisplatin	9,3 ± 3	6,5 ± 2,4	40 ± 4,4

FIGURA 02. Estructura de los compuestos de platino con iminas polifuncionalizadas sintetizados y tabla con sus valores de IC_{50} sobre las tres líneas tumorales ensayadas. Se incluyen también los ligandos libres, usados como referencia.

Capítulo 1c. Caracterización de la actividad antiproliferativa de compuestos de platino y paladio derivados del pirazol

Se ha estudiado el efecto de compuestos organometálicos de platino y de paladio derivados del pirazol sobre la viabilidad de células de cáncer de pulmón A549, así como sobre la viabilidad de células tumorales de mama MDA-MB231 y MCF7. En todos los casos, los compuestos organometálicos exhiben una actividad biológica sobre la proliferación de las líneas tumorales más potente que la de los ligandos libres, que también fueron ensayados como referencia (ver **figura 3**). Además, varios de los compuestos ensayados presentan concentraciones de IC_{50} más bajas que el cisplatino, que es usado de manera rutinaria en la práctica clínica en el tratamiento del cáncer de pulmón.

Valores de IC50 (μM)

Compuesto	A549	MDA-MB231	MCF7
1a	>100	>100	>100
1b	>100	>100	>100
1c	55 ± 14	64 ± 24	52 ± 10
2a	3 ± 1	57 ± 8,5	20 ± 3,6
2b	12 ± 5	62 ± 9,3	51 ± 10,4
2c	13 ± 5,8	14 ± 1,7	17 ± 2,2
4c	7 ± 2,8	6,2 ± 1,3	9,3 ± 3,4
3a	>100	>100	>100
3b	73,5 ± 2,1	>100	>100
5c	38,5 ± 4,9	16,2 ± 4,6	38,4 ± 16,5
cisplatin	9,3 ± 3	6,5 ± 2,4	19 ± 4,5

FIGURA 03. Estructura de los compuestos de platino y paladio derivados del pirazol sintetizados y tabla con sus valores de IC_{50} sobre las tres líneas tumorales ensayadas. Se incluyen también los ligandos libres, usados como referencia.

También se han realizado estudios acerca de la capacidad de los compuestos para afectar a la movilidad electroforética de un plásmido de ADN *pBluescript*. La alteración de esta movilidad por parte de los compuestos implica la existencia de una interacción con el ADN capaz de alterar su estructura terciaria, lo que puede resultar indicativo de sus mecanismos de acción,. El compuesto **2a**, que es el que presenta una menor concentración de IC_{50} en células A549 es, junto con **5c**, el que mayor efecto presenta sobre la movilidad del ADN. El compuesto **4c**, en cambio, a pesar de ser el segundo compuesto con una actividad más potente sobre la viabilidad de las células tumorales de pulmón, no provoca ningún efecto visible sobre esta movilidad.

Capítulo 1d. Caracterización de la actividad antiproliferativa de compuestos híbridos ferroceno-indol

Se ha estudiado el efecto sobre la viabilidad de células tumorales de compuestos ferroceno-indólicos de nueva síntesis sobre la línea de adenocarcinoma pulmonar A549 (ver **figura 4**).

Todos los compuestos sintetizados, con la excepción de los compuestos **4** y **7**, presentan valores de IC_{50} a 72 horas inferiores a 100 μM. Los compuestos **11**, **12** y **13** presentan valores de IC_{50} por debajo de 10 μM, siendo el compuesto **11** el que cuenta con una actividad antiproliferativa más potente, con un valor de IC_{50} de tan solo 5 μM.

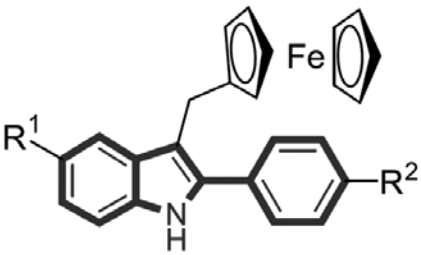

Valores de IC50 (μM) en células A549

Compuesto	Tipo de molécula	R1	R2	X	IC_{50} (μM)
1	Orgánica	H	H	H	30 ± 7
2	Orgánica	H	Cl	H	33 ± 8
3	Orgánica	H	F	H	31 ± 8
4	Orgánica	OHC_3	H	H	118 ± 4
5	Orgánica	NO_2	H	H	14 ± 3
6	Orgánica	Cl	H	H	15 ± 5
7	Orgánica	H	H	N	120 ± 10
8	Organometálica	H	H	H	13 ± 4
9	Organometálica	H	Cl	H	15 ± 1
10	Organometálica	H	F	H	26 ± 1
11	Organometálica	OHC_3	H	H	5 ± 1
12	Organometálica	NO_2	H	H	7 ± 1
13	Organometálica	Cl	H	H	10 ± 1
14	Organometálica	H	H	N	27 ± 3

FIGURA 04. Estructura de los compuestos híbridos ferroceno-indol sintetizados y tabla con sus valores de IC_{50} sobre la línea celular de adenocarcinoma pulmonar A549.

Capítulo 1e. Caracterización de la actividad antiproliferativa de compuestos de platino(II) derivados del ferroceno

Se ha estudiado el efecto de tres pares de compuestos de platino(II) diastereoméricamente puros derivados del ferroceno. La actividad de estos compuestos sobre la viabilidad de células tumorales se ha ensayado utilizando como modelo la línea de adenocarcinoma de pulmón A549, así como las líneas tumorales de colon y mama HCT116 y MDA-MB231 (ver **figura 5**).

El ligando libre **1a**, un iminoalcohol, presenta un efecto moderado sobre la viabilidad de las células de cáncer de pulmón A549 (IC_{50}=33 μM). Los tres pares de compuestos de platino(II) de nueva síntesis **2a**-**7a**, en cambio, presentan potentes actividades biológicas, y la mayoría de ellos tienen valores de IC_{50} por debajo del cisplatino tanto en la línea A549 como en el resto de líneas celulares estudiadas. El compuesto **3a**, el isómero cis de **2a**, es el menos potente de todos los estudiados con un valor de IC_{50} de alrededor de 20 μM, siendo **2a** (el isómero trans) alrededor de 4 veces más potente. Los isómeros **4a** y **5a** presentan valores de IC_{50} similares entre ellos e inferiores a los de **2a** y **3a**. El par de platinaciclos isómeros **6a** y **7a** tienen también una gran capacidad de inhibir la viabilidad de las células de cáncer de pulmón, con un valor de IC_{50} inferior a 10 μM y, en el caso del compuesto **6a**, inferior a la del cisplatino.

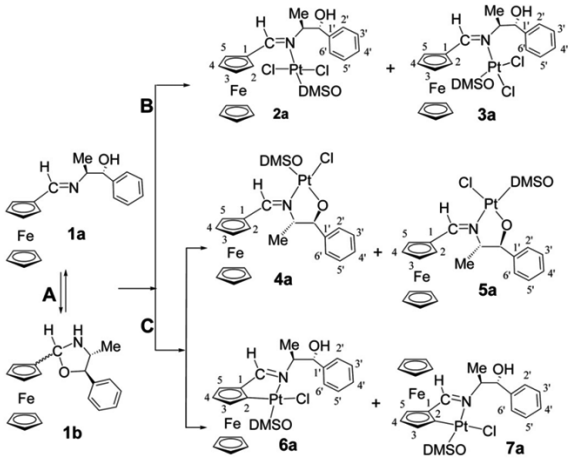

Valores de IC50 (μM)

Compuesto	A549	MDA-MB231	HCT116
1a	33,5 ± 0,2	>100	>100
2a	5,7 ± 0,4	3,9 ± 0,6	4,,4 ± 2,8
3a	21,7 ± 6,5	1,04 ± 4,0	14 ± 2,6
4a	4,1 ± 0,8	1,4 ± 0,1	1,4 ± 2,8
5a	2,8 ± 0,6	1,4 ± 0,5	1,4 ± 2,0
6a	8,8 ± 1,8	2,7 ± 0,2	2,0 ± 0,18
7a	10 ± 0,7	9,5 ± 0,5	8,1 ± 0,6
cisplatin	9,3 ± 3,0	6,5 ± 2,4	40 ± 4,4

FIGURA 05. Estructura de los compuestos de platino derivados del ferroceno sintetizados y tabla con sus valores de IC_{50} sobre las tres líneas tumorales ensayadas.

También se ha estudiado la capacidad de los compuestos de nueva síntesis para alterar la movilidad del ADN de un plásmido pBluescript mediante un ensayo electroforético. El ligando libre **1a** no fue capaz de provocar un cambio en la movilidad del ADN, pero la mayoría del resto de compuestos de platino(II) sí lo hicieron. Aunque ningún compuesto fue capaz de ejercer un efecto sobre la movilidad del ADN a concentraciones ≤ 25 μM, los compuestos **3a** y **4a** provocaron un efecto a una concentración de 50 μM, mientras que los compuestos **2a**, **6a** y **7a** lo hicieron a una concentración de 100 μM. El compuesto **5a**, de manera análoga al compuesto **1a**, tampoco provoca ningún efecto sobre la movilidad del ADN.

Por último, también se ha llevado a cabo un estudio de la estabilidad de los compuestos en DMSO y en una mezcla de DMSO:D_2O. Los resultados de este estudio, realizado mediante espectrometría de resonancia magnética nuclear (NMR, del inglés *Nuclear Magnetic Ressonance*), indican que el par de isómeros **6a**-**7a** son mucho más estables en solución que el resto de compuestos sintetizados, ya que sus espectros de protón tras días en disolución son idénticos a las que tienen cuando están recién sintetizados.

4.1.2. *(Capítulo 02)* El complejo ciclometalado Pt(II)-ferroceno 6a induce localización nuclear de FOXO3a y apoptosis, y presenta un comportamiento sinérgico con el cisplatino en la inhibición de la proliferación de células de cáncer de pulmón.

Se ha estudiado el mecanismo por el que el complejo de Pt(II) derivado del ferroceno **6a** ejerce su acción antiproliferativa sobre las células de cáncer de pulmón. Este compuesto, cuya actividad sobre la viabilidad de células tumorales de pulmón A549 ha sido evaluada en el Capítulo 1 de esta Tesis, es capaz de inducir la translocación al núcleo celular del factor de transcripción FOXO3a en la línea celular U2foxRELOC, un sistema celular basado en células de osteosarcoma humano U2OS que ha sido usado previamente para estudiar mediante microscopía confocal el tránsito de FOXO3a entre el citoplasma y el núcleo (Zanella, Rosado et al. 2008; Link, Oyarzabal et al. 2009; Zanella, Rosado et al. 2009). FOXO3a es un factor de transcripción considerado un supresor tumoral, y únicamente puede ejercer sus funciones reguladoras de la proliferación cuando se encuentra localizado en el núcleo celular. El compuesto **8**, que presenta similitudes estructurales con el compuesto **6a** pero que tiene una menor actividad sobre la viabilidad celular, no es capaz de provocar cambios significativos en la localización de FOXO3a en las células U2foxRELOC a las concentraciones utilizadas con **6a**.

El efecto de **6a** sobre la localización de FOXO en las células tumorales de pulmón A549 también fue evaluado mediante la transfección de las mismas con un plásmido de FOXO-GFP, que permite observar la localización de FOXO mediante microscopía confocal. **6a** también es capaz de inducir un cambio de localización de FOXO3a, haciendo que este pase de estar en el citoplasma a concentrarse en el núcleo celular, en el que puede llevar a cabo su función antiproliferativa. Enayos de Western Blot determinaron que el tratamiento con **6a** hace aumentar la concentración de FOXO3a (activo) en el núcleo, disminuyendo al mismo tiempo la concentración de FOXO3a-P (inhibido por fosforilación) en el citoplasma, lo que valida las observaciones realizadas observando la localización de FOXO-GFP. La fosforilación de FOXO3a mediante AKT es uno de los mecanismos de regulación más comunes de este factor de transcripción, y ensayos de Western Blot indicaron que la incubación de las células A549 con **6a** provoca un descenso en la concentración tanto de fosfo-AKT como de fosfo-PRAS40, uno de los sustratos de AKT. La incubación con cisplatino, en cambio, no provocó efectos apreciables sobre los niveles de fosfo-AKT ni de fosfo-PRAS40.

Los factores de transcripción FOXO son capaces de ejercer su actividad supresora de tumores a través de la regulación del ciclo celular (Dijkers, Medema et al. 2000; Schmidt, Fernandez de Mattos et al. 2002; Eijkelenboom and

Burgering 2013) y de la apoptosis (Dijkers, Medema et al. 2000; Tang, Dowbenko et al. 2002), por lo que también se han realizado estudios de FACS para determinar el efecto de **6a** sobre ambos procesos. Los resultados indicaron que el tratamiento de células A549 con **6a** no es capaz de alterar de manera importante la distribución de células en las distintas fases del ciclo celular, pero sí de desencadenar un proceso apoptótico muy evidente. Estudios de integridad del ADN confirmaron la inducción de apoptosis por parte del compuesto, y los Western Blot realizados indicaron que la incubación de las células con **6a** provoca un descenso de los niveles de pro-caspasas 3 y 9, así como un aumento de los niveles del marcador apoptótico PARP.

El compuesto **6a** también resulta activo sobre otra línea de cáncer de pulmón de células no pequeñas como NCIH460, tanto en lo que respecta a la inhibición de la viabilidad celular como en lo que respecta a la inducción de apoptosis. Por otra parte, la IC_{50} de **6a** sobre adipocitos 3T3-L1 diferenciados y no proliferantes es entre 3 y 15 veces mayor que en todas las líneas tumorales ensayadas.

4.1.3. *(Capítulo 03)* El estudio del metabolismo de las líneas tumorales de pulmón A549 y NCIH460 revela dianas terapéuticas metabólicas explotables en tratamientos combinados con complejos de platino.

Se han estudiado las tasas de producción de lactato y glutamato y las tasas de consumo de glucosa y glutamina de la línea no tumoral de pulmón BEAS2B y de las líneas tumorales de pulmón A549 (adenocarcinoma) y NCIH460 (carcinoma de célula grande), así como sus tasas de duplicación. Tras normalizar los resultados por millón de células y por hora de incubación, estos indican que las dos líneas tumorales consumen más glucosa y glutamina y producen más lactato y glutamato que la línea no tumoral. En concreto, NCIH460 es la línea celular que consume más glucosa y glutamina, así como la que produce más lactato, mientras que A549 es la línea celular con mayor producción de glutamato.

Se ha realizado un estudio metabolómico basado en el uso de trazadores usando los sustratos marcados con ^{13}C [1,2-^{13}C]-glucosa y [3-^{13}C]-glutamina, para evaluar las diferencias en los flujos del metabolismo central entre las tres líneas de pulmón. Los resultados indican que la actividad relativa de la rama no oxidativa de la vía de las pentosas fosfato es mayor en las líneas de células tumorales, y especialmente en NCIH460. Además, únicamente las células tumorales utilizan la glutamina como fuente de carbonos para la síntesis de ácidos grasos, a través de una vía que implica la activación de la lanzadera de citrato y la acción del enzima málico.

En general, los resultados sugieren la existencia de una dependencia de la glutamina en las líneas tumorales A549 y NCIH460, por lo que se ha estudiado el efecto de BPTES, un inhibidor de la glutaminasa, sobre las tres líneas celulares en estudio. BPTES es capaz de inhibir la viabilidad celular de las dos líneas celulares que presentan consumos de glutamina elevados (A549 y NCIH460), mientras que las concentraciones ensayadas no provocan grandes efectos sobre la viabilidad de las células no tumorales BEAS-2B.

4.1.4. *(Capítulo 04)* Las alteraciones metabólicas pueden explotarse en la detección no invasiva de cáncer y pulmón y COPD mediante el análisis de muestras de aire exhalado.

Se ha puesto a punto un método para la detección de los compuestos orgánicos volátiles (VOCs) de la respiración mediante cromatografía de gases acoplada a espectrometría de masas (GC-MS). Se ha realizado un estudio piloto en el que las muestras de respiración eran tomadas utilizando bolsas de Tedlar, y los VOCs presentes en las muestras eran preconcentrados en una fibra de carboxen/PDMS mediante microextracción en fase sólida. En un estudio piloto inicial se tomaron muestras de respiración de sujetos sanos y pacientes con enfermedad pulmonar obstructiva crónica (EPOC), y se intentó usar el patrón de VOCs del aire exhalado para separar los grupos en función de la presencia o ausencia de la enfermedad.

La clasificación de los datos mediante Análisis de Componentes Principales (PCA, del inglés *principal component analysis*) revela que el reciclado de bolsas de Tedlar genera una gran variabilidad en el patrón de VOCs de las bolsas reutilizadas. Esta variabilidad es mayor que la inducida por la presencia de la enfermedad, por lo que se decidió descartar la reutilización de las bolsas de Tedlar y tomar muestras únicamente con bolsas nuevas.

Mediante un nuevo análisis de PCA, realizado únicamente a partir de las muestras tomadas con bolsas de Tedlar nuevas, se advirtió que el calendario del muestreo (parte de las muestras se tomaron en febrero, mientras que el resto se tomaron en noviembre) también introduce una gran variabilidad en los patrones de VOCs del aire exhalado. Mediante el análisis de los VOCs presentes en el aire ambiental de la habitación en la que las muestras de respiración eran tomadas, se ha visto que los dos componentes principales de una PCA son capaces de agrupar las muestras de aire ambiental en función del mes en el que fueron tomadas, de manera similar al agrupamiento observado con las muestras de aire exhalado. Aunque un análisis de PCA simple no es capaz

de separar gráficamente los grupos de sanos y enfermos de COPD, seleccionando los 14 componentes principales de la PCA y llevando a cabo con ellos un análisis discriminante lineal ha sido posible separar los grupos en función de la presencia o ausencia de COPD. Tras una validación interna del modelo, se ha conseguido una especificidad del 72% y una sensibilidad del 58% en la detección del COPD, con un porcentaje de acierto global del 66%.

Los resultados resultan prometedores, teniendo en cuenta el reducido número de muestras incluidas en el estudio piloto y la gran variabilidad presente en los patrones de VOCs de las muestras estudiadas. A partir de las conclusiones obtenidas en el estudio piloto, se ha desarrollado y puesto a punto un nuevo sistema de toma de muestra que utiliza Sorbent Traps (tubos rellenos de una fibra de Tenax/Unicarb) para captar y almacenar los VOCs de las muestras de respiración. Además, los sujetos participantes en esta segunda fase del estudio respiraron aire medicinal durante todo el proceso de toma de muestra, para reducir la variabilidad que las distintas composiciones de VOCs del aire ambiental durante los distintos meses del año provocan en los patrones de VOCs del aire exhalado.

Con este nuevo método de toma de muestra se han analizado las muestras de aire exhalado de 83 sujetos distintos, incluyendo voluntarios sanos (grupo CONTROL), pacientes con cáncer de pulmón (grupo LC), pacientes con EPOC (grupo COPD, del inglés *chronic obstructive pulmonary disease*) y pacientes que padecían ambas enfermedades (grupo COPDLC). Se han generado, mediante el método estadístico conocido como *Random Forest*, 6 modelos binarios (CONTROL vs. LC, CONTROL vs COPD, Control vs COPDLC, COPD vs LC, COPD vs COPDLC and COPDLC vs LC), y se ha realizado una prueba de permutación para comprobar si estos modelos binarios eran capaces de separar las muestras de respiración de sus dos grupos correspondientes en función del patrón de VOCs de las mismas. Los modelos que pasaron la prueba de permutación (todos excepto los modelos Control vs COPDLC y COPDLC vs LC) fueron validados externamente con muestras que no habían sido utilizadas para generar el modelo.

Los resultados indican que es posible conseguir una buena separación con los modelos COPD vs LC y CONTROL vs COPD. También hay evidencias de las diferencias entre los patrones de VOCs de las muestras de respiración de los grupos CONTROL y LC, pero la clasificación es algo menos exitosa que en la que se produce en los modelos anteriores, sobretodo en lo que respecta a la sensibilidad del modelo.

Los modelos binarios que pasaron el test de permutación fueron utilizados para construir un modelo combinado capaz de indicar a cuál de los cuatro grupos (CON-

TROL, LC, COPD y COPDLC) pertenece una muestra cualquiera. Al aplicar este modelo sobre todas las muestras generadas, se obtuvo un éxito de clasificación del 52%, siendo el éxito esperado en una clasificación llevada a cabo al azar de un 26%. Los mayores errores se cometieron con las muestras del grupo COPDLC, que con frecuencia fueron clasificadas como correspondientes a los grupos LC o COPD, así como con muestras del grupo LC que fueron clasificadas en el grupo COPDLC.

4.2. DISCUSIÓN GLOBAL

El bajo índice de supervivencia a cinco años del cáncer de pulmón que se sitúa actualmente alrededor del 15%, hace indispensable la aparición de nuevas terapias capaces de combatir la enfermedad. Esto es especialmente cierto en el caso de los tumores pulmonares con mutaciones en KRAS, que no suelen responder a los tratamientos dirigidos a inhibir el receptor del factor de crecimiento epidérmico EGFR. Aunque el cisplatino sigue siendo uno de los tratamientos quimioterapéuticos de referencia en cáncer de pulmón, su uso no está exento de desventajas que hacen que su utilidad se vea reducida. De entre estas desventajas destacan, por su importancia, los efectos secundarios del cisplatino y la resistencia de muchas células tumorales al mismo. El descubrimiento de compuestos con una actividad biológica más potente que la del cisplatino, o que ejerzan su actividad antiproliferativa mediante mecanismos diferentes, podría ayudar a solucionar ambas limitaciones. Además, el uso conjunto del cisplatino con estos compuestos puede potenciar su acción antiproliferativa, en una sinergia explotable en el diseño de terapias combinadas con actividad aumentada.

En el primer capítulo de esta Tesis, hemos explorado la actividad biológica de distintos grupos de complejos metálicos de nueva síntesis sobre las células de adenocarcinoma pulmonar A549, que presentan mutación en el gen KRAS. El análisis de la Relación Estructura-Actividad (SAR, del inglés *Structure-Activity Relationship*) de estos compuestos puede resultar de gran interés para el diseño futuro de nuevas moléculas con una actividad antitumoral aún más potente.

Los **compuestos cicloplatinados de 7 miembros** ensayados presentan, todos ellos, una IC_{50} menor que el cisplatino. Los valores de IC_{50} de todos los compuestos ensayados son muy similares, lo que no permite extraer conclusiones acerca de la influencia de los distintos sustituyentes presentes en cada uno de ellos sobre su actividad biológica. El hecho de que el cisplatino, aun contando con una IC_{50} más alta que los compuestos de nueva síntesis, sea capaz de afectar la movilidad electroforética del ADN en un grado mayor al resto de los mismos,

incluso a concentraciones más pequeñas, sugiere que la actividad antiproliferativa de los compuestos cicloplatinados de siete miembros es de naturaleza distinta a la del cisplatino. Los resultados de los ensayos de ciclo y apoptosis indican que el compuesto **1c** (así como, probablemente, el resto de compuestos de la serie) parece estar ejerciendo su efecto antiproliferativo sobre las células A549 a través de la parada o ralentización de su ciclo celular, lo que provoca que disminuya la velocidad de duplicación de esas células tumorales.

Los **compuestos de platino con iminas polifuncionalizadas** presentan actividad antiproliferativa sobre las células de adenocarcinoma pulmonar, aunque sus valores de IC_{50} no son, en general, más bajos que los del cisplatino. La sustitución de un grupo fenilo en los compuestos **4**, **6a** y **8a** por un grupo ferrocenilo, lo que da como resultado los compuestos respectivos **5**, **7** y **9**, no provoca un aumento en la citotoxicidad. Sin embargo, la presencia de un ligando metilo no lábil en **8c** (en vez del ligando cloruro lábil de **8a**) sí provoca un aumento en la actividad biológica del compuesto. En general, los compuestos con ligandos bidentados presentan actividades menores que las de los compuestos con ligandos tridentados.

Los resultados sobre la capacidad antiproliferativa de **compuestos de platino y paladio derivados del pirazol** indican que algunos de ellos tienen una actividad biológica sobre las células A549 más potente que la del cisplatino. El compuesto **4c** se forma mediante la coordinación de los dos átomos de nitrógeno y la formación de un enlace σ(Pt-C), lo que genera un sistema tetracíclico [6.5.5.6]. Por lo tanto, el compuesto **4c** tiene una mayor rigidez y linearidad que el compuesto **2c**, y dado que los compuestos metálicos planos con ligandos aromáticos se unen al ADN por intercalación (Erkkila, Odom et al. 1999; Collins, Rixon et al. 2000; Ma and Che 2003), es posible que **4c** se una al ADN no sólo por alquilación sino también como agente intercalante, lo que podría explicar la mayor potencia biológica del compuesto **4c** frente al compuesto **2c**. Los compuestos **4c** y **5c**, por otro lado, se diferencian únicamente en la naturaleza de su átomo metálico, y el hecho de que el compuesto **4c**, con Pt(II), sea considerablemente más potente que **5c**, se debe probablemente a la mayor labilidad y facilidad de hidrólisis de los compuestos de paladio en comparación con sus equivalentes de platino (Khan, Bhatt et al. 1991). Finalmente, aunque el compuesto **2a** (que presenta la menor concentración de IC_{50} en células A549) es, junto con **5c**, el que mayor efecto presenta sobre la movilidad del ADN, el compuesto **4c** no provoca ningún efecto visible sobre esta movilidad a pesar de ser el segundo compuesto con una actividad más potente sobre la viabilidad de las células tumorales de pulmón. Esto indica que las diferencias entre las estructuras de estos compuestos implican que su actividad biológica asume mecanismos diferentes, lo que puede resultar de especial interés en posibles terapias combinadas.

La actividad antiproliferativa de los **híbridos ferroceno-indol** sobre la línea de adenocarcinoma pulmonar A549 también ha resultado elevada, con concentraciones de IC_{50} por debajo de 10 µM para los compuestos **11**, **12** y **13**. La sustitución del átimo de hidrógeno de la posición 5 del anillo indólico aumenta la actividad biológica de la molécula, con el siguiente orden de potencia: 5-OMe (**11**)> 5-NO_2(**12**)> 5-Cl(**13**). En cambio, las sustituciones en la posición *para* del anillo arilo provocaron una disminución de la actividad de los compuestos de la siguiente manera: p-H (**8**)> p-Cl (**9**)> p-F (**10**). En cualquier caso, la combinación del núcleo de ferroceno con la estructura 2-fenilindólica siempre crea moléculas híbridas más potentes que las originales. Así, los híbridos ferroceno-indol **8-14** son más activos biológicamente que los compuestos orgánicos puros correspondientes **1-7**.

Finalmente, también se ha caracterizado la actividad antiproliferativa de **compuestos de platino(II) derivados del ferroceno**, que resulta superior a la del cisplatino en la mayoría de los casos. Los isómeros **4a** y **5a** presentan valores de IC_{50} inferiores a **2a** y **3a**, lo que sugiere que el cambio en el modo de unión del ligando **1a**, de N-donador a $(N,O)^-$, implica un aumento de la actividad biológica de los complejos resultantes. El hecho de que los compuestos **4a** y **5a**, que se diferencian en la disposición relativa del ligando Cl^- y el N de la imina (trans en **4a** y cis en **5a**), muestren una actividad biológica similar, parece sugerir que esta disposición no tiene efectos importantes sobre la actividad de las moléculas. Pero aunque la IC_{50} de estos dos compuestos sea similar, el compuesto **5a** (a diferencia de **4a**) no provoca ningún efecto sobre la movilidad del DNA, lo que sugiere que en realidad los mecanismos de acción de ambos compuestos son diferentes. En este sentido, el cisplatino es capaz de alterar la movilidad electroforética del ADN a concentraciones inferiores a las de cualquiera de los compuestos sintetizados, aunque alguno de estos presenta valores de IC_{50} inferiores en las líneas estudiadas. Así, la actividad antiproliferativa de estos compuestos no se debe únicamente a su capacidad para alquilar el ADN, sino que debe implicar otros mecanismos alternativos diferentes. Por último, la mayor estabilidad en solución de los compuestos ciclometalados **6a** y **7a** con respecto al resto de complejos de platino(II) derivados del ferroceno implica que, en sistemas in vivo, **6a** y **7a** tienen más posibilidades de alcanzar su diana biológica intactos (Rouhi, Jensen et al. 2010), lo que resulta de especial interés para su potencial desarrollo como tratamientos antitumorales.

En general, los resultados obtenidos revelan la capacidad de los nuevos complejos metálicos para inhibir la viabilidad de la línea de adenocarcinoma pulmonar A549, muchas veces con concentraciones de IC_{50} inferiores a la del cisplatino y/o mediante lo que parecen ser mecanismos alternativos a la distorsión de la estructura del ADN mediante unión covalente al mismo, que es como el cisplatino ejerce su acción antiproliferativa. Los estudios de Relacion Estructura-Actividad sobre los compuestos de nueva síntesis resultan de especial interés para

el diseño futuro de nuevos compuestos con estructuras específicas que permitan obtener actividades biológicas aún más potentes.

De entre los compuestos ensayados, el **compuesto de platino(II) derivado del ferroceno 6a** fue escogido para realizar estudios que profundizaran en el mecanismo de su actividad antiproliferativa. Se escogió este compuesto tanto por la gran potencia de su actividad sobre la viabilidad de las células A549 (con un valor de IC_{50} inferior a 10 μM) como por sus propiedades de estabilidad en solución, que apuntan a que en sistemas biológicos *in vivo* el compuesto tendrá más posibilidades de alcanzar su diana biológica estructuralmente intacto.

El compuesto **6a** provoca, tanto en células U2foxRELOC como en células A549, la traslocación del supresor de tumores FOXO3a al núcleo. FOXO3a, al ser un factor de transcripción, necesita estar en el núcleo celular para realizar sus funciones de control de la proliferación celular, con lo que el efecto de **6a** sobre la localización intracelular de FOXO parece estar relacionado con su actividad antiproliferativa. El hecho de que el compuesto **8**, que presenta similitudes estructurales con el compuesto **6a** pero que tiene una menor actividad sobre la viabilidad celular, no sea capaz de provocar cambios significativos en la localización de FOXO en las células U2foxRELOC a las concentraciones utilizadas con **6a**, también sugiere que existe una relación entre esta translocación y el efecto antiproliferativo de **6a**. El descenso de los niveles de FOXO3a fosforilado en el citoplasma, que se corresponde con un aumento de los niveles de FOXO3a activo en el núcleo celular, confirma las observaciones realizadas acerca de la localización de la proteína. El hecho de que 6a sea capaz de inhibir la fosforilación tanto de AKT como de su sustrato PRAS40 sugiere que el efecto del compuesto sobre la localización de FOXO3a está mediado por la vía AKT, una de las principales reguladoras de FOXO3a.

FOXO3a tiene descritas funciones tanto de regulación del ciclo celular como de activación de la apoptosis. Los resultados obtenidos con **6a** indican que el compuesto no tiene un gran efecto sobre el ciclo celular, pero en cambio es capaz de activar la apoptosis en menos de 24 horas, efecto que se mantiene para todos los tiempos de incubación ensayados. El efecto de **6a** sobre la fragmentación del ADN de las células A549 confirma la existencia de apoptosis, y el hecho de que disminuyan los niveles de las pro-caspasas 3 y 9 indica que esta es activada a través de la vía intrínseca, también llamada vía mitocondrial.

La actividad de **6a** sobre la viabilidad, el ciclo celular y la apopotosis de las células de carcinoma pulmonar de célula grande NCIH460 (que, como la línea A549, también cuenta con KRAS mutado) es similar a la observada con las célu-

las A549, lo que indica que el compuesto es activo también sobre otros modelos de cáncer de pulmón de células no pequeñas. Además, la IC_{50} del compuesto sobre adipocitos 3T3-L1 diferenciados y no proliferantes es entre 3 y 15 veces mayor que en todas las líneas tumorales ensayadas, lo que apunta a que existe una especificidad del efecto de **6a** sobre células tumorales. Tanto los resultados sobre la movilidad electroforética del ADN (que aparecen en el capítulo 1 de esta Tesis doctoral) como los resultados sobre los niveles de AKT y PRAS40 fosforilados indican que **6a** y cisplatino actúan sobre la viabilidad celular mediante mecanismos diferentes, lo que abre la puerta a la posibilidad de realizar un tratamiento combinado con ambos compuestos. Los ensayos combinados de **6a** y cisplatino sobre la línea celular A549 confirman la existencia de una sinergia entre ambos compuestos, señalando el potencial de esta posibilidad. Todo ello hace que **6a** se presente como un compuesto con una interesante actividad antitumoral en distintos modelos de cáncer de pulmón, y por lo tanto resulta un excelente candidato para llevar a cabo estudios adicionales que profundicen en su potencial uso terapéutico en el tratamiento del cáncer.

Dos maneras alternativas de mejorar la baja supervivencia asociada al cáncer de pulmón consisten en la detección de nuevas dianas moleculares específicas que puedan ser atacadas para evitar la progresión tumoral y en el desarrollo de nuevos métodos que permitan realizar un diagnóstico temprano de la enfermedad. Ambos objetivos pueden ser alcanzados mediante el estudio del metabolismo tumoral, ya que impedir la reprogramación metabólica asociada al cáncer puede suponer un modo de impedir la proliferación celular, mientras que los metabolitos generados por un metabolismo alterado pueden ser explotados como biomarcadores con potencial diagnóstico.

El estudio del metabolismo de las líneas de cáncer de pulmón A549 y NCIH460 y de la línea de pulmón no tumoral BEAS2B revela que las líneas tumorales consumen más glutamina y más glucosa que la línea tumoral, además de producir más lactato y glutamato. El peso relativo de la rama no oxidativa de la vía de las pentosas fosfato con respecto a la vía oxidativa es también mayor en las líneas tumorales, y especialmente en la línea NCIH460, que es la que presenta una mayor tasa de proliferación. Este resultado sugiere que la actividad de la rama no oxidativa de las pentosas fosfato es capaz de facilitar la proliferación de las células tumorales, lo que está en concordancia con resultados previos que indican que la expresión de TKTL1, una de las enzimas más importantes de esta rama metabólica, promueve la proliferación y correlaciona con la agresividad de distintos tumores (Langbein, Zerilli et al. 2006; Staiger, Coy et al. 2006; Foldi, Stickeler et al. 2007; Zhang, Yang et al. 2007; Krockenberger, Honig et al. 2007; Diaz-Moralli, Tarrado-Castellarnau et al. 2011; Hartmannsberger, Mack et al. 2011).

Tras incubación de las células con glutamina marcada con ^{13}C, la marca aparece en moléculas de ácidos grasos únicamente en las líneas tumorales A549 y NCIH460. Esto sugiere que únicamente las células tumorales utilizan la glutamina como fuente de carbonos para la síntesis de ácidos grasos. Dado que el sustrato trazador utilizado es [3-^{13}C]-glutamina, la marca no puede llegar a ácidos grasos si no es a través de la lanzadera de citrato y la enzima málica, que usa el malato para generar piruvato que puede ser reintroducido en el Ciclo de Krebs. La acción de la enzima málica es capaz de generar reductor en forma de NADPH, que puede ser utilizados por las células tumorales para equilibrar su estado redox o para sintetizar ácidos grasos (Santidrian, Matsuno-Yagi et al. 2013), lo que constituye una ventaja adicional en la activación de esta vía.

En general, los resultados sugieren la existencia de una dependencia de la glutamina en las líneas tumorales A549 y NCIH460. El efecto antiproliferativo de BPTES, un inhibidor de la glutaminasa capaz de inhibir la viabilidad celular de ambas líneas de forma selectiva, confirma la existencia de esta dependencia.

El metabolismo genera compuestos orgánicos volátiles que están presentes en el aire exhalado. El estudio del cambio que se produce en el patrón de estos compuestos como consecuencia de un metabolismo alterado nos puede ayudar a diagnosticar una enfermedad como el cáncer de pulmón, que entre otras cosas se caracteriza por implicar una profunda reprogramación metabólica.

Los resultados obtenidos a partir del análisis de muestras de respiración mediante GC-MS demuestran que hay diferencias entre los patrones de VOCs de muestras de respiración de sujetos sanos, con cáncer de pulmón y con enfermedad pulmonar obstructiva crónica, aunque la gran variabilidad que existe entre miembros de la misma clasificación clínica puede dificultar la correcta clasificación de las muestras. Por tanto, hay que tomar todas las medidas posibles para limitar esa variabilidad. Los resultados sugieren que la composición de VOCs del aire ambiental cambia en función de la época del año, y que esta composición, a su vez, tiene una gran influencia en los patrones de VOCs del aire exhalado, por lo que una manera de reducir la variabilidad de las muestras consiste en hacer que los pacientes respiren aire medicinal durante el proceso de toma de muestra. El grupo COPDLC, que contiene a pacientes con cáncer de pulmón y EPOC, fue el que más errores provocó en la clasificación de las muestras. Al tener ambas enfermedades, los pacientes del grupo pueden potencialmente expresar un fenotipo muy cercano al cáncer de pulmón, a la EPOC o cualquier fenotipo intermedio entre los de cada una de estas enfermedades. Además, en los grupos con pacientes de cáncer de pulmón (COPDLC y LC), la heterogeneicidad entre el tipo de cáncer que estos padecen (adenocarcinoma, carcinoma escamoso, leimiosarcoma…) y entre el grado de desarrollo de los tumores

provoca una dispersión de las muestras que dificulta su correcta clasificación, especialmente si tenemos en cuenta que estas diferencias implican también que los pacientes estén sometidos a tratamientos distintos. La solución a estos problemas pasa por homogeneizar los grupos en estudio o bien aumentar el tamaño del muestreo.

En cualquier caso, los resultados indican que la toma de muestras de aire exhalado y su análisis posterior mediante GC-MS es un método con potencial en la detección del cáncer de pulmón y la EPOC atendiendo a los patrones particulares de VOCs que estas enfermedades generan en el aire exhalado. Las decisiones tomadas tras el estudio piloto mejoran la clasificación de muestras de sujetos sanos y pacientes con EPOC, incluso con el método de validación mucho más riguroso que ha sido utilizado en el estudio extendido. Además, la buena clasificación obtenida entre muestras de pacientes con EPOC y con cáncer de pulmón demuestra que el método no detecta únicamente la existencia de una disfunción pulmonar de cualquier tipo, sino que es capaz de detectar los patrones de VOCs específicos de cada una de estas dos enfermedades.

4.3. CONCLUSIONES

01. Se ha ensayado la actividad biológica sobre células tumorales de una nueva familia de compuestos cicloplatinados de 7 miembros, que presentan valores de IC_{50} inferiores a los del cisplatino pero que no interaccionan con el ADN en tanta extensión como este, lo que sugiere que tienen un mecanismo de acción diferente. El compuesto **1c** de la serie ejerce su efecto antiproliferativo sobre las células A549 mediante la parada de su ciclo celular.

02. Se ha ensayado la actividad biológica sobre células tumorales de una nueva familia de compuestos de platino con iminas polifuncionalizadas, que en general no presentan valores de IC_{50} inferiores a los del cisplatino. Se ha observado que los compuestos con ligandos bidentados presentan actividades menores a las de los compuestos con ligandos tridentados.

03. Se ha ensayado la actividad biológica sobre células tumorales de una nueva familia de compuestos de platino y paladio derivados del pirazol, algunos de los cuales tienen valores de IC_{50} inferiores a los del cisplatino. La sustitución de un átomo de paladio por uno de platino aumenta la actividad de los compuestos a la vez que disminuye la ca-

pacidad de alterar la movilidad electroforética del ADN, lo que puede estar relacionado con la menor facilidad de hidrólisis de los compuestos con platino con respecto a los de paladio.

04. Se ha ensayado la actividad biológica sobre células de adenocarcinoma pulmonar de una nueva familia de compuestos híbridos ferroceno-indol, algunos de los cuales tienen valores de IC_{50} inferiores a los del cisplatino. La combinación del núcleo de ferroceno con la estructura 2-fenilindólica siempre crea moléculas híbridas más potentes que las originales. La sustitución del H de la posición 5 del anillo indólico aumenta la actividad biológica, mientras que las sustituciones en la posición *para* del anillo arilo la disminuyen.

05. Se ha ensayado la actividad biológica sobre células tumorales de una nueva familia de compuestos de platino(II) derivados del ferroceno, que resulta superior a la del cisplatino en la mayoría de los casos. El cambio en el modo de unión del ligando, de N-donador a $(N,O)^-$, implica un aumento de la actividad. La disposición relativa del ligando Cl^- y el N de la imina no conlleva un aumento de la actividad antiproliferativa, pero sí hace que varíe la capacidad de unión al ADN. El compuesto **6a** de la serie combina una elevada acción sobre la viabilidad celular con una elevada estabilidad en disolución.

06. El compuesto de platino(II) derivado del ferroceno **6a** es capaz de inhibir la fosforilación del factor de transcripción FOXO3a a través de la vía AKT, permitiendo así su activación mediante su translocación del citoplasma al núcleo celular. **6a** es capaz de provocar apoptosis en células de adenocarcinoma pulmonar A549 a través de la vía intrínseca de las caspasas.

07. El compuesto de platino(II) derivado del ferroceno **6a** también es efectivo sobre la línea de carcinoma pulmonar de célula grade NCIH460, mientras que su IC_{50} sobre adipocitos 3T3-L1 diferenciados y no proliferantes es entre 3 y 15 veces mayor que sobre las líneas tumorales. Su mecanismo de acción, distinto al del cisplatino, hace que exista sinergia en el uso combinado de ambos compuestos.

08. El estudio de las alteraciones metabólicas de las líneas de cáncer de pulmón A549 y NCIH460 ha revelado la existencia de una dependencia metabólica de la glutamina explotable en la inhibición selectiva de su proliferación.

09. Se ha desarrollado un método para analizar los compuestos orgánicos volátiles (VOCs) de muestras de aire exhalado mediante cromatografía de gases acoplada a espectrometría de masas, y se ha diseñado un nuevo sistema de muestreo.

10. Se ha determinado que hay fuentes de variabilidad que no tienen que ver con el estado clínico de los sujetos cuyas muestras han sido tomadas. Una de las más importantes es el cambio de la composición de VOCs del aire ambiental en distintos meses del año, que afecta a la composición de VOCs en el aire exhalado.

11. Se ha determinado que los patrones de VOCs permiten clasificar las muestras de respiración en función de la presencia o ausencia de enfermedades como cáncer de pulmón o enfermedad pulmonar obstructiva crónica, aunque la elevada variabilidad de algunos de los grupos de clasificación dificulta el proceso.

05.
BIBLIOGRAFÍA

Abu-Surrah, A. S. and M. Kettunen (2006). "Platinum group antitumor chemistry: design and development of new anticancer drugs complementary to cisplatin." Curr Med Chem **13**(11): 1337-1357.

Adamson, E. D. (1987). "Oncogenes in development." Development **99**(4): 449-471.

Adekola, K., S. T. Rosen, et al. (2012). "Glucose transporters in cancer metabolism." Curr Opin Oncol **24**(6): 650-654.

Al Zaid Siddiquee, K., M. J. Arauzo-Bravo, et al. (2004). "Metabolic flux analysis of pykF gene knockout Escherichia coli based on 13C-labeling experiments together with measurements of enzyme activities and intracellular metabolite concentrations." Appl Microbiol Biotechnol **63**(4): 407-417.

Bailey, K. M., J. W. Wojtkowiak, et al. (2012). "Targeting the metabolic microenvironment of tumors." Adv Pharmacol **65**: 63-107.

Bajtarevic, A., C. Ager, et al. (2009). "Noninvasive detection of lung cancer by analysis of exhaled breath." BMC Cancer **9**: 348.

Bijland, L. R., M. K. Bomers, et al. (2013). "Smelling the diagnosis: a review on the use of scent in diagnosing disease." Neth J Med **71**(6): 300-307.

Biswas, S., J. Lunec, et al. (2012). "Non-glucose metabolism in cancer cells--is it all in the fat?" Cancer Metastasis Rev **31**(3-4): 689-698.

Blake, D. C., Jr., O. R. Mikse, et al. (2010). "FOXO3a elicits a pro-apoptotic transcription program and cellular response to human lung carcinogen nicotine-derived nitrosaminoketone (NNK)." Lung Cancer **67**(1): 37-47.

Boren, J., W. N. Lee, et al. (2003). "The stable isotope-based dynamic metabolic profile of butyrate-induced HT29 cell differentiation." J Biol Chem **278**(31): 28395-28402.

Boren, J., A. R. Montoya, et al. (2002). "Metabolic control analysis aimed at the ribose synthesis pathways of tumor cells: a new strategy for antitumor drug development." Mol Biol Rep **29**(1-2): 7-12.

Bray, F., A. Jemal, et al. (2012). "Global cancer transitions according to the Human Development Index (2008-2030): a population-based study." Lancet Oncol **13**(8): 790-801.

Budzisz, E., I.-P. Lorenz, et al. (2008). "Synthesis, crystal structure, theoretical calculation and cytotoxic effect of new Pt(ii), Pd(ii) and Cu(ii) complexes with pyridine-pyrazoles derivatives." New Journal of Chemistry **32**(12): 2238-2244.

Burgess, S. C., T. He, et al. (2007). "Cytosolic phosphoenolpyruvate carboxykinase does not solely control the rate of hepatic gluconeogenesis in the intact mouse liver." Cell Metab **5**(4): 313-320.

Calusic, A. L., V. M. Varnai, et al. (2011). "Acute effects of smoking and food consumption on breath condensate pH in healthy adults." Exp Lung Res **37**(2): 92-100.

Cardarella, S. and B. E. Johnson (2013). "The impact of genomic changes on treatment of lung cancer." Am J Respir Crit Care Med **188**(7): 770-775.

Cascante, M., J. J. Centelles, et al. (2000). "Role of thiamin (vitamin B-1) and transketolase in tumor cell proliferation." Nutr Cancer **36**(2): 150-154.

Cascante, M. and S. Marin (2008). "Metabolomics and fluxomics approaches." Essays Biochem **45**: 67-81.

Collins, J. G., R. M. Rixon, et al. (2000). "Interaction of [Pt(en)(phen)]2+ and [Pt(en)(phi)]2+ with the hexanucleotide d(GTCGAC)2: evidence for minor groove binding." Inorg Chem **39**(19): 4377-4379.

Collins, J. M., M. J. Neville, et al. (2011). "De novo lipogenesis in the differentiating human adipocyte can provide all fatty acids necessary for maturation." J Lipid Res **52**(9): 1683-1692.

Cooper, W. A., D. C. Lam, et al. (2013). "Molecular biology of lung cancer." J Thorac Dis **5**(Suppl 5): S479-S490.

Cornforth, A. N., J. S. Davis, et al. (2008). "FOXO3a mediates the androgen-dependent regulation of FLIP and contributes to TRAIL-induced apoptosis of LNCaP cells." Oncogene **27**(32): 4422-4433.

Crown, S. B. and M. R. Antoniewicz (2013). "Parallel labeling experiments and metabolic flux analysis: Past, present and future methodologies." Metab Eng **16**: 21-32.

Chan, H. P., C. Lewis, et al. (2010). "Oxidative stress and exhaled breath analysis: a promising tool for detection of lung cancer." Cancers (Basel) **2**(1): 32-42.

Chan, K. S., C. G. Koh, et al. (2012). "Mitosis-targeted anti-cancer therapies: where they stand." Cell Death Dis **3**: e411.

Chen, M. K., N. J. Espat, et al. (1993). "Influence of progressive tumor growth on glutamine metabolism in skeletal muscle and kidney." Ann Surg **217**(6): 655-666; discussion 666-657.

Cheng, N., A. Chytil, et al. (2008). "Transforming growth factor-beta signaling-deficient fibroblasts enhance hepatocyte growth factor signaling in mammary carcinoma cells to promote scattering and invasion." Mol Cancer Res **6**(10): 1521-1533.

Cheng, T., J. Sudderth, et al. (2011). "Pyruvate carboxylase is required for glutamine-independent growth of tumor cells." Proc Natl Acad Sci U S A **108**(21): 8674-8679.

Chetty, R. and D. Govender (2013). "Gene of the month: KRAS." J Clin Pathol **66**(7): 548-550.

Cheung, T. H. and T. A. Rando (2013). "Molecular regulation of stem cell quiescence." Nat Rev Mol Cell Biol **14**(6): 329-340.

Christofk, H. R., M. G. Vander Heiden, et al. (2008). "Pyruvate kinase M2 is a phosphotyrosine-binding protein." Nature **452**(7184): 181-186.

Daitoku, H., J. Sakamaki, et al. (2011). "Regulation of FoxO transcription factors by acetylation and protein-protein interactions." Biochim Biophys Acta **1813**(11): 1954-1960.

Dansen, T. B. and B. M. Burgering (2008). "Unravelling the tumor-suppressive functions of FOXO proteins." Trends Cell Biol **18**(9): 421-429.

Das, M. K., S. C. Bishwal, et al. (2014). "Investigation of gender-specific exhaled breath volatome in humans by GCxGC-TOF-MS." Anal Chem **86**(2): 1229-1237.

Daye, D. and K. E. Wellen (2012). "Metabolic reprogramming in cancer: unraveling the role of glutamine in tumorigenesis." Semin Cell Dev Biol **23**(4): 362-369.

de Atauri, P., A. Benito, et al. (2011). "Carbon metabolism and the sign of control coefficients in metabolic adaptations underlying K-ras transformation." Biochim Biophys Acta **1807**(6): 746-754.

DeBerardinis, R. J., A. Mancuso, et al. (2007). "Beyond aerobic glycolysis: transformed cells can engage in glutamine metabolism that exceeds the requirement for protein and nucleotide synthesis." Proc Natl Acad Sci U S A **104**(49): 19345-19350.

Diaz-Moralli, S., M. Tarrado-Castellarnau, et al. (2011). "Transketolase-like 1 expression is modulated during colorectal cancer progression and metastasis formation." PLoS One **6**(9): e25323.

Diaz-Moralli, S., M. Tarrado-Castellarnau, et al. (2013). "Targeting cell cycle regulation in cancer therapy." Pharmacol Ther **138**(2): 255-271.

Dijkers, P. F., R. H. Medema, et al. (2000). "Expression of the pro-apoptotic Bcl-2 family member Bim is regulated by the forkhead transcription factor FKHR-L1." Curr Biol **10**(19): 1201-1204.

Doherty, J. R. and J. L. Cleveland (2013). "Targeting lactate metabolism for cancer therapeutics." J Clin Invest **123**(9): 3685-3692.

Duran, R. V., W. Oppliger, et al. (2012). "Glutaminolysis activates Rag-mTORC1 signaling." Mol Cell **47**(3): 349-358.

Edwards, G. L., D. S. C. Black, et al. (2005). "Effect of charge and surface area on the cytotoxicity of cationic metallointercalation reagents." Canadian Journal of Chemistry **83**(6-7): 969-979.

Eijkelenboom, A. and B. M. Burgering (2013). "FOXOs: signalling integrators for homeostasis maintenance." Nat Rev Mol Cell Biol **14**(2): 83-97.

Elkholi, R., K. V. Floros, et al. (2011). "The Role of BH3-Only Proteins in Tumor Cell Development, Signaling, and Treatment." Genes Cancer **2**(5): 523-537.

Erkkila, K. E., D. T. Odom, et al. (1999). "Recognition and reaction of metallointercalators with DNA." Chem Rev **99**(9): 2777-2796.

Fadok, V. A., D. R. Voelker, et al. (1992). "Exposure of phosphatidylserine on the surface of apoptotic lymphocytes triggers specific recognition and removal by macrophages." J Immunol **148**(7): 2207-2216.

Faux, S. P., T. Tai, et al. (2009). "The role of oxidative stress in the biological responses of lung epithelial cells to cigarette smoke." Biomarkers **14 Suppl 1**: 90-96.

Foldi, M., E. Stickeler, et al. (2007). "Transketolase protein TKTL1 overexpression: A potential biomarker and therapeutic target in breast cancer." Oncol Rep **17**(4): 841-845.

Fu, G. and C. Peng (2011). "Nodal enhances the activity of FoxO3a and its synergistic interaction with Smads to regulate cyclin G2 transcription in ovarian cancer cells." Oncogene **30**(37): 3953-3966.

Fu, L., C. Zhang, et al. (2011). "Wnt2 secreted by tumour fibroblasts promotes tumour progression in oesophageal cancer by activation of the Wnt/beta-catenin signalling pathway." Gut **60**(12): 1635-1643.

Gaglio, D., C. M. Metallo, et al. (2011). "Oncogenic K-Ras decouples glucose and glutamine metabolism to support cancer cell growth." Mol Syst Biol **7**: 523.

Gallorini, M., A. Cataldi, et al. (2012). "Cyclin-dependent kinase modulators and cancer therapy." BioDrugs **26**(6): 377-391.

Ganapathy, S., Q. Chen, et al. (2010). "Resveratrol enhances antitumor activity of TRAIL in prostate cancer xenografts through activation of FOXO transcription factor." PLoS One **5**(12): e15627.

Gao, P., I. Tchernyshyov, et al. (2009). "c-Myc suppression of miR-23a/b enhances mitochondrial glutaminase expression and glutamine metabolism." Nature **458**(7239): 762-765.

Gasser, G., I. Ott, et al. (2011). "Organometallic anticancer compounds." J Med Chem **54**(1): 3-25.

Gillies, R. J., I. Robey, et al. (2008). "Causes and consequences of increased glucose metabolism of cancers." J Nucl Med **49 Suppl 2**: 24S-42S.

Goldstraw, P. (2013). "New staging system: how does it affect our practice?" J Clin Oncol **31**(8): 984-991.

Gordon, S. M., L. A. Wallace, et al. (2002). "Volatile organic compounds as breath biomarkers for active and passive smoking." Environ Health Perspect **110**(7): 689-698.

Gorjanacz, M. (2014). "Nuclear assembly as a target for anti-cancer therapies." Nucleus **5**(1).

Greaves, M. and C. C. Maley (2012). "Clonal evolution in cancer." Nature **481**(7381): 306-313.

Greer, E. L. and A. Brunet (2005). "FOXO transcription factors at the interface between longevity and tumor suppression." Oncogene **24**(50): 7410-7425.

Gross, D. N., M. Wan, et al. (2009). "The role of FOXO in the regulation of metabolism." Curr Diab Rep **9**(3): 208-214.

Hammill, A. K., J. W. Uhr, et al. (1999). "Annexin V staining due to loss of membrane asymmetry can be reversible and precede commitment to apoptotic death." Exp Cell Res **251**(1): 16-21.

Hanahan, D. and R. A. Weinberg (2011). "Hallmarks of cancer: the next generation." Cell **144**(5): 646-674.

Hennings, H., A. B. Glick, et al. (1993). "Critical aspects of initiation, promotion, and progression in multistage epidermal carcinogenesis." Proc Soc Exp Biol Med **202**(1): 1-8.

Hensley, C. T., A. T. Wasti, et al. (2013). "Glutamine and cancer: cell biology, physiology, and clinical opportunities." J Clin Invest **123**(9): 3678-3684.

Hitosugi, T. and J. Chen (2013). "Post-translational modifications and the Warburg effect." Oncogene.

Hitosugi, T., S. Kang, et al. (2009). "Tyrosine phosphorylation inhibits PKM2 to promote the Warburg effect and tumor growth." Sci Signal **2**(97): ra73.

Holford, J., P. J. Beale, et al. (2000). "Mechanisms of drug resistance to the platinum complex ZD0473 in ovarian cancer cell lines." Eur J Cancer **36**(15): 1984-1990.

Honasoge, A. and H. Sontheimer (2013). "Involvement of tumor acidification in brain cancer pathophysiology." Front Physiol **4**: 316.

Hu, M. C., D. F. Lee, et al. (2004). "IkappaB kinase promotes tumorigenesis through inhibition of forkhead FOXO3a." Cell **117**(2): 225-237.

Huang, H., K. M. Regan, et al. (2005). "Skp2 inhibits FOXO1 in tumor suppression through ubiquitin-mediated degradation." Proc Natl Acad Sci U S A **102**(5): 1649-1654.

Jiang, P., W. Du, et al. (2011). "p53 regulates biosynthesis through direct inactivation of glucose-6-phosphate dehydrogenase." Nat Cell Biol **13**(3): 310-316.

Jiang, P., W. Du, et al. (2013). "A critical role of glucose-6-phosphate dehydrogenase in TAp73-mediated cell proliferation." Cell Cycle **12**(24): 3720-3726.

Johnson, S. W., P. A. Swiggard, et al. (1994). "Relationship between platinum-DNA adduct formation and removal and cisplatin cytotoxicity in cisplatin-sensitive and -resistant human ovarian cancer cells." Cancer Res **54**(22): 5911-5916.

Jones, R. G. and C. B. Thompson (2009). "Tumor suppressors and cell metabolism: a recipe for cancer growth." Genes Dev **23**(5): 537-548.

Jung, Y. and S. J. Lippard (2007). "Direct cellular responses to platinum-induced DNA damage." Chem Rev **107**(5): 1387-1407.

Kabashima, T., T. Kawaguchi, et al. (2003). "Xylulose 5-phosphate mediates glucose-induced lipogenesis by xylulose 5-phosphate-activated protein phosphatase in rat liver." Proc Natl Acad Sci U S A **100**(9): 5107-5112.

Kastan, M. B. and J. Bartek (2004). "Cell-cycle checkpoints and cancer." Nature **432**(7015): 316-323.

Kelland, L. (2007). "The resurgence of platinum-based cancer chemotherapy." Nat Rev Cancer **7**(8): 573-584.

Kelland, L. R., P. Mistry, et al. (1992). "Mechanism-related circumvention of acquired cis-diamminedichloroplatinum(II) resistance using two pairs of human ovarian carcinoma cell lines by ammine/amine platinum(IV) dicarboxylates." Cancer Res **52**(14): 3857-3864.

Kennedy, K. M. and M. W. Dewhirst (2010). "Tumor metabolism of lactate: the influence and therapeutic potential for MCT and CD147 regulation." Future Oncol **6**(1): 127-148.

Khan, B. T., J. Bhatt, et al. (1991). "Synthesis, antimicrobial, and antitumor activity of a series of palladium(II) mixed ligand complexes." J Inorg Biochem **44**(1): 55-63.

Khan, K. H., M. Blanco-Codesido, et al. (2014). "Cancer therapeutics: Targeting the apoptotic pathway." Crit Rev Oncol Hematol **90**(3): 200-219.

Kikuno, N., H. Shiina, et al. (2007). "Knockdown of astrocyte-elevated gene-1 inhibits prostate cancer progression through upregulation of FOXO3a activity." Oncogene **26**(55): 7647-7655.

Kilburn, D. G., M. D. Lilly, et al. (1969). "The energetics of mammalian cell growth." J Cell Sci **4**(3): 645-654.

Kim, D. H., T. Zhang, et al. (2013). "FoxO6 in glucose metabolism (FoxO6)." J Diabetes **5**(3): 233-240.

Klagge, A., C. Weidinger, et al. (2011). "The role of FOXO3 in DNA damage response in thyrocytes." Endocr Relat Cancer **18**(5): 555-564.

Kousteni, S. (2012). "FoxO1, the transcriptional chief of staff of energy metabolism." Bone **50**(2): 437-443.

Krockenberger, M., A. Honig, et al. (2007). "Transketolase-like 1 expression correlates with subtypes of ovarian cancer and the presence of distant metastases." Int J Gynecol Cancer **17**(1): 101-106.

Kuwana, T., M. R. Mackey, et al. (2002). "Bid, Bax, and lipids cooperate to form supramolecular openings in the outer mitochondrial membrane." Cell **111**(3): 331-342.

Lam, E. W., J. J. Brosens, et al. (2013). "Forkhead box proteins: tuning forks for transcriptional harmony." Nat Rev Cancer **13**(7): 482-495.

Langbein, S., M. Zerilli, et al. (2006). "Expression of transketolase TKTL1 predicts colon and urothelial cancer patient survival: Warburg effect reinterpreted." Br J Cancer **94**(4): 578-585.

Link, W., J. Oyarzabal, et al. (2009). "Chemical interrogation of FOXO3a nuclear translocation identifies potent and selective inhibitors of phosphoinositide 3-kinases." J Biol Chem **284**(41): 28392-28400.

Lippi, G. and G. Cervellin (2012). "Canine olfactory detection of cancer versus laboratory testing: myth or opportunity?" Clin Chem Lab Med **50**(3): 435-439.

Lobo, C., M. A. Ruiz-Bellido, et al. (2000). "Inhibition of glutaminase expression by antisense mRNA decreases growth and tumourigenicity of tumour cells." Biochem J **348 Pt 2**: 257-261.

Ma, D. L. and C. M. Che (2003). "A bifunctional platinum(II) complex capable of intercalation and hydrogen-bonding interactions with DNA: binding studies and cytotoxicity." Chemistry **9**(24): 6133-6144.

Machado, R. F., D. Laskowski, et al. (2005). "Detection of lung cancer by sensor array analyses of exhaled breath." Am J Respir Crit Care Med **171**(11): 1286-1291.

Malumbres, M. and M. Barbacid (2009). "Cell cycle, CDKs and cancer: a changing paradigm." Nat Rev Cancer **9**(3): 153-166.

Marin, S., K. Chiang, et al. (2003). "Metabolic strategy of boar spermatozoa revealed by a metabolomic characterization." FEBS Lett **554**(3): 342-346.

Martinez-Gac, L., M. Marques, et al. (2004). "Control of cyclin G2 mRNA expression by forkhead transcription factors: novel mechanism for cell cycle control by phosphoinositide 3-kinase and forkhead." Mol Cell Biol **24**(5): 2181-2189.

Matito, C., F. Mastorakou, et al. (2003). "Antiproliferative effect of antioxidant polyphenols from grape in murine Hepa-1c1c7." Eur J Nutr **42**(1): 43-49.

Mazzone, P. J., J. Hammel, et al. (2007). "Diagnosis of lung cancer by the analysis of exhaled breath with a colorimetric sensor array." Thorax **62**(7): 565-568.

McCracken, A. N. and A. L. Edinger (2013). "Nutrient transporters: the Achilles' heel of anabolism." Trends Endocrinol Metab **24**(4): 200-208.

McIlwain, D. R., T. Berger, et al. (2013). "Caspase functions in cell death and disease." Cold Spring Harb Perspect Biol **5**(4): a008656.

Menendez, J. A. and R. Lupu (2007). "Fatty acid synthase and the lipogenic phenotype in cancer pathogenesis." Nat Rev Cancer **7**(10): 763-777.

Meng, M., S. Chen, et al. (2010). "Nitrogen anabolism underlies the importance of glutaminolysis in proliferating cells." Cell Cycle **9**(19): 3921-3932.

Mikse, O. R., D. C. Blake, Jr., et al. (2010). "FOXO3 encodes a carcinogen-activated transcription factor frequently deleted in early-stage lung adenocarcinoma." Cancer Res **70**(15): 6205-6215.

Miller, K. A., N. Yeager, et al. (2009). "Oncogenic Kras requires simultaneous PI3K signaling to induce ERK activation and transform thyroid epithelial cells in vivo." Cancer Res **69**(8): 3689-3694.

Mistry, P., L. R. Kelland, et al. (1991). "The relationships between glutathione, glutathione-S-transferase and cytotoxicity of platinum drugs and melphalan in eight human ovarian carcinoma cell lines." Br J Cancer **64**(2): 215-220.

Mitro, N., P. A. Mak, et al. (2007). "The nuclear receptor LXR is a glucose sensor." Nature **445**(7124): 219-223.

Mitsuishi, Y., K. Taguchi, et al. (2012). "Nrf2 redirects glucose and glutamine into anabolic pathways in metabolic reprogramming." Cancer Cell **22**(1): 66-79.

Moradell, S., J. Lorenzo, et al. (2003). "Platinum complexes of diaminocarboxylic acids and their ethyl ester derivatives: the effect of the chelate ring size on antitumor activity and interactions with GMP and DNA." J Inorg Biochem **96**(4): 493-502.

Mosmann, T. (1983). "Rapid colorimetric assay for cellular growth and survival: application to proliferation and cytotoxicity assays." J Immunol Methods **65**(1-2): 55-63.

Nunez, R. (2001). "DNA measurement and cell cycle analysis by flow cytometry." Curr Issues Mol Biol **3**(3): 67-70.

Oltvai, Z. N. and A. L. Barabasi (2002). "Systems biology. Life's complexity pyramid." Science **298**(5594): 763-764.

Ortega, A. D., M. Sanchez-Arago, et al. (2009). "Glucose avidity of carcinomas." Cancer Lett **276**(2): 125-135.

Ostman, A. and M. Augsten (2009). "Cancer-associated fibroblasts and tumor growth--bystanders turning into key players." Curr Opin Genet Dev **19**(1): 67-73.

Padda, S. K., B. M. Burt, et al. (2014). "Early-stage non-small cell lung cancer: surgery, stereotactic radiosurgery, and individualized adjuvant therapy." Semin Oncol **41**(1): 40-56.

Paik, J. H., R. Kollipara, et al. (2007). "FoxOs are lineage-restricted redundant tumor suppressors and regulate endothelial cell homeostasis." Cell **128**(2): 309-323.

Paul Lee, W. N., P. N. Wahjudi, et al. (2010). "Tracer-based metabolomics: concepts and practices." Clin Biochem **43**(16-17): 1269-1277.

Peng, G., M. Hakim, et al. (2010). "Detection of lung, breast, colorectal, and prostate cancers from exhaled breath using a single array of nanosensors." Br J Cancer **103**(4): 542-551.

Phillips, M., R. N. Cataneo, et al. (2013). "Detection of an extended human volatome with comprehensive two-dimensional gas chromatography time-of-flight mass spectrometry." PLoS One **8**(9): e75274.

Phillips, M., R. N. Cataneo, et al. (2000). "Effect of age on the breath methylated alkane contour, a display of apparent new markers of oxidative stress." J Lab Clin Med **136**(3): 243-249.

Phillips, M., K. Gleeson, et al. (1999). "Volatile organic compounds in breath as markers of lung cancer: a cross-sectional study." Lancet **353**(9168): 1930-1933.

Pojarova, M., D. Kaufmann, et al. (2007). "[(2-Phenylindol-3-yl)methylene]propanedinitriles inhibit the growth of breast cancer cells by cell cycle arrest in G(2)/M phase and apoptosis." Bioorg Med Chem **15**(23): 7368-7379.

Qing, G., B. Li, et al. (2012). "ATF4 regulates MYC-mediated neuroblastoma cell death upon glutamine deprivation." Cancer Cell **22**(5): 631-644.

Rattigan, Y. I., B. B. Patel, et al. (2012). "Lactate is a mediator of metabolic cooperation between stromal carcinoma associated fibroblasts and glycolytic tumor cells in the tumor microenvironment." Exp Cell Res **318**(4): 326-335.

Ren, D., H. C. Tu, et al. (2010). "BID, BIM, and PUMA are essential for activation of the BAX- and BAK-dependent cell death program." Science **330**(6009): 1390-1393.

Reungwetwattana, T. and G. K. Dy (2013). "Targeted therapies in development for non-small cell lung cancer." J Carcinog **12**: 22.

Riganti, C., E. Gazzano, et al. (2012). "The pentose phosphate pathway: an antioxidant defense and a crossroad in tumor cell fate." Free Radic Biol Med **53**(3): 421-436.

Rodriguez-Prados, J. C., P. G. Traves, et al. (2010). "Substrate fate in activated macrophages: a comparison between innate, classic, and alternative activation." J Immunol **185**(1): 605-614.

Rouhi, P., L. D. Jensen, et al. (2010). "Hypoxia-induced metastasis model in embryonic zebrafish." Nat Protoc **5**(12): 1911-1918.

Roy, S. K., R. K. Srivastava, et al. (2010). "Inhibition of PI3K/AKT and MAPK/ERK pathways causes activation of FOXO transcription factor, leading to cell cycle arrest and apoptosis in pancreatic cancer." J Mol Signal **5**: 10.

Rubin, H. (2003). "Microenvironmental regulation of the initiated cell." Adv Cancer Res **90**: 1-62.

Salmela, A. L. and M. J. Kallio (2013). "Mitosis as an anti-cancer drug target." Chromosoma **122**(5): 431-449.

Santidrian, A. F., A. Matsuno-Yagi, et al. (2013). "Mitochondrial complex I activity and NAD+/NADH balance regulate breast cancer progression." J Clin Invest **123**(3): 1068-1081.

Schmidt, M., S. Fernandez de Mattos, et al. (2002). "Cell cycle inhibition by FoxO forkhead transcription factors involves downregulation of cyclin D." Mol Cell Biol **22**(22): 7842-7852.

Semenza, G. L. (2008). "Tumor metabolism: cancer cells give and take lactate." J Clin Invest **118**(12): 3835-3837.

Seoane, J., H. V. Le, et al. (2004). "Integration of Smad and forkhead pathways in the control of neuroepithelial and glioblastoma cell proliferation." Cell **117**(2): 211-223.

Shukla, S., N. Bhaskaran, et al. (2013). "Deregulation of FoxO3a accelerates prostate cancer progression in TRAMP mice." Prostate **73**(14): 1507-1517.

Staiger, W. I., J. F. Coy, et al. (2006). "Expression of the mutated transketolase TKTL1, a molecular marker in gastric cancer." Oncol Rep **16**(4): 657-661.

Suzuki, S., T. Tanaka, et al. (2010). "Phosphate-activated glutaminase (GLS2), a p53-inducible regulator of glutamine metabolism and reactive oxygen species." Proc Natl Acad Sci U S A **107**(16): 7461-7466.

Szablewski, L. (2013). "Expression of glucose transporters in cancers." Biochim Biophys Acta **1835**(2): 164-169.

Tang, T. T., D. Dowbenko, et al. (2002). "The forkhead transcription factor AFX activates apoptosis by induction of the BCL-6 transcriptional repressor." J Biol Chem **277**(16): 14255-14265.

Tarnoki, D. L., A. Bikov, et al. (2014). "Lack of heritability of exhaled volatile compound pattern: an electronic nose twin study." J Breath Res **8**(1): 016001.

Tzivion, G., M. Dobson, et al. (2011). "FoxO transcription factors; Regulation by AKT and 14-3-3 proteins." Biochim Biophys Acta **1813**(11): 1938-1945.

Valavanidis, A., T. Vlachogianni, et al. (2013). "Pulmonary oxidative stress, inflammation and cancer: respirable particulate matter, fibrous dusts and ozone as major causes of lung carcinogenesis through reactive oxygen species mechanisms." Int J Environ Res Public Health **10**(9): 3886-3907.

Vander Heiden, M. G., L. C. Cantley, et al. (2009). "Understanding the Warburg effect: the metabolic requirements of cell proliferation." Science **324**(5930): 1029-1033.

Vizan, P., G. Alcarraz-Vizan, et al. (2009). "Modulation of pentose phosphate pathway during cell cycle progression in human colon adenocarcinoma cell line HT29." Int J Cancer **124**(12): 2789-2796.

Wang, D. and S. J. Lippard (2005). "Cellular processing of platinum anticancer drugs." Nat Rev Drug Discov **4**(4): 307-320.

Wang, J. B., J. W. Erickson, et al. (2010). "Targeting mitochondrial glutaminase activity inhibits oncogenic transformation." Cancer Cell **18**(3): 207-219.

Ward, P. S. and C. B. Thompson (2012). "Metabolic reprogramming: a cancer hallmark even warburg did not anticipate." Cancer Cell **21**(3): 297-308.

Watroba, M., D. Maslinska, et al. (2012). "Current overview of functions of FoxO proteins, with special regards to cellular homeostasis, cell response to stress, as well as inflammation and aging." Adv Med Sci **57**(2): 183-195.

Webb, A. E. and A. Brunet (2014). "FOXO transcription factors: key regulators of cellular quality control." Trends Biochem Sci **39**(4): 159-169.

Weinberg, R. A. (1991). "Tumor suppressor genes." Science **254**(5035): 1138-1146.

Weinstein, I. B. and A. K. Joe (2006). "Mechanisms of disease: Oncogene addiction--a rationale for molecular targeting in cancer therapy." Nat Clin Pract Oncol **3**(8): 448-457.

Winter, G. and J. O. Kromer (2013). "Fluxomics - connecting 'omics analysis and phenotypes." Environ Microbiol **15**(7): 1901-1916.

Wise, D. R., R. J. DeBerardinis, et al. (2008). "Myc regulates a transcriptional program that stimulates mitochondrial glutaminolysis and leads to glutamine addiction." Proc Natl Acad Sci U S A **105**(48): 18782-18787.

Xie, Q., J. Chen, et al. (2012). "Post-translational regulation of FOXO." Acta Biochim Biophys Sin (Shanghai) **44**(11): 897-901.

Yan, S., Y. Z. Li, et al. (2013). "HuGE systematic review and meta-analysis demonstrate association of CASP-3 and CASP-7 genetic polymorphisms with cancer risk." Genet Mol Res **12**(2): 1561-1573.

Yang, J. Y., C. S. Zong, et al. (2008). "ERK promotes tumorigenesis by inhibiting FOXO3a via MDM2-mediated degradation." Nat Cell Biol **10**(2): 138-148.

Ying, H., A. C. Kimmelman, et al. (2012). "Oncogenic Kras maintains pancreatic tumors through regulation of anabolic glucose metabolism." Cell **149**(3): 656-670.

Zanella, F., A. Rosado, et al. (2008). "Chemical genetic analysis of FOXO nuclear-cytoplasmic shuttling by using image-based cell screening." Chembiochem **9**(14): 2229-2237.

Zanella, F., A. Rosado, et al. (2009). "Using multiplexed regulation of luciferase activity and GFP translocation to screen for FOXO modulators." BMC Cell Biol **10**: 14.

Zarogoulidis, K., P. Zarogoulidis, et al. (2013). "Treatment of non-small cell lung cancer (NSCLC)." J Thorac Dis **5**(Suppl 4): S389-S396.

Zhang, S., Y. Zhao, et al. (2013). "FoxO3a modulates hypoxia stress induced oxidative stress and apoptosis in cardiac microvascular endothelial cells." PLoS One **8**(11): e80342.

Zhang, X., N. Tang, et al. (2011). "Akt, FoxO and regulation of apoptosis." Biochim Biophys Acta **1813**(11): 1978-1986.

Zhang, Y., B. Gan, et al. (2011). "FoxO family members in cancer." Cancer Biol Ther **12**(4): 253-259.

06.
PUBLICACIONES

CAPÍTULO 01

ESTUDIO DEL EFECTO DE COMPLEJOS METÁLICOS DE NUEVA SÍNTESIS SOBRE LA PROLIFERACIÓN DE CÉLULAS TUMORALES DE PULMÓN.

CAPÍTULO 1A

COMPLEJOS CICLOPLATINADOS DE SIETE MIEMBROS COMO UNA NUEVA FAMILIA DE AGENTES ANTITUMORALES. CARACTERIZACIÓN POR RAYOS-X Y ESTUDIOS BIOLÓGICOS PRELIMINARES.

Roldán Cortés [a], Margarita Crespo [b,*], Laia Davin [b], Raquel Martín [b], Josefina Quirante [c,*], Daniel Ruiz [c], Ramon Messeguer [d], Carme Calvis [d], Laura Baldomà [e], Josefa Badia [e], Mercè Font-Bardía [f,g], Teresa Calvet [f], Marta Cascante [a]

[a] Departament de Bioquímica i Biologia Molecular, Facultat de Biologia, Institut de Biomedicina de la Universitat de Barcelona (IBUB) y IDIBAPS, Unidad Asociada al CSIC, Diagonal 643, 08028 Barcelona, España

[b] Departament de Química Inorgànica y Institut de Biomedicina de la Universitat de Barcelona (IBUB), Facultat de Química, Universitat de Barcelona, Diagonal 645, 08028 Barcelona, España

[c] Laboratori de Química Orgànica, Facultat de Farmàcia, Institut de Biomedicina, (IBUB), Universitat de Barcelona, Av. Joan XXIII s/n, 08028 Barcelona, España

[d] Biomed Division LEITAT Technological Center, Parc Científic de Barcelona, Edifici Hèlix, C/Baldiri Reixach, 15-21, 08028 Barcelona, España

[e] Departament de Bioquímica i Biologia Molecular, Facultat de Farmàcia, Institut de Biomedicina de la Universitat de Barcelona (IBUB), Av. Joan XXIII s/n, 08028 Barcelona, España

[f] Departament de Cristal·lografia, Mineralogia i Dipòsits Minerals, Facultat de Geologia, Universitat de Barcelona, Martí i Franquès s/n, 08028 Barcelona, España

[g] Unitat de Difracció de Raigs-X, Centre Científic i Tecnològic de la Universitat de Barcelona (CCiTUB), Solé i Sabarís, 1-3, 08028 Barcelona, España

Resumen

Se ha desarrollado una serie de complejos cicloplatinados de Pt(II) de siete miembros que contienen un ligando tridentado [C,N,N'] (**1a**-**1c** y **2a**-**2c**), como potenciales agentes de unión al ADN. Mediante reacciones de *cis*-[Pt(4-$C_6H_4Me)_2(\mu\text{-}SEt_2)]_2$ o *cis*-$[Pt(C_6H_5)_2(SMe_2)_2]$ con iminas 2-$ClC_6H_4CH{=}NCH_2CH_2NMe_2$ (**b**) o 2-F,6-$ClC_6H_3CH{=}NCH_2CH_2NMe_2$ (**c**), los nuevos compuestos **1b**, **1c** y **2c** fueron sintetizados y caracterizados. Los complejos **1b** y **1c** fueron también caracterizados mediante cristalografía de rayos-X. La evaluación de la citotoxicidad de complejos cicloplatinados de siete miembros **1** (**1a**-**1c**) y **2** (**2a**-**2c**) sobre un panel de células humanas de adenocarcinoma (A549 de pulmón, HCT116 de colon y MDA-MB231 de mama) reveló que los seis complejos cicloplatinados exhiben una destacable actividad antiproliferativa, mayor aún que la del cisplatino, en las tres líneas celulares. Desde un punto de vista farmacológico, los compuestos cicloplatinados **1** (**1a**-**1c**) y **2** (**2a**-**2c**) pueden representar compuestos con potencial para desarrollar una nueva clase de drogas antitumorales. Estudios de migración electroforética del ADN demuestran que todos los compuestos modifican la estructura ternaria del DNA. La inducción de una parada del ciclo celular en las fases S y G2/M y de apoptosis también fueron evaluadas en un compuesto representativo (**1c**) de la serie.

European Journal of Medicinal Chemistry 54 (2012) 557–566

Contents lists available at SciVerse ScienceDirect

European Journal of Medicinal Chemistry

journal homepage: http://www.elsevier.com/locate/ejmech

Original article

Seven-membered cycloplatinated complexes as a new family of anticancer agents. X-ray characterization and preliminary biological studies

Roldán Cortés [a], Margarita Crespo [b,*], Laia Davin [b], Raquel Martín [b], Josefina Quirante [c,*], Daniel Ruiz [c], Ramon Messeguer [d], Carme Calvis [d], Laura Baldomà [e], Josefa Badia [e], Mercè Font-Bardía [f,g], Teresa Calvet [f], Marta Cascante [a]

[a] Department of Biochemistry and Molecular Biology, Faculty of Biology, Institute of Biomedicine of University of Barcelona (IBUB) and IDIBAPS, Unit Associated with CSIC, Diagonal 643, 08028 Barcelona, Spain
[b] Departament de Química Inorgànica and Institut de Biomedicina, (IBUB), Facultat de Química, Universitat de Barcelona, Diagonal 645, 08028 Barcelona, Spain
[c] Laboratori de Química Orgànica, Facultat de Farmàcia, Institut de Biomedicina, (IBUB), Universitat de Barcelona, Av. Joan XXIII s/n, 08028 Barcelona, Spain
[d] Biomed Division LEITAT Technological Center, Parc Científic de Barcelona, Edifici Hèlix, C/Baldiri Reixach, 15-21, 08028 Barcelona, Spain
[e] Departament de Bioquímica i Biologia Molecular, Facultat de Farmàcia, Institut de Biomedicina de la Universitat de Barcelona (IBUB), Av. Joan XXIII s/n, 08028 Barcelona, Spain
[f] Departament de Cristal·lografia, Mineralogia i Dipòsits Minerals, Facultat de Geologia, Universitat de Barcelona, Martí i Franquès s/n, 08028 Barcelona, Spain
[g] Unitat de Difracció de Raigs-X, Centre Científic i Tecnològic de la Universitat de Barcelona (CCiTUB), Solé i Sabarís, 1-3, 08028 Barcelona, Spain

ARTICLE INFO

Article history:
Received 13 February 2012
Received in revised form
10 May 2012
Accepted 2 June 2012
Available online 12 June 2012

Keywords:
Platinum(II)
Cyclometallated compounds
Seven-membered platinacycles
Cancer
Cytotoxicity
Anticancer drugs

ABSTRACT

A series of seven-membered cyclometallated Pt(II) complexes containing a terdentate [C,N,N′] ligand (**1a**–**1c** and **2a**–**2c**) have been developed as potential monofunctional DNA binding agents. By reactions of *cis*-[Pt(4-$C_6H_4Me)_2(\mu$-$SEt_2)]_2$ or *cis*-[$Pt(C_6H_5)_2(SMe_2)_2$] with imines 2-$ClC_6H_4CH{=}NCH_2CH_2NMe_2$ (**b**) or 2-F,6-$ClC_6H_3CH{=}NCH_2CH_2NMe_2$ (**c**) the new compounds **1b**, **1c** and **2c** were synthesized and characterized. Complex **1b** and **1c** were further characterized by X-ray crystallography. The cytotoxicity assessment of the seven-membered platinacycles **1** (**1a**–**1c**) and **2** (**2a**–**2c**) against a panel of human cancer cell lines (A549 lung, HCT116 colon, and MDA MB231 breast adenocarcinomas) revealed that the six cycloplatinated complexes exhibit a remarkable antiproliferative activity, even greater than cisplatin in the three human cancer cell lines. From a pharmacological point of view, platinacycles **1** (**1a**–**1c**) and **2** (**2a**–**2c**) may represent compounds for a new class of antitumor drugs. Electrophoretic DNA migration studies showed that all of them modify the DNA tertiary structure. Induction of S-G2/M arrest and apoptosis were also observed for one of the representative compounds (**1c**) of the series.

1. Introduction

Since the discovery by Rosenberg that *cis*-[$PtCl_2(NH_3)_2$] (cisplatin) inhibits cell division [1] the search for new and effective chemotherapeutic agents with anticancer properties has led to tremendous activity. Over the last three decades thousands of Pt-containing compounds have been designed and tested [2,3], but just a few of them have entered clinical use (carboplatin, oxaliplatin and nedaplatin) or are in clinical trials [4]. Despite the therapeutic benefit of the approved platinum drug, the efficacy of the treatments is still limited due to side effects [5,6] and intrinsic and acquired resistances [7].

Recent advances in the knowledge of how cisplatin induces its antitumor effects and how tumours are or become resistant [8–10], have contributed to a renewed interest [11] in the development of a cisplatin based therapy safer to patients, providing oral bioavailability and able to overcome drug resistance. It is believed that DNA is the main target of platinum drug and that cisplatin and its analogues form an intrastrand d(GpG) adduct with platinum cross-linking N7 atoms of neighbour guanine residues of DNA [8,9,12]. It has been also shown that carrier amine ligands of cisplatin analogues appear to modulate the antitumor properties of this class of drugs [2]. There are many possible roles for the carrier ligand of

Abbreviations: CDDP, *cis*-diamminedichloroplatinum(II), cisplatin; DMEM, Dulbecco's Modified Eagle Medium; MTT, 3-(4,5-Dimethylthiazol-2-yl)-2,5-diphenyltetrazolium bromide; FACS, Fluorescence-Activated Cell Sorting; FITC, Fluorescein Isothiocyanate; PI, Propidium Iodide; PS, Phosphatidylserine.

* Corresponding authors. Tel.: +34 934039132; fax: +34 934907725.
E-mail addresses: margarita.crespo@qi.ub.es (M. Crespo), quirantese@ub.edu (J. Quirante).

0223-5234/$ – see front matter © 2012 Elsevier Masson SAS. All rights reserved.
http://dx.doi.org/10.1016/j.ejmech.2012.06.002

the platinum anticancer compounds, such as affect pharmacokinetics, rates and type of DNA adduct formation, influence on the recognition of damaged DNA by repair enzymes or regulatory/binding proteins [13]. Subsequently, *cis*- and *trans*-$[Pt(L)_2Cl_2]$ complexes have been prepared with a wide variety of ligands, where L = pyridine and picoline derivatives [14,15], pyrazole [16,17], benzimidazole [18], purine derivatives [19,20] and many others. On the other hand, cyclometalating N-donor ligands may offer an alternative approach to give structures quite different from that of cisplatin and analogs with the possibility that those could interact in a different way with DNA, and consequently show a different spectrum of activity and toxicity profile.

Cyclometallated compounds containing not only Pd(II) and Pt(II), but also Ru(II), Ir(III), Rh(III) and Au(III), have revealed promising anticancerous activities [21–32]. It is noteworthy that the presence of a metal-carbon σ-bond appears to increase the stability of the complexes, and therefore the cyclometallated complexes would be more likely to reach their biological target intact [33]. The cytotoxicities of several platinum compounds containing bidentate [C,N] cyclometallated ligands such as 2-(dimethylaminomethyl)phenyl [34], 2-phenylpyridine, 2-phenylpyrazole, and analogues [35–39] or terdentate [C,N,N] ligands such as 6-phenyl-2,2′-bipyridine [40,41] have been studied. In all reported cases, the platinacycle is a planar five-membered ring.

We have been involved recently in the synthesis of a novel class of seven-membered platinacycles [42,43] and the lack of information on the biological activity of these compounds prompted us to undertake the present study. On the other hand it has been reported for chelated diamines that 1,4-butanediamine complex (seven-membered rings) show greater antiproliferative activity than 1,2-ethanediamine complex (five-membered rings) and 1,3-propanediamine complex (six-membered rings) [44–46], in front of L1210 cell line. Hence we want to compare the behaviour of the seven-membered platinacycles investigated in this study with the five-membered cyclometallated complexes previously reported [33–41].

Compound **1a** (Scheme 1) containing a terdentate [C,N,N′] cyclometallated ligand and a seven-membered platinacycle has been prepared from the reaction of ligand 2,6-$Cl_2C_6H_3CH{=}NCH_2CH_2NMe_2$ (**a**) and *cis*-$[Pt(4\text{-}C_6H_4Me)_2(\mu\text{-}SEt_2)]_2$ [43].Compounds **2a** and **2b** (Scheme 1) have been previously prepared from the reactions of *cis*-$[Pt(C_6H_5)_2(SMe_2)_2]$ with imines 2,6-$Cl_2C_6H_3CH{=}NCH_2CH_2NMe_2$ (**a**) and 2-$ClC_6H_4CH{=}NCH_2CH_2NMe_2$ (**b**), respectively [42]. Preliminary biological studies suggested a high activity for the synthesized seven-membered platinacycles and therefore, the synthesis of new compounds **1b**, **1c** and **2c** (Scheme 1) was envisaged and it was undertaken in this study. In all cases our strategy has been the use of terdentate, cyclometallated ligands to form stable seven-membered cycloplatinated complexes. The square planar coordination around the platinum of compounds **1** (**1a**–**1c**) and **2** (**2a**–**2c**) contains always a strong platinum-carbon σ bond *cis* to a non-labile imine function and two mutually *cis* labile positions, the chloro ligand and the amine fragment. Platinacycles **1** (**1a**–**1c**) and **2** (**2a**–**2c**) differ from one another in the nature of the substituents R_1 (H, F, Cl), and R_2 (H, CH_3) in order to evaluate how the modifications in the physico-chemical properties of the molecules (hydrophobicity, steric hindrance or binding capabilities [47]), provided by the substituents, influence the antiproliferative activity of these complexes. The cytotoxicity effectiveness of complexes **1** (**1a**–**1c**) and **2** (**2a**–**2c**) was evaluated in A549 lung, MDA MB231 breast and HCT116 colon human cancer cell lines. To gain insight into the action mechanism of the investigated complexes, studies of electrophoretic shift DNA-migration, cell cycle arrest and apoptosis were performed.

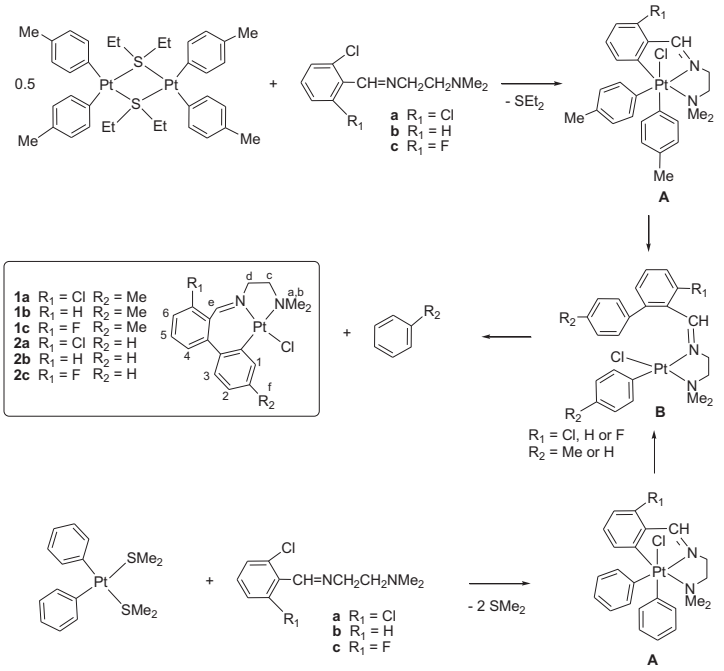

Scheme 1. Synthesis of compounds **1a** [43], **2a** and **2b** [42], **1b**, **1c** and **2c** [this work].

2. Results and discussion

2.1. Preparation of the compounds

2.1.1. Synthesis and characterization of compounds *1b*, *1c* and *2c*

Following the previously reported procedures for compounds **1a**, **2a** and **2b** [41,42], the reactions of *cis*-[Pt(4-$C_6H_4Me)_2(\mu$-$SEt_2)]_2$ with ligands2-$ClC_6H_4CH{=}NCH_2CH_2NMe_2$ (**b**), and 2-Cl,6-$FC_6H_3CH{=}NCH_2CH_2NMe_2$ (**c**) were carried out in toluene under reflux for 4 h and produced respectively compounds [PtCl{$(MeC_6H_3)(C_6H_4CHNCH_2CH_2NMe_2$}] (**1b**) and [PtCl{$(MeC_6H_3)(FC_6H_3CHNCH_2CH_2NMe_2$}] (**1c**) (Scheme 1). An analogous reaction carried out using *cis*-$[Pt(C_6H_5)_2(SMe_2)_2]$ and imine **c** produced compound [PtCl{$(C_6H_4)(FC_6H_3CHNCH_2CH_2NMe_2$}] (**2c**). In these synthetical procedures, intramolecular activation of one *ortho* C—Cl bond of the ligand to produce platinum(IV) intermediate **A** is followed by a reductive elimination process to produce intermediate **B** and by a final cyclometallation step with release of one arene molecule. The proposed structures, shown in Scheme 1, contain a terdentate [C,N,N′] ligand and a seven-membered platinacycle arising from formation of a C—C bond between the aryl ring of the ligand and either a phenyl or a *para*-tolyl ligand. In order to produce the required platinum(IV) intermediates **A**, ligands containing at least one *ortho* C—Cl bond as well as diarylplatinum(II) substrates, without substituents that might hamper the intramolecular oxidative addition process, are needed in this synthetic method. These requirements limit the choice of substituents R_1 and R_2 in the reported compounds.

The new compounds were characterised by elemental analyses, ESI mass spectra and NMR spectroscopy, and compounds **1b** and **1c** were also characterised crystallographically. NMR data are in good agreement to those reported for analogous compounds [42,43].

2.1.2. Crystal structures

Suitable crystals of compounds **1b** and **1c** were grown from dichloromethane-methanol at room temperature.

The crystal structures are composed of discrete molecules separated by van der Waals distances. The structure of **1b** consists in the packing in the asymmetric unit of two independent molecules with bond parameters equal within experimental error [3σ]. Compound **1c** crystallises as the hydrate **1c**·$0.5H_2O$. The structures are shown in Fig. 1 and selected molecular dimensions are listed in Table 1.

The molecular structures confirm the geometries predicted from spectroscopic data and are similar to that reported for **1a**. Square-planar coordination of the platinum(II) is achieved with a terdentate [C,N,N′] and a chloro ligand. The metallacycle consists in a non-planar seven-membered system in which the imine functionality and two aryl rings tilted 54.2(5)° (**1b**) or 50.6(3)° (**1c**) from each other are included. These values are similar to these

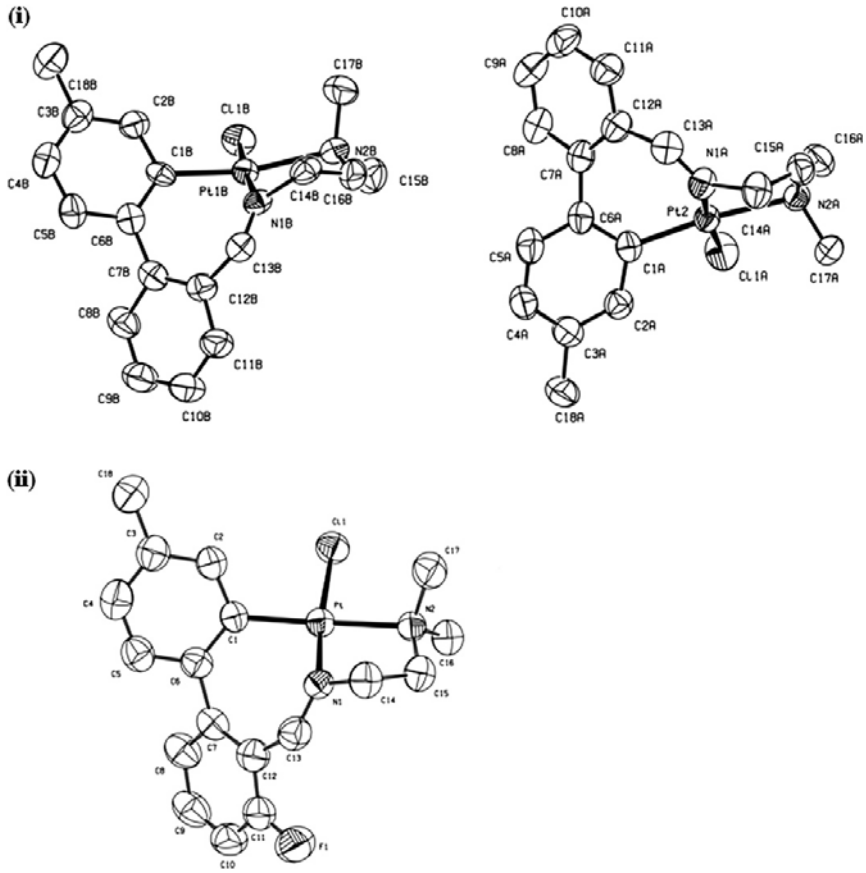

Fig. 1. (i) Molecular structure of compound **1b**. (ii) Molecular structure of compound **1c**.

Table 1
Selected bond lengths (Å) and angles (deg.) for compounds **1b** and **1c** with estimated standard deviations.

Compound **1b** (molecule 1)		Compound **1c**	
Pt(1)–N(1)	1.983(6)	Pt–N(1)	1.935(4)
Pt(1)–C(1)	2.014(8)	Pt–C(1)	2.024(4)
Pt(1)–N(2)	2.189(8)	Pt–N(2)	2.187(4)
Pt–Cl(1)	2.307(3)	Pt–Cl(1)	2.3087(14)
N(1)–Pt(1)–C(1)	92.5(3)	N(1)–Pt–C(1)	92.48(17)
N(1)–Pt–N(2)	82.5(3)	N(1)–Pt–N(2)	81.99(15)
C(1)–Pt–Cl(1)	92.4(2)	C(1)–Pt–Cl(1)	93.68(13)
N(2)–Pt–Cl(1)	93.4(2)	N(2)–Pt–Cl(1)	91.66(11)

found for compound **1a** (50.6(2)°) [43]. No interactions (either inter o intramolecular) involving the fluorine substituent were detected for **1c**.

Bond lengths and angles are well within the range of values obtained for analogous compounds. In particular, the Pt–C and Pt–Cl bonds distances are in the range found for analogous complexes of platinum (II) and the platinum-amine distances are larger than platinum-imine distances consistent with the weaker ligating ability of amines for platinum. Most bond angles at platinum are close to the ideal value of 90°, and the smallest angles correspond to the chelate N–Pt–N bite angle.

2.2. Biological studies

2.2.1. Antiproliferative assay

Compounds **1** (**1a**–**1c**) and **2** (**2a**–**2c**) were evaluated in vitro by testing for inhibition of cell proliferation activity against human lung, breast and colon cancer cell lines (A549, MDA MB231 and HCT116, respectively), using cisplatin as a positive control.

The effects of the assayed platinacycles on the growth of the selected cell lines were evaluated after 72 h and the obtained IC_{50} values are listed in Table 2. It can be seen from Table 2 that compounds **1** (**1a**–**1c**) and **2** (**2a**–**2c**) exhibit a great antiproliferative activity, showing little differences in their cytotoxic effectiveness and lower IC_{50} values than cisplatin itself in the three cellular lines. Platinacycle **1c** exhibited the lowest IC_{50} values, being approximately 4-fold more potent than cisplatin in A549 lung cancer cells, 6-fold more potent than cisplatin in MDA MB231 breast cancer cells, and 40-fold more potent than cisplatin in HCT116 colon cancer cells (Fig. 2).

Compounds **1** (**1a**–**1c**) contain a methyl group at R_2 in order to evaluate the shift in cytotoxicity with regard to the unsubstituted complexes **2** (**2a**–**2c**). It has been reported for five-membered cycloplatinated complexes that the substitution around the periphery of the aromatic ligand gives rise to significant antitumor activity [33]. A methyl substituent for instance may provide a steric barrier to dislodgement of an intercalated cyclometallated complex, accounting for the observed increase in activity. However, no increase in potency is observed when compounds **2** (**2a**–**2c**) (R_2=H) are compared with compounds **1** (**1a**–**1c**) (R_2=CH_3) in pairs: **1a**–**2a**, **1b**–**2b**, and **1c**–**2c**. Actually, there is a decrease in potency in the methylated compound **1a** with regard to the demethylated compound **2a** in the HCT116 colon and MDA MB231 breast cancer cell lines.

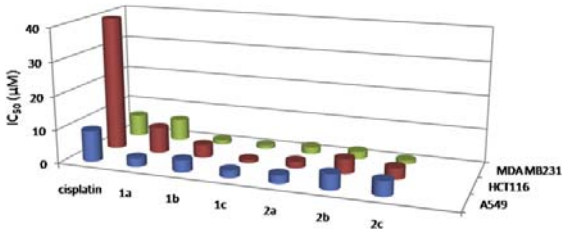

Fig. 2. Cytotoxicity of complexes **1** (**1a**–**1c**), **2** (**2a**–**2c**) and cisplatin (IC_{50} μM) against A549 lung, HCT-116 colon and MDA-MB231 breast human cancer cell lines.

While five-membered metallacycles are often planar and therefore able to intercalate into DNA [33], the seven-membered metallacycles studied in the present work are not planar. As stated in section 2.1.2, the tilt angle between both aryl rings contained in the seven-membered ring is in the range 50.6–54.2°. In addition, deviation from the planarity is also observed for the five-membered chelate formed upon coordination of both nitrogen atoms to the platinum as deduced from the sum of the internal angles of the chelate (511.0° for **1b** and 513.6° for **1c**) [48].

clog *P* Value is an important lipophilic parameter associated with prediction of drug-like physical properties in ADME models. In order to study the influence of the lipophilicity of the synthesized complexes, provided by the substituents at R_1 (H, F, Cl) and R_2 (H, Me) on the inhibition of cell growth proliferation, the clog *P* values of the platinacycles **1** (**1a**–**1c**) and **2** (**2a**–**2c**) were calculated. The obtained values of clog *P* fall in the range 4.65–5.72 and are depicted in Table 3. No correlation between the clog *P* values and the cytotoxic effectiveness of the synthesized complexes has been observed in the three cellular lines.

The effect of fluorination on acidity, basicity or functional group hydrogen bonding still remains controversial [47]. Hydrogen bond to F-atom are weaker than those to other heteroatoms, but they could be observed in structures like the synthesized complexes **1c** and **2c** which lack other heteroatoms (O, N) that would compete for the hydrogen bonds.

Table 2
Cytotoxic activities on A549 lung, HCT-116 colon and MDA-MB231 breast human cancer cell lines for the platinacycles **1** (**1a**–**1c**) and **2** (**2a**–**2c**) and cisplatin. Data are shown as the mean values of two or more experiments performed in triplicate with the corresponding standard deviation (SD).

	IC_{50} values (μM)		
	Cell line		
Complex	A549	HCT116	MDA MB231
1a	2.6 ± 0.1	7.7 ± 0.9	6.3 ± 1.0
1b	3.6 ± 0.1	3.9 ± 0.2	1.3 ± 0.3
1c	2.2 ± 0.5	0.95 ± 0.2	1.1 ± 0.2
2a	2.6 ± 0.1	2.0 ± 0.4	2.0 ± 0.2
2b	4.6 ± 1.4	4.3 ± 0.3	2.2 ± 0.5
2c	4.4 ± 0.1	3.4 ± 0.5	1.1 ± 0.2
Cisplatin	9.3 ± 3.0	40 ± 4.40	6.5 ± 2.4

Table 3
clog *P* of platinacycles **1** (**1a**–**1c**) and **2** (**2a**–**2c**) and cisplatin.

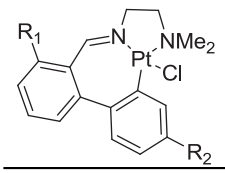

Complex	R_1	R_2	Clog *P*[a]
1a	Cl	Me	5.72
1b	H	Me	5.01
1c	F	Me	5.15
2a	Cl	H	5.22
2b	H	H	4.51
2c	F	H	4.65
Cisplatin			−2.5

[a] clog *P* is the calculated logarithmic value of the *n*-octanol/water partition coefficient, and was calculated using the computer program ChemBioDraw Ultra 12.0 (ChemBioOffice 2010).

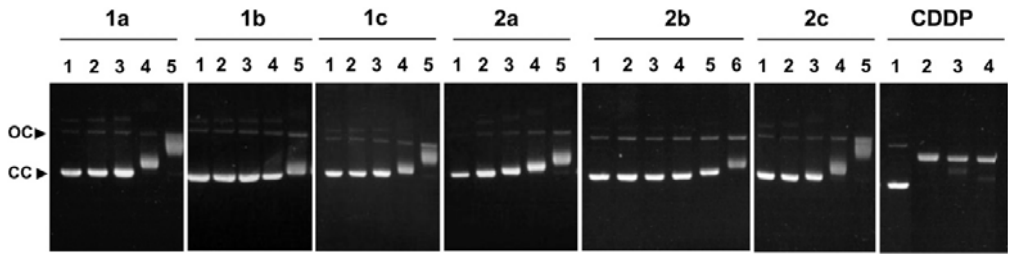

Fig. 3. Interaction of pBluescript SK + plasmid DNA (40 μg/ml) with increasing concentrations of the indicated compounds. Lanes 1, DNA only; lanes 2, 10 μM drug; lanes 3, 25 μM drug, lanes 4, 50 μM drug; lanes 5, 100 μM drug; and lane 6, 200 μM drug. Unwinding assay with cisplatin (CDDP) was performed for comparison. ccc, supercoiled closed circular DNA form; oc, open circular DNA form.

In spite of the IC_{50} values of the compounds **1** (**1a**–**1c**) and **2** (**2a**–**2c**) being extremely close, in MDA MB231 breast and HCT116 colon cancer cell lines a six- to eight-fold increase in potency respectively was observed for the fluorinated complex **1c** (R_1=F, R_2=Me) with regard to the chlorinated complex **1a** (R_1=Cl, R_2=Me), and a four-fold increase in HCT116 colon cancer cell line with regard to the non-halogenated compound **1b** (R_1=H, R_2=Me). However, the above mentioned increase in potency was not observed for the fluorinated compound **2c** (R_1=F, R_2=H) with regard to the chlorinated compound **2a** (R_1=Cl, R_2=H) and the non-halogenated compound **2b** (R_1=H, R_2=H).

2.2.2. DNA migration studies

The effect of binding of the compounds investigated in this study on supercoiled DNA was determined by their ability to alter the electrophoretic mobility of pBluescript plasmid DNA: supercoiled closed circular (ccc) and open circular (oc) forms.

Fig. 3 shows the electrophoretic mobility of native pBluescript DNA incubated with the synthesized compounds (**1a**–**c**, **2a**–**c**) at increasing amounts ranging from 10 μM to 100 μM. Compound **2b** was also analysed at 200 μM concentration. To provide a basis for comparison, incubation of DNA with cisplatin (CDDP) was also performed. As expected, cisplatin greatly altered the electrophoretic mobility of pBluescript DNA at all concentrations tested.

At concentrations up to 25 μM none of the assayed compounds produced a significant effect on the electrophoretic mobility of native pBluescript DNA. At this concentration, the rate of migration of the supercoiled closed circular form was only slightly decreased by compound **2a**. Compounds with R_1=Cl or F (**1a**, **1c**, **2a**, **2c**) greatly alter the mobility of plasmid DNA at 50 μM and 100 μM. At these concentrations, the rate of migration of supercoiled band (ccc) decreases and tends to approach to that of the nicked relaxed band (oc). Compounds containing H in position R_1 (**1b** and **2b**) displayed a lower effect on plasmid DNA mobility. Significant

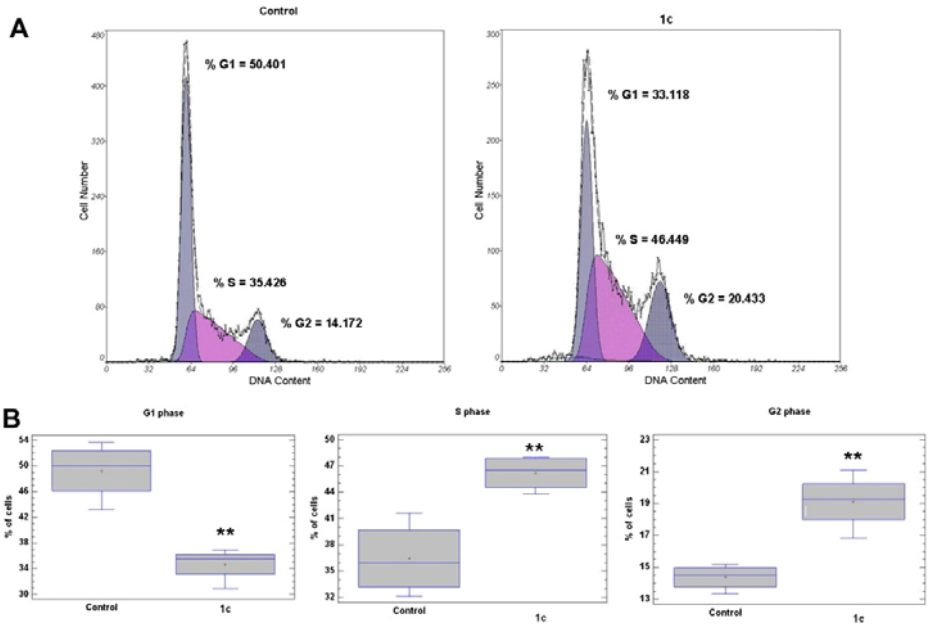

Fig. 4. A: Cell cycle analysis of A549 cells untreated (Control) or treated with **1c** at a concentration equal to its IC_{50} value (2.2 μM) for 72 h. The harvested cells were stained with PI and their DNA content analysed by flow cytometry. These histograms are from one out of three representative experiments. B: Box and whisker plot depicting the variation of the percentage of cells in each phase of the cell cycle.

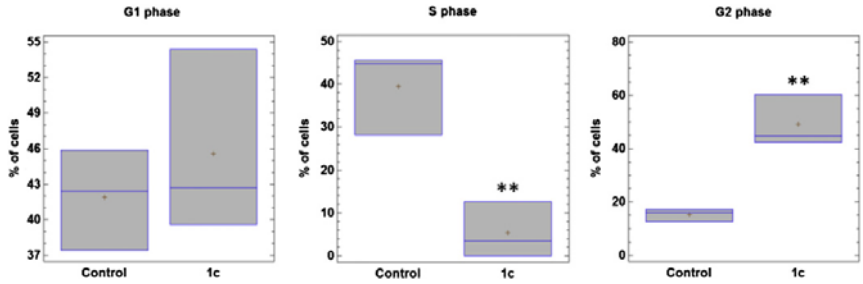

Fig. 5. Box and whisker plot depicting the variation of the percentage of VA13 cells in each phase of the cell cycle after treatment with 2.2 μM **1c**.

changes in the rate of migration of supercoiled band were observed at 100 μM for compound **1b** and at 200 μM for **2b**.

It is worth mentioning that compounds with hydrogen or a methyl group at position R_2 but with the same substituent at position R_1 (H, F, Cl) displayed similar effects on plasmid DNA mobility. Thus, in the pairs **1a**–**2a**, **1b**–**2b**, and **1c**–**2c** the shift on the DNA electrophoretic mobility is very similar.

In summary, these results indicated that all the compounds investigated in this study alter the electrophoretic mobility of pBluescript plasmid DNA and hence all of them interact with DNA as the standard reference, cisplatin. Compounds with R_1=Cl or F (**1a**, **1c**, **2a** and **2c**) have a greater effect on plasmid DNA mobility, which is in agreement with their low IC_{50} values. However compounds **1b** and **2b**, with similar IC_{50} values, showed a weak effect on DNA electrophoresis. These results underscore the importance of additional factors in predicting anticancer activity.

2.2.3. *Effect of compound **1c** on cell cycle distribution*

It is well known that one of the main hallmarks of cancer cells is cell cycle dysregulation, and proteins controlling critical events of the cell cycle have been proposed as useful antitumor targets [49–51]. To study the effect of **1c** at a concentration equal to its IC_{50} value on the cell cycle distribution, A549 tumoral cells were treated with the compound for 72 h and then analysed by FACS.

The cell cycle is typically divided into mitosis and interphase, which on turn consists on different phases: quiescent and gap 1 (G0/G1 phase), synthesis (S phase) and gap 2 (G2 phase). As shown in Fig. 4, treatment with compound **1c** provokes a redistribution of the percentage of the cells in each of the cell cycle phases. Specifically, after 72 h of incubation with 2.2 μM **1c**, significant increases in the population at the S and G2 phases were observed (after treatment with **1c**, the number of cells in phases S and G2 increased respectively by 27% and 33% with regard to the untreated controls), with a concomitant decrease of around 30% in the percentage of cells at the G0/G1 phase. The results are concordant with several examples in the literature about platinum compounds provoking arrest in S and G2 phases of the cell cycle [52–54]. Since these results highlight the cytostatic effect of compound **1c** on A549 lung cancer cells, we performed the cell cycle assay on VA13 human fibroblast non-tumoral cells, in order to see if there were any differences in its behaviour. As shown in Fig. 5, treatment with 2.2 μM **1c** also affects the distribution of VA13 cells in each of the cell cycle phases, although differently: whereas the percentage of cells in G2 phase is also increased, the number of cells in S phase decreases, while the distribution of cells in G0/G1 phase remains stable.

2.2.4. *Effect of compound **1c** on apoptosis induction*

Since cell cycle arrest may sometimes lead to apoptosis, in the next series of experiments we analysed whether necrosis or apoptosis was involved in the mechanism of action of complex **1c**. In the earlier events of the apoptotic process, plasma membrane asymmetry is lost, accompanied by PS translocation from the inner to the outer membrane [55]. Thus, PS is exposed to the external environment and can bind to the annexin V-FITC conjugate, to which PS has a high affinity for [55,56]. On the latest stages of the apoptotic process, as well as in necrotic processes, cell membranes lose their integrity, allowing PI to access the nucleus and intercalate between the DNA bases. FACS analysis using both annexin V-FITC staining and PI accumulation was used to differentiate non-apoptotic cells (annexin V^- and PI^-) from early apoptotic (annexin V^+ and PI^-) and necrotic or late apoptotic (PI^+) cells.

As seen on Fig. 6, treatment of A549 cells with 2.2 μM **1c** for 72 h generated early apoptosis in 6.2% of the cells, as compared to the 2.5% of the early apoptotic cells in the untreated controls. In spite of this difference, the results suggest **1c** exercises its antiproliferative effect mostly through cell cycle arrest.

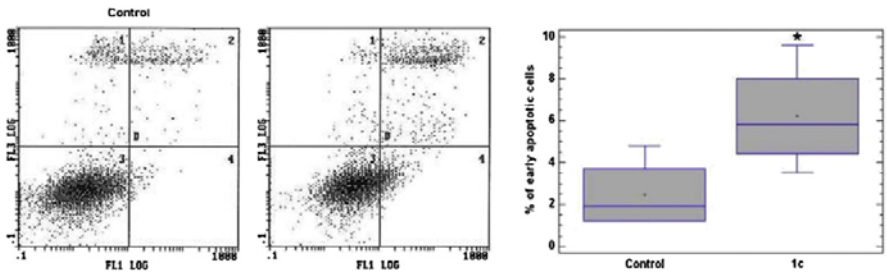

Fig. 6. A: Representative flow cytometric plots for the quantification of apoptosis in A549 cells untreated (Control) or treated with **1c** at a concentration equal to its IC_{50} value (2.2 μM) for 72 h. Quadrant 4 (annexin V^+ and PI^-) represents early apoptotic cells. B: Box and whisker plot depicting the variation of the percentage of cells in early apoptosis.

Table 4
Crystallographic and refinement data for compounds **1b** and **1c**.

	Compound **1b**	Compound **1c**
Formula	$C_{18}H_{21}ClN_2Pt$	$2C_{18}H_{20}ClFN_2Pt\cdot H_2O$
Fw	495.91	1045.82
Temp, K	293(2)	293(2)
Wavelength, Å	0.71073	0.71073
Crystal system	Monoclinic	Monoclinic
Space group	$P2_1/c$	$P2_1/c$
a, Å	14.154(5)	12.349(2)
b, Å	16.039(5)	12.248(5)
c, Å	18.354(17)	12.025(4)
α, deg	90	90
β, deg	124.39(5)	100.83(2)
γ, deg	90	90
V, Å^3; Z	3438(4); 8	1786.4(10); 2
d (calcd), Mg/m^3	1.916	1.944
Abs coeff, mm^{-1}	8.315	8.017
F(000)	1904	1004
rflns coll./unique	35,336/10,529 [*R*(int) = 0.0519]	16,540/5014 [*R*(int) = 0.0525]
Data/restraints/parameters	10,529/0/404	6114/2/236
GOF on F^2	1.113	1.132
$R_1(I > 2\sigma(I))$	0.0603	0.0370
wR_2 (all data)	0.1738	0.1056
Peak and hole, e.Å^{-3}	4.699 and −3.315	2.150 and −1.227

3. Conclusions

Six cyclometallated platinum(II) compounds containing a novel framework have been tested as a new class of antitumour drugs. Complexes **1b**, **1c** and **2c** were synthesized in this work and characterized by spectral and elemental analysis. The molecular structures of the compounds **1b** and **1c** confirmed by X-ray analysis indicated a non-planar arrangement for both the seven-membered metallacycle and the five-membered chelate ring. Cytotoxicity studies revealed the high effectiveness of compounds **1** (**1a**–**1c**) and **2** (**2a**–**2c**) against human lung carcinoma, breast and colon cancer cell lines (A549, MDA MB231 and HCT116 respectively). All of them exhibited IC_{50} values lower than cisplatin, which was used as a positive control. Complex **1c** was found to inhibit cell growth proliferation at the level four times higher (A549 lung cancer cells), six times higher (MDA MB231 breast cancer cells) and 40 times higher (colon HCT116 cancer cells) to that of cisplatin. The behaviour observed for the electrophoretic mobility of complexes **1** (**1a**–**1c**) and **2** (**2a**–**2c**) indicates alteration of the degree of superhelicity of the DNA molecules, in a similar way than cisplatin. As a representative complex of the series, platinacycle **1c** was found to suppress A549 lung cancer cell growth through cell cycle arrest and, in a lesser way, apoptosis. Further studies on seven-membered cycloplatinacycles are in progress for both understanding structure–activity relationships and developing prospective pharmaceutics.

4. Experimental

4.1. Chemistry

General. Microanalyses were performed at the *Serveis Cientifico-Tècnics (Universitat de Barcelona).* Electrospray mass spectra were performed at the *Servei d'Espectrometria de Masses (Universitat de Barcelona)* in an LC/MSD-TOF spectrometer using H_2O–CH_3CN 1:1 to introduce the sample. NMR spectra were performed at the *Unitat de RMN d'Alt Camp de la Universitat de Barcelona* using a Mercury-400 (^{1}H, 400 MHz; ^{19}F, 376.5 MHz) spectrometer, and referenced to $SiMe_4$ (^{1}H) and $CFCl_3$ (^{19}F). δ values are given in ppm and *J* values in Hz. Abbreviations used: s = singlet; d = doublet; t = triplet; m = multiplet; br = broad; NMR labelling as shown in Scheme 1.

4.1.1. Preparation of the complexes

The synthesis of compounds **1a**, **2a** and **2b** was previously reported [42,43], *cis*-$[Pt(C_6H_5)_2(SMe_2)_2]$ [57,58], *cis*-$[Pt(4\text{-}C_6H_4CH_3)_2(\mu\text{-}SEt_2)]_2$ [59] and ligands **b** and **c** [60] were prepared as reported elsewhere.

*4.1.1.1. [PtCl{(MeC$_6$H$_3$)(C$_6$H$_4$CHNCH$_2$CH$_2$NMe$_2$}] (**1b**).* Compound (**1b**) was obtained from 200 mg (0.21 mmol) of compound *cis*-$[Pt(4\text{-}C_6H_4CH_3)_2(\mu\text{-}SEt_2)]_2$ and 90 mg of imine **b** after reaction in refluxing toluene for 4 h. The solvent was removed and the residue was treated with ether to produce a solid which was filtered and dried *in vacuo*. Yield 121 mg (58%). ^{1}H NMR (400 MHz, $CDCl_3$): δ = 8.77 [s, ^3J(Pt-H) = 148.0, 1H, H^e]; 7.60 [td, *J*(H-H) = 7.6 and 1.6, 1H]; 7.47 [d, ^3J(H-H) = 7.2, 1H]; 7.33 [t, ^3J(H-H) = 7.6, 1H]; 7.29 [m, 1H]; 7.22 [s, 1H]; 6.84–6.80 [m, 2H]; 4.44 [td, *J*(H-H) = 12.0 and 4.0, 1H, H^d]; 3.85 [dd, ^2J(H-H) = 12.0, *J*(H-H) = 3.0, 1H, H^d]; 2.98 [s, 3H, H^a]; 2.70 [s, 3H, H^b]; 2.60 [m, 2H, H^c]; 2.31 [s, 3H, H^f]. ESI-MS, *m*/*z*: 497.11 [M + H]$^+$; 460.14 [M-Cl]$^+$. Anal. Found (calc. for $C_{18}H_{21}ClN_2Pt$): C: 43.1 (43.60); H: 4.3 (4.27); N: 5.8 (5.65).

*4.1.1.2. [PtCl{(MeC$_6$H$_3$)(C$_6$H$_3$FCHNCH$_2$CH$_2$NMe$_2$}] (**1c**).* Compound (**1c**) was obtained from 200 mg (0.21 mmol) of compound *cis*-$[Pt(4\text{-}C_6H_4CH_3)_2(\mu\text{-}SEt_2)]_2$ and 96 mg of imine **c** after reaction in refluxing toluene for 4 h. The solvent was removed and the residue was treated with ether to produce a solid which was filtered and dried *in vacuo*. Yield 137 mg (63%). ^{1}H NMR (400 MHz, $CDCl_3$): δ = 9.10 [s, ^3J(Pt-H) = 148.0, 1H, H^e]; 7.55 [td, ^3J(H-H) = 8.0, *J*(H-F) = 6.0, 1H, H^5]; 7.46 [d, *J*(H-H) = 1.6, 1H, H^1]; 7.25 [d, ^3J(H-H) = 8.0, 1H, H^4]; 7.02 [ddd, *J*(H-F) = 10.4, *J*(H-H) = 8.0 and 1.0, 1H, H^6]; 6.87 [d, ^3J(H-H) = 8.0, 1H, H^3]; 6.80 [dd, *J*(H-H) = 8.0 and 1.6, 1H, H^2]; 4.50 [td, *J*(H-H) = 12.0 and 4.0, 1H, H^d]; 3.92 [dd, *J*(H-H) = 12.0; 3.0, *J*(H-Pt) = 58.0, 1H, H^d]; 3.01 [s, 3H, H^a]; 2.74 [s, 3H, H^b]; 2.64 [m, 2H, H^c]; 2.31 [s, 3H, H^f]. ^{19}F NMR (376.5 MHz, $CDCl_3$): δ = −118.83. ESI-MS, *m*/*z*: 515.10 [M + H]$^+$; 478.13 [M-Cl]$^+$. Anal. Found (calc. for $C_{18}H_{20}ClFN_2Pt$): C: 41.6 (42.07); H: 3.9 (3.92); N: 5.7 (5.45).

*4.1.1.3. [PtCl{(C$_6$H$_4$)(C$_6$H$_3$FCHNCH$_2$CH$_2$NMe$_2$}] (**2c**).* Compound (**2c**) was obtained from 199 mg (0.42 mmol) of compound $[Pt(C_6H_5)_2(SMe_2)_2]$ and 95 mg of imine **c** after reaction in refluxing toluene for 4 h. The solvent was removed and the residue was treated with ether to produce a solid which was filtered and dried *in vacuo*. Yield 147 mg (70%). ^{1}H NMR (400 MHz, $CDCl_3$): δ = 9.09[s, ^3J(Pt-H) = 148.0, 1H, H^e]; 7.63 [d, ^3J(H-H) = 7.2, 1H]; 7.56 [d, ^3J(H-H) = 8.0, 1H]; 7.25 [d, ^3J(H-H) = 8.0, 1H]; 7.05 [d, ^3J(H-H) = 8.0, 1H]; 7.01 [t, ^3J(H-H) = 8.0, 1H]; 6.96 [m, 2H]; 4.48 [td, *J*(H-H) = 12.0 and 4.0, 1H, H^d]; 3.92 [dd, *J*(H-H) = 12.0 and 4.0, *J*(H-Pt) = 49.2, 1H, H^d]; 3.00 [s, 3H, H^a]; 2.72 [s, 3H, H^b]; 2.66 [m, 1H, H^c]; 2.60 [td, *J*(H-H) = 12.0 and 4.0, 1H, H^c]. ^{19}F NMR (376.5 MHz, $CDCl_3$): δ = −118.68. ESI-MS, *m*/*z*: 501.09 [M + H]$^+$; 464.11 [M − Cl]$^+$. Anal. Found (calc. for $C_{17}H_{18}ClFN_2Pt\cdot H_2O$): C: 39.0 (39.42); H: 3.7 (3.89); N: 4.9 (5.41).

4.1.2. X-ray structure analysis

Prismatic crystals were selected and mounted on a MAR345 diffractometer with an image plate detector. Intensities were collected with graphite monochromatized Mo Kα radiation. The structures were solved by direct methods using SHELXS computer program [61] and refined by the full-matrix least-squares method, with the SHELXL97 computer program using 2 reflections (very negative intensities were not assumed). The function minimized was $\Sigma w\,||Fo|^2 - |Fc|^2|^2$, where $w = [\sigma^2(I) + (0.0912P)^2 + 16.3408P]^{-1}$ (**1b**) and $w = [\sigma^2(I) + (0.0568P)^2 + 0.4527P]^{-1}$ (**1c**) and

$P = (|Fo|^2 + 2|Fc|^2)/3$. f, f' and f'' were taken from International Tables of X-Ray Crystallography [62]. All hydrogen atoms were computed and refined using a riding model with an isotropic temperature factor equal to 1.2 times the equivalent temperature factor of the atom to which they are linked. Further details are given in Table 4.

4.2. Biological studies

4.2.1. Cell culture

Human lung carcinoma A549 cells, colon adenocarcinoma HCT116 cells and MBA MD231 breast cancer cells were grown as a monolayer culture in minimum essential medium (DMEM with L-glutamine, without glucose and without sodium pyruvate) in the presence of 10% heat-inactivated fetal calf serum, 10 mM D-glucose and 0.1% streptomycin/penicillin, in standard culture conditions (humidified air with 5% CO_2 at 37 °C). VA13 lung fibroblast cells were grown as a monolayer culture in MEM in the presence of 10% heat-inactivated fetal calf serum, 1 mM sodium pyruvate and 0.1% streptomycin/penicillin, also in standard culture conditions.

4.2.2. Cell viability assay

For A549 cell viability assays, compounds were suspended in DMSO at 20 mM as stock solution. To obtain final assay concentrations, they were diluted in DMEM (final concentration of DMSO was always lower than 1%). The assay was performed by a variation of the MTT assay described by Mosmann et al. [63] as specified by Matito and coworkers [64], which is based on the ability of live cells to cleave the tetrazolium ring of the MTT thus producing formazan, which absorbs at 550 nm. In brief, 3×10^3 A549 cells/well were cultured in 96 well plates for 24 h prior to the addition of the different compounds at different concentrations, in triplicate. After incubation for 72 h more, the supernatant was aspirated and 100 μL of filtered MTT (0.5 mg/mL) was added to each well. Following 1 h of incubation with the MTT, the supernatant was removed and the precipitated formazan was dissolved in 100 μL DMSO. Relative cell viability, compared to the viability of untreated cells, was measured by absorbance at 550 nm on an ELISA plate reader (Tecan Sunrise MR20-301, TECAN, Salzburg, Austria). Concentrations that inhibited cell growth by 50% (IC_{50}) after 72 h of treatment were subsequently calculated.

For MDA MB231 and HCT116 cell viability assays, compounds were dissolved in 100% DMSO at 50 mM as stock solution; then, serial dilutions have been done in DMSO (1:1) (in this way DMSO concentration in cell media was always the same); finally, 1:500 dilutions of the serial dilutions of compounds on cell media were done. The assay was performed as described by Givens et al. [65]. In brief, HCT116 and MDA MB231 cells were plated at 5000 cells/well, respectively, in 100 μL media in tissue culture 96 well plates (Cultek). After 24 h, media was replaced by 100 μL/well of serial dilution of drugs. Control wells did not contain compounds. Each point concentration was run in triplicate. Reagent blanks, containing media plus colorimetric reagent without cells were run on each plate. Blank values were subtracted from test values and were routinely 5–10% of uninhibited control values. Plates were incubated 72 h. Hexosaminidase activity was measured according to the following protocol: the media containing was removed and cells were washed once with PBS 60 μL of substrate solution (*p*-nitrophenol-*N*-acetyl-β-D-glucosamide 7.5 mM [Sigma N-9376], sodium citrate 0.1 M, pH 5.0, 0.25% Triton X-100) was added to each well and incubated at 37 °C for 1–2 h; after this incubation time, a bright yellow appears; then, plates could be developed by adding 90 μL of developer solution (Glycine 50 mM, pH 10.4; EDTA 5 mM), and absorbance was recorded at 410 nm.

4.2.3. DNA migration studies

Compounds were dissolved in high purity DMSO at 10 mM as stock solution. Then, serial dilutions were made in milliQ water (1:1). Plasmid pBluescript SK+ (Stratagene) was obtained using a QIAGEN plasmid midi kit as described by the manufacturer. Interaction of drugs with pBluescript SK + plasmid DNA was analysed by agarose gel electrophoresis following a modification of the method described by Abdullah et al. [66]. In brief, plasmid DNA aliquots (40 μg mL^{-1}) were incubated in TE buffer (10 mM Tris–HCl, 1 mM EDTA, pH 7.5) with different concentrations of the compounds (ranging from 0 μM to 100 μM) at 37 °C for 24 h. When indicated 200 μM concentration was also analysed. Final DMSO concentration in the reactions was always lower than 1%. For comparison, cisplatin was used as a positive control. Aliquots of 20 μL of compound: DNA complexes containing 0.8 μg of DNA were subjected to 1% agarose gel electrophoresis in TAE buffer (40 mM Tris–acetate, 2 mM EDTA, pH 8.0). The gel was stained in the same buffer containing ethidium bromide (0.5 mg mL^{-1}) and visualized and photographed under UV light.

4.2.4. Cell cycle analysis

Cell cycle was assessed by flow cytometry using a fluorescence-activated cell sorter (FACS). For this assay, 3×10^4 A549 cells or 5×10^4 VA13 cells per well were seeded in 6 well plates with 2 ml of medium. After 24 h of incubation, **1c** was added at its IC_{50} value (2.2 μM). Following 72 h of incubation, cells were harvested by mild tripsinization, collected by centrifugation and resuspended in Tris-buffered saline (TBS) containing 50 μg/mL PI, 10 μg/mL DNase-free RNase and 0.1% Igepal CA-630. The cell suspension was incubated for 1 h at room temperature to allow for the staining of the cells with the PI, and afterwards FACS analysis was carried out at 488 nm in an Epics XL flow cytometer (Coulter Corporation, Hialeah, FL). Data from 1×10^4 cells were collected and analysed using the Multicycle program (Phoenix Flow Systems, San Diego, CA).

4.2.5. Apoptosis assay

Apoptosis is assessed evaluating the annexin-V binding to phosphatidylserine (PS), which is externalized early in the apoptotic process. 3×10^4 A549 cells per well were seeded in 6 well plates with 2 mL of medium and treated as described above for the cell cycle analysis assay. After cell collection and centrifugation, cells were resuspended in 95 μL binding buffer (10 mM HEPES/NaOH, pH 7.4, 140 mM NaCl, 2.5 mM $CaCl_2$). 3 μL of Annexin-V FITC conjugate (1 μg/mL) were then added and the suspension was incubated in darkness for 30 min, at room temperature. Just before FACS analysis, the cell suspension was added to a vial containing 500 μL of binding buffer, and then stained with 20 μL of 1 mg/mL PI solution. Data from 1×10^4 cells were collected and analysed.

4.2.6. Statistical analysis

For each compound, a minimum of three independent experiments with triplicate values to measure cell viability and a minimum of three independent experiments for cell cycle analysis and assessment of apoptosis were conducted. Data are given as the mean ± standard deviation (SD). Statistical analysis was performed by using two-way analysis of variance (ANOVA). Differences between treated and control groups were considered significant when $p < 0.05$ (*) or $p < 0.01$ (**).

Acknowledgments

This work was supported by the Ministerio de Ciencia y Tecnología (projects CTQ2009-11501 and CTQ2009-07021/BQU) and the *AGAUR, Generalitat de Catalunya* (Grants 2009-SGR-1111, 2009SGR01308, 2006ITT-10007 and 2009CTP-00026). This study

was also supported by the project SAF2011-25726 and by RD06/0020/0046 from Red Temática de Investigación Cooperativa en Cáncer (RTICC), Instituto de Salud Carlos III, both funded by the Ministerio de Ciencia e Innovación-Spanish government and European Regional Development Funds (ERDF) "Una manera de hacer Europa". Marta Cascante acknowledges the support received through the prize "ICREA Academia", funded by ICREA foundation-Generalitat de Catalunya.

Appendix A. Supplementary material

Supplementary material associated with this article can be found, in the online version, at http://dx.doi.org/10.1016/j.ejmech.2012.06.002.

References

[1] B. Rosenberg, L. van Camp, T. Krigas, Inhibition of cell division in Escherichia coli by electrolysis products from a platinum electrode, Nature 205 (1965) 698–699.
[2] Á.M. Montaña, C. Batalla, The rational design of anticancer platinum complexes: the importance of the structure-activity relationship, Curr. Med. Chem. 16 (2009) 2235–2260.
[3] E. Wong, M. Giandomenico, Current status of platinum-based anticancer drugs, Chem. Rev. 99 (1999) 2451–2466.
[4] N.J. Wheate, S. Walker, G.E. Craig, R. Oun, The status of platinum anticancer drugs in the clinic and in clinical trials, Dalton Trans. 39 (2010) 8113–8127.
[5] R.Y. Tsang, T. Al-Fayea, H. Au, Cisplatin overdose: toxicities and management, Drug Safety 32 (2009) 1109–1122.
[6] M.J. Sullivan, Hepatoblastoma, cisplatin, and ototoxicity: good news on deaf ears, Cancer 115 (2009) 5623–5626.
[7] B. Köberle, M.T. Tomicic, S. Usanova, B. Kaina, Cisplatin resistance: preclinical findings and clinical implications, Biochim. Biophys. Acta Rev. Cancer 1806 (2010) 172–182.
[8] D. Wang, S.J. Lippard, Cellular processing of platinum anticancer drugs, Nat. Rev. Drug Discov. 4 (2005) 307–320.
[9] D. Gibson, The mechanism of action of platinum anticancer agents - What do we really know about it? Dalton Trans. (2009) 10681–10689.
[10] F. Arnesano, G. Natile, Mechanistic insight into the cellular uptake and processing of cisplatin 30 years after its approval by FDA, Coord. Chem. Rev. 253 (2009) 2070–2081.
[11] L. Kelland, The resurgence of platinum-based cancer chemotherapy, Nat. Rev. Cancer 7 (2007) 573–584.
[12] Y. Jung, S.J. Lippard, Direct cellular responses to platinum-induced DNA damage, Chem. Rev. 107 (2007) 1387–1407.
[13] J.T. Reardon, A. Vaisman, S.G. Chaney, A. Sancar, Efficient nucleotide excision repair of cisplatin, oxaliplatin, and bis- acetoammine-dichloro-cyclohexylamine-platinum(IV) (JM216) platinum intrastrand DNA diadducts, Cancer Res. 59 (1999) 3968–3971.
[14] C. Tessier, F.D. Rochon, Multinuclear NMR study and crystal structures of complexes of the types cis- and trans-Pt(Ypy)2X2, where Ypy=pyridine derivative and X=Cl and I, Inorg. Chim. Acta 295 (1999) 25–38.
[15] Y. Chen, Z. Guo, S. Parsons, P.J. Sadler, Stereospecific and kinetic control over the hydrolysis of a sterically hindered platinum picoline anticancer complex, Chem. Eur. J. 4 (1998) 672–676.
[16] E. Budzisz, M. Malecka, B. Nawrot, Synthesis and structure of highly substituted pyrazole ligands and their complexes with platinum(II) and palladium(II) metal ions, Tetrahedron 60 (2004) 1749–1759.
[17] E. Budzisz, M. Miernicka, I.-P. Lorenz, P. Mayer, U. Krajewska, M. Rozalski, Synthesis and X-ray structure of platinum(II), palladium(II) and copper(II) complexes with pyridine-pyrazole ligands: Influence of ligands' structure on cytotoxic activity, Polyhedron 28 (2009) 637–645.
[18] M. Gökçe, S. Utku, S. Gür, A. Özkul, F. Gümü&scedil, Synthesis, in vitro cytotoxic and antiviral activity of cis-[Pt(R(-) and S(+)-2-α-hydroxybenzylbenzimidazole)2Cl2] complexes, Eur. J. Med. Chem. 40 (2005) 135–141.
[19] Z. Trávníček, M. Maloň, M. Zatloukal, K. Doležal, M. Strnad, J. Marek, Mixed ligand complexes of platinum(II) and palladium(II) with cytokinin-derived compounds Bohemine and Olomoucine: X-ray structure of [Pt(BohH+-N7)Cl3]·9/5H2O {Boh=6-(benzylamino)-2-[(3-(hydroxypropyl)-amino]-9-isopropylpurine, Bohemine}, J. Inorg. Biochem. 94 (2003) 307–316.
[20] M. Quirós, J.M. Salas, M.P. Sánchez, A.L. Beauchamp, X. Solans, Palladium(II)-purine nucleoside complexes: synthesis, characterization and X-ray determination, Inorg. Chim. Acta 204 (1993) 213–220.
[21] A.C.F. Caires, Recent advances involving palladium (II) complexes for the cancer therapy, Anti-Cancer Agents Med. Chem. 7 (2007) 484–491.
[22] G. Gasser, I. Ott, N. Metzler-Nolte, Organometallic anticancer compounds, J. Med. Chem. 54 (2011) 3–25.
[23] M.R. Crimmin, D.A. Colby, J.A. Ellman, R.G. Bergman, Synthesis and coordination chemistry of tri-substituted benzamidrazones, Dalton Trans. 40 (2011) 514–522.
[24] J.-P. Djukic, J.-B. Sortais, L. Barloy, M. Pfeffer, Cycloruthenated compounds - Synthesis and applications, Eur. J. Inorg. Chem. (2009) 817–853.
[25] S.P. Fricker, R.M. Mosi, B.R. Cameron, I. Baird, Y. Zhu, V. Anastassov, J. Cox, P.S. Doyle, E. Hansell, G. Lau, J. Langille, M. Olsen, L. Qin, R. Skerlj, R.S.Y. Wong, Z. Santucci, J.H. McKerrow, Metal compounds for the treatment of parasitic diseases, J. Inorg. Biochem. 102 (2008) 1839–1845.
[26] W. Kandioller, C.G. Hartinger, A.A. Nazarov, C. Bartel, M. Skocic, M.A. Jakupec, V.B. Arion, B.K. Keppler, Maltol-derived ruthenium-cymene complexes with tumor inhibiting properties: the impact of ligand-metal bond stability on anticancer activity in vitro, Chem. Eur. J. 15 (2009) 12283–12291.
[27] P.-K. Lee, H.-W. Liu, S.-M. Yiu, M.-W. Louie, K.K.-W. Lo, Luminescent cyclometallated iridium(iii) bis(quinolylbenzaldehyde) diimine complexes - Synthesis, photophysics, electrochemistry, protein cross-linking properties, cytotoxicity and cellular uptake, Dalton Trans. 40 (2011) 2180–2189.
[28] S.-K. Leung, K.Y. Kwok, K.Y. Zhang, K.K.-W. Lo, Design of luminescent biotinylation reagents derived from cyclometalated iridium(III) and rhodium(III) bis(pyridylbenzaldehyde) complexes, Inorg. Chem. 49 (2010) 4984–4995.
[29] Z. Liu, L. Salassa, A. Habtemariam, A.M. Pizarro, G.J. Clarkson, P.J. Sadler, Contrasting reactivity and cancer cell cytotoxicity of isoelectronic organometallic iridium(III) complexes, Inorg. Chem. 50 (2011) 5777–5783.
[30] R.W.-Y. Sun, D.-L. Ma, E.L.-M. Wong, C.-M. Che, Some uses of transition metal complexes as anti-cancer and anti-HIV agents, Dalton Trans. (2007) 4884–4892.
[31] J.J. Yan, A.L.-F. Chow, C.-H. Leung, R.W.-Y. Sun, D.-L. Ma, C.-M. Che, Cyclometalated gold(III) complexes with N-heterocyclic carbene ligands as topoisomerase i poisons, Chem. Commun. 46 (2010) 3893–3895.
[32] J. Quirante, D. Ruiz, A. Gonzalez, C. López, M. Cascante, R. Cortés, R. Messeguer, C. Calvis, L. Baldomà, A. Pascual, Y. Guérardel, B. Pradines, M. Font-Bardía, T. Calvet, C. Biot, Platinum(II) and palladium(II) complexes with (N, N′) and (C, N, N′)- ligands derived from pyrazole as anticancer and antimalarial agents: synthesis, characterization and in vitro activities, J. Inorg. Biochem. 105 (2011) 1720–1728.
[33] G.L. Edwards, D.S.C. Black, G.B. Deacon, L.P.G. Wakelin, Effect of charge and surface area on the cytotoxicity of cationic metallointercalation reagents, Can. J. Chem. 83 (2005) 969–979.
[34] J. Ruiz, V. Rodríguez, C. De Haro, A. Espinosa, J. Pérez, C. Janiak, New 7-azaindole palladium and platinum complexes: crystal structures and theoretical calculations in vitro anticancer activity of the platinum compounds, Dalton Trans. 39 (2010) 3290–3301.
[35] I.M. El-Mehasseb, M. Kodaka, T. Okada, T. Tomohiro, K.- Okamoto, H. Okuno, Platinum (II) complex with cyclometalating 2-phenylpyridine ligand showing high cytotoxicity against cisplatin-resistant cell, J. Inorg. Biochem. 84 (2001) 157–158.
[36] T. Okada, I.M. El-Mehasseb, M. Kodaka, T. Tomohiro, K. Okamoto, H. Okuno, Mononuclear platinum(II) complex with 2-phenylpyridine ligands showing high cytotoxicity against mouse sarcoma 180 cells acquiring high cisplatin resistance, J. Med. Chem. 44 (2001) 4661–4667.
[37] J. Ruiz, V. Rodríguez, N. Cutillas, A. Espinosa, M.J. Hannon, Novel C, N-chelate platinum(II) antitumor complexes bearing a lipophilic ethisterone pendant, J. Inorg. Biochem. 105 (2011) 525–531.
[38] G.L. Edwards, D.S.C. Black, G.B. Deacon, L.P.G. Wakelin, In vitro and in vivo studies of neutral cyclometallated complexes against murine leukæmias, Can. J. Chem. 83 (2005) 980–989.
[39] H. Samouei, M. Rashidi, F.W. Heinemann, A cyclometalated diplatinum complex containing 1,1′-bis(diphenylphosphino)ferrocene as spacer ligand: antitumor study, J. Organomet. Chem. 696 (2011) 3764–3771.
[40] P. Wang, C.-H. Leung, D.-L. Ma, R.W.-Y. Sun, S.-C. Yan, Q.-S. Chen, C.-M. Che, Specific blocking of CREB/DNA binding by cyclometalated platinum(II) complexes, Angew. Chem. Int. Ed. 50 (2011) 2554–2558.
[41] D.-L. Ma, C.-M. Che, A bifunctional platinum(II) complex capable of intercalation and hydrogen-bonding interactions with DNA: binding studies and cytotoxicity, Chem. Eur. J. 9 (2003) 6133–6144.
[42] M. Crespo, M. Font-Bardia, X. Solans, Compound [$PtPh_2(SMe_2)_2$] as a versatile metalating agent in the preparation of new types of [C, N, N′] cyclometalated platinum compounds, Organometallics 23 (2004) 1708–1713.
[43] R. Martin, M. Crespo, M. Font-Bardia, T. Calvet, Five- and seven-membered metallacycles in [C, N, N′] and [C, N] cycloplatinated compounds, Organometallics 28 (2009) 587–597.
[44] A. Alvarez-Valdés, J.M. Pérez, I. López-Solera, R. Lannegrand, J.M. Continente, P. Amo-Ochoa, M.J. Camazón, X. Solans, M. Font-Bardía, C. Navarro-Ranninger, C. Navarro-Ranninger, Preparation and characterization of platinum(II) and (IV) complexes of 1,3-diaminepropane and 1,4-diaminebutane: circumvention of cisplatin resistance and DNA interstrand cross-link formation in CH1cisR ovarian tumor cells, J. Med. Chem. 45 (2002) 1835–1844.
[45] J.M. Pérez, E.I. Montero, A.M. González, A. Alvarez-Valdés, C. Alonso, C. Navarro-Ranninger, Apoptosis induction and inhibition of H-ras overexpression by novel trans-[$PtCl_2$(isopropylamine)(amine')] complexes, J. Inorg. Biochem. 77 (1999) 37–42.
[46] S. Moradell, J. Lorenzo, A. Rovira, M.S. Robillard, F.X. Avilés, V. Moreno, R. De Llorens, M.A. Martinez, J. Reedijk, A. Llobet, Platinum complexes of diaminocarboxylic acids and their ethyl ester derivatives: the effect of the chelate ring size on antitumor activity and interactions with GMP and DNA, J. Inorg. Biochem. 96 (2003) 493–502.
[47] B.E. Smart, Fluorine substituent effects (on bioactivity), J. Fluorine Chem. 109 (2001) 3–11.

[48] H.F. Klein, S. Camadanli, R. Beck, D. Leukel, U. Flörke, Angew. Chem. Int. Ed. 44 (2005) 975–977.
[49] M. Zanuy, A. Ramos-Montoya, O. Villacañas, N. Canela, A. Miranda, E. Aguilar, N. Agell, O. Bachs, J. Rubio-Martinez, M.D. Pujol, W.-P. Lee, S. Marin, M. Cascante, Cyclin-dependent kinases 4 and 6 control tumor progression and direct glucose oxidation in the pentose cycle, Metabolomics (2011) 1–11.
[50] J. Pietzsch, F. Graf, L. Koehler, T. Kniess, F. Wuest, B. Mosch, Cell cycle regulating kinase cdk4 as a potential target for tumor cell treatment and tumor imaging, J. Oncol. (2009) 1–12.
[51] M. Malumbres, M. Barbacid, Is Cyclin D1-CDK4 kinase a bona fide cancer target? Cancer Cell 9 (2006) 2–4.
[52] F.J. Ramos-Lima, V. Moneo, A.G. Quiroga, A. Carnero, C. Navarro-Ranninger, The role of p53 in the cellular toxicity by active trans-platinum complexes containing isopropylamine and hydroxymethylpyridine, Eur. J. Med. Chem. 45 (2010) 134–141.
[53] H. Zheng, W. Hu, D. Yu, D.- Shen, S. Fu, J.J. Kavanagh, I.- Wei, D.J. Yang, Diammine dicarboxylic acid platinum enhances cytotoxicity in platinum-resistant ovarian cancer cells through induction of apoptosis and S-phase cell arrest, Pharm. Res. 25 (2008) 2272–2282.
[54] V. Horváth, K. Souček, L. Švihálková-Šindlerová, J. Vondráček, O. Blanářová, J. Hofmanová, P. Sova, A. Kozubík, Different cell cycle modulation following treatment of human ovarian carcinoma cells with a new platinum(IV) complex vs cisplatin, Invest. New Drugs 25 (2007) 435–443.
[55] D.L. Bratton, E. Dreyer, J.M. Kailey, V.A. Fadok, K.L. Clay, P.M. Henson, The mechanism of internalization of platelet-activating factor in activated human neutrophils: enhanced transbilayer movement across the plasma membrane, J. Immunol. 148 (1992) 514–523.
[56] A.K. Hammill, J.W. Uhr, R.H. Scheuermann, Annexin V staining due to loss of membrane asymmetry can be reversible and precede commitment to apoptotic death, Exp. Cell Res. 251 (1999) 16–21.
[57] D. Song, S. Wang, Structures of $Pt_2(CH_3)_4(S(CH_3)_2)_2$ and $[PtPh_2(S(CH_3)_2)]_n$ (n=2,3), J. Organomet. Chem. 648 (2002) 302–305.
[58] M. Rashidi, Z. Fakhroeian, R. Puddephatt, Studies of binuclear methyl and phenyl derivatives of platinum(II), J. Organomet. Chem. 406 (1990) 261–267.
[59] B.R. Steele, K. Vrieze, Complexes with metal-carbon bonds, part III(1). Preparation and properties of binuclear diarylplatinum(II) compounds, Transit. Metal Chem. 2 (1977) 140–144.
[60] C.M. Anderson, M. Crespo, M.C. Jennings, A.J. Lough, G. Ferguson, R.J. Puddephatt, Competition between intramolecular oxidative addition and ortho metalation in organoplatinum(II) compounds: activation of aryl-halogen bonds, Organometallics 10 (1991) 2672–2679.
[61] G.M. Sheldrick, SHELXS97, A Computer Program for Crystal Structure Determination, University of Göttingen, Germany, 1997.
[62] International Tables of X-Ray Crystallography, vol. IV, Kynoch Press, Birmingham, UK, 1974, pp. 99–100, and 149.
[63] T. Mosmann, Rapid colorimetric assay for cellular growth and survival: application to proliferation and cytotoxicity assays, J. Immunol. Methods 65 (1983) 55–63.
[64] C. Matito, F. Mastorakou, J.J. Centelles, J.L. Torres, M. Cascante, Antiproliferative effect of antioxidant polyphenols from grape in murine Hepa-1c1c7, Eur. J. Nutr. 42 (2003) 42–49.
[65] K.T. Givens, S. Kitada, A.K. Chen, J. Rothschiller, D.A. Lee, Proliferation of human ocular fibroblasts: an assessment of in vitro colorimetric assays, Invest. Ophthalmol. Vis. Sci. 31 (1990) 1856–1862.
[66] A. Abdullah, F. Huq, A. Chowdhury, H. Tayyem, P. Beale, K. Fisher, BMC Chem. Biol. 6 (2006) 3.

CAPÍTULO 1B

COMPLEJOS DE PT(II) CON LIGANDOS (N,N') O (C,N,E)$^-$ (E = N,S): ESTUDIOS CITOTÓXICOS, EFECTO SOBRE LA ESTRUCTURA TERCIARIA DEL ADN Y RELACIONES ESTRUCTURA-ACTIVIDAD.

Joan Albert [a,b], Ramon Bosque [a,b], Margarita Crespo [a,b], Jaume Granell [a,b], Concepción López [a], Roldán Cortés [b,c], Asensio Gonzalez [b,d], Josefina Quirante [b,d], Carme Calvis e, Ramon Messeguer [e], Laura Baldomà [b,f], Josefa Badia [b,f], Marta Cascante [b,c]

[a] Departament de Química Inorgànica, Facultat de Química, Universitat de Barcelona, Diagonal 645, E-08028 Barcelona, España

[b] Institut de Biomedicina (IBUB), Universitat de Barcelona, E-08028 Barcelona, España

[c] Department of Biochemistry and Molecular Biology, Facultat de Biologia, IDIBAPS, Unidad asociada al CSIC, Diagonal 643, E-08028 Barcelona, España

[d] Laboratori de Química Orgànica, Facultat de Farmàcia, Universitat de Barcelona, Av. Joan XXIII, s/n, E-08028 Barcelona, España

[e] Biomed Division LEITAT Tecnological Center, Parc Científic de Barcelona, Edificio Hèlix, Baldiri i Reixach, 15-21, E-08028 Barcelona, España

[f] Departament de Bioquímica i Biologia Molecular, Facultat de Farmàcia, Universitat de Barcelona, Av. Joan XXIII, s/n, E-08028 Barcelona, España

Resumen

Se presenta la actividad citotóxica de dos series de complejos de platino(II) que contienen las iminas polifuncionales R^1–CH=N–R^2 [R^1 es la unidad fenil o ferrocenil, y R^2 es $(CH_2)n$–CH_2–NMe_2 en el que $n = 1$ o 2) (**1** y **2**) o C_6H_4-2-SMe (**3**)] actuando como un ligando bidentado (N,N') (**4**–**7**) o tridentado [C(fenil o ferrocenil),N,N']$^-$ (**8**–**10**) o [C(ferrocenil),N,S]$^-$ (**11**) frente a líneas humanas de adenocarcinoma de pulmón (A549), mama (MDA-MD231) y colon (HCT116). Los resultados revelan que la mayoría de los complejos de platino(II) son activos sobre las tres líneas celulares ensayadas y que los complejos 6, 7 y los ciclo-platinados 10 y 11 exhoben una destacable actividad antiproliferativa, superior incluso a la del cisplatino, en la línea tumoral humana HCT116. Estudios sobre la migración electroforética del ADN indicaron que la mayoría de los compuestos modifican la estructura terciaria del ADN de manera similar al cisplatino, usado como referencia. También se han llevado a cabo estudios de solubilidad de una selección de los complejos más relevantes para evaluar: (a) su estabilidad en medio acuoso biológico y/o la formación de especies biológicamente activas y (b) su propensión a reaccionar con 9-metilguanina (9-MeG), utilizada como modelo de nucleobase. También se han realizado estudios computacionales mediante teoría de funcionales de densidad (DFT).

Bioorganic & Medicinal Chemistry 21 (2013) 4210–4217

Contents lists available at SciVerse ScienceDirect

Bioorganic & Medicinal Chemistry

journal homepage: www.elsevier.com/locate/bmc

Pt(II) complexes with (N,N′) or (C,N,E)$^-$ (E = N,S) ligands: Cytotoxic studies, effect on DNA tertiary structure and structure–activity relationships

Joan Albert [a,b], Ramon Bosque [a,b], Margarita Crespo [a,b], Jaume Granell [a,b], Concepción López [a,*], Roldán Cortés [b,c], Asensio Gonzalez [b,d], Josefina Quirante [b,d,*], Carme Calvis [e], Ramon Messeguer [e], Laura Baldomà [b,f], Josefa Badia [b,f], Marta Cascante [b,c]

[a] Departament de Química Inorgànica, Facultat de Química, Universitat de Barcelona, Diagonal 645, E-08028 Barcelona, Spain
[b] Institut de Biomedicina (IBUB), Universitat de Barcelona, 08028 Barcelona, Spain
[c] Department of Biochemistry and Molecular Biology, Faculty of Biology, IDIBAPS, Unit Associated with CSIC, Diagonal 643, E-08028 Barcelona, Spain
[d] Laboratori de Química Orgànica, Facultat de Farmàcia, Universitat de Barcelona, Av. Joan XXIII, s/n, E-08028 Barcelona, Spain
[e] Biomed Division LEITAT Tecnological Center, Parc Científic de Barcelona, Edifici Hèlix, Baldiri i Reixach, 15-21, E-08028 Barcelona, Spain
[f] Departament de Bioquímica i Biologia Molecular, Facultat de Farmàcia, Universitat de Barcelona, Av. Joan XXIII, s/n, E-08028 Barcelona, Spain

ARTICLE INFO

Article history:
Received 1 March 2013
Revised 26 April 2013
Accepted 3 May 2013
Available online 14 May 2013

Keywords:
Platinum(II)
Cycloplatinated complexes
Cytotoxicity
Anticancer drugs

ABSTRACT

The cytotoxic activity of two series of platinum(II) complexes containing the polyfunctional imines R^1–CH=N–R^2 [R^1 = phenyl or ferrocenyl unit and $R^2 = (CH_2)_n$–CH_2–NMe_2 where n = 1 or 2) (**1** and **2**) or C_6H_4-2-SMe (**3**)] acting as a bidentate (N,N′) (**4**–**7**) or terdentate [C(phenyl or ferrocenyl),N,N′]$^-$ (**8**–**10**) or [C(ferrocenyl),N,S]$^-$ ligand (**11**) in front of A549 lung, MDA-MB231 breast and HCT116 colon human adenocarcinoma cell lines is reported. The results reveal that most of the platinum(II) complexes are active against the three assayed lines and compounds **6**, **7** and the platinacycles **10** and **11** exhibit a remarkable antiproliferative activity, even greater than *cisplatin* itself, in the *cisplatin* resistant HCT116 human cancer cell line. Electrophoretic DNA migration studies showed that most of them modify the DNA tertiary structure in a similar way as the reference *cisplatin*. Solution studies of a selection of the most relevant complexes have also been performed in order to test: (a) their stability in the aqueous biological medium and/or the formation of biologically active species and (b) their proclivity to react with 9-methylguanine (9-MeG), as a model nucleobase. Computational studies at DFT level have also been performed in order to explain the different solution behaviour of the complexes and their proclivity to react with the nucleobase.

1. Introduction

The potential of metal-based anticancer agents has been widely explored and recognised[1–3] since the landmark discovery of the biological activity of *cisplatin*.[4] To date this prototypical anticancer drug remains one of the most effective chemotherapeutic agents in clinical use.[5] However, its utility against cancer is limited by (a) severe dose-limiting toxicity, such as neuro-, hepato-, and nephrotoxicity[6–9] and/or (b) inherent or acquired resistance.[10]

A better understanding of the cellular response to *cisplatin* and how tumours are or become resistant,[11–14] will contribute to the design of novel platinum compounds[15] with improving anticancer properties. *Cisplatin* enters cells by passive diffusion[16] and also, as discovered later, by active transport mediated by the copper transporter Ctr1p in yeast and mammals.[17,18] Once inside the cell, the low chloride concentration (4–20 mM) results in drug aquation with the loss of one or both of the chlorido ligands. The resulting aquo-platinum complex binds to its target, DNA, by the formation of covalent cross-links; being the 1,2-intrastrand d(GpG) cross-link the major adduct. Binding of *cisplatin* to DNA causes significant distortion of the helical structure and results in inhibition of DNA replication and transcription,[16,19] which ultimately leads to cell cycle arrest and cellular apoptosis. The distorted, platinated DNA

Abbreviations: DMEM, Dulbecco's modified eagle medium; MTT, 3-(4,5-dimethylthiazol-2-yl)-2,5-diphenyltetrazolium bromide; G, guanine; 9-MeG, 9-methylguanine; 9-AA, 9-aminoacridine; ELISA, enzyme-linked immunosorbent assay; DFT, density functional theory; B3LYP, Becke 3-parameter (exchange)—Lee, Yang and Parr (correlation) functional; LANL2DZ, Los Alamos National Laboratory 2 double zeta basis set; C-PCM, conductor polarized continuum model.

* Corresponding authors. Tel.: +34 934039134; fax: +34 934907725 (C.L.), tel.: +34 934035849; fax: +34 934024539 (J.Q.).
E-mail addresses: conchi.lopez@qi.ub.es (C. López), quirantese@ub.edu (J. Quirante).

0968-0896/$ - see front matter © 2013 Elsevier Ltd. All rights reserved.
http://dx.doi.org/10.1016/j.bmc.2013.05.005

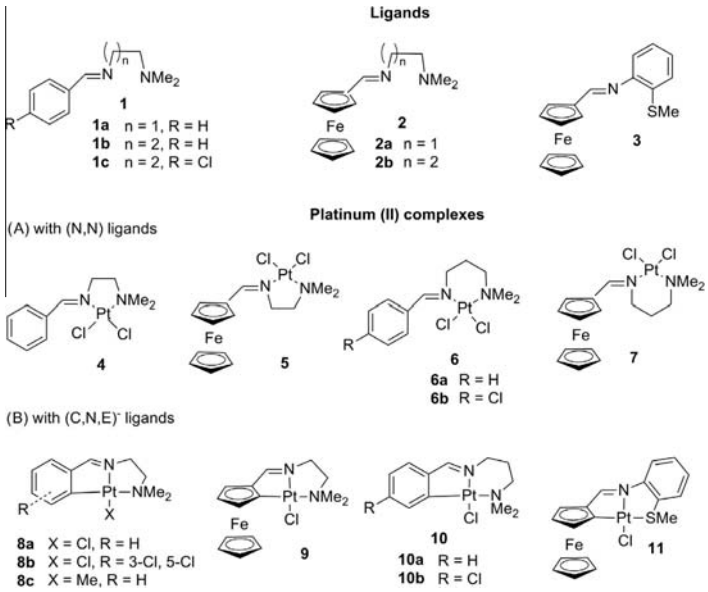

Figure 1. Chemical formulae of the free ligands (**1**–**3**) and the platinum(II) complexes (**4**–**11**) selected for this study.

Table 1
Cytotoxic activities (IC_{50} values[a]) on A549 lung, MDA-MB231 breast human and HCT116 colon cancer cell lines for the free ligands (**1a**–**1c** and **3**)[b] the platinum complexes (**4**–**11**) and *cisplatin*

Type of product	Mode of binding of the ligand	IC_{50}(μM) for the cell lines:		
		A549	MDA-MB231	HCT116
Ligand[b]				
1a	—	>100	>100	>100
1b	—	>100	>100	>100
1c	—	>100	>100	>100
3	—	173 ± 25	nd	44 ± nd
Platinum(II) complexes with bidentate ligands				
4	(N,N′)	26 ± 12	47 ± nd	35 ± 2.2
5	(N,N′)	>100	57 ± nd	55 ± 6.8
6a	(N,N′)	95 ± 7	14.1 ± 2.4	11.9 ± 9 2
6b	(N,N′)	>200	10.7 ± 4.6	10.6 ± 1.7
7	(N,N′)	178 ± 32	28 ± 0.3	30 ± 4.2
Platinum(II) complexes with terdentate ligands				
8a	[C(phenyl), N,N′]⁻	95 ± 7	10.7 ± 4.6	60 ± 1.7
8b	[C(phenyl), N,N′]⁻	38 ± 18	42.2 ± 9.5	>100
8c	[C(phenyl), N,N′]⁻	27.0 ± 10	30 ± 10.2	44 ± 8.5
9	[C(ferrocenyl), N,N′]⁻	75 ± 14	87 ± nd	45 ± 7.8
10a	[C(phenyl), N,N′]⁻	40 ± 14	28 ± 2.4	28 ± 6.7
10b	[C(phenyl), N,N′]⁻	23 ± 4	17 ± 1.1	18 ± 1.9
11	[C(ferrocenyl), N,S′]⁻	23 ± 8	32 ± 6.2	20.7 ± 3.8
Cisplatin	(N)	9.3 ± 3.0	6.5 ± 2.4	40 ± 4.4

[a] Data are shown as the mean values of two or more experiments performed in triplicate with the corresponding standard deviation (SD).
[b] Ref. 32.

structure also serves as a recognition binding site for cellular proteins,[11,12] such transcription factors, histones, high-mobility group (HMG)-domain proteins, and nucleotide excision repair (NER) proteins, which may modulate the *cisplatin* effectiveness and/or resistance.

Taking these findings into account, one of the strategies for developing new anticancer agents include the design of platinum complexes that bind to DNA in a fundamentally different manner than *cisplatin*. One of them consists in the synthesis of new organic compounds with one or more N atoms with donor abilities (i.e., amines, oximes, thiosemicarbazones, functionalized azoles, etc.) and their use as ligands for Pt(II).[20–23] Despite the great number of studies on this field and the variety of complexes reported in recent years, to the best of our knowledge, none of these studies deals with sets of platinum(II) complexes derived from closely related ligands, exhibiting different coordination modes. Structure–activity relationship (SAR) upon this sets of platinum(II) compounds may provide interesting information of how their cytotoxic activity could be influenced by several structural factors such as (a) the donor atoms of the ligand, (b) its mode of binding [i.e., (N),

(N,E), (C,N,E)$^-$, E = additional heteroatom], (c) the chelate size, (d) the presence of substituents or even (e) the nature of additional ancillary ligands.

During the last decade, we have prepared different families of polyfunctional imines (**1**–**3**, Fig. 1)[24–28] and used them as ligands to build up a wide variety of platinum(II) complexes (**4**–**11**),[24,26–31] in which the Schiff bases behave as neutral and bidentate (N,N′) ligands (in compounds **4**–**7** of Fig. 1) or as monoanionic and terdentate (C,N,N′)$^-$ (in **8**–**10**) or (C,N,S)$^-$ (in **11**) ligands.

Now we report comparative studies of the cytotoxic activity of the platinum(II) complexes (**4**–**11**) in front of A549 lung, MDA-MB231 breast and HCT116 colon (*cisplatin* resistant) human adenocarcinoma cell lines, together with the investigation of their effect on the electrophoretic mobility of DNA. The results presented here provide conclusive evidences of the influence of the type of ligands and their binding mode on their biological effectiveness.

2. Results and discussion

2.1. Biological studies

2.1.1. Antiproliferative assay

Human lung, breast and colon cancer cell lines (A549, MDA-MB231 and HCT116, respectively) were used to test the cytotoxic activity of the Pt(II) complexes with (N,N′) ligands (**4**–**7**) and the platinacycles (**8**–**11**). For comparison purposes *cisplatin* (as positive control) and the free ligands **1**–**3** were evaluated under the same experimental conditions.[32]

Data presented in Table 1 shows that the investigated compounds exhibit variable selectivity in front of the adenocarcinoma cell lines tested (Table 1, Fig. 2). Several complexes showed greater cytotoxicity effectiveness than that of *cisplatin* versus the platinum resistant HCT116 cancer cell line selected, namely compounds **4**, **6a**, **6b**, **7**, **10a**, **10b**, and **11** (Fig. 3).

Regarding the chelated (N,N′) Pt(II) complexes (**4**–**7**), it has been reported that the five membered 1,2-ethanediamine complexes showed greater antiproliferative activity than the six membered 1,3-propanediamine complexes in front of L1210 cell line.[20,33] In our study, the chelated five-membered complex **4** exhibited greater potency than compound **6a** (six-membered chelate ring) in A549 lung cancer cell line. However, for the other cancer cell lines tested (MDA-MB231 breast and HCT116 colon) complex **4** showed higher IC_{50} values than that of complex **6a**. In *cisplatin* resistant HCT116 colon adenocarcinoma cell line, the six-membered complexes **6a** and **6b** exhibited a cytotoxic effectiveness approximately fourfold greater than that of *cisplatin*. It should be mentioned that a

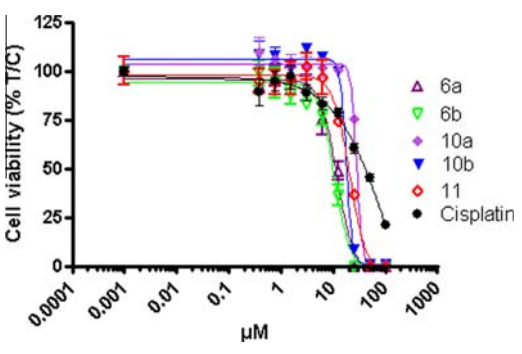

Figure 2. Inhibition of cell growth proliferation in HCT116 colon cancer cells line, after 72 h of exposure to the compounds **6** (**6a**–**6b**), **10** (**10a**–**10b**), **11** and *cisplatin*.

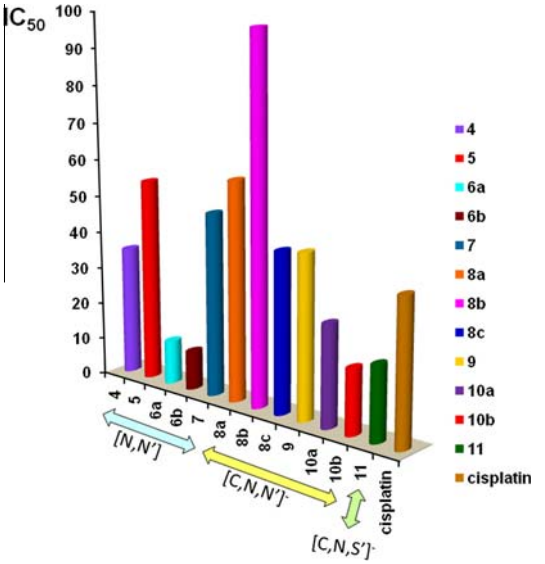

Figure 3. Comparison of the IC_{50} (μM) values obtained for the platinum(II) complexes with bidentate (N,N′) ligands (**3**–**7**), the cyclometallated compounds (**8**–**11**) and *cisplatin* in front of the HCT-116 cell line.

similar variable effect, depending of the assayed cancer cell line, has also been observed for Pt(II) complexes with 2,3-diaminopropanoate or 2,4-diaminobutiroate ligands towards A431, Hela and HL-60 cell lines.[33] Furthermore the ferrocene derivative **7** (six membered) exhibited greater cytotoxic effectiveness than the corresponding five membered ferrocene derivative **5** in the three cancer cells lines assayed. No increase in potency is observed when the ferrocenyl compounds **5** and **7** are compared with the phenyl complexes **4** and **6a** in pairs: **5**–**4** and **7**–**6a**.

Considering the cyclometallated complexes **8** (**8a**–**8b**) having a tricyclic [6.5.5] system, the non-substituted compound **8a** exhibits a slight greater cytotoxic activity than the 3,5-dichlorido derivative **8b** in A549 lung and HCT116 colon cancer cell lines; and the opposite situation is given for MDA-MB231 breast cancer cell line. Surprisingly, the platinacycle **8c**, having a methyl ligand instead of the Cl^- ligand showed lower IC_{50} values in the three human cancer cell lines than the corresponding monofuntional complex **8a**.

Finally, the cyclometallated complexes **10** (**10a** and **10b**) and **11** having a tricyclic [6.5.6] and tetracyclic [5.5.5.6] system, respectively, showed a remarkable cytotoxic effectiveness, although not so high as the seven-membered platinacycles previously investigated in our research group.[34,35] In *cisplatin* resistant HCT116 colon adenocarcinoma cell line, platinacycle **10b** exhibited a low IC_{50} value, being approximately 2.2-fold more potent than *cisplatin*. Considering the two cycloplatinated ferrocene derivatives **9** and **11**, it is noteworthy that complex **11**, with Pt–S bond exhibits lower IC_{50} than compound **9** with a Pt–N(amine) bond.

2.1.2. DNA migration studies

The effect of binding of the compounds investigated in this study on supercoiled DNA was determined by their ability to alter the electrophoretic mobility of pBluescript plasmid DNA: supercoiled closed circular (ccc) and open circular (oc) forms. The ccc form usually moves faster due to its compact structure, so it showed almost one band in gel. When the test compounds (**1**–**11**) were incubated with plasmid DNA at 37 °C, most of them could coordinate to the DNA molecule, which in some extend was

cleaved into fragments, and the brightness of band was diminished in gel.

Figure 4 shows the electrophoretic mobility of native pBluescript DNA (40 μg/mL) incubated with the selected compounds (**1**–**11**) ranging from 2.5 to 200 μM concentrations. To provide a basis for comparison, incubation of DNA with *cisplatin* and 9-AA was also performed using the same concentrations and conditions. As expected, at the lowest concentration (2.5 μM) assayed, *cisplatin* greatly altered the electrophoretic mobility of pBluescript DNA.

For the free ligands **1** (**1a**–**1c**) an increase in the presence of nicked relaxed forms without shifting the plasmid DNA mobility of supecoiled form was observed when increasing the concentration of the compounds. For the ferrocenyl ligand **3** almost no decrease in mobility was observed at any assayed concentration (Fig. 4A).

The chelated complexes having five (**4** and **5**) and six (**6a** and **6b**) membered rings greatly alter the electrophoretic mobility of plasmid DNA (Fig. 4B). When increasing the concentration of the platinum complex, the migration rate of the supercoiled band decreases until it comigrates with the nicked relaxed band. In these titration experiments, the coalescence point (defined as the amount of platinum complex that is necessary for complete removal of all supercoils from DNA) occurs at 75 μM concentration of **4** and **5** and at 10 μM concentration of **6a** and **6b**. At high concentration of complexes **4** and **5** (lanes 8 and 9) and **6** (**6a**–**6b**, lanes 5, 6 and 7), a strong unwinding of negative supercoiled DNA to positive supercoiled DNA was displayed in the electrophoretogram (Fig. 4B). The same effect was observed for *cisplatin*[36] (Fig. 4D, lines 5 and 6). For the ferrocene complex **7** a slight decrease in plasmid DNA mobility was observed in a dose dependent manner.

Platinacycles **8** (**8a**–**8c**) greatly alter the mobility of plasmid DNA. For these three compounds (Fig. 4C) the coalescence point, obtained in the titration assay occurs at 10 μM concentration of **8a** and **8b**, and at 50 μM concentration of **8c**. The lower efficiency of complex **8c** than that of **8a** in removing the supercoils from DNA could be related to the nature of the ancillary ligand {Cl (in **8a**) or Me (in **8c**)}. It is well known that Pt–Cl bonds are more labile than Pt–C bonds, thus metallacycle **8a** is expected to be more reactive than the methyl derivative **8c**. At high concentration of complexes **8a**–**8b** (lanes 5, 6 and 7) and complex **8c** (lanes 7, 8 and 9), the strong unwinding of negative supercoiled DNA to positive supercoiled DNA was also observed. Regarding the ferrocene platinacycle **9** a weaker effect on the migration rate of supercoiled closed circular plasmid DNA in a dose dependent manner was displayed. Paradoxically, compound **9** (ferrocenylimine) exhibits a similar structure as complex **8a** (benzylimine), which is able to produce a great unwinding effect on DNA.

The Pt(II) complexes **10a** and **10b** greatly alter the electrophoretic mobility of plasmid DNA (Fig. 2D). In the unwinding experiment the coalescence point for complexes **10a** and **10b** takes place with 5 and 25 μM, respectively. Interestingly these two compounds are even more potent than *cisplatin* in HCT116 colon

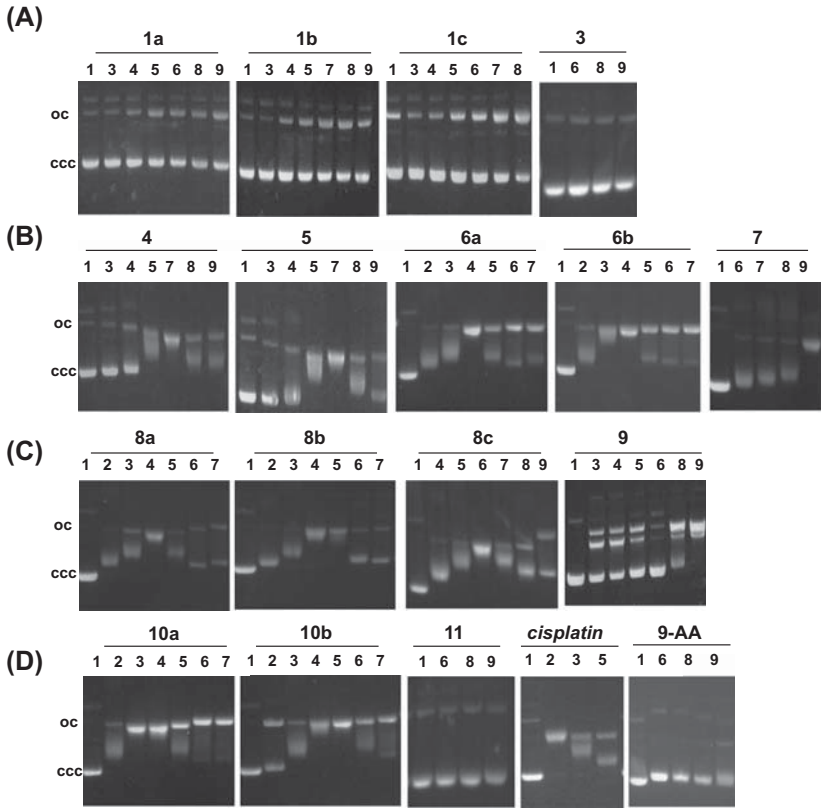

Figure 4. Interaction of pBluescript SK+ plasmid DNA (40 μg/ml) with increasing concentrations of: (A), free ligands (**1**–**3**), (B) their platinum(II) derivatives with (N,N′) ligands (**4**–**7**), and (C–D) 5-membered metallacycles (**8**–**11**) and *cisplatin* and 9-AA used for comparison purposes. Lanes 1, DNA only; lanes 2, 2.5 μM compound; lanes 3, 5 μM compound; lanes 4, 10 μM compound; lanes 5, 25 μM compound; and lane 6, 50 μM compound; lanes 7, 75 μM compound; lanes 8, 100 μM compound; and lane 9, 200 μM compound. [Abbreviations: ccc = supercoiled closed circular DNA form and oc = open circular DNA form].

cancer cell line (*cisplatin* resistant). With regard to the ferrocenyl-containing platinacycle **11**, although it exhibits a strong antiproliferative activity versus HCT116 adenocarcinoma cell line, no changes on the plasmid DNA migration rate were observed in the electrophoretogram. Compound **11**, with a polycyclic [5.5.5.6] system, is hypothesized to behave as 9-AA, which is used as intercalator reference in the experiment, or through another target/mechanism.

In general, the five-membered platinacycles under study exhibit a greater effect on DNA migration than that of the non-planar seven-membered platinacycle previously investigated in our group.[34,35] In recent studies centered on five-membered cyclometallated complexes, the metallacycle showed a planar five-membered ring structure[37–44] and hence it was hypothesized that they may act by intercalating into DNA.[41–44] However, the five-membered platinacycles **8** (**8a**–**8c**) and **10** (**10a**–**10b**) investigated in this study greatly alter the superhelicity of the DNA molecules in a similar way as the model *cisplatin*.

2.2. Solution studies

Given that the assayed compounds were insoluble in water, their stabilities in the aqueous biological media were evaluated, recording the ^{1}H NMR spectra of the solubilized compounds (**6a**, **8a**, **8c**, and **11**) in a mixture of DMSO-d_6 and D_2O (1:1). Then, the ^{1}H NMR spectra of the freshly prepared samples was compared with those obtained after different storage periods (Figs. S1–S4).

As shown in Figures S2 and S3 the solution behavior of **8a** and **8c** with identical terdentate ligands were markedly different. While **8c** was stable in aqueous solution for 48 h, for **8a**, a new compound was formed upon addition of D_2O. An analogous behavior to that of **8a** in D_2O was observed for the coordination compound **6a**, while for complex **11** no significant changes in the ^{1}H NMR spectra were detected after four days.

In a further step we also studied the effect produced by the presence of equimolar amounts of 9-methylguanine on the complexes solutions (Figs. S5–S7). In contrast with the results obtained above, in the presence of the nucleobase, complex **11** degradated (Fig. S7); whereas for compound **10a** (Fig. S6) the spectral changes detected were consistent with the coordination of 9-methylguanine to platinum. For **8c**, the quality of the ^{1}H NMR spectra decreased with time, but new signals were detected (in the range $7.7 < \delta < 8.4$ ppm) after 24 h of storage (Fig. S5-C).

2.3. Theoretical interpretation

It is well-known that the mechanism of action of *cisplatin* involves aquation prior to the binding to DNA[12–14] and we have proved that the length of the aliphatic chain (in **8a** and **10a**) and the nature of the ancillary ligand {Cl^- (in **8a**) or Me (in **8c**)} affects their cytotoxic activity, their effect on the electrophoretic mobility of DNA and their solution behavior. In view of this, and in order to compare the effect produced by the size of the chelate (in **8a** and **10a**) in the aquation process and the subsequent formation of the mono- or bis (adducts) with a nucleobase such as guanine, we undertook computational studies to determine the variations of the free energy (ΔG) of the process involving the incorporation of a H_2O molecule in the coordination sphere of the Pt(II), by either a simple ligand exchange reaction (Scheme 1, **a**) or the cleavage of the Pt–N(amine) bond and the coordination of the H_2O molecule (Scheme 1, **b**) to give the neutral species (**II**).

In a first stage the geometries of the complexes were optimized, afterwards the free energy and solvation corrections were calculated and finally we determined the ΔG values in water of each one of the reactions under study. Data presented in Scheme 1, show that differences ΔG (path **a**)$-\Delta G$ (path **b**) are 5.4 (for **8a**) and 8.5 kcal/mol (for **10a**). These values indicate that from a thermodynamic point of view the aquation is expected to proceed through path **b**. In addition, for **8a** the ΔG (for the formation of type **II** complex) is (ca. 2.7 kcal/mol) greater than for **10a**; thus suggesting that **10a** is more prone to give the aquo-complex **II** than **8a**.

It should be noted that for complex **II** with $n = 2$ the ΔG value for the aquation of the Pt–Cl bond and the formation of the mono-adduct with guanine (**V**) (steps **e** and **f**), is greater than for its analogue with $n = 1$. These differences could be attributed to the

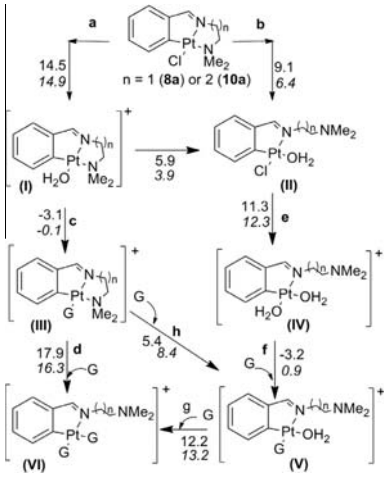

Scheme 1. Sequences of reactions chosen in the computational studies undertaken to the evaluate the aquation processes and the subsequent formation of the Pt(II)–guanine complexes {the mono-(**III**) or **V**) or bis (**VI**) aduct. The calculated ΔG value (in kcal/mol) of each one of the reactions, (in H_2O at 298 K) is presented next or close to the arrows and the values in itallics correspond to complexes with $n = 2$.

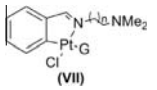

Figure 5. Guanine–platinum(II) monoadducts (**VII**) used in the computational studies.

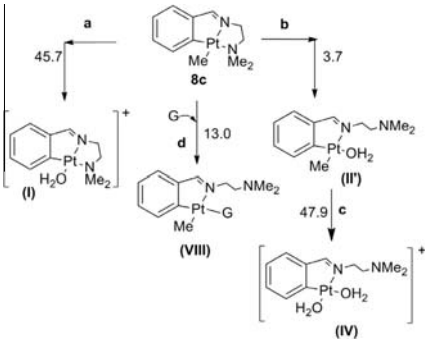

Scheme 2. Sequences of reactions choosen for the computational studies for the evaluation of the aquation processes of the cycloplatinated complex **8c**. Transformation of the species formed (**I** and **II'**) into the mono- or bis-Pt(II)-guanine adducts would proceed as shown in Scheme 1, {from **I**: steps; **c** or (**c** and **h**); from **II** or **II'**: **e** and **f** to the monoadducts aducts **II**, and **V**, or step **g** for the bis(guanine) derivative}. The calculated ΔG for these processes (in kcal/mol) are presented next to the arrow.

presence of a larger and more flexible pendant arm. Furthermore, the computational studies also showed that the reactions of **8a** or **10a** with the guanine to give the monoadducts **VII**, shown in Figure 5, are even less favored than steps **a** and **b** of Scheme 1.

In order to clarify the role of the ancillary ligand {Cl (in **8a**) or Me (in **8c**)}, a parallel study on the aquation process of **8c** was also performed. As shown in Scheme 2, (steps **a** and **b**), the formation of **I** (in **a**) is less likely to occur than that of **II′** (by a ring opening process and coordination of water in step **b**). The ΔG for the following step **c** is more than four times higher than for the chlorido-complexes (**8a**). A similar result was obtained for the formation of the mono- or bis(guanine) adducts. These findings suggest that in **II′** the ancillary Me ligand inhibits the binding of the nucleobase. It should be noted that for the direct conversion of **8c** into the guanine monoadduct (**VIII** in Scheme 2, **d**) ΔG (13 kcal/mol) is smaller than that of the transformation of **II′** into the aquo-guanine derivative **V**—shown in Scheme 1—(44.7 kcal/mol).

3. Conclusions

The evaluation of the in vitro cytotoxic activity of five Pt(II) complexes with bidentate (N,N′) ligands (**4**–**7**) and eight 5-membered platinacycles with $(C,N,E)^-$ pincer ligands (**8**–**11**) revealed that all of them exhibit growth inhibitory activity against lung (A549), colon (HCT116) and breast (MDA-MB231 and MCF7) human cancer cell lines. For SAR analysis some preliminary conclusions could be highlighted when comparing the framework and the substitution pattern of the tested compounds: (1) the investigated compounds showed a variable selectivity towards the selected human adenocarcinoma cell lines assayed. For instance the chelated 1,3-propanediamine Pt(II) complexes **6** (**6a**–**6b**) exhibited four-times greater antiproliferative activity than that of *cisplatin* in HCT116 colon (*cisplatin* resistant) cancer cell line and no activity in A549 lung cancer cell line; (2) the [6.5.6] fused polycylic complexes **10** (**10a**–**10b**) and the [5.5.5.6] fused polycyclic complex **11** showed greater cytotoxic effectiveness than the corresponding [6.5.5] fused polycylic complexes **8** and [5.5.5] fused polycylic complex **9**; in particular complex **10b** inhibits cell growth proliferation at the level two times higher to that of *cisplatin* in HTC116 (*cisplatin* resistant) colon cancer cell line; (3) the substitution of a phenyl by a ferrocenyl group in compounds **4**, **6a** and **8a** to give complexes **5**, **7** and **9**, respectively did not show any increase in cytotoxicity; (4) the presence of a non-labile methyl ligand in **8c**, instead of the labile chlorido-ligand in **8a** interestingly give rise to an increase in potency.

Most of the complexes evaluated in this study show an effect on DNA electrophoretic mobility. Complexes **6**, **8** and **10** are those exhibiting the strongest interaction with DNA and display moderate to good cytotoxic activities towards the three cancer cell lines assayed. Solution studies and DFT calculations suggest that the replacement of the Me in (**8c**) by a Cl (in **8a**) is important as to modify the mode of action of the two products. Further studies on these areas are in progress centered on both (1) the mechanistic elucidation (cell cycle arrest, induction of apoptosis, etc) of the investigated complex, and (2) the development of more potent complex containing bidentate [(N,N′) or (N,S)], and terdentate $[(C,N,N')^-$ or $(C,N,S)^-]$ donor ligands based on SAR analysis.

4. Experimental

4.1. Chemistry

4.1.1. Synthesis

The free ligands **1**–**3** and the platinum(II) complexes **4**–**11** were prepared according to procedures developed in our group[24–31] and characterized by NMR spectroscopy and X-ray crystallography (**3**–**4** and **7**, **8a**, **9**–**11**). The synthesis of the ligands **1**–**3** was accomplished by condensation reaction of equimolar amounts of the appropriate aldehyde and the corresponding amine in refluxing benzene. The synthesis was usually carried out using a Dean–Stark apparatus to remove the benzene–water azeotrope formed in the course of the reaction. Ligand **1a**[24] and **1b**–**1c**[25] were synthesized by reaction between the corresponding benzaldehide and the diamine $Me_2N(CH_2)_2NH_2$ or $Me_2N(CH_2)_3NH_2$. Ligands **2** (**2a**–**2b**)[26,28] were prepared by reaction between ferrocenecarbaldehyde and the appropriate diamine. Finally ligand **3**[27] was obtained by reaction of ferrocenecarbaldehyde with 2-mercaptoaniline. Complex **4**,[29] **5**,[26] **6** (**6a**–**6b**)[30] and **7**[28] were prepared by reaction of the corresponding ligand with *cis*$[PtCl_2(DMSO)_2]$ in MeOH at reflux temperature. Complexes **8a**,[29] **9**,[26] **10** (**10a**–**10b**),[30] by reaction of the corresponding ligand with *cis*$[PtCl_2(DMSO)_2]$/NaOAc in the same reaction conditions. Compound **8c**,[24] by reaction of ligand **1a** with $[Pt_2Me_4(\mu\text{-}SMe_2)_2]$ in acetone at reflux temperature. Complex **8b**[31] by reaction of a methyl precursor with CH_3COCl in CH_2Cl_2/MeOH at room temperature. Finally complex **11**,[27] by reaction of ligand **3** with *cis*-$[PtCl_2(PhCN)_2]$ in toluene at reflux temperature.

4.1.2. Study of the stability of the platinum(II) complexes in solution

These studies were performed using the following methodology: the corresponding complex [5.0 mg (of **6a**), 4.4 mg (of **8a**), 4.6 mg (of **8c**), or 5 mg (of **11**)] was introduced in a NMR tube, then 0.7 mL of a DMSO-d_6/D_2O (1:1) mixture were added, the tubes were sealed and the mixtures were shaken at 298 K to complete homogenization. The stability of the compounds in this solvent was studied by comparison of the ^1H NMR spectra of these freshly prepared solutions and those obtained after different periods of storage (t) at 298 K.

4.1.3. Study of the effect produced by 9-methylguanine on the platinum(II) complexes

A solution formed by the selected compound [4.4 mg (of **8c**), or 5.8 mg (of **10a**) or 4 mg (of **11**)] and 0.7 mL of a DMSO-d_6/D_2O (1:1) mixture was introduced in a NMR-tube. Then, the equimolar amount of 9-methylguanine was added, the resulting solution was shaken at 298 K to complete the homogenization and the tube was sealed. ^1H NMR spectra of these freshly prepared solutions were recorded at 298 K and the progress of the reaction was monitored by NMR after different periods of storage at 298 K.

4.2. Biological studies

4.2.1. Cell culture

Human lung A549, colon HCT116 cells and MBA-MD231 breast adenocarcinoma cells were grown as a monolayer culture in minimum essential medium (DMEM with L-glutamine, without glucose and without sodium pyruvate) in the presence of 10% heat-inactivated fetal calf serum, 10 mM D-glucose and 0.1% streptomycin/penicillin, in standard culture conditions (humidified air with 5% CO_2 at 37 °C).

4.2.2. Cell viability assay

For A549 cell viability assays, compounds were suspended in high purity DMSO at 20 mM as stock solution. To obtain final assay concentrations, they were diluted in DMEM (final concentration of DMSO was the same for all conditions and was always lower than 1%). The assay was performed by a variation of the MTT assay described by Mosmann[45] as specified by Matito et al.[46] which is based on the ability of live cells to cleave the tetrazolium ring of the MTT thus producing formazan, which absorbs at 550 nm. In brief, 3×10^3 A549 cells/well were cultured in 96 well plates for

24 h prior to the addition of the different compounds at different concentrations, in triplicate. After incubation for 72 h more, the supernatant was aspirated and 100 μL of filtered MTT (0.5 mg/mL) was added to each well. Following 1 h of incubation with the MTT, the supernatant was removed and the precipitated formazan was dissolved in 100 μL DMSO. Relative cell viability, compared to the viability of untreated cells, was measured by absorbance at 550 nm on an ELISA plate reader (Tecan Sunrise MR20-301, TECAN, Salzburg, Austria). Concentrations that inhibited cell growth by 50% (IC_{50}) after 72 h of treatment were subsequently calculated.

For MDA-MB231 and HCT116 cell viability assays, compounds were dissolved in high purity DMSO at 50 mM as stock solution. Then, serial dilutions were made with DMSO (1:1). In this way DMSO concentration in cell media was always the same. Finally, 1:500 dilutions of the serial dilutions of compounds on cell media were prepared. The assay was performed as described by Givens et al.[47] In brief, HCT116 and MDA-MB231 cells were plated at 5000 cells/well, respectively, in 100 μL media in tissue culture 96 well plates (Cultek). After 24 h, media was replaced by 100 μL/well of serial dilution of drugs. Control wells did not contain compounds. Each point concentration was run in triplicate. Reagent blanks, containing media and colorimetric reagent without cells were run on each plate. Blank values were subtracted from test values and were routinely 5–10% of uninhibited control values. Plates were incubated 72 h. Hexosaminidase activity was measured according to the following protocol: the media was removed and cells were washed once with PBS. 60 μL of substrate solution (*p*-nitrophenol-*N*-acetyl-β-D-glucosamide 7.5 mM, sodium citrate 0.1 M, pH 5.0, 0.25% Triton X-100) was added to each well and incubated at 37 °C for 1–2 h. After this incubation time, a bright yellow appears. Then, plates could be developed by adding 90 μL of developer solution (Glycine 50 mM, pH 10.4; EDTA 5 mM) and absorbance was recorded at 410 nm.

4.2.3. DNA migration studies

Compounds were dissolved in high purity DMSO at 10 mM as stock solution. Then, serial dilutions were made in milliQ water (1:1). Plasmid pBluescript SK+ (Stratagene) was obtained using a QIAGEN plasmid midi kit as described by the manufacturer. Interaction of drugs with pBluescript SK+ plasmid DNA was analyzed by agarose gel electrophoresis following a modification of the method described by Abdullah et al.[48] In brief, plasmid DNA aliquots (40 μg mL^{-1}) were incubated in TE buffer (10 mM Tris–HCl, 1 mM EDTA, pH 7.5) with different concentrations of the compounds (ranging from 0 μM to 100 μM) at 37 °C for 24 h. When indicated 200 μM concentration was also analyzed. Final DMSO concentration in the reactions was always lower than 1%. For comparison, *cisplatin* and 9-AA were used as reference controls. Aliquots of 20 μL of compound: DNA complexes containing 0.8 μg of DNA were subjected to 1% agarose gel electrophoresis in TAE buffer (40 mM Tris–acetate, 2 mM EDTA, pH 8.0). The gel was stained in the same buffer containing ethidium bromide (0.5 mg mL^{-1}) and visualized and photographed under UV light.

4.3. Computational studies

DFT calculations of all the platinum(II) complexes depicted in Schemes 1 and 2 and in Figure 5 have been performed at the B3LYP level[49,50] using the GAUSSIAN 03 software.[51] The basis set has been chosen as follows: LANL2DZ[52,53] for Pt and Cl, including polarization functions for Cl,[54] 6-31G[55] for hydrogen, and 6-31G(d) including polarization functions[55,56] for the remaining atoms. Solvent effects have been calculated on the optimized structures using the C-PCM model.[57]

Acknowledgments

This work was supported by the *Ministerio de Ciencia y Tecnología* (Projects CTQ2009-11501 and CTQ2009-07021/BQU) and the *AGAUR, Generalitat de Catalunya* (Grants 2009-SGR-1111, 2009SGR01308, 2006ITT-10007 and 2009CTP-00026). This study was also supported by the project SAF2011-25726 and by RD06/0020/0046 from Red Temática de Investigación Cooperativa en Cáncer (RTICC), Instituto de Salud Carlos III, both funded by the *Ministerio de Ciencia e Innovación*-Spanish government and European Regional Development Funds (ERDF) 'Una manera de hacer Europa'. Marta Cascante acknowledges the support received through the prize 'ICREA Academia', funded by ICREA foundation-*Generalitat de Catalunya*.

Supplementary data

Supplementary data (stability studies of the complexes (**6a**, **8a**, **8c**, and **11**) in solution, by comparison of the ^1H NMR spectra of freshly prepared samples and those obtained after different storage periods (Figs. S1–S4). Effect produced by the presence of equimolar amounts of 9-methylguanine on the complexes solutions (Figs. S5–S7)) associated with this article can be found, in the online version, at http://dx.doi.org/10.1016/j.bmc.2013.05.005.

References and notes

1. Gasser, G.; Ott, I.; Metzler-Nolte, N. *J. Med. Chem.* **2011**, *54*, 3.
2. Dyson, P. J.; Sava, G. *Dalton Trans.* **2006**, 1929.
3. Thompson, K. H.; Orvig, C. *Dalton Trans.* **2006**, 761.
4. Rosenberg, B.; van Camp, L.; Krigas, T. *Nature* **1965**, *205*, 698.
5. Wheate, N. J.; Walker, S.; Craig, G. E.; Oun, R. *Dalton Trans.* **2010**, *39*, 8113.
6. Kannarkat, G.; Lasher, E. E.; Schiff, D. *Curr. Opin. Neurol.* **2007**, *20*, 719.
7. Markman, M. *Expert Opin. Drug Saf.* **2003**, *2*, 597.
8. Tsang, R. Y.; Al-Fayea, T.; Au, H.-J. *Drug Saf.* **2009**, *32*, 1109.
9. Sullivan, M. J. *Cancer* **2009**, *115*, 5623.
10. Köberle, B.; Tomicic, M. T.; Usanova, S.; Kaina, B. *BBA-Rev. Cancer* **2010**, *1806*, 172.
11. Jung, Y.; Lippard, S. J. *Chem. Rev.* **2007**, *107*, 1387.
12. Wang, D.; Lippard, S. J. *Nat. Rev. Drug Disc.* **2005**, *4*, 307.
13. Arnesano, F.; Natile, G. *Coord. Chem. Rev.* **2009**, *253*, 2070.
14. Gibson, D. *Dalton Trans.* **2009**, 10681.
15. Kelland, L. *Nat. Rev. Cancer* **2007**, *7*, 573.
16. Jamieson, E. R.; Lippard, S. J. *Chem. Rev.* **1999**, *99*, 2467.
17. Ishida, S.; Lee, J.; Thiele, D. J.; Herskowitz, I. *Proc. Natl. Acad. Sci. U.S.A.* **2002**, *99*, 14298.
18. Lin, X.; Okuda, T.; Holzer, A.; Howell, S. B. *Mol. Pharmacol.* **2002**, *62*, 1154.
19. Lee, K.-B.; Wang, D.; Lippard, S. J.; Sharp, P. A. *Proc. Natl. Acad. Sci. U.S.A.* **2002**, *99*, 4239.
20. Montaña, Á. M.; Batalla, C. *Curr. Med. Chem.* **2009**, *16*, 2235.
21. Ling, E. C. H.; Allen, G. W.; Vickery, K.; Hambley, T. W. *J. Inorg. Biochem.* **2000**, *78*, 55.
22. Chellan, P.; Land, K. M.; Shokar, A.; Au, A.; An, S. H.; Clavel, C. M.; Dyson, P. J.; Kock, C. D.; Smith, P. J.; Chibale, K.; Smith, G. S. *Organometallics* **2012**, *31*, 5791.
23. Miernicka, M.; Szulawska, A.; Czyz, M.; Lorenz, I.-P.; Mayer, P.; Karwowski, B.; Budzisz, E. *J. Inorg. Biochem.* **2008**, *102*, 157.
24. Anderson, C. M.; Crespo, M.; Jennings, M. C.; Lough, A. J.; Ferguson, G.; Puddephatt, R. J. *Organometallics* **1991**, *10*, 2672.
25. Gómez, M.; Granell, J.; Martinez, M. *Inorg. Chem. Commun.* **2002**, *5*, 67.
26. López, C.; Solans, X.; Font-Bardía, M. *Inorg. Chem. Commun.* **2005**, *8*, 631.
27. Pérez, S.; López, C.; Caubet, A.; Bosque, R.; Solans, X.; Bardía, M. F.; Roig, A.; Molins, E. *Organometallics* **2004**, *23*, 224.
28. Pérez, S.; López, C.; Caubet, A.; Solans, X.; Font-Bardía, M. *New J. Chem.* **2003**, *27*, 975.
29. Crespo, M.; Font-Bardia, M.; Granell, J.; Martínez, M.; Solans, X. *J. Chem. Soc., Dalton Trans.* **2003**, 3763.
30. Capapé, A.; Crespo, M.; Granell, J.; Font-Bardía, M.; Solans, X. *J. Organomet. Chem.* **2005**, *690*, 4309.
31. Crespo, M.; Granell, J.; Solans, X.; Font-Bardia, M. *Organometallics* **2002**, *21*, 5140.
32. Ligands **2a** and **2b** hydrolyze in polar solvents (i.e., water, alcohols, DMSO) and this precluded the calculation of their IC_{50} values. Also, for the same reason it was imposible to determine for this two compounds the shift mobility of plasmid DNA.
33. Moradell, S.; Lorenzo, J.; Rovira, A.; Robillard, M. S.; Avilés, F. X.; Moreno, V.; de Llorens, R.; Martinez, M. A.; Reedijk, J.; Llobet, A. *J. Inorg. Biochem.* **2003**, *96*, 493.

34. Martin, R.; Crespo, M.; Font-Bardia, M.; Calvet, T. *Organometallics* **2009**, *28*, 587.
35. Cortés, R.; Crespo, M.; Davin, L.; Martín, R.; Quirante, J.; Ruiz, D.; Messeguer, R.; Calvis, C.; Baldomà, L.; Badia, J.; Font-Bardía, M.; Calvet, T.; Cascante, M. *Eur. J. Med. Chem.* **2012**, *54*, 557.
36. Chang, T. T.; More, S. V.; Lu, N.; Jhuo, J.-W.; Chen, Y.-C.; Jao, S.-C.; Li, W.-S. *Bioorg. Med. Chem.* **2011**, *19*, 4887.
37. El-Mehasseb, I. M.; Kodaka, M.; Okada, T.; Tomohiro, T.; Okamoto, K.-I.; Okuno, H. *J. Inorg. Biochem.* **2001**, *84*, 157.
38. Okada, T.; El-Mehasseb, I. M.; Kodaka, M.; Tomohiro, T.; Okamoto, K.; Okuno, H. *J. Med. Chem.* **2001**, *4*, 4661.
39. Ruiz, J.; Rodríguez, V.; Cutillas, N.; Espinosa, A.; Hannon, M. J. *J. Inorg. Biochem.* **2011**, *105*, 525.
40. Samouei, H.; Rashidi, M.; Heinemann, F. W. *J. Organomet. Chem.* **2011**, *696*, 3764.
41. Edwards, G. L.; Black, D. S. C.; Deacon, G. B.; Wakelin, L. P. G. *Can. J. Chem.* **2005**, *83*, 969.
42. Edwards, G. L.; Black, D. S. C.; Deacon, G. B.; Wakelin, L. P. G. *Can. J. Chem.* **2005**, *83*, 980.
43. Wang, P.; Leung, C.-H.; Ma, D.-L.; Sun, R. W.-Y.; Yan, S.-C.; Chen, Q.-S.; Che, C.-M. *Angew. Chem., Int. Ed.* **2011**, *50*, 2554.
44. Ma, D.-L.; Che, C.-M. A. *Chem. Eur. J.* **2003**, *9*, 6133.
45. Mosmann, T. *J. Immunol. Methods* **1983**, *65*, 55.
46. Matito, C.; Mastorakou, F.; Centelles, J. J.; Torres, J. L.; Cascante, M. *Eur. J. Nutr.* **2003**, *42*, 42.
47. Givens, K. T.; Kitada, S.; Chen, A. K.; Rothschiller, J.; Lee, D. A. *Invest. Ophthalmol. Vis. Sci.* **1856**, *1990*, 31.
48. Abdullah, A.; Huq, F.; Chowdhury, A.; Tayyem, H.; Beale, P.; Fisher, K. *BMC Chem. Biol.* **2006**, *6*, 3.
49. Becke, A. D. *J. Chem. Phys.* **1993**, *98*, 5648.
50. Lee, C.; Yang, W.; Parr, R. G. *Phys. Rev. B* **1988**, *37*, 785.
51. Frisch, M. J.; Trucks, G. W.; Schlegel, H. B.; Scuseria, G. E.; Robb, M. A.; Cheeseman, J. R.; Montgomery, J. A.; Vreven, T.; Kudin, K. N.; Burant, J. C.; Millam, J. M.; Iyengar, S. S.; Tomasi, J.; Barone, V.; Mennucci, B.; Cossi, M.; Scalmani, G.; Rega, N.; Petersson, G. A.; Nakatsuji, H.; Hada, M.; Ehara, M.; Toyota, K.; Fukuda, R.; Hasegawa, J.; Ishida, M.; Nakajima, T.; Honda, Y.; Kitao, O.; Nakai, H.; Klene, M.; Li, X.; Knox, J. E.; Hratchian, H. P.; Cross, J. B.; Bakken, V.; Adamo, C.; Jaramillo, J.; Gomperts, R.; Stratmann, R. E.; Yazyev, O. A.; Austin, J.; Cammi, R.; Pomelli, C.; Ochterski, J. W.; Ayala, P. Y.; Morokuma, K.; Voth, G. A.; Salvador, P.; Dannenberg, J. J.; Zakrzewski, V. G.; Dapprich, S.; Daniels, A. D.; Strain, M. C.; Farkas, O.; Malick, D. K.; Rabuck, A. D.; Raghavachari, K.; Foresman, J. B.; Ortiz, J. V.; Cui, Q.; Baboul, A. G.; Clifford, S.; Cioslowski, J.; Stefanov, B. B.; Liu, G.; Liashenko, A.; Piskorz, P.; Komaromi, I.; Martin, R. L.; Fox, D. J.; Keith, T.; Al-Laham, M. A.; Peng, C. Y.; Nanayakkara, A.; Challacombe, M.; Gill, P. M. W.; Johnson, B.; Chen, W.; Wong, M. W.; González, C.; Pople, J. A. GAUSSIAN *03, (Revision C.02)*; Gaussian: Wallingford, CT, 2004.
52. Wadt, W. R.; Hay, P. J. *J. Chem. Phys.* **1985**, *82*, 284.
53. Hay, P. J.; Wadt, W. R. *J. Chem. Phys.* **1985**, *82*, 299.
54. Höllwarth, A.; Böhme, M.; Dapprich, S.; Ehlers, A. W.; Gobbi, A.; Jonas, V.; Köhler, K. F.; Stegmann, R.; Veldkamp, A.; Frenking, G. *Chem. Phys. Lett.* **1993**, *208*, 237.
55. Hehre, W. J.; Ditchfield, K.; Pople, J. A. *J. Chem. Phys.* **1972**, *56*, 2257.
56. Hariharan, P. C.; Pople, J. A. *Theor. Chim. Acta* **1973**, *28*, 213.
57. Cossi, M.; Rega, N.; Scalmani, G.; Barone, V. *J. Comput. Chem.* **2003**, *24*, 669.

CAPÍTULO 1C

COMPLEJOS DE PLATINO(II) Y DE PALADIO(II) CON LIGANDOS (N,N') Y (C,N,N')⁻ DERIVADOS DEL PIRAZOL COMO AGENTES ANTITUMORALES Y ANTIMALÁRICOS: SÍNTESIS, CARACTERIZACIÓN Y ACTIVIDADES IN VITRO.

Josefina Quirante [a], Daniel Ruiz [a], Asensio Gonzalez [a], Concepción López [b,*], Marta Cascante [c], Roldán Cortés [c], Ramon Messeguer [d], Carme Calvis [d], Laura Baldomà [e], Aurélie Pascual [f], Yann Guérardel [g,h], Bruno Pradines [f], Mercè Font-Bardía [i], Teresa Calvet [j], Christophe Biot [g,h,]**

[a] Laboratori de Química Orgànica, Facultat de Farmàcia, Institut de Biomedicina, (IBUB), Universitat de Barcelona, Av. Joan XXIII, s/n, 08028 Barcelona, España

[b] Departament de Química Inorgànica, Facultat de Química, Universitat de Barcelona, Martí i Franquès 1-11, 08028 Barcelona, España

[c] Departament de Bioquímica i Biologia Molecular, Facultat de Biologia, Institut de Biomedicina de la Universitat de Barcelona (IBUB) y IDIBAPS, Unidad Asociada al CSIC, Diagonal 643, 08028 Barcelona, España

[d] Leitat Tecnological Center, Parc Cientific de Barcelona, Edifici Hèlix, C/Baldiri Reixach, 15-21, 08028 Barcelona, España

[e] Departament de Bioquímica i Biologia Molecular, Facultat de Farmàcia, Institut de Biomedicina de la Universitat de Barcelona (IBUB), Av. Joan XXIII s/n, 08028 Barcelona, España

[f] Institut de Recherche Biomédicale des Armées, Antenne de Marseille, Unité de Parasitologie, URMITE-UMR 6236, Allée du Médecin Colonel Jamot, Parc le Pharo, BP 60109, 13262 Marsella Cedex 07, Francia

[g] Université Lille Nord de France, Université Lille 1, Unité de Glycobiologie Structurale et Fonctionnelle, 59650 Villeneuve d'Ascq, Francia

[h] UMR CNRS 8576, Francia

[i] Unitat de Difracció de Raig-X, Centre Científici Tecnològic de La Universitat de Barcelona, Solé I Sabarís 1-5, 08028 Barcelona, España

[j] Departament de Cristal·lografia, Mineralogia I Dipòsits Minerals, Facultat de Geologia, Universitat de Barcelona, Martí i Franquès s/n. 08028 Barcelona, España

Resumen

El estudio de la reactividad de tres derivados de 1-(2-dimetilaminoetil)-1H-pirazol, de fórmula general [1-(CH_2)2NMe_2}-3,5-R_2-pzol] {donde pzol representa pirazol y R representa H (**1a**), Me (**1b**) o Ph (**1c**)} con [$MCl_2(DMSO)_2$] (M representa Pt o Pd) bajo diferentes condiciones experimentales nos ha permitido aislar y caracterizar *cis*-[M{κ^2-*N,N'*-{[1-(CH_2)$_2$$NMe_2$}-3,5-$R_2$-pzol])}Cl2] {MM representa PtPt (**2a**–**2c**) o Pd (**3a**–**3c**)} y los dos complejos ciclometalados [M{κ^3-*C,N,N'*-{[1-(CH_2)$_2$$NMe_2$}-3-($C_5H_4$)-5-Ph-pzol])}Cl] {M representa Pt(II) (**4c**) o Pd(II) (**5c**)}. Los compuestos **4c** y **5c** se generan por la ortometalación del anillo 3-fenilo del ligando **1c**. El complejo **2a** ha sido también caracterizado mediante cristalografía de rayos-X. Se ha evaluado la actividad antimalárica in vitro sobre *Plasmodium falciparum*, así como las actividades antiproliferativas sobre líneas de cáncer de pulmón (A549) y de mama (MDA-MB231 y MCF7). Los complejos **2a**-**2c** y **5c** exhibieron una actividad antimalárica moderada sobre dos cepas de *P. falciparium* (3D7 y W2). En cambio, los ensayos de viabilidad celular revelaron que el cicloplatinado **4c** exhibe mayor actividad que el cisplatino en las tres líneas tumorales, y que el complejo **2a** genera una notable actividad selectiva sobre células de pulmón (IC_{50}=3 µM) con respecto a células de mama (IC_{50}>20 µM). Así, los complejos **2c** y **4c** resultan prometedores puntos de partida en la creación de una nueva familia de agentes antitumorales. También se han llevado a cabo estudios de movilidad electroforética del ADN con los compuestos sintetizados, con el objetivo de obtener información acerca de su mecanismo de acción.

Journal of Inorganic Biochemistry 105 (2011) 1720–1728

Contents lists available at SciVerse ScienceDirect

Journal of Inorganic Biochemistry

journal homepage: www.elsevier.com/locate/jinorgbio

Platinum(II) and palladium(II) complexes with (N,N′) and (C,N,N′)$^-$ ligands derived from pyrazole as anticancer and antimalarial agents: Synthesis, characterization and in vitro activities

Josefina Quirante [a], Daniel Ruiz [a], Asensio Gonzalez [a], Concepción López [b,*], Marta Cascante [c], Roldán Cortés [c], Ramon Messeguer [d], Carme Calvis [d], Laura Baldomà [e], Aurélie Pascual [f], Yann Guérardel [g,h], Bruno Pradines [f], Mercè Font-Bardía [i], Teresa Calvet [j], Christophe Biot [g,h,**]

[a] Laboratori de Química Orgànica, Facultat de Farmàcia, Institut de Biomedicina, (IBUB), Universitat de Barcelona, Av. Joan XXIII, s/n, 08028 Barcelona, Spain
[b] Departament de Química Inorgànica, Facultat de Química, Universitat de Barcelona, Martí i Franquès 1-11, 08028 Barcelona, Spain
[c] Department of Biochemistry and Molecular Biology, Faculty of Biology, Institute of Biomedicine of University of Barcelona (IBUB) and IDIBAPS, Unit Associated with CSIC, Diagonal 645, 08028 Barcelona, Spain
[d] Leitat Tecnological Center, Parc Cientific de Barcelona, Edifici Hèlix, C/Baldiri Reixach, 15-21, 08028 Barcelona, Spain
[e] Departament de Bioquímica i Biologia Molecular, Facultat de Farmàcia, Institut de Biomedicina de la Universitat de Barcelona (IBUB), Av. Joan XXIII s/n, 08028 Barcelona, Spain
[f] Institut de Recherche Biomédicale des Armées, Antenne de Marseille, Unité de Parasitologie, URMITE-UMR 6236, Allée du Médecin Colonel Jamot, Parc le Pharo, BP 60109, 13262 Marseille Cedex 07, France
[g] Université Lille Nord de France, Université Lille 1, Unité de Glycobiologie Structurale et Fonctionnelle, 59650 Villeneuve d'Ascq, France
[h] UMR CNRS 8576, France
[i] Unitat de Difracció de Raig-X, Centre Científici Tecnològic de La Universitat de Barcelona, Solé I Sabarís 1-5, 08028 Barcelona, Spain
[j] Departament de Cristal.lografia, Mineralogia I Dipòsits Minerals, Facultat de Geologia, Universitat de Barcelona, Martí i Franquès s/n. 08028 Barcelona, Spain

ARTICLE INFO

Article history:
Received 31 May 2011
Received in revised form 12 September 2011
Accepted 14 September 2011
Available online 22 September 2011

Keywords:
Cancer
Malaria
Palladium
Platinum

ABSTRACT

The study of the reactivity of three 1-(2-dimethylaminoethyl)-1*H*-pyrazole derivatives of general formula [1-(CH$_2$)$_2$NMe$_2$}-3,5-R$_2$-pzol] {where pzol represents pyrazole and R═H (**1a**), Me (**1b**) or Ph (**1c**)} with [MCl$_2$(DMSO)$_2$] (M═Pt or Pd) under different experimental conditions allowed us to isolate and characterize *cis*-[M{κ^2-*N*,*N*′-{[1-(CH$_2$)$_2$NMe$_2$}-3,5-R$_2$-pzol]}Cl$_2$] {MM═PtPt (**2a**–**2c**) or Pd (**3a**–**3c**)} and two cyclometallated complexes [M{κ^3-*C*,*N*,*N*′-{[1-(CH$_2$)$_2$NMe$_2$}-3-(C$_5$H$_4$)-5-Ph-pzol]}Cl] {M═Pt(II) (**4c**) or Pd(II) (**5c**)}. Compounds **4c** and **5c** arise from the orthometallation of the 3-phenyl ring of ligand **1c**. Complex **2a** has been further characterized by X-ray crystallography. Ligands and complexes were evaluated for their in vitro antimalarial against *Plasmodium falciparum* and cytotoxic activities against lung (A549) and breast (MDA MB231 and MCF7) cancer cellular lines. Complexes **2a**–**2c** and **5c** exhibited only moderate antimalarial activities against two *P. falciparum* strains (3D7 and W2). Interestingly, cytotoxicity assays revealed that the platinacycle **4c** exhibits a higher toxicity than cisplatin in the three human cell lines and that the complex **2a** presents a remarkable cytotoxicity and selectivity in lung (IC$_{50}$ = 3 μM) versus breast cancer cell lines (IC$_{50}$ > 20 μM). Thus, complexes **2c** and **4c** appear to be promising leads, creating a novel family of anticancer agents. Electrophoretic DNA migration studies in presence of the synthesized compounds have been performed, in order to get further insights into their mechanism of action.

1. Introduction

Platinum drugs have played a key role among the metal-based anticancer agents [1]. The discovery of the antitumor properties of *cis*-[PtCl$_2$(NH$_3$)$_2$] *cisplatin* [2] (Fig. 1) in 1965 was rapidly followed by clinical trials and finally in 1978, FDA granted approval. Platinum(II) complexes such as cisplatin and carboplatin (Fig. 1) are widely used to treat cancers such as testicular, ovarian, urinary bladder, melanoma, etc. The cytotoxicity of Pt-based drugs is mainly attributed to their ability to bind DNA and to induce DNA damage leading then to apoptosis [3–5].

Unfortunately, the use of cisplatin is restricted due to dose-limiting toxicity, including nephrotoxicity, neurotoxicity and ototoxicity [6,7]. Additional side effects such as blood pressure increase, severe nausea, vomiting and diarrhea have also been reported. Moreover, the biochemical resistance mode limits the clinical utility of the Pt-based drugs in current use [1].

* Corresponding author. Tel.: +34 934039134; fax: +34 934907725.
** Correspondence to: C. Biot, Université Lille Nord de France, Université Lille 1, Unité de Glycobiologie Structurale et Fonctionnelle, 59650 Villeneuve d'Ascq, France. Tel.: +33 3 20436941; fax: +33 3 20436555.
E-mail addresses: conchi.lopez@qi.ub.es (C. López), christophe.biot@univ-lille1.fr (C. Biot).

0162-0134/$ – see front matter © 2011 Elsevier Inc. All rights reserved.
doi:10.1016/j.jinorgbio.2011.09.021

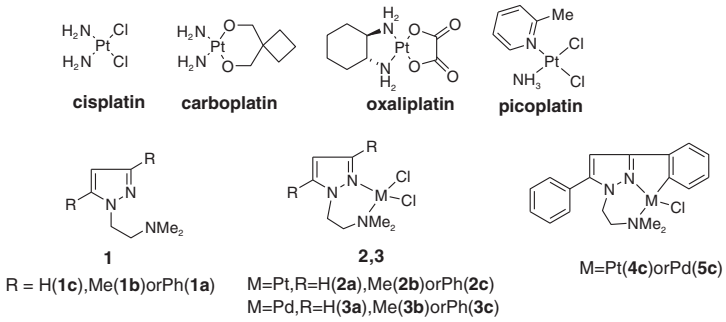

Fig. 1. Chemical structure of some platinum(II) based anticancer agents and compounds used in this study.

In the search of new metallodrugs avoiding toxicity and resistance, special attention has been paid to the replacement of one or both NH_3 ligands of *cisplatin* by other *N*-donor ligand(s). This strategy gave rise to oxaliplatin and picoplatin [8] (Fig. 1). In oxaliplatin, which is active in patients with colorectal cancer, both NH_3 units have been replaced by (1*R*,2*R*)-cyclohexane-1,2-diamine (*R*,*R*-dach); while picoplatin, that is in clinical development for the treatment of patients with solid tumors, contains a 2-methylpyridine instead of one NH_3 ligand.

The search of novel *N*-donor ligands (i.e. amines, oximes, imines or azoles) for the synthesis of optimized platinum(II) and palladium(II) drugs is still in progress [9,10]. In addition, it is well-known that azoles are valuable reagents in coordination chemistry and that their binding to a transition metal ion affects their properties and activities. Few complexes with pyrazole ligands showing an antitumor activity similar to that of cisplatin have been reported [11–20], but the effect produced by the substituents on the heterocycle has not been clarified so far. Within this therapeutic context, and in order to clarify this point and to elucidate the influence of mode of binding of this family of ligands in the biological activity of the complexes, we decided to synthesize the new pyrazole derivatives **1a**–**1c** (Fig. 1) and to study their reactivity with Pt(II) and Pd(II). Due to the relative disposition of the two nitrogen atoms, compounds **1a**–**1c** may bind to the M(II) center as a neutral (*N*) or (*N*,*N*′) ligand. Moreover, for **1c**, the presence of the phenyl ring on position 3 of the heterocycle may also allow the formation of metallacycles containing **1c** as a *mer*-terdentate $(C,N,N')^-$ ligand.

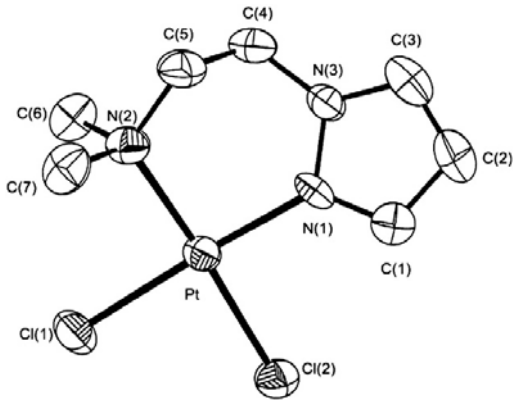

Fig. 2. ORTEP plot of complex **2a**. Hydrogen atoms have been omitted for clarity. Selected bond lengths (in Å) and angles (in deg.) for **2a**: Pt–N(1), 2.010(3); Pt–N(3), 2.091(4); Pt–Cl(1), 2.3056(13); Pt–Cl(2), 2.3058(13); N(1)–C(1),1.339(6); N(1)–N(2), 1.370(6); N(3)–C(7), 1.499(5); N(3)–C(6), 1.499(7); N(3)–C(8), 1.506(6); C(1)–C(2), 1.409(8); C(2)–C(3), 1.367(10); C(3)–N(2), 1.349(7); N(2)–C(5), 1.453(7); C(5)–C(6), 1.483(7); N(1)–Pt–N(3), 93.57(15); N(1)–Pt–Cl(1), 176.60(11), N(3)–Pt–Cl(1), 89.61(12); N(1)–Pt–Cl(2), 89.32(12); N(3)–Pt–Cl(2), 177.03(12); Cl(1)–Pt–Cl(2), 87.52(5); C(1)–N(1)–N(2), 105.3(4); C(1)–N(1)–Pt, 129.5(3); N(2)–N(1)–Pt, 125.2(3); C(7)–N(3)–C(6), 108.2(4); C(7)–N(3)–C(8), 108.3(4); C(6)–N(3)–C(8), 106.6(4); C(7)–N(3)–Pt, 109.7(3); C(6)–N(3)–Pt, 113.5(3); C(8)–N(3)–Pt, 110.4(3); N(1)–C(1)–C(2), 111.0(5); C(3)–C(2)–C(1), 104.7(5); N(2)–C(3)–C(2), 108.5(6); C(3)–N(2)–N(1), 110.6(4); C(3)–N(2)–C(5), 129.1(5); N(1)–N(2)–C(5), 120.1(4); N(2)–C(5)–C(6), 111.5(4) and C(5)–C(6)–N(3), 113.8(4).

In this work, we present the study of the reactivity of ligands **1a**–**1c** with syntheses of *cis*-$[MCl_2(DMSO)_2]$, the new compounds **2a**–**2c** and **3a**–**3c** and the cyclometallated complexes **4c** and **5c**, together with a comparative study of their antineoplastic activity against lung (A549) and breast (MDA MB231 and MCF7) human cancer cell lines. As our interests lie also in the area of antiparasitic drugs [42,43] and since a few Pt(II) [44] and Pd(II) based complexes [45] with antimalarial activity (in the micromolar range) have been reported, we also tested the potential of the free ligands (**1a**–**1c**) and the complexes **2a**–**5c** against the chloroquine-susceptible strain (3D7) and the chloroquine-resistant strain (W2) of *Plasmodium falciparum*.

Cyclometallated complexes derived from *N*-donor ligands have attracted great interest during the last decade due to their properties and applications in a wide variety of fields [10,20–36] and compounds of this kind containing Pd(II), Pt(II), Ru(II), Ir(III) Rh(III) and Au have shown promising cytotoxic activities [10,20,27–36]. Few cyclopalladated complexes derived from pyrazole are known [37–41] and, to the best of our knowledge, their cytotoxicity has only been reported once [41]. On the other hand despite the interest for Pt(II) complexes, platinacycles with pyrazolyl ligands are scarce and studies on their biological activity have not been performed so far.

2. Experimental

2.1. Chemistry

2.1.1. Materials and methods

Reagents were obtained from commercial sources and used as received. *Cis*-$[MCl_2(DMSO)_2]$ (M═Pd or Pt) were prepared according to literature protocols [46,47]. All reactions were carried out with dry and freshly distilled solvents. Column chromatography refers to flash chromatography and was carried out on SiO_2 (silica gel 60, SDS, 230–240 mesh) or Al_2O_3 (neutral alumina, 63–200 μm). Analytical TLC was performed on SiO_2 (Merck silica gel 60 F_{254}) plates. Elemental analyses were carried out at the Serveis Cientifico-Tècnics (*Universitat Barcelona*). Mass spectra (electrospray ionization, ESI^+) were performed at the Servei d'Espectrometria de Masses (*Universitat de Barcelona*). Infrared spectra were obtained with a Nicolet 400FTIR instrument using KBr pellets. Only noteworthy IR absorptions are listed. Unless otherwise noted ^1H and ^{13}C NMR spectra were recorded in $CDCl_3$ at 298 K with a Mercury-400 MHz. ^1H and ^{13}C chemical shifts (δ) are reported in ppm downfield and referred to $SiMe_4$ and to the resonance of $CDCl_3$, respectively and coupling constants (*J*) are given in Hz. All NMR assignments were

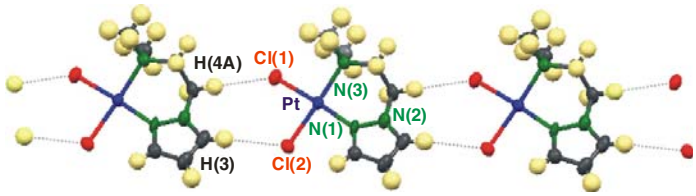

Fig. 3. Assembly of molecules of **2a** in the crystal by multiple weak C–H···Cl intermolecular interactions involving: a) the two chlorides {Cl(1) and Cl(2)} the unit at (*x*, *y*, *z*) (represented as the central unit) and the H(4B) and H(3) atoms, respectively of another and close molecule at (*x*, *1 + y*, *z*) and b) these two hydrogen atoms and the two Cl^- ligands of the molecule located at (*− 1 + x*, *y*, *z*).

made on the basis of two dimensional NMR experiments (gradient correlation spectroscopy gCOSY, gradient heteronuclear single quantum correlation gHSQC, and gradient Heteronuclear Single Quantum Correlation gHMBC). In all cases the atom labeling scheme for the assignment of the signals corresponds to that shown in Scheme 1. If not specified, ^{195}Pt{^{1}H} NMR spectra of **2a**, **2c** and **4c** were recorded in $CDCl_3$ with a Bruker 250DXR instrument using $CDCl_3$ as solvent and $H_2[PtCl_6]$ {δ^{195}Pt($H_2[PtCl_6]$) = 0.0 ppm} as reference. The splitting of proton resonances in the reported ^{1}H NMR spectra is defined as s = singlet, d = doublet, dd = doublet of doublet, t = triplet, td = triplet of doublet and m = multiplet.

*2.1.2. Synthesis of ligands [1-(CH$_2$)$_2$NMe$_2$}-3,5-R$_2$-pzol] {R═H (**1a**), Me (**1b**) or Ph (**1c**)}*

*2.1.2.1. Preparation of 1-(2-dimethylaminoethyl)-1H-pyrazole (**1a**).* A mixture of 1*H*-pyrazole (1.92 g, 2.8×10^{-3} mol) and sodamide (1.56 g, 4×10^{-3} mol) in dry toluene (20 mL) was heated at reflux temperature with stirring for 2.5 h. The mixture was cooled, 2-dimethylaminoethyl chloride hydrochloride (2.6 g, 2.8×10^{-3} mol) was added, and the mixture was heated under reflux for 4 h. Water (20 mL) was added, the toluene layer was separated and the aqueous phase was extracted with toluene (20 mL). The joined organic phases was extracted with aqueous 0.1 M HCl solution, basified with aqueous saturated Na_2CO_3, extracted with CH_2Cl_2, dried with Na_2SO_4 and finally evaporated to dryness to give **1a** as a colorless oil (2.6 g, 67%). IR (cm^{-1}): 3423, 2946, 2772, 1461, 1397, 1283, 1092, 1054, 751. ^{1}H NMR (gCOSY): 2.27 (s, 6 H, NMe_2), 2.76 (t, J = 7 Hz, 2 H, $-CH_2-^b$), 4.24 (t, J = 7 Hz, 2 H, $-CH_2-^a$), 6.24 (m, 1 H, H^4), 7.45 (d, J = 2 Hz, 1 H, H^5), 7.50 d, J = 1.6 Hz, 1 H, H^3). ^{13}C NMR (gHSQC, gHMBC): 45.6 (NMe_2), 50.2 (C^a), 59.2 (C^b), 105.3 (C^4), 129.3 (C^5), 139.2 (C^3). EM (ESI^+): m/z = 140.12 (Calc. 140.11) $\{[M]+H\}^+$. $C_7H_{13}N_3$ (FW = 139.11).

*2.1.2.2. Preparation of 1-(2-dimethylaminoethyl)-3,5-dimethyl-1H-pyrazole (**1b**).* This product **1b** was obtained as a colorless oil following the same procedure as described for **1a**. Yield 75%. IR (cm^{-1}): 3423, 2945, 2771, 1554, 1461, 1425, 1386, 1042, 1018, 773. ^{1}H NMR (gCOSY): 2.21 (s, 3H, Me), 2.21 (s, 3H, Me), 2.28 (s, 6H, $-NMe_2$), 2.68 (t, J = 3.2, 2H, $-CH_2-^b$), 4.06 (t, J = 3.4, 2H, $-CH_2-^a$), 5.77 (s, 1H, H^4). ^{13}C NMR (gHSQC, gHMBC): 11.0 (Me), 22.0 (Me), 45.7 ($-NMe_2$), 46.0 (C^a), 59.1 (C^b), 104.9 (C^4), 140.0 (C^5), 147.4 (C^3). EM (ESI^+): m/z = 168.15 (Calc. 168.14) $\{[M]+H\}^+$. $C_9H_{17}N_3$ (FW = 167.14).

*2.1.2.3. 1-(2-dimethylaminoethyl)-3,5-diphenyl-1H-pyrazole (**1c**).* To a suspension of 3,5-diphenylpyrazole (1.26 g, 5.74×10^{-3} mol) in toluene (100 mL) Aliquat 336 (1 g), 40% aqueous NaOH solution (50 mL) and $ClCH_2CH_2NMe_2\cdot HCl$ (2.5 g, 23.04×10^{-3} mol) were added and the resulting mixture was stirred at 95 °C for 24 h. After this period water (50 mL) was added, the organic phase was extracted, dried with Na_2SO_4 and finally evaporated to dryness. The crude material was chromatographed on silica gel (Et_2O to Et_2O:CH_2Cl_2 1:1), to yield the ligand **1c** as a clear viscous oil (1.28 g, 77%). An analytical sample was recrystallized from hexane/CH_2Cl_2 to obtain colorless crystals. IR (cm^{-1}): 3463, 3040, 2945, 2819, 2775, 1483, 1460, 1438, 1299, 763, 694. ^{1}H NMR (gCOSY): 2.17 (s, 6H, NMe_2), 2.79 (t, J = 7.2, 2H, $-CH_2-^b$), 2.25 (t, J = 7.2, 2H, $-CH_2-^a$), 6.57 (s, 1H, H^4), 7.25–7.48 (m, 8H, ArH), 7.83 (dd, J = 8 and 1.4, 2H, $H^{2'}$ and $H^{6'}$). ^{13}C NMR (gHSQC): 45.6 (NMe_2), 47.8 (C^a), 59.1 (C^b), 103.4 (C^4), 125.6, 127.5, 128.5, 128.7, 129.0 (Ar) 130.8, 135.5 ($C^{1'}$ and $C^{1''}$), 145.1 (C^5), 150.7 (C^3). EM (ESI^+): m/z = 292.18 (Calc. 292.17) $\{[M]+H\}^+$. Anal (%) Calc. for $C_{19}H_{21}N_3.1/4\ H_2O$: C, 77.12; H, 7.32; N, 14.20. Found: C, 77.5; H, 7.4; N, 14.4. $C_{19}H_{21}N_3$ (FW = 291.17).

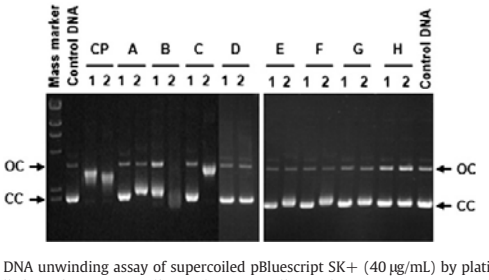

Fig. 4. DNA unwinding assay of supercoiled pBluescript SK+ (40 μg/mL) by platinum and palladium drugs at 5 μM (lanes 1) or 50 μM (lanes 2). A, **2c**; B, **5c**; C, **2a**; D, **4c**; E, **3b**; F, **3a**; G, **2b**, H, **1c**. Cisplatin (CP) was analyzed in parallel for comparison. The molecular mass marker was lambda DNA digested with HindIII. cc, closed circular DNA form (supercoiled form); oc, open circular DNA form.

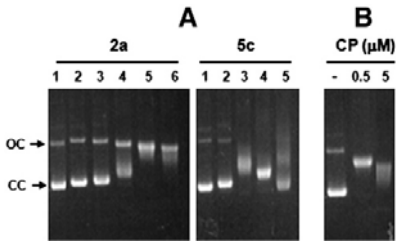

Fig. 5. (A) Interaction of pBluescript SK+ plasmid DNA (40 μg/mL) with increasing concentrations of the platinum(II) complex **2a** and the palladium(II) complex **5c**. Lanes 1, DNA only; lanes 2, 5 μM drug; lanes 3, 10 μM drug, lanes 4, 25 μM drug; lanes 5, 50 μM drug; and lanes 6, 100 μM drug. (B) Unwinding assay with cisplatin (CP) at the indicated concentrations for comparison. cc, closed circular DNA form; oc, open circular DNA form.

*2.1.3. Synthesis of compounds cis-[Pt{κ^2-N,N′-[1-(CH$_2$)$_2$NMe$_2$]-3,5-R$_2$-pzol}Cl$_2$] (**2**)*

*2.1.3.1. Cis-[Pt{κ^2-N,N′-[1-(CH$_2$)$_2$NMe$_2$]pzol}Cl$_2$] (**2a**).* A suspension of *cis*-$[PtCl_2(DMSO)_2]$ (52.8 mg, 125×10^{-3} mol) and ligand **1a** (17.4 mg, 125×10^{-3} mol) in toluene (10 mL) was heated at reflux temperature for 2 h. The reaction mixture was evaporated to dryness and the obtained

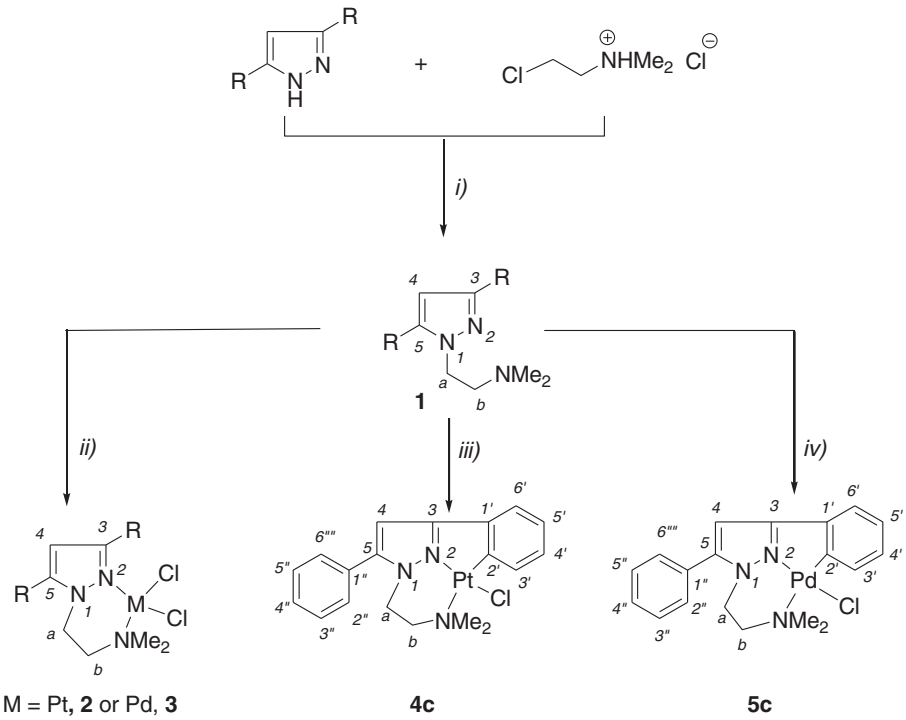

Scheme 1. Synthesis of ligands (**1a**–**1c**) and their palladium(II) and platinum(II) derivatives with **1** acting as a bidentate (N,N′) ligand (**2**, ·**3**) and the cyclometallated compounds **4c** and **5c**. In order to ease the visualization of the reactions, letters **a**, **b** and **c** refer to the substituents on positions 3 and 5 of the pyrazole {R═H (**a**), Me (**b**) or Ph (**c**)}. Reagents and conditions: i) in toluene, in the presence of sodamine (for R═H or Me) or using Aliquat 336 and NaOH (40%) for R═Ph. ii) *Cis*-[$MCl_2(DMSO)_2$] (M═Pt or Pd for **2** and **3**, respectively) (1:1) toluene, reflux; iii) *Cis*-[$PtCl_2(DMSO)_2$] and NaOAc in toluene:MeOH (12:1) mixture, reflux 3 h. iv) *Cis*-[$PdCl_2(DMSO)_2$] and NaOAc in toluene:MeOH (12:1) mixture, reflux 1 h.

residue was purified by column chromatography (Al_2O_3, hexane: acetone 50:50 to 25:75) to yield 33 mg (65%) of the title complex as a yellow solid. An analytical sample was recrystallized from CH_2Cl_2/MeOH. IR (cm^{-1}): 3430, 3085, 2921, 1740, 1627, 1517, 1447, 1422, 1156, 1020, 756. ^1H NMR (DMSO-d_6, 500 MHz, gCOSY): 2.85 (m, 2H, $-CH_2-^b$), 2.94 (s, 6H, NMe_2), 4.53 (m, 2H, $-CH_2-^a$), 6.45 (m, 1H, H^4), 8.07 (m, 2H, H^3 and H^5). ^{13}C NMR (DMSO-d_6, 125.9 MHz, gHSQC, gHMBC): 47.5 (C^a), 52.4 ($-NMe_2$), 62.6 (C^b), 105.8 (C^4), 133.8 (C^5), 141.3 (C^3). $^{195}Pt\{^1H\}$ NMR (DMSO-d_6, 54 MHz): −2178 (s).[1] EM (ESI^+): m/z = 422.05 (Calc. 422.05) $\{[M]+NH_4\}^+$. Anal (%) Calc. for $C_7H_{13}Cl_2N_3Pt$ (FW = 404.01): C, 20.75; H, 3.23; N, 10.37. Found: C, 20.9; H, 3.3; N, 10.3.

*2.1.3.2. Cis-[Pt{κ²-N,N′-[1-$(CH_2)_2NMe_2$]-3,5-Me_2pzol}Cl_2] (**2b**).* A suspension of *cis*-[$PtCl_2(DMSO)_2$] (52.8 mg, 125×10^{-3} mol) and ligand **1b** (20.9 mg, 125×10^{-3} mol) in toluene (10 mL) was heated at reflux temperature for 3 h. The reaction mixture was evaporated to dryness and the residue was treated with MeOH (10 mL). The obtained suspension was stirred for 2 h and filtered out. The solid was washed with two 5 mL portions of CH_2Cl_2 to remove the MeOH, and finally dried under vacuum to yield 32.5 mg (60%) of complex **2b** as a yellow solid. IR (cm^{-1}): 3427, 2916, 2342, 1553, 1465, 1450, 1156, 987, 808. ^1H NMR (DMSO-d_6, 500 MHz, gCOSY): 2.33 (s, 3H, Me), 2.43 (s, 3H, Me), 2.45 (m, 2H, $-CH_2-^b$), 2.83 (s, 6H, NMe_2), 4.40 (m, 2H, $-CH_2-^a$), 6.09 (s, 1H, H^4). ^{13}C NMR (DMSO-d_6, 125.9 MHz, gHSQC, gHMBC): 11.1 (Me), 14.7 (Me), 45.4 (C^a), 53.1 (NMe_2), 64.1 (C^b), 107.8 (C^4), 143.5 (C^5), 153.1 (C^3). EM (ESI^+): m/z = 450.10 (Calc. 450.08) $\{[M]+NH_4\}^+$. Anal (%) Calc. for $C_9H_{17}Cl_2N_3Pt$ (FW = 432.04): C, 24.95; H, 3.96; N, 9.70. Found: C, 25.0; H, 4.0; N, 9.4.

*2.1.3.3. Cis-[Pt{κ²-N,N′-[1-$(CH_2)_2NMe_2$]-3,5-Ph_2-pzol}Cl_2] (**2c**).* A suspension of *cis*-[$PtCl_2(DMSO)_2$] (26.4 mg, 62.5×10^{-3} mol) and ligand **1c** (18.2 mg, 62.5×10^{-3} mol) in toluene (5 mL) was heated at reflux for 1.5 h. The solid formed was filtered out and purified by column chromatography {Al_2O_3, hexane: CH_2Cl_2 (25:75)} to yield 23 mg (66%) of the title complex as a yellow solid. IR (cm^{-1}): 3430, 2925, 1628, 1480, 1023, 768, 698. ^1H NMR (gCOSY): 2.66 (b m, 2H, $-CH_2-^b$), 3.18 (s, 6H, $-NMe_2$), 4.6 (b m, 2H, $-CH_2-^a$), 6.65 (s, 1H, H^4), 7.45 (m, 2H, $H^{2''}$ and $H^{6''}$), 7.44–7.54 (m, 6H,), 8.30 (d, J = 8.4, 2H, $H^{2'}$ and $H^{6'}$). ^{13}C NMR (gHSQC, gHMBC): 48.7 ($-NMe_2$), 54.0 (C^a), 64.8 (C^b), 107.3 ($C^{4'}$), 127.6 (C^4), 128.4 ($C^{3''}$ and C^*), 128.4 ($C^{2''}$ and $C^{6''}$), 128.8 ($C^{2'}$ and $C^{6'}$), 129.3 ($C^{1'}$), 129.4 ($C^{3'}$ and $C^{5'}$), 130.4 ($C^{4''}$), 131.5 ($C^{1''}$), 148.8 (C^5), 157.1 (C^3). $^{195}Pt\{^1H\}$ NMR (54 MHz): −2165 (s). EM (ESI^+): m/z = 521.11 (Calc. 520.58) $\{[M]-Cl\}^+$. Anal (%) Calc. for $C_{19}H_{21}Cl_2N_3Pt.1/2\ H_2O$: C, 40.29; H, 3.92; N, 7.42. Found: C, 40.25; H, 3.8; N, 7.4. $C_{19}H_{21}Cl_2N_3Pt$ (FW = 556.08).

*2.1.4. Synthesis of compounds cis-[Pd{κ²-N,N′-[1-$(CH_2)_2NMe_2$]-3,5-R_2-pzol}Cl_2] (**3**)*

*2.1.4.1. Cis-[Pd{κ²-N,N′-[1-$(CH_2)_2NMe_2$]pzol}Cl_2] (**3a**).* A suspension of *cis*-[$PdCl_2(DMSO)_2$] (41.7 mg, 125×10^{-3} mol) and ligand **1a** (17.4 mg, 125×10^{-3} mol) in toluene (10 mL) was heated at reflux temperature for 2 h. The reaction mixture was evaporated to dryness and the obtained residue was purified by column chromatography {Al_2O_3, CH_2Cl_2: MeOH

[1] During the acquisition time (more than 24 h) of the $^{195}Pt\{^1H\}$ NMR data the presence of an additional signal at δ = −2982 ppm was also observed in the spectrum. Its intensity increased with time, thus suggesting the formation of a new species in solution.

(from 2% to 5%)} to yield 28 mg (71%) of the title complex as an orange solid. IR (cm^{-1}): 3447, 3086, 2920, 1628, 1421, 1277, 1109, 1078, 796, 760. ^{1}H NMR (acetone-d_6, 500 MHz, gCOSY): 2.82 (masked m, 2H, $-CH_2-^b$), 2.91 (s, 6 H, NMe_2), 4.70 (m, 2H, $-CH_2-^a$), 6.39 (t, $J=2.5$, 1H, H^4), 7.91 (dd, $J=2.5$, 1H, H^5), 8.17 (d, $J=2.5$, 1H, H^3). ^{13}C NMR (acetone-d_6, 125.9 MHz, gHSQC, gHMBC): 48.4 (C^a), 52.0 (NMe_2), 63.2 (C^b), 106.5 (C^4), 134.2 (C^5), 143.9 (C^3). EM (ESI^+): m/z = 321.0 (320.45) $\{[M]\text{-}Cl+CH_3CN\}^+$. Anal (%) Calc. for $C_7H_{13}Cl_2NPd\cdot 1H_2O\cdot 1/4C_7H_8$: C, 29.40; H, 4.76; N, 11.70. Found: C, 29.5; H, 4.9; N, 11.0.[2] $C_7H_{13}Cl_2NPd$ (FW = 314.95).

*2.1.4.2. Cis-[Pd{κ^2-N,N′-[1-$(CH_2)_2NMe_2$]-3,5-Me_2-pzol}Cl_2] (**3b**).* A suspension of *cis*-$[PdCl_2(DMSO)_2]$ (41.7 mg, 125×10^{-3} mol) and ligand **1b** (20.9 mg, 125×10^{-3} mol) in toluene (10 mL) was heated at reflux temperature for 2 h. The reaction mixture was evaporated to dryness and the obtained residue was purified by column chromatography (Al_2O_3, CH_2Cl_2: MeOH 1% to 8%) to yield 30 mg (70%) of complex **3b** as an orange solid. IR (cm^{-1}): 3449, 3003, 2916, 2860, 1151, 1465, 1430, 1310, 1091, 1026, 991, 810. ^{1}H NMR (acetone-d_6, 500 MHz, gCOSY): 2.36 (s, 3H, Me), 2.52 (s, 3H, Me), 2.56 (m, 2H, $-CH_2-^b$), 2.80 (s, 6H, NMe_2), 4.68 (m, 2H, $-CH_2-^a$), 6.09 (s, 1H, H^4). ^{13}C NMR (acetone-d_6, 125.9 MHz, gHSQC, gHMBC): 11.1 (Me), 15.6 (Me), 48.9 (C^a), 53.1 (NMe_2), 64.1 (C^b), 106.5 (C^4), 134.0 (C^5), 142.6 (C^3). EM (ESI^+): m/z = 377 (Calc. 375.0) $\{[M]+MeOH\}^+$. Anal (%) Calc. for $C_9H_{17}Cl_2N_3Pd\cdot 3/2H_2O\cdot 1/4C_7H_8$: C, 32.71; H, 5.51; N, 10.65. Found: C, 32.7; H, 5.2; N, 10.7. $C_9H_{17}Cl_2N_3Pd$ (FW = 342.98).

2.1.5. Synthesis of the cyclometallated compounds

*2.1.5.1. [Pt{κ^2-C,N,N′-{[1-$(CH_2)_2NMe_2$}-3-(C_5H_4)-5-Ph-pzol]}Cl_2] (**4c**).* To a suspension of *cis*-$[PtCl_2(DMSO)_2]$ (52.8 mg, 125×10^{-3} mol) and ligand **1c** (18.2 mg, 125×10^{-3} mol) in toluene (5 mL), a MeOH (1 mL) solution of NaOAc (11.2 mg, 138×10^{-3} mol). The resulting mixture was heated at reflux for 3 h and later on concentrated to dryness. The solid formed was dissolved in CH_2Cl_2 and filtered very slowly through a short pad of celite. The filtrate was evaporated and the obtained residue was submitted to column chromatography {Al_2O_3, hexane:CH_2Cl_2 (75:25)}, to yield 47 mg (72%) of the title complex as a yellow solid. IR (cm^{-1}): 3438, 3046, 2923, 1506, 1448, 1335, 1022, 799, 759, 695. ^{1}H NMR (gCOSY): 2.95 (s, 6H, NMe_2), 3.27 (m, 2H, $-CH_2-^b$), 4.31 (m, 2H, $-CH_2-^a$), 6.50 (s, 1 H, H^4), 6.97–7.08 (m, 2H, $H^{4'}$ and $H^{5'}$), 7.24 (m, 1H, $H^{3'}$), 7.40–7.47 (m, 2 H, $H^{2''}$ and $H^{6''}$), 7.48–7.57 (m, 2H, $H^{3''}$ and $H^{5''}$), 7.71 (dd, $J=5.6$, 3.2 Hz, 1H, $H^{4''}$), 7.89 (dd, $J=7.2$ and 1.6 Hz, 1H, $H^{6'}$). ^{13}C NMR (gHSQC, gHMBC): 45.7 (C^a), 49.2 ($-NMe_2$), 61.7 (C^b), 101.3 (C^4), 121.7 ($C^{3'}$), 123.7 ($C^{5'}$), 127.5 ($C^{4'}$), 128.8 ($C^{2''}$, $C^{4''}$ and $C^{6''}$), 129.3 ($C^{3''}$ and $C^{5''}$), 129.8 ($C^{1''}$), 135.0 ($C^{6'}$), 137.5 ($C^{1'}$), 144.6 (C^5), 160.5 (C^3 and $C^{2'}$). ^{195}Pt{^{1}H} NMR (54 MHz): −3555 (s). EM (ESI^+): m/z = 521.11 (Calc. 521.10){[M] + H}$^+$. Anal (%) Calc. for $C_{19}H_{20}ClN_3Pt$ (FW = 520.10): C, 43.81; H, 3.87; N, 8.07. Found: C, 43.81; H, 3.84; N, 7.77.

*2.1.5.2. [Pd{κ^2-C,N,N′-{[1-$(CH_2)_2NMe_2$}-3-(C_5H_4)-5-Ph-pzol]}Cl_2] (**5c**).* To a suspension of *cis*-$[PdCl_2(DMSO)_2]$ (41.7 mg, 125×10^{-3} mol) and ligand **1c** (36.4 mg, 125×10^{-3} mol) in toluene (12 mL), a MeOH (1 mL) solution of NaOAc (11.2 mg, 138×10^{-3} mol) was added. The resulting mixture was heated at reflux for 1 h. Afterwards the solvent was evaporated to dryness and the residue formed was dissolved in CH_2Cl_2 and filtered very slowly through a short pad of celite. The filtrate was evaporated and the obtained residue was passed through a Al_2O_3 column using CH_2Cl_2:MeOH (100:1) mixture as eluent. The band collected gave, after concentration to dryness, **5c** as a white solid (38 mg, 70%). IR (cm^{-1}): 3448, 3038, 2924, 2856, 1528, 1449, 1387, 796, 758, 698. ^{1}H NMR (gCOSY): 2.77 (s, 6H, NMe_2), 2.99 (m, 2H, $-CH_2-^b$), 4.25 (m, 2H, $-CH_2-^a$), 6.45 (s, 1 H, H^4), 6.95 (td, J = 7.6 and 1.6, 1H, $H^{4'}$), 7.01 (td, J = 7.2 and 1.2, 1H, H5′), 7.23(dd, J = 7.6 and 1.6, 1H, $H^{3'}$), 7.40–7.46 (m, 2H, $H^{2''}$ and $H^{6''}$), 7.50–7.56 (m, 3H, $H^{3''}$, $H^{4''}$ and $H^{5''}$), 7.87 (d, J = 7.2, 1H, $H^{6'}$). ^{13}C NMR (gHSQC, gHMBC): 45.2(C^a), 48.5 ($-NMe_2$), 60.9 (C^b), 101.0 (C^4), 122.1 ($C^{3'}$), 124.5 ($C^{5'}$), 127.1 ($C^{4'}$), 128.9 ($C^{2''}$, $C^{4''}$ and $C^{6''}$), 129.2 ($C^{3''}$ and $C^{5''}$), 129.8 ($C^{1''}$), 136.6 ($C^{6'}$), 137.5 ($C^{1'}$), 145.1 (C^5), 148.4 ($C^{2'}$), 160.5 (C^3). EM (ESI^+): m/z = 396.07 $\{[M]\text{-}Cl\}^+$. Anal (%) Calc. for $C_{19}H_{20}ClN_3Pd$ (FW = 431.04): C, 52.80; H, 4.66; N, 9.72. Found: C, 52.55; H, 4.6; N, 9.9.

2.2. Crystallography

A prismatic crystal of **2a** (sizes in Table 1) was selected and mounted on a MAR345 diffractometer with an image plate detector. Unit-cell parameters were determined from 5843 reflections (3°<θ<31°) and refined by least-squares method. Intensities were collected with graphite monochromatized Mo K_α radiation. 9754 reflections were measured (in the range $2.39°\le\theta\le32.38°$) of which 2861 were non-equivalent by symmetry $\{R_{int}(on\ I)=0.072\}$ and 2741 reflections were assumed as observed applying the condition $I>2\sigma(I)$. Lorentz-polarization and absorption corrections were made.

The structure was solved by Direct methods using SHELXS computer program [48] and refined by full-matrix least-squares method with SHELX97 computer program [49] using 9754 reflections, (very negative intensities were not assumed). The function minimized was $\Sigma w(|Fo|^2-|Fc|^2|^2$, where $w=[\sigma^2(I)+(0.0518P)^2+0.5576P]^{-1}$, and $P=(|Fo|^2+2|Fc|^2)/3$; f, f' and f'' were taken from *International Tables of X-Ray Crystallography* [50]. All H atoms were computed and refined, using a riding model, with an isotropic temperature factor equal to 1.2 times the equivalent temperature factor of the atom to which is linked. The final R(on F) factor was 0.033, wR(on $|F|^2$) = 0.085 and goodness of fit = 1.062 for all observed reflections. Number of refined parameters was 118. Max. shift/esd = 0.00, Mean shift/esd = 0.00. Max. and min. peaks in final difference synthesis were 2.767 and −2.054 eÅ^{-3}, respectively.

Table 1
Crystal data and details of the structure refinement for **2a**. Standard deviations are given in parentheses.

Empirical formula	$C_7H_{13}Cl_2N_3Pt$
Formula weight	405.19
Temperature (K)	293 (2)
λ (Å)	0.71073
Crystal size (mm × mm × mm)	0.2 × 0.1 × 0.1
Crystal system	Monoclinic
Space group	$P2_1/c$
a (Å)	7.162 (3)
b (Å)	8.725 (3)
c (Å)	17.478 (4)
α = γ (deg.)	90
β (deg.)	102.76 (2)
Volume (Å^3)	1065.2 (6)
Z	4
$D_{calc.}$ (Mg × m^{-3})	2.527
μ (mm^{-1})	13.633
F(000)	752
Θ for data collection (deg.)	From 2.39 to 32.38
N. of reflections collected	9754
N. of unique reflections, [R(int)]	2861[0.0721]
N. of parameters	118
Completeness to Θ = 25.00°	94.2%
Goodness-of-fit on F^2	1.062
Final R indices [$I>2\sigma(I)$]	$R_1=0.0327$, $wR_2=0.0850$
R indices (all data)	$R_1=0.0338$, $wR_2=0.0859$
Largest diff. peak and hole	2.767 and −2.054 e.Å^{-3}

[2] Compounds **3a** and **3b** retain solvents. Evidence of the presence of small amounts of toluene is in the ^{1}H NMR spectra (a singlet at 2.3 ppm). Despite the fact that the two compounds were dried in the vacuum for a week, it was impossible to evaporate the solvents. The best analytical results are presented above.

2.3. Biological studies

2.3.1. Cell culture

Human lung carcinoma A549 cells (from the American Type Culture Collection), MBA MD231 and MCF7 (from the European Collection of Cell Cultures — ECACC) were used in all the experiments. Cells were grown as a monolayer culture in minimum essential medium (DMEM with L-glutamine, without glucose and without sodium pyruvate) in the presence of 10% heat-inactivated fetal calf serum, 10 mM of D-glucose and 0.1% streptomycin/penicillin in standard culture conditions.

2.3.2. Cell proliferation assay

The assay was performed by a variation of the method described by Mosmann et al. [51] as specified by Matito and coworkers [52]. In brief, 3×10^3 A549 cells/well were cultured in 96 well plates. Concentrations that inhibited cell growth by 50% (IC_{50}) after 72 h of treatment were calculated based on the survival rate compared with untreated cells. Relative cell viability was measured by the absorbance on an ELISA (enzyme-linked immunosorbent assay) plate reader (Tecan Sunrise MR20-301, TECAN, Salzburg, Austria) at 550 nm.

2.3.3. Cell viability assay

The compounds were dissolved in 100% DMSO at 50 mM as stock solution. Then, serial dilutions have been done in DMSO (1:1), in this way DMSO concentrations in cell media were always the same. Finally, 1:500 dilutions of the serial dilutions of compounds on cell media were done. The assay was performed as described by Givens et al. [53]. In brief, MDA MB231 and MCF7 cells were plated at 5000 and 10,000 cells/well, respectively, in 100 μL media in tissue culture 96 well plates (Cultek). After 24 h, media was replaced by 100 μL/well of serial dilution of drugs. Control wells did not contain compounds. Each point concentration was run in triplicate. Reagent blanks, containing media plus colorimetric reagent without cells were run on each plate. Blank values were subtracted from test values and were routinely 5–10% of uninhibited control values. Plates were incubated 72 h. Hexosaminidase activity was measured according to the following protocol: the media containing was removed and cells were washed once with PBS 60 μL of substrate solution (*p*-nitrophenol-*N*-acetyl-β-*D*-glucosamide 7.5 mM [Sigma N-9376], sodium citrate 0.1 M, pH 5.0, 0.25% Triton X-100) was added to each well and incubated at 37 °C for 1–2 h; after this incubation time, a bright yellow appears; then, plates could be developed by adding 90 μL of developer solution (glycine 50 mM, pH 10.4; EDTA 5 mM), and absorbance was recorded at 410 nM.

2.3.4. DNA migration studies

Plasmid pBluescript SK+ was obtained using a QIAGEN plasmid midi kit as described by the manufacturer. Interaction of drugs with pBluescript SK+ plasmid DNA (Stratagene) was analyzed by agarose gel electrophoresis following a modification of the method described by Abdullah et al.[54]. In brief, plasmid DNA aliquots (40 μg/mL) were incubated with different concentrations of the platinum and palladium compounds (ranging from 5 μM to 100 μM) at 37 °C for 24 h. For comparison, cisplatin was used as a positive control. Aliquots of 20 μL of compound: DNA complexes containing 0.8 μg of DNA were subjected to 1% agarose gel electrophoresis in TAE buffer (40 mM Tris–acetate, 2 mM EDTA, pH 8.0). The gel was stained in the same buffer containing ethidium bromide (0.5 $mg.mL^{-1}$) and visualized and photographed under UV light.

2.3.5. In vitro antimalarial assay

The 3D7 chloroquine-susceptible *P. falciparum* clone (Africa) and the W2 chloroquine resistant clone (Indochina) were maintained in culture in RPMI 1640 (Invitrogen, Paisley, United Kingdom), supplemented with 10% human serum (Abcys S.A., Paris, France) and buffered with 25 mM HEPES ((4-(2-hydroxyethyl)-1-piperazineethanesulfonic acid) and 25 mM $NaHCO_3$. Parasites were grown in A-positive human blood under controlled atmospheric conditions that consisted of 10% O_2, 5% CO_2 and 85% N_2 at 37 °C with a humidity of 95%. All strains were synchronized twice with sorbitol before use. Clonality was verified using PCR genotyping of polymorphic genetic markers, *msp1*, *msp2* and microsatellite loci [55,56].

Chloroquine (CQ) diphosphate was purchased from Sigma (Saint Louis, MO). CQ was suspended in water in concentrations ranging from 5 to 3200 nM. Compounds **1**–**5** were suspended in methanol and then diluted in RPMI to obtain final concentrations ranging from 0.01 μM to 500 μM.

For in vitro isotopic microtests, 25 μL/well of antimalarial drug and 200 μL/well of the parasitized red blood cell suspension (final parasitemia, 0.5%; final hematocrit, 1.5%) were distributed into 96 well plates. Parasite growth was assessed by adding 1 μCi of tritiated hypoxanthine with a specific activity of 14.1 Ci/mmol (Perkin-Elmer, Courtaboeuf, France) to each well at time zero. The plates were then incubated for 48 h in controlled atmospheric conditions. Immediately after incubation, the plates were frozen and thawed to lyse erythrocytes. The contents of each well were collected on standard filter microplates (Unifilter GF/B; Perkin-Elmer) and washed using a cell harvester (Filter-Mate Cell Harvester; Perkin-Elmer). Filter microplates were dried, and 25 μL of scintillation cocktail (Microscint O; Perkin-Elmer) was placed in each well. Radioactivity incorporated by the parasites was measured with a scintillation counter (Top Count; Perkin-Elmer).

The IC_{50}, the drug concentration able to inhibit 50% of parasite growth, was assessed by identifying the drug concentration corresponding to 50% of the uptake of tritiated hypoxanthine by the parasite in the drug-free control wells. The IC_{50} value was determined by nonlinear regression analysis of log-based dose–response curves (Riasmart™, Packard, Meriden, USA). IC_{50} are expressed as means of 3 to 4 experiments ± standard deviation.

3. Results and discussion

3.1. Synthesis and characterization

The preparation of ligands **1a** and **1b** was carried out by a modification of former literature protocols [57,58] consisting in the alkylation of 1*H*-pyrazole and 3,5-dimethyl-1*H*-pyrazole respectively with 2-dimethylaminoethyl chloride using sodamide as a base (Scheme 1). The best yield for the synthesis of **1c** was obtained by alkylation of 3,5-diphenyl-1*H*-pyrazole using Aliquat 336 as a phase transfer catalyst. The three ligands were fully characterized by NMR, IR and mass spectroscopy. To the best of our knowledge, these data were found to be absent or incomplete in the literature.

The reactivity of ligands **1a**–**1c** with *cis*-$[MCl_2(DMSO)_2]$ {M═Pt(II) or Pd(II)} was studied under different experimental conditions. Treatment of equimolar amounts of the corresponding ligand (**1a**–**1c**) and of *cis*-$[PtCl_2(DMSO)_2]$ in toluene under reflux gave after work up yellow solids that were identified as the corresponding *cis*-$[Pt\{\kappa^2\text{-}N,N'\text{-}\{[1\text{-}(CH_2)_2NMe_2\}\text{-}3,5\text{-}R_2\text{-}pzol]\}Cl_2]$ (**2a**–**2c** in Scheme 1). The palladium(II) analogs (**3a**–**3c**) were isolated using the same strategy.

However, treatment of **1c** with *cis*-$[PtCl_2(DMSO)_2]$ in a toluene: methanol (12:1) mixture in the presence of a slight excess (~10%) of NaOAc, produced the activation of the *ortho* σ(C–H) bond of the phenyl ring on position 3 giving the platinacycle $[Pt\{\kappa^3\text{-}C,N,N'\text{-}[1\text{-}\{(CH_2)_2NMe_2\}\text{-}3\text{-}(C_6H_4)\text{-}5\text{-}Ph\text{-}pzol]\}Cl]$ **4c**. When *cis*-$[PtCl_2(DMSO)_2]$ was replaced by its palladium(II) analog, the palladacycle $[Pd\{\kappa^3\text{-}C,N,N'\text{-}[1\text{-}\{(CH_2)_2NMe_2\}\text{-}3\text{-}(C_6H_4)\text{-}5\text{-}Ph\text{-}pzol]\}Cl]$ **5c** was achieved. It should be noted that this product could also be isolated in the absence of the base in the reaction medium.

The new complexes were characterized by elemental analyses, mass spectrometry, infrared spectroscopy and ^1H, ^{13}C and two-dimensional homo (gCOSY) and heteronuclear (gHSQC and gHMBC) correlations. In the $^{13}C\{^1H\}$ NMR spectra of cyclometallated compounds **4c** and **5c** the intensity of the signal due to the $C^{2'}$ atom decreased substantially and was low-field shifted when compared with that of the free ligand **1c**. In

addition, no evidence of cross-peak between the resonance of the $C^{2'}$ nuclei and those of the aromatic protons was detected in the [^{1}H–^{13}C]-HSQC spectra of compounds **4c** and **5c**. According to previous studies [59,60], these observations suggested the existence of a σ(M–$C^{2'}$) bond and the presence of five membered ring metallacycle in **4c** and **5c**. ^{195}Pt{^{1}H} NMR spectra not only provided convincing evidence of the coordination sphere of the platinum and structure of **2c** and **4c**, but also explained the variations produced by the different mode of binding of ligand **1c**. The spectrum of **2c** showed a singlet at −2165 ppm, the position of which is consistent with the values reported for related complexes with a "(*N,N′*)Cl_2" environment around the platinum(II) [60–62]. For **2c** the signal appeared at higher fields (δ = −3555 ppm); this trend agrees with those reported for complexes containing R–CH=N–$(CH_2)_n$$NMe_2$ (R = phenyl or ferrocenyl moieties) as bidentate (*N,N′*) or terdentate (*C,N,N′*)$^-$ ligands [61,62]. The ^{195}Pt NMR spectrum of **2b** was not recorded due to the low solubility of this product and for **2a**, two singlets of relative intensities (1.0:0.3) centered at δ = −2178 and −2982 ppm were observed. The chemical shift of the former one is similar to that of **2c** and the presence of the second and less intense signal suggested that this product is less stable in $CDCl_3$ than its analog **2c**.

Complex **2a** was also characterized by X-ray diffraction. Its molecular structure and the atom numbering scheme are presented in Fig. 2. The crystal contains molecules of [Pt{κ^2-*N,N′*-[1-$(CH_2)_2NMe_2$]-Ph_2-pzol}Cl_2] (**2a**) in which the platinum(II) atom is bound to the two nitrogen atoms [N(1) and N(3)] of the pyrazolyl ligand and to two chlorides [Cl(1) and Cl(2)], in a slightly distorted square-planar environment thus confirming the mode of binding of the ligand. The Pt–Cl(1) and Pt–Cl (2) bond lengths are practically identical (the differences do not clearly exceed 3σ) and fall in the range found in Pt(II) complexes having *cis*-coordinated chlorido ligands trans to N-donor ligands.[63–68] The Pt–N(1) [2.010(3) Å] and Pt–N(3) [Pt–N(3) 2.091(4) Å] bond lengths are within the normal distances (1.98–2.06 Å) reported for the same type of complexes and the differences may be attributed to the different basicities of the two donor atoms {N(amine) versus N(heterocycle)}[69].

Each molecule of *cis*-[Pt{κ^2-*N,N′*-[1-$(CH_2)_2NMe_2$]-3,5-Ph_2-pzol}Cl_2] (**2a**) contains a [5.6] bicyclic system formed by the pyrazolyl unit that shares the N(2)–N(3) bond with the six membered chelate ring generated by the coordination of the platinum(II) to the N(1) and N(2) atoms of the ligand. Bond lengths and angles of the pyrazolyl unit agree with those reported for most metal complexes containing this azole. The heterocycle is planar[3] and it forms an angle of ca. 22.3° with the coordination plane of the platinum(II). The puckering analyses of the six-membered chelate ring is formed by the set of atoms Pt, N(1), N(2), C(4), C(5) and N(3) [θ = 106.6(4)° and ϕ = 30.3 (4)° indicates that it adopts a twisted-boat conformation.

In each molecule of *cis*-[Pt{κ^2-*N,N′*[1-{$(CH_2)_2NMe_2$}pzol]}Cl_2], the distances Cl(1)···H(7B) [2.642 Å], Cl(1)···H(6C) [2.699 Å], and Cl (2)···H(1) [2.721 Å] are smaller than the sum of the van der Waals radii of these atoms (Cl, 1.7 Å and H, 1.0 Å) [70] thus suggesting weak C–H···Cl intramolecular interactions.

In the crystal a molecule at (*x*, *y*, *z*) is connected to two different and vicinal ones [at (*x*, *1 + y*, *z*) and (*−1 + x*, *y*, *z*)] by four weak intermolecular C–H···Cl interactions (Fig. 3) forming chains.

3.2. Biological studies

A human lung carcinoma cell line (A549) and two human breast cancer cell lines (MDA MB231 and MCF7) were used to test the cytotoxic activity of the synthesized compounds. Cisplatin was used as a positive control, showing a value of IC_{50} below 20 μM in the three cancer cellular lines (Table 2).

[3] Deviations from the mean plane: N(1), −0.005(4); N(2), 0.008(5); C(1) 0.001(5), C(2), 0.004(6) and C(3), −0.008(7) Å.

Table 2
Cytotoxic activities on A549 human lung carcinoma and MDA-MB231 and MCF7 breast cancer cell lines for the free ligands and their platinum(II) or palladium(II) complexes, using cisplatin as reference. Data are shown as the mean SD of two or more experiments performed in triplicate.

IC_{50} values (μM)			
	A549	MDA-MB231	MCF/
A) Free ligands			
1a	>100	>100	>100
1b	>100	>100	>100
1c	55 ± 14	64 ± 24	52 ± 10
B) Platinum(II) complexes			
2a	3 ± 1	57 ± 8.5	20 ± 3.6
2b	12 ± 5	62 ± 9.3	51 ± 10.4
2c	13 ± 5.8	14 ± 1.7	17 ± 2.2
4c	7 ± 2.8	6.2 ± 1.3	9.3 ± 3.4
C) Palladium(II) complexes			
3a	>100	>100	>100
3b	73.5 ± 2.1	>100	>100
5c	38.5 ± 4.9	16.2 ± 4.6	38.4 ± 16.5
Cisplatin	9.3 ± 3.0	6.5 ± 2.4	19 ± 4.5

For the purely organic ligands **1a**–**1c**, a moderate activity was observed for the 3,5 diphenyl substituted compound **1c** (IC_{50} values between 52 and 64 μM). In all cases, the Pd(II) and Pt(II) complexes were more potent than their corresponding parent ligand and compound **2a** exhibited in human lung A549 cancer cell line the highest potency (IC_{50} = 3 μM) of the synthesized complexes and a notable selectivity for lung cancer cell line versus the two breast cancer cell lines (MDA MB 231 and MCF7) selected. Interestingly, **2a** turned out to be three times more potent than cisplatin in lung A549 cancer cell line. In the three cancer cell lines, the platinacycle **4c** exhibited the highest cytotoxic activity with IC_{50} values in the range of 6.2–9.3 μM. It was more effective against human lung carcinoma (A549) cells and breast cancer (MDA MB231 and MCF7) cells than the reference drug cisplatin. Cytotoxicity effectiveness of **4c** was approximately twice that of the coordination complex **2c** in the three cancer cell lines. Compound **4c** arises from the coordination of the two nitrogen atoms and the formation of a σ(Pt–C) bond, this leads to a [6.5.5.6] tetracyclic system. Consequently, it has a higher degree of rigidity and planarity than **2c**. It is well-known that square-planar metal complexes with aromatic ligands bind to DNA by intercalation [71–74] and consequently compound **4c** may behave not only as alkylating but also as an intercalating agent. This potential dual behavior may account for the increased potency of the platinacycle **4c** when compared with **2c**.

Although compounds **4c** and **5c** only differ by the nature of the M(II) ion, the platinum(II) complex **4c** is (2.6–5.5 times depending on the cell line) more potent than its Pd(II) analog **5c**. This may be due to the greater lability and faster hydrolysis rate of palladium complexes compared to their platinum equivalents [75]. Therefore, higher cytotoxicity of **5c** could be also connected to slower hydrolysis of Pt–Cl bond and to the stability of this compound compared to the palladium(II) derivative **5c**.

The effect of binding of the compounds investigated in this study on supercoiled DNA was determined by their ability to alter the electrophoretic mobility of pBluescript plasmid DNA: supercoiled closed circular (cc) and open circular (oc) forms.

Fig. 4 shows the electrophoretic mobility of native pBluescript DNA incubated with the synthesized compounds (**1c** and **2**–**5**) at 5 μM or 50 μM concentration. To provide a basis for comparison, incubation of DNA with cisplatin was also performed using the same concentrations and conditions. As expected, at both 5 μM and 50 μM concentrations, cisplatin greatly altered the electrophoretic mobility of pBluescript DNA. At 5 μM concentration, none of the assayed compounds produced a significant effect on the electrophoretic mobility of native pBluescript DNA. At this concentration, the mobility of the supercoiled closed circular form was only slightly decreased by the platinum(II) compound **2a** and the

palladium(II) compound **5c**. Consistently, at 50 μM, both compounds greatly alter the mobility of plasmid DNA. For these two compounds (**2a** and **5c**), an unwinding assay was performed with increasing amounts of drugs ranging from 5 μM to 100 μM (Fig. 5). For complex **2a**, the migration rate of supercoiled band decreases until it comigrates with the nicked relaxed band. In this titration experiment of 40 μg/mL pBluescript, the coalescence point, defined as the amount of platinum complex that is necessary for complete removal of all supercoils from DNA, occurs with 50 μM concentration of **2a**. The lowest efficiency of complex **2a** than cisplatin in removing the supercoils from DNA could be related to the shorter incubation time (24 h) of the experiments compared to the incubation time in the experiments with cancer cell lines (72 h). Under these conditions, hydrolysis of the platinum complex should not occur.

For the palladium(II) compound **5c**, the rate of migration of supercoiled band also decreases as drug concentration increases up to 10 μM. At higher concentrations the migration rate begins to increase again in parallel to a decrease in the bands intensity. At higher concentrations of **5c** (more than 100 μM), DNA is no longer visible.

Regarding the other assayed complexes (Fig. 4), at 50 μM concentration, small changes on the migration rate of the supercoiled closed circular plasmid DNA were observed for most of them, with the exception of the free ligand **1c** and the platinum(II) complex **4c**. When assayed at higher concentrations (500 μM), the synthesized compounds dramatically altered plasmid DNA mobility (data not shown). Again, compounds **1c** and **4c** did not produce any effect. Paradoxically, as it was mentioned before, complex **4c** exhibited a great cytotoxicity in the three selected human cancer cell lines.

Overall, these results indicated that most of the compounds investigated in this study interact with DNA, **2a** and **5c** exhibiting the highest effect on plasmid DNA mobility. These two compounds may behave as alkylating agents acting by the same mechanism as cisplatin. However, compound **4c** is hypothesized to act on tumor cells through a different mechanism than cisplatin.

We also evaluated the potential activities of products **1**–**5** against the chloroquine-susceptible strain (3D7) and the chloroquine-resistant strain (W2) of *P. falciparum* (Table 3). The free ligands exhibited poor (for **1a**–**1b**) to moderate (for **1c**) antimalarial activities. In contrast with these results, the platinum(II) complexes (**2a**–**2c**) with a $(N,N')Cl_2$ environment demonstrated higher in vitro activity against *P. falciparum* chloroquine-susceptible and chloroquine-resistant clones than their corresponding parent ligand. The toxicity of platinacycle **4c** was low on *P. falciparum* parasites (IC_{50} of 111.7 μM on 3D7 and 138.0 μM on W2). The cyclopalladated complex **5c** was 10-times more potent than its platinum(II) analog **4c** against *P. falciparum*. Compound **2c** showed similar cytotoxic activity on *P. falciparum* parasites and cancer cells. Compound **5c** was 2 to 3-times more potent against *P. falciparum* parasites than against cancer cells.

In vivo efficiency of platinum derivatives has been already demonstrated in malaria. Cisplatin (Fig. 1) cured mice infected with *Plasmodium berghei* at a dose of 6 mg/kg body weight [76]. The Pd-cyclometallated derivative **5c** was more efficient than Pt-protoporphyrin against *P. falciparum* (38 μM) [77]. However, these compounds were less potent against the two *P. falciparum* clones 3D7 and W2 than Fe-derivatives, such as ferroquine and analogs [78,79], ferrocenic derivatives from ciprofloxacin [80], or Ru, such as ruthenoquine and analogs [42].

Table 3
In vitro activity of ligands **1**, compounds **2**–**5** and chloroquine against chloroquine susceptible *P. falciparum* 3D7 clone and the chloroquine resistant W2 clone. IC_{50} are expressed as means of 3 to 4 experiments ± standard deviation.

IC_{50} values (μM)		
	3D7	W2
A) Free ligands		
1a	182.3 ± 19.6	196.3 ± 13.8
1b	248.0 ± 15.5	183.3 ± 16.6
1c	38.4 ± 4.2	20.2 ± 4.3
B) Platinum(II) complexes		
2a	18.9 ± 1.2	22.5 ± 0.8
2b	18.3 ± 0.7	24.9 ± 2.4
2c	13.8 ± 4.5	16.1 ± 1.1
4c	111.7 ± 18.0	138.0 ± 6.2
B) Palladium(II) complexes		
3a	133.3 ± 11.6	111.0 ± 10.6
3b	132.0 ± 10.1	85.8 ± 3.1
5c	10.3 ± 5.5	19.2 ± 0.8
Chloroquine	0.020 ± 0.004	0.56 ± 0.09

4. Conclusions

The study of the reactivity of the three pyrazolyl ligands [1-$(CH_2)_2NMe_2$]-3,5-R_2-pzol] {with R═H (**1a**), Me (**1b**) or Ph (**1c**)} with $[MCl_2(DMSO)_2]$ (M═Pd or Pt) under different experimental conditions reveals that they may act as a bidentate (*N,N′*) (in **2a**–**2c** and **3a**–**3c**) or as terdentate $(C,N,N')^-$ ligand (in **4c** and **5c**). It is noteworthy that **4c** and **5c** are the first examples of platina- and palladacycles with $(C,N\text{-}_{pyrazole},N')^-$ pincer ligands reported so far. The in vitro antimalarial activity was evaluated against one chloroquine susceptible strain 3D7 and three chloroquine-resistant strains W2 of *P. falciparum*. Compounds **2a**–**2c** and **5c** were found to exhibit significant in vitro activity (with IC_{50} in the microM range). On the contrary, compound **4c** was inactive in similar experimental conditions. The evaluation of the in vitro cytotoxic activity of complexes **2c**–**5c** revealed that they exhibit growth inhibitory activity against lung (A549) and breast (MDA MB 231 and MCF7) human cancer cell lines. The comparison of the results obtained for the three types of complexes in human carcinoma A549 cell line indicates that the obtained IC_{50} values follow the trend **2a**<**4c**<cisplatin<**2b**<**2c**<**5c**<**3b**<**3a**. This means that: a) the platinum(II) derivatives are more potent than their palladium(II) analogs, b) for the platinum(II) complexes the change of binding mode of the ligand from (*N,N′*) in **2c** to (*C,N,N′*) in **4c** increases the cytotoxic activity, and c) compound **2a** is specially relevant due to remarkable potency in lung cancer A549 cell line (twice that of **4c** and three times more potent than cisplatin). It is noteworthy that complex **4c**, the first example of a pyrazole containing platinacycle, shows greater antitumoral in vitro activity than cisplatin. The platinum and palladium complexes evaluated in this study more or less exhibit an effect on DNA electrophoretic mobility. Complexes **2a** and **5c** are those exhibiting the strongest interaction with DNA, and both display moderate to good cytotoxic activities towards different cancer cell lines. In particular complex **2a** is the most potent of the new synthesized compounds in human lung carcinoma A549 cell line (IC_{50} value of 3 μM). An exception occurs in the case of compound **4c** that exhibits a considerable cytotoxicity in several cancer cell lines but has no effect on plasmid DNA mobility. These results underscore the importance of additional factors in predicting anticancer activity.

New Pt- and Pd-cyclometallated derivatives will be synthetized to improve antimalarial activity. Finally it should be noted that the methods and strategies described here, especially those concerning complex **4c**, constitute the first step toward the development of new but closely related platinum(II) complexes with pincer $(C,N;N')^-$ ligands derived from pyrazole. These compounds may exhibit improved biological activities owing to the conversion of **4c** into ionic products of the type [Pt(*C,N,N′*)(L)]X (L = neutral ligand and X = monoanion), which may be more soluble in polar solvents, or [Pt(*C,N,N′*)(CCPh)] that have an additional interest in view of their potential luminescence. The rich chemistry of pyrazole ligands also permits to introduce changes on the pendant arm of the nitrogen N_1 or on the pyrazole ring. These strategies open up a vast array of possibilities.

Acknowledgments

The authors thank R. Amalvict, M. Mokrane and D. Travers for technical support. Financial support from the *Ministerio de Ciencia e Innovación* of Spain (Project: CTQ2009-07021/BQU and CTQ2009-11501) and the *AGAUR*, *Generalitat de Catalunya* (Grant 2009-SGR-1111) is gratefully acknowledged. C.B. thanks the Ministère de l'Enseignement Supérieur, Université Lille Nord de France, and CNRS for financial support.

Appendix A. Supplementary material

The electronic crystallographic information file (.cif) for **2a**. will be deposited at the *Cambridge Crystallographic Data Centre*, 12 Union Road, Cambridge CB21EZ, UK.

References

[1] N.J. Wheate, S. Walker, G.E. Craig, R. Oun, Dalton Transactions 39 (2010) 8113–8127.
[2] B. Rosenberg, L. van Camp, T. Krigas, Nature 205 (1965) 698–699.
[3] Y. Jung, S.J. Lippard, Chemical Reviews 107 (2007) 1387–1407.
[4] L. Kelland, Nature Reviews. Cancer 7 (2007) 573–584.
[5] D. Gibson, Dalton Transactions (2009) 10681–10689.
[6] G. Kannarkat, E.E. Lasher, D. Schiff, Current Opinion in Neurology 20 (2007) 719–725.
[7] M. Markman, Expert Opinion on Drug Safety 2 (2003) 597–607.
[8] E. Wong, M. Giandomenico, Chemical Reviews 99 (1999) 2451–2466.
[9] A.M. Montaña, C. Batalla, Current Medicinal Chemistry 16 (2009) 2235–2260.
[10] A.C.F. Caires, Anti-Cancer Agents in Medicinal Chemistry. 7 (2007) 484–491.
[11] E. Budzisz, I.P. Lorenz, P. Mayer, P. Paneth, L. Szatkowski, U. Krajewska, M. Rozalski, M. Miernicka, New Journal Chemistry. 32 (2008) 2238–2244.
[12] A.S. Abu-Surrah, K.A. Abu Safieh, I.M. Ahmad, M.Y. Abdalla, M.T. Ayoub, A.K. Qaroush, A.M. Abu-Mahtheieh, European Journal of Medicinal Chemistry 45 (2010) 471–475.
[13] K. Sakai, Y. Tomita, T. Ue, K. Goshima, M. Ohminato, T. Tsubomura, K. Matsumoto, K. Ohmura, K. Kawakami, Inorganica Chimica Acta 297 (2000) 64–71.
[14] E. Pantoja, A. Gallipoli, S. van Zutphen, S. Komeda, D. Reddy, D. Jaganyi, M. Lutz, D.M. Tooke, A.L. Spek, C. Navarro-Ranninger, J. Reedijk, Journal of Inorganic Biochemistry 100 (2006) 1955–1964.
[15] G.B. Onoa, V. Moreno, M. Font-Bardia, X. Solans, J.M. Pérez, C. Alonso, Journal of Inorganic Biochemistry 75 (1999) 205–212.
[16] E. Budzisz, M. Miernicka, I.P. Lorenz, P. Mayer, U. Krajewska, M. Rozalski, Polyhedron 28 (2009) 637–645.
[17] F.K. Keter, S.O. Ojwach, O.A. Oyetunji, I.A. Guzei, J. Darkwa, Inorganica Chimica Acta 362 (2009) 2595–2602.
[18] M. Miernicka, A. Szulawska, M. Czyz, I.P. Lorenz, P. Mayer, B. Karwowski, E. Budzisz, Journal of Inorganic Biochemistry 102 (2008) 157–165.
[19] N.J. Wheate, C. Cullinane, L.K. Webster, J.G. Collins, Anti-Cancer Drug Design 16 (2001) 91–98.
[20] F.K. Keter, S. Kanyanda, S.S.L. Lantagaye, J. Darwa, D.J.G. Rees, M. Meyer, Cancer Chemotherapy and Pharmacology 63 (2008) 127–138.
[21] J. Dupont, M. Pfeffer, Palladacycles. Synthesis, Characterization and Applications, Wiley-VCH, Weinheim (Germany, 2008.
[22] M. Ghedini, I. Aiello, A. Crispini, A. Golemme, M. La Deda, D. Pucci, Coordination Chemistry Reviews 250 (2006) 1373–1390.
[23] D.A. Alonso, C. Najera, Chemical Society Reviews 39 (2010) 2891–2902.
[24] I. Omae, Journal of Organometallic Chemistry 692 (2007) 2608–2632.
[25] K. Godula, D. Sames, Science 312 (2006) 67–72.
[26] J. Dupont, C.S. Consorti, J. Spencer, Chemical Reviews 105 (2005) 2527–2571.
[27] Z. Liu, L. Salassa, A. Habtemariam, A.M. Pizarro, G.J. Clarkson, P.J. Sadler, Inorganic Chemistry 50 (2011) 5777–5783.
[28] P. Wang, C.-H. Leung, D.-L. Ma, R.W.-Y. Sun, S.-C. Yan, Q.-S. Chen, C.-M. Che, Angewandte Chemie (International Ed. in English) 50 (2011) 2554–2558.
[29] W. Kandioller, C.G. Hartinger, A.A. Nazarov, C. Bartel, M. Skocic, M.A. Jakupec, V.B. Arion, B.K. Keppler, Chemistry—A European Journal 13 (2009) 12283–12291.
[30] J.J. Yan, A.L.-F. Chow, C.-H. Leung, R.W.-Y. Sun, D.-L. Ma, C.-M. Che, Chemical Communications 46 (2010) 3893–3895.
[31] J.P. Djukic, J.B. Sortais, L. Barloy, M. Pfeffer, European Journal of Inorganic Chemistry (2009) 817–853.
[32] G. Gasser, I. Ott, N. Metzler-Nolte, Journal of Medicinal Chemistry 54 (2011) 3–25.
[33] M.R. Crimmin, D.A. Colby, J.A. Ellman, R.G. Bergman, Dalton Transactions 40 (2011) 514–522.
[34] P.-K. Lee, H.-W. Liu, S.-M. Yiu, M.-W. Louie, K.K.-W. Lo, Dalton Transactions 40 (2011) 2180–2189.
[35] S.P. Fricker, Metallomics 2 (2010) 366–377.
[36] S.-K. Leung, K.Y. Kwok, K.Y. Zhang, K.K.-W. Lo, Inorganic Chemistry 49 (2010) 4984–4995.
[37] H.P. Dijkstra, M.D. Meijer, J. Patel, R. Kreiter, G.P.M. van Klink, M. Lutz, A.L. Spek, A.J. Canty, G. van Koten, Organometallics 20 (2001) 3159–3168.
[38] A.J. Canty, R.T. Honeyman, B.W. Skelton, A.H. White, Journal of Organometallic Chemistry 430 (1992) 245–257.
[39] P.K. Basu, A. Gonzalez, C. López, M. Font-Bardia, T. Calvet, Journal of Organometallic Chemistry 694 (2009) 3633–3642.
[40] G. Aragay, J. Pons, J. Garcia-Anton, X. Solans, M. Font-Bardia, J. Ros, Journal of Organometallic Chemistry 693 (2008) 21–22.
[41] G.L. Edwards, D.S.C. Black, G.B. Deacon, L.P.G. Wakelin, Canadian Journal of Chemistry 83 (2005) 980–989.
[42] F. Dubar, T.J. Egan, B. Pradines, D. Kuter, K.K. Ncokazi, D. Forge, J.F. Paul, C. Pierrot, H. Kalamou, J. Khalife, E. Buisine, C. Rogier, H. Vezin, I. Forfar, C. Slomianny, X. Trivelli, S. Kapishnikov, L. Leiserowitz, D. Dive, C. Biot, ASC Chemical Biology 6 (2011) 275–287.
[43] J. Quirante, F. Dubar, A. González, C. López, M. Cascante, R. Cortés, I. Forfar, B. Pradines, C. Biot, Journal of Organometallic Chemistry 696 (2011) 1011–1017.
[44] T.J. Egan, K.R. Koch, P.L. Swan, C. Clarkson, D.A. van Schalkwyk, P.J. Smith, Journal of Medicinal Chemistry 47 (2004) 2926–2934.
[45] P. Chellan, S. Nasser, L. Vivas, K. Chibale, G.S. Smith, Journal of Organometallic Chemistry 695 (2010) 2225–2232.
[46] J.H. Price, A.N. Williamson, R.F. Schramm, B.B. Wayland, Inorganic Chemistry 11 (1972) 1280–1284.
[47] Z. Szafran, R.M. Pike, M.M. Singh, Microscale Inorganic Chemistry, A Comprehensive Laboratory Experience, John Wiley & Sons, New York (USA, 1991, p. 218.
[48] G.M. Sheldrick, SHELXS, A Program for Automatic Solution of Crystal Structure Refinement, Univ. Goettingen, Germany, 1997.
[49] G.M. Sheldrick, SHELX97, A Program for Crystal Structure Refinement, Univ. Goettingen, Germany, 1997.
[50] International Tables of X-Ray Crystallography, IV, Kynoch press, Birmingham (UK, 1974, pp 99–100 and 149.
[51] T. Mosmann, Journal of Immunological Methods 65 (1983) 55–63.
[52] C. Matito, F. Mastorakou, J.J. Centelles, J.L. Torres, M. Cascante, European Journal of Nutrition 42 (2003) 43–49.
[53] K.T. Givens, S. Kitada, A.K. Chemn, J. Rothschiller, D.A. Lee, Investigative Ophthalmology & Visual Science 31 (1990) 1856–1862.
[54] A. Abdullah, F. Huq, A. Chowdhury, H. Tayyem, P. Beale, K. Fisher, BMC Chemical Biology 6 (2006) 3.
[55] H. Bogreau, F. Renaud, H. Bouchiba, P. Durand, S.B. Assi, M.C. Henry, E. Garnotel, B. Pradines, T. Fusai, B. Wade, E. Adehossi, P. Parola, M.A. Kamil, O. Puijalon, C. Rogier, The American Journal of Tropical Medicine and Hygiene 74 (2006) 953–959.
[56] M. Henry, I. Diallo, J. Bordes, S. Ka, B. Pradines, B. Diatta, P.S. M'Baye, M. Sane, M. Thiam, P.M. Gueye, B. Wade, J.E. Touze, J.M. Debonne, C. Rogier, T. Fusai, The American Journal of Tropical Medicine and Hygiene 75 (2006) 146–151.
[57] J. Buchi, H.R. Meyer, R. Hirt, F. Hunziker, E. Eichenberger, R. Lieberherr, Helvetica Chimica Acta 38 (1955) 670–679.
[58] J.B. Wright, W.E. Dulin, J.H. Markillie, Journal of Medicinal Chemistry 7 (1963) 102–105.
[59] C. López, A. Gonzalez, C. Moya, R. Bosque, X. Solans, M. Font-Bardía, Journal of Organometallic Chemistry 693 (2008) 2877–2886.
[60] S. Pérez, C. López, A. Caubet, X. Solans, M. Font-Bardía, M. Gich, E. Molins, Journal of Organometallic Chemistry 692 (2007) 2402–2414.
[61] P.S. Pregosin, Coordination Chemistry Reviews 44 (1982) 247–291.
[62] S. Pérez, C. López, A. Caubet, X. Solans, M. Font-Bardía, New Journal Chemistry 27 (2003) 975–982.
[63] F.H. Allen, Acta Crystallographica Section B 58 (2002) 380–388.
[64] R. Cini, F.P. Fanizzi, F.P. Intini, G. Natile, Journal of the American Chemical Society 113 (1991) 7805–7806.
[65] L. Cerasino, K.M. Williams, F.P. Intini, R. Cini, L.G. Marzilli, G. Natile, Inorganic Chemistry 36 (1997) 6070–6079.
[66] G. Bandoli, P.A. Caputo, F.P. Intini, M.F. Sivo, G. Natile, Journal of the American Chemical Society 119 (1997) 10370–10376.
[67] F.P. Fanizzi, M. Lanfranchi, G. Natile, A. Tiripicchio, Inorganic Chemistry 33 (1994) 3331–3339.
[68] S.D. Kirik, A.K. Starkov, G.A. Kozhuhovskay, Acta Crystallographica Section C: Crystal Structural Communications. 62 (2006) m249–m251.
[69] M.B. Smith, J. March, March's Advanced Organic Chemistry: Reactions, Mechanism and Structure, sixth ed. John Wiley & Sons, New York, 2007.
[70] A. Bondi, The Journal of Physical Chemistry 68 (1964) 441–451.
[71] S.J. Lippard, Accounts of Chemical Research 11 (1978) 211–217.
[72] K.E. Erkkila, D.T. Odom, J.K. Barton, Chemical Reviews 99 (1999) 2777–2795.
[73] J.G. Collins, R.M. Rixon, J.R. Aldrich-Wright, Inorganic Chemistry 39 (2000) 4377–4379.
[74] D.L. Ma, C.-M. Che, Chemistry 9 (2003) 6133–6144.
[75] B. Taqui Khan, K. Najmuddin, S. Shamsuddin, K. Annapoorna, J. Bhatt, Journal of Inorganic Biochemistry 44 (1991) 55–63.
[76] L. Nair, V.K. Bhasin, Japanese Journal of Medical Science & Biology 47 (1994) 241–252.
[77] K. Begum, H.S. Kim, V. Kumar, I. Stojiljkovic, Y. Wataya, Parasitology Research 90 (2003) 221–224.
[78] C. Biot, B. Pradines, M.H. Sergeant, J. Gut, P.J. Rosenthal, K. Chibale, Bioorganic & Medicinal Chemistry Letters 17 (2007) 6434–6338.
[79] C. Biot, N. Chavain, F. Dubar, B. Pradines, X. Trivelli, J. Brocard, I. Forfar, D. Dive, Journal of Organometallic Chemistry 694 (2009) 845–854.
[80] F. Dubar, G. Anquetin, B. Pradines, D. Dive, J. Khalife, C. Biot, Journal of Medicinal Chemistry 52 (2009) 7954–7957.

CAPÍTULO 1D

HÍBRIDOS FERROCENO-INDÓLICOS CONTRA EL CÁNCER Y LA MALARIA.

Josefina Quirante [a,*,1], Faustine Dubar [b,2], Asensio González [a], Concepción Lopez [c], Marta Cascante [d], Roldán Cortés [d], Isabelle Forfar [e], Bruno Pradines [f], Christophe Biot [b,,2]**

[a] Laboratori de Química Orgànica, Facultat de Farmàcia, Institut de Biomedicina, (IBUB), Universitat de Barcelona, Barcelona, España

[b] Université de Lille1, Unité de Catalyse et Chimie du Solidee UMR CNRS 8181, ENSCL, Bâtiment C7, B.P. 90108, 59652 Villeneuve d'Ascq Cedex, Francia

[c] Departament de Química Inorgànica, Facultat de Química, Universitat de Barcelona, Martí i Franquès 1-11. E-08028-Barcelona, España

[d] Departament de Bioquímica i Biologia Molecular, Facultat de Biologia, Institut de Biomedicina de la Universitat de Barcelona (IBUB) y IDIBAPS, Unidad Asociada al CSIC, Diagonal 643, 08028 Barcelona, España

[e] Université de Bordeaux, Pharmacochimie EA 4138, Bordeaux, France

[f] Institut de Recherche Biomédicale des Armées, Antenne de Marseille, Unité de Recherche en Biologie et Epidémiologie Parasitaires, URMITE-UMR 6236, Allée du Médecin Colonel Jamot, Parc le Pharo, BP 60109, 13262 Marsella Cedex 07, Francia

Resumen

Presentamos la síntesis, caracterización y actividad antiproliferativa y antimalárica de los híbridos ferroceno-indólicos **8**-**14**. Se ha escogido el 2-fenilindol como estructura de partida por su potente actividad antimitótica, y el ferroceno fue escogido teniendo en cuenta el desarrollo de ferrocifenos, derivados del tamoxifeno y el ferroceno, que constituyen prototipos de una nueva familia de anti-estrógenos organometálicos. Los híbridos ferroceno-indólicos **8**-**14**, y sus correspondientes análogos orgánicos **1**-**7**, presentan actividades antimaláricas moderadas, mientras que los híbridos ferroceno-indólicos 11 y 12 demuestran una excelente actividad *in vitro* sobre células humanas de adenocarcinoma pulmonar A549, con valores de IC_{50} de 5 y 7 μM, respectivamente. Estos compuestos híbridos resultaron hasta 25 veces más potentes en su actividad antiproliferativa que sus análogos puramente orgánicos.

Journal of Organometallic Chemistry 696 (2011) 1011–1017

Contents lists available at ScienceDirect

Journal of Organometallic Chemistry

journal homepage: www.elsevier.com/locate/jorganchem

Review

Ferrocene–indole hybrids for cancer and malaria therapy

Josefina Quirante [a,*,1], Faustine Dubar [b,2], Asensio González [a], Concepción Lopez [c], Marta Cascante [d], Roldán Cortés [d], Isabelle Forfar [e], Bruno Pradines [f], Christophe Biot [b,**,2]

[a] Laboratori de Química Orgànica, Facultat de Farmàcia, Institut de Biomedicina, (IBUB), Universitat de Barcelona, Barcelona, Spain
[b] Université de Lille1, Unité de Catalyse et Chimie du Solide–UMR CNRS 8181, ENSCL, Bâtiment C7, B.P. 90108, 59652 Villeneuve d'Ascq Cedex, France
[c] Departament de Química Inorgànica, Facultat de Química, Universitat de Barcelona, Martí i Franquès 1-11. E-08028-Barcelona, Spain
[d] Department of Biochemistry and Molecular Biology, Faculty of Biology, Institute of Biomedicine of University of Barcelona (IBUB) and IDIBAPS, Unit Associated with CSIC, Diagonal 645, 08028 Barcelona, Spain
[e] Université de Bordeaux, Pharmacochimie EA 4138, Bordeaux, France
[f] Institut de Recherche Biomédicale des Armées, Antenne de Marseille, Unité de Recherche en Biologie et Epidémiologie Parasitaires, URMITE-UMR 6236, Allée du Médecin Colonel Jamot, Parc le Pharo, BP 60109, 13262 Marseille Cedex 07, France

ARTICLE INFO

Article history:
Received 11 October 2010
Received in revised form
12 November 2010
Accepted 15 November 2010

Keywords:
Cancer
Malaria
Hybrid drug
Indole
Ferrocene

ABSTRACT

We report the synthesis, characterization, and cytotoxic and antimalarial activity of ferrocene–indole hybrids **8**–**14**. The 2-phenylindole scaffold was chosen because of its potent antimitotic activity and ferrocene was chosen following the development of ferrocifens, ferrocene derivatives of tamoxifen, which are prototypes of a new family of organometallic anti-estrogens. Ferrocene–indole hybrids **8**–**14** and their corresponding organic analogues **1**–**7** showed only moderate antimalarial activities, while ferrocene–indole hybrids **11** and **12** showed excellent *in vitro* activities against the A549 human carcinoma cell line, with IC_{50} values of 5 and 7 μM respectively. These ferrocene–indole hybrids were up to 25-fold more potent as cytotoxic agents than their purely organic analogues.

Contents

1. Introduction 1012
2. Results and discussion 1013
 2.1. Chemistry 1013
 2.2. Biology 1013
  2.2.1. Cytotoxic activities 1013
  2.2.2. Antimalarial activities 1013
3. Conclusion 1014
4. Experimental 1014
 4.1. Chemistry 1014
  4.1.1. Full description of ^{1}H, ^{19}F and ^{13}C NMR spectra for 2-pheylylindoles (**1**–**7**) [19] 1014
   4.1.1.1. 2-Phenyl-1H-indole (**1**) 1014
   4.1.1.2. 2-(4-Chlorophenyl)-1H-indole (**2**) 1014
   4.1.1.3. 2-(4-Fluorophenyl)-1H-indole (**3**) 1014
   4.1.1.4. 5-Methoxy-2-phenyl-1H-indole (**4**) 1014
   4.1.1.5. 5-Nitro-2-phenyl-1H-indole (**5**) 1015

* Corresponding author.
** Corresponding author. Tel.: +33 320436941; fax: +33 320434893.
E-mail addresses: quirantese@ub.edu (J. Quirante), christophe.biot@univ_lille1.fr (C. Biot).
[1] Present adress: Laboratori de Química Orgànica, Facultat de Farmàcia, Institut de Biomedicina, (IBUB), Universitat de Barcelona, Av. Joan XXIII, s/n, 08028-Barcelona, Spain.
[2] Present address: Université de Lille1, Unité de Glycobiologie Structurale et Fonctionnelle, CNRS UMR 8576, IFR 147, 59650 Villeneuve d'Ascq Cédex, France.

0022-328X/$ – see front matter © 2010 Elsevier B.V. All rights reserved.
doi:10.1016/j.jorganchem.2010.11.021

4.1.1.6. 5-Chloro-2-phenyl-1H-indole (**6**) 1015
4.1.1.7. 2-(2pyiridyl)-1H-indole (**7**) 1015
4.1.2. General synthetic procedure for the preparation of 3-ferrocenylmethyl-2-pheylindoles (**8**–**14**) 1015
4.1.2.1. 3-Ferrocenylmethyl-2-phenyl-1H-indole (**8**) 1015
4.1.2.2. 2-(4-Chlorophenyl)-3-ferrocenylmethyl-1H-indole (**9**) 1015
4.1.2.3. 3-Ferrocenylmethyl-2-(4-fluorophenyl)-1H-indole (**10**) 1015
4.1.2.4. 3-Ferrocenylmethyl-5-methoxy-2-phenyl-1H-indole (**11**) 1015
4.1.2.5. 3-Ferrocenylmethyl-5-nitro-2-phenyl-1H-indole (**12**) 1015
4.1.2.6. 5-Chloro-3-ferrocenylmethyl-2-phenyl-1H-indole (**13**) 1015
4.1.2.7. 3-Ferrocenylmethyl-2-(2pyridyl)-1H-indole (**14**) 1016
4.2. Biology 1016
4.2.1. Cell culture 1016
4.2.2. Cell proliferation assay 1016
4.2.3. Antiplasmodial assay 1016
Acknowledgment 1016
References 1016

1. Introduction

Organometallic medicinal chemistry is the most promising branch of bioorganometallic chemistry [1]. Pioneered by the group of Paul Dyson [2], an extensive series of ruthenium–arene complexes have shown selective effects on metastasis. Moreover, the group of Eric Meggers [3] developed ruthenium–cyclopentadienyl half-sandwich compounds based on the structure of staurosporine that proved to be very effective kinase inhibitors. Thanks to its unique properties such as aromaticity, aqueous stability, and redox behaviour [4], ferrocene is increasingly used in the development of new anticancer drugs [5]. Impressive results have been obtained by the group of Gérard Jaouen [6], with the development of ferrocifens (i.e. ferrocene-modified tamoxifens), which exhibit strong antiproliferative effects not only in hormone-dependent but also in hormone-independent breast cancer cells.

Another example of a ferrocene based drug is ferroquine [7] (FQ, SSR97193), a new antimalarial highly active against chloroquine-resistant malaria strains, and currently in phase IIb clinical trials piloted by Sanofi-Aventis. In addition, FQ has been found to display potent anticancer activity by interfering with DNA [8]. These results suggested a relation between the antitumor and the antimalarial activities of this compound [9]. Among the available strategies to design affordable and efficient drugs, the use of organometallics [10], and especially of ferrocene [5a], clearly offers new possibilities since these compounds may exhibit enhanced chemical and pharmacological properties compared to the purely organic parent drugs [6e,7b] (Chart 1).

Various anticancer drugs including vinblastine, paclitaxel, colchicine, and combretastatin have been shown to modulate microtubule assembly by inhibiting tubulin polymerization or by blocking microtubule disassembly. Tubulin polymerization inhibitors characterized by the presence of an indole nucleus have been obtained from natural sources or have been prepared by semi-synthesis. Small molecules such as indole itself have been extensively studied [11]. Indeed, they are very attractive as lead compounds due to their cheap and easy synthesis. This is evidenced by the studies of the group of von Angerer [12] that has synthesized a series of 2-phenylindole derivatives and assessed their anticancer activities in human breast cancer cell lines. These compounds prevent the polymerization of the α/β-tubulin dimers to functional microtubules by binding to the colchicine-binding site and provoking cell cycle arrest in G2/M phase [12b]. The 2-phenylindole-3-carbaldehydes of this series showed pronounced cytotoxic activity. Thus the development of new 2-phenylindole derivatives as anticancer agents is of great interest. Modifications of the structure of the antimitotic 2-phenylindole-3-carbaldehydes by substitution of the 3-formyl group gave rise to methylene propanedinitrile [12c] and hydrazone [12d] derivatives that did not inhibit tubulin polymerization but were still able to block the cell cycle in G_2/M phase. QSAR [13], CoMFA, and docking studies [14] have been carried out upon 2-phenylindole derivatives to find out the structural requirements for more active antimitotic agents.

In the light of these findings, we decided to study the synthesis and characterization of new ferrocene–indole hybrids in order to compare them to their organic parent compounds. In our design, the ferrocene core was introduced into the 3 position of the 2-phenylindole scaffold (Chart 2). We studied the contribution of

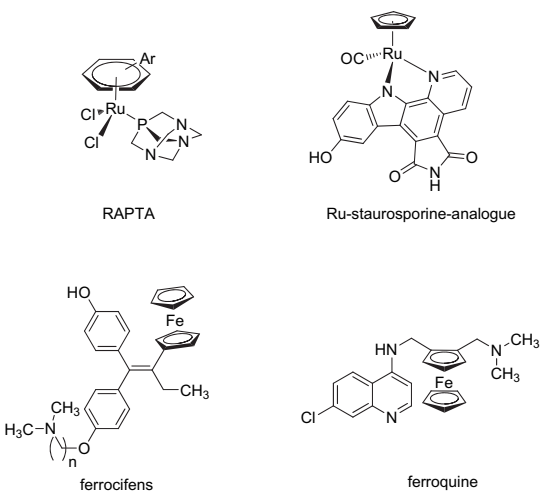

Chart 1. Chemical structures of organometallics with anticancer and antimalarial activity.

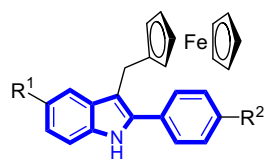

Chart 2. Compounds investigated in this study.

the ferrocene core of these new hybrid molecules in their anticancer activity against the A549 human carcinoma cell line. In addition, we tested the potential of our new derivatives against chloroquine-susceptible and chloroquine-resistant strains of *Plasmodium falciparum*.

2. Results and discussion

2.1. Chemistry

The starting 2-phenylindole derivatives (**1**–**7**) were synthesized by the classical Bischler [15] or Fischer [16] indole synthesis. The ferrocene–indole hybrids (**8**–**14**) were synthesized using a modified procedure of Boev and coworkers [17] (Scheme 1).

The 2-phenylindole derivatives were reacted with ferrocenemethanol in dichloromethane in the presence of an aqueous solution of HBF_4 at room temperature during 1 h. The two-phase system reaction is based on the generation of the corresponding α-ferrocenylcarbocation from ferrocenemethanol in strong acids and their further reaction on the nucleophilic indol 3-position. Purification of the crude products by column chromatography on silica gel using diethylether as eluent afforded the ferrocene–indole hybrids in very good yield (Scheme 1). The chemical structures of the 2-phenylindole derivatives (**1**–**7**) and the ferrocene–indole hybrids (**8**–**14**) were established unequivocally by NMR techniques using 2D homonuclear (COSY) and heteronuclear (HSQC, HMBC) experiments.

2.2. Biology

2.2.1. Cytotoxic activities

The A549 human lung carcinoma cell line was used to test the cytotoxic activity of the synthesized compounds. With the exception of **4** and **7**, all compounds exhibited cytotoxic activities with IC_{50} values below 100 μM. 5-Fluorouracil (5-FU) was used as a positive control in the cell proliferation assay, showing an IC_{50} value below 5 μM. Compounds **11**, **12** and **13** showed the highest antiproliferative effect, with IC_{50} values below 10 μM. Among these molecules, ferrocene–indole hybrid **11** showed the strongest cytotoxic activity with an IC_{50} value of 5 μM (Table 1).

For SAR analysis, some elements could be highlighted when comparing the substitution pattern of the tested compounds (**1**–**14**). The 5-position of the indole ring (R^1) is sensitive to the substitution pattern because compounds **11**, **12** and **13** had the lowest IC_{50} values. The order of potency was as follows: 5-OMe (**11**)> 5-NO_2 (**12**) > 5-Cl (**13**). The IC_{50} values of the 5-position unsubstituted compounds (R^1 = H) were higher than those of the 5-substituted compounds. Halogen substituents at the *p*-position (R^2) of the aryl ring decreased the cytotoxic properties as follows: *p*-H (**8**) > *p*-Cl (**9**) > *p*-F (**10**). The unsubstituted **8** was two-fold more active than the fluoro derivative **10**. The introduction of basic nitrogen in the isosteric exchange benzene/pyridine, ferrocene–indole hybrid **14** decreased its activity two-fold.

Table 1
Cytotoxic activities on A549 human lung carcinoma cell line of the ferrocene–indole hybrids **8**–**14** in contrast to the organic analogues **1**–**7**.

compound	Type	R^1	R^2	X	IC_{50}
1	Organic molecule	H	H	H	30 ± 7
2	Organic molecule	H	Cl	H	33 ± 8
3	Organic molecule	H	F	H	31 ± 8
4	Organic molecule	OCH_3	H	H	118 ± 4
5	Organic molecule	NO_2	H	H	14 ± 3
6	Organic molecule	Cl	H	H	15 ± 5
7	Organic molecule	H	H	N	120 ± 10
8	Organometallic molecule	H	H	H	13 ± 4
9	Organometallic molecule	H	Cl	H	15 ± 1
10	Organometallic molecule	H	F	H	26 ± 1
11	Organometallic molecule	OCH_3	H	H	5 ± 1
12	Organometallic molecule	NO_2	H	H	7 ± 1
13	Organometallic molecule	Cl	H	H	10 ± 1
14	Organometallic molecule	H	H	N	27 ± 3
5-FU	Reference				<5

5-FU, 5-Fluorouracil.

The combination of the ferrocene core and the 2-phenylindol scaffold always increased the cytotoxicity of hybrid molecules: ferrocene–indole hybrids **8**–**14** were all more active than the corresponding purely organic compounds **1**–**7**. In this regard, ferrocene–indole hybrids **9**, **10** and **12**, with *p*-Cl, *p*-F and 5-NO_2 substituents were two-fold more active than their corresponding organic analogues **2**, **9** and **5**, respectively. The ferrocene–indole hybrids **8** and **14** were three-fold and four-fold more active than their corresponding organic analogues **1** and **7**, respectively. Finally, the ferrocene–indole hybrid **11** (with R^2 = OMe) was the most potent of the synthesized compounds (with an IC_{50} value of 5 μM) and was 25-fold more active than its corresponding precursor **4**.

2.2.2. Antimalarial activities

The *in vitro* screening assays are described in the experimental protocols section. The biological activities of the new aryl and ferrocenyl indole derivatives were compared to those of the widely used chloroquine (CQ). All the compounds were tested against a larger panel of well characterized *P. falciparum* laboratory strains or strains obtained from isolates grown in culture for an extended period of time [18] (Table 2).

Whatever the CQ susceptibility of the *P. falciparum* strains, the new derivatives only exhibited weak inhibitory effects. Moreover, no clear difference between the organic **1**–**7** and ferrocene–indole hybrids **8**–**14** could be noted. Although the interpretation of these results in terms of the structure–activity relationship (SAR) is difficult at this stage, some elements could be highlighted concerning R^1 and R^2 substituents. In the organic series, the introduction of a chlorine atom as an R^2 substituent (compound **2**) or a methoxy group as an R^1 substituent (compound **4**) caused an enhancement of the activity against *P. falciparum*. In the ferrocenic series, the most active compound was the unsubstituted indole **8**. We found no correlation between anticancer activities and antimalarial activities of these compounds. In contrast to our previous work, the most cytotoxic hybrids were not the most active on CQ-resistant strains [8].

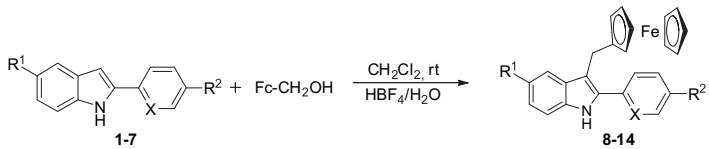

Scheme 1. Synthesis of ferrocene-indole hybrids 8–14. Reagents and conditions: 2-arylindole (1 mmol), ferrocenemethanol (1 mmol), CH_2Cl_2, aqueous solution of HBF_4 (6 mL of 50% commercial acid + 4 mL of water), rt, 1 h.

Table 2
In vitro antiplasmodial activity of 2-phenylindoles and 3-ferrocenylmethyl-2-phenylindoles.

	IC_{50} in μM[a]							
Strains	3D7	D6	FCM29	IMT 10500	K14	K4	PA	W2
Origin	Africa	Sierra Leone	Cameroon	Comoros	Cambodia	Cambodia	Uganda	Indochina
1	>100	44.0	35.3	44.6	28.7	90.1	31.5	35.8
2	26.4	30.2	43.2	32.8	25.1	18.2	15.1	26.5
3	18.6	25.4	100	28.5	>100	52.2	>100	26.2
4	23.0	24.7	28.2	21.2	27.3	25.1	37.3	17.6
5	22.8	22.3	21.0	30.5	24.9	22.2	31.5	24.0
6	34.0	29.5	33.0	32.4	26.9	27.1	12.3	19.7
7	>100	29.2	25.6	43.3	30.9	39.4	>100	30.8
8	28.2	22.7	25.4	25.8	22.3	18.8	24.6	26.7
9	30.6	33.3	25.2	36.4	37.7	38.4	31.0	33.2
10	38.2	43.6	31.9	29.7	40.8	14.8	17.6	29.3
11	38.6	29.0	44.0	26.4	36.4	32.1	31.0	29.6
12	31.5	28.0	26.0	25.7	25.3	19.4	25.1	28.6
13	31.9	13.3	25.8	30.3	25.2	14.2	20.4	30.0
14	28.3	26.0	30.8	41.0	27.5	22.3	16.9	28.2
IC_{50} in nM								
CQ	25	25	502	51	662	491	287	539
FQ	3.5	5.2	6.8	4.6	13.0	7.5	6.4	6.6

[a] IC_{50} are geometric means of 3–4 experiments.

3. Conclusion

In summary, we report a convenient one-step, high yield synthetic procedure for the preparation of the 3-ferrocenyl-2-phenylindole derivatives, **8**–**14**. The design of these compounds constitutes the first bioorganometallic approach for modifying the 2-phenylindole framework present in several potent antimitotic drugs. These new ferrocene–indole hybrids and their organic analogues were tested for their cytotoxic and antiplasmodial activities. These compounds showed only moderate antimalarial activity and the presence or absence of the ferrocenyl moiety only slightly affected this. Ferrocene–indole hybrids **11**, **12**, and **13** were the most potently cytotoxic compounds with IC_{50} values below 10 μM. The ferrocene–indole hybrids **8**–**14** were found to be markedly more cytotoxic than the organic series (compounds **1**–**7**). Notably we observed a 25-fold increase in potency for the ferrocenic 5-OMe derivative **11**, with an IC_{50} value of 5 μM. Future work will be aimed at the evaluation of the mode of action of the synthesized hybrids molecules and the preparation of new analogues bearing alkyl groups at R^1 and alkoxy substituents at R^2, taking into account QSAR and CoMFA analysis carried out previously on 3-carbaldehyde-2-phenylindole derivatives.

4. Experimental

4.1. Chemistry

Materials and methods. Reagents were obtained from commercial sources and used as received. All reactions were carried out with dry, freshly distilled solvents. Column chromatography refers to flash chromatography and was carried out on SiO_2 (silica gel 60, SDS, 230–240 mesh). Analytical TLC was performed on SiO_2 (Merck silica gel 60 F_{254}) plates. Melting points were determined on a Gallenkamp apparatus and are not corrected. Elemental analyses were carried out at the Serveis Cientifico-Tècnics (*Universitat Barcelona*). Mass spectra (ESI^+) were performed at the Servei d'Espectrometria de Masses (*Universitat de Barcelona*). Infrared spectra were obtained with a Nicolet 400FTIR instrument using KBr pellets. Only noteworthy IR absorptions are listed (cm^{-1}). Chemical shifts of ^1H NMR spectra are reported in ppm downfield (δ) from Me_4Si. For ^{13}C NMR spectra chemical shifts are reported relative to the δ 77.00 resonance of $CDCl_3$. Unless otherwise noted ^1H and ^{13}C NMR spectra were recorded in $CDCl_3$ solution at 400 and 100 MHz, respectively and registered with a Mercury-400 MHz. Coupling constants (J) are reported in Hz. All NMR assignments were made on the basis of two-dimensional NMR experiments (gCOSY gHSQC and gHMBC). ^{19}F NMR spectra of **2** and **10** were recorded with a Mercury 400 instrument and the reference was TFA [δ (^{19}F) = −78.5 ppm].

4.1.1. Full description of ^1H, ^{19}F and ^{13}C NMR spectra for 2-pheylylindoles (**1**–**7**) [19]

The full description of ^1H, ^{19}F and ^{13}C NMR spectra for 2-phenylylindoles (**1**–**7**) is given, as these data, to the best of our knowledge, were found to be incomplete in the literature [15,16].

*4.1.1.1. 2-Phenyl-1H-indole (**1**).* ^1H NMR (gCOSY) 8.31 (b s, 1H, NH-indol), 7.64 (d, J = 8 Hz, 2H, H-2′ and H-6′), 7.63 (d, J = 8 Hz, 1H, H-4), 7.43 (m, 2H, H-3′ and H-5′), 7.39 (d, J = 8 Hz, 1H, H-7), 7.32 (tt, J = 7.6 and 1.2 Hz, 1H, H-4′), 7.19 (td, J = 8 and 1.1 Hz, 1H, H-6), 7.14 (td, J = 8 and 1.1 Hz, 1H, H-5), 6.82 (s, 1H, H-3). ^{13}C NMR (gHSQC, gHMBC) 137.8 (C-1′), 136.8 (C-7a), 132.3 (C-2), 129.2 (C-3a), 129.0 (C-2′ and C-6′), 127.7 (C-4′), 125.1 (C-3′ and C-5′), 122.3 (C-6), 120.6 (C-4), 120.3 (C-5), 110.9 (C-7), 99.9 (C-3).

*4.1.1.2. 2-(4-Chlorophenyl)-1H-indole (**2**).* ^1H NMR (gCOSY) 8.23 (b s, 1H, NH-indol), 7.62 (d, J = 7.8 Hz, 1H, H-4), 7.56 (m, 2H, H-2′ and H-6′), 7.40 (m, 2H, H-3′ and H-5′), 7.38 (dd, J = 8 and 0.9 Hz, 1H, H-7), 7.20 (ddd, J = 8.0, 7.1 and 1.1 Hz, 1H, H-6), 7.13 (ddd, J = 7.7, 7.0 and 1.1 Hz, 1H, H-5), 6.80 (dd, J = 2.1 and 0.9 Hz, 1H, H-3). ^{13}C NMR (gHSQC, gHMBC) 136.9 (C-7a), 136.6 (C-2), 133.4 (C-4′), 130.8 (C-1′), 129.2 (C-3′ and C-5′), 129.1 (C-3a), 126.3 (C-2′ and C-6′), 122.7 (C-6), 120.7 (C-4), 120.4 (C-5), 110.9 (C-7), 100.4 (C-3).

*4.1.1.3. 2-(4-Fluorophenyl)-1H-indole (**3**).* ^1H NMR (gCOSY) 8.25 (b s, 1H, NH-indol), 7.58–7.65 (m, 3 H, H-4, H-2′ and H-6′), 7.39 (dd, J = 8 and 1 Hz, 1H, H-7), 7.20 (td, J = 8 and 1.2 Hz, 1H, H-6), 7.10–7.18 (m, 3 H, H-5, H-3′ and H-5′), 6.76 (d, J = 3 Hz, 1H, H-3). ^{13}C NMR (gHSQC, gHMBC) 163.6, 161.2 (C-4′), 137.0 (C-7a), 136.8 (C-2), 129.2 (C-3a), 128.8 (C-1′), 126.9, 126.8 (C-2′ and C-6′), 122.4 (C-6), 120.6 (C-4), 120.4 (C-5), 116.2, 115.9 (C-3′ and C-5′), 110.9 (C-7), 99.9 (C-3). ^{19}F NMR -114.37.

*4.1.1.4. 5-Methoxy-2-phenyl-1H-indole (**4**).* ^1H NMR (gCOSY) 8.20 (b s, 1H, NH-indol), 7.64 (m, 2H, H-2′ and H-6′), 7.43 (t, J = 7.6 Hz, 2H, H-3′ and H-5′), 7.31 (m, 1H, H-4′), 7.29 (d, J = 8.8 Hz, 1H, H-7), 7.09

(d, $J = 2$ Hz, 1H, H-4), 6.86 (dd, $J = 8.8$ and 2.4 Hz, 1H, H-6), 6.76 (d, $J = 2$ Hz, 1H, H-3), 3.87 (s, 3 H, OCH_3). ^{13}C NMR (gHSQC, gHMBC) 154.5, (C-5), 138.6 (C-2), 132.5 (C-1′), 132.0 (C-7a), 129.7 (C-3a), 129.0 (C-3′ and C-5′), 127.6 (C-4′), 125.0 (C-2′ and C-6′), 112.6 (C-6), 111.6 (C-7), 102.3 (C-4), 99.8 (C-3), 55.8 (CH_3).

*4.1.1.5. 5-Nitro-2-phenyl-1H-indole (**5**).* ^1H NMR (gCOSY) 8.78 (b s, 1H, NH-indol), 8.59(d, $J = 2$ Hz, 1H, H-4), 8.12 (dd, $J = 9.2$ and 2 Hz, 1H, H-6), 7.70 (m, 2H, H-2′ and H-6′), 7.50 (td, $J = 7.6$ and 1.4 Hz, 2H, H-3′ and H-5′), 7.44 (d, $J = 9.2$ Hz, 1H, H-7), 7.41 (tt, $J = 7.4$ and 1.6 Hz, 1H, H-4′), 6.98 (s, 1H, H-3). ^{13}C NMR (gHSQC, gHMBC) 142.3, (C-3a), 141.2 (C-2), 139.7 (C-7a), 131.1 (C-1′), 129.3 (C-3′ and C-5′), 128.8 (C-4′), 128.6 (C-5), 125.4 (C-2′ and C-6′), 118.0 (C-6), 117.7 (C-4), 110.9 (C-7), 101.6 (C-3).

*4.1.1.6. 5-Chloro-2-phenyl-1H-indole (**6**).* ^1H NMR (gCOSY) 8.37 (b s, 1H, NH-indol), 7.64 (dt, $J = 7.2$ and 1.2 Hz, 2H, H-2′ and H-6′), 7.58 (d, $J = 2$ Hz, 1H, H-4), 7.44 (td, $J = 7.4$ and 1.4 Hz, 2H, H-3′ and H-5′), 7.34 (tt, $J = 7.4$ and 1.2 Hz, 1H, H-4′), 7.29 (d, $J = 8.8$ Hz, 1H, H-7), 7.13 (dd, $J = 9$ and 2 Hz, 1H, H-6), 6.75 (s, 1H, H-3). ^{13}C NMR (gHSQC, gHMBC) 139.3 (C-2), 135.1 (C-7a), 131.8 (C-1′), 130.3 (C-3a), 129.1 (C-3′ and C-5′), 128.1 (C-4′), 125.8 (C-5), 125.2 (C-2′ and C-6′), 122.5 (C-6), 120.0 (C-4), 111.9 (C-7), 99.5 (C-3).

*4.1.1.7. 2-(2pyiridyl)-1H-indole (**7**).* ^1H NMR (gCOSY) 9.86 (b s, 1H, NH-indol), 8.57 (dm, $J = 4.8$ Hz, 1H, H-3′), 7.80 (m, 1H, H-6′), 7.70 (td, $J = 7.6$ and 1.6 Hz, 1H, H-5′), 7.65 (d, $J = 7.6$ Hz, 1H, H-4), 7.37 (dm, $J = 8$ Hz, 1H, H-7), 7.21 (ddd, $J = 8.2$, 7 and 1.2 Hz, 1H, H-6), 7.16 (ddd, $J = 7.4$, 4.8 and 1 Hz, 1H, H-4′), 7.11 (ddd,, $J = 7.8$, 7.1 and 0.9 Hz, 1H, H-5), 7.02 (m, 1H, H-3). ^{13}C NMR (gHSQC, gHMBC) 150.4 (C-1′), 149.1 (C-3′), 136.7 (C-2), 136.62 (C-5′), 136.59 (C-7a), 129.1 (C-3a), 123.1 (C-6), 122.0 (C-4′), 121.1 (C-4), 120.1 (C-5), 119.9 (C-6′), 111.4 (C-7), 100.6 (C-3).

*4.1.2. General synthetic procedure for the preparation of 3-ferrocenylmethyl-2-pheylindoles (**8**–**14**)*

A slightly modified procedure of Boev and coworkers [17] was followed for the synthesis of the 3-ferrocenylmethyl-2-phenylindoles. To a stirred solution of the parent 2-phenylindole derivative (**1**–**7**, 1 mmoL) and ferrocenemethanol (216 mg, 1 mmoL) in dichloromethane (25 mL), 10 mL of an aqueous solution of HBF_4 (6 mL of 50% commercial acid + 4 mL H_2O) was added dropwise. After vigorous stirring for 1 h, the mixture was quenched with water (40 mL). The phases were separated, and the aqueous phase extracted with dichloromethane (2 × 20 mL) [20]. The combined organic extracts were washed with water (2 × 10 mL), dried over Na_2SO_4 and evaporated under reduced pressure. The crude product was purified by column chromatography on a short pad of silica gel using diethylether as eluent. The ether was evaporated under reduced pressure to yield the desired 3-ferrocenylmethyl derivatives (**8**–**14**) in very high yield.

*4.1.2.1. 3-Ferrocenylmethyl-2-phenyl-1H-indole (**8**).* Yellow solid, mp 128–130 °C. Yield 92%. Anal. Calc. For $C_{25}H_{21}FeN$: C, 76.92; H, 5.37; N, 3.58. Found: C, 76.59; H, 5.31; N, 3.78%. MS (ESI^+): $m/z = 391.11$ [M^+]. IR: 3500, 3403, 3383, 1456, 765, 746, 699, 501, 484. ^1H NMR (gCOSY) 8.00 (b s, 1H, NH-indol), 7.60–7.70 (m, 3 H, H-6, H-2′ and H-6′), 7.51 (t, $J = 7.6$ Hz, 1H, H-3′ and H-5′), 7.41 (d, $J = 7.6$ Hz, 1H, H-7), 7.36 (m, 1H, H-4), 7.18 (td, $J = 7.4$ and 1.2 Hz, 1H, H-5), 7.12 (m, 1H, H-4′), 4.13 (s, 2H, H^2 and H^5, C_5H_4), 4.02 (s, 7 H, H^3, H^4, C_5H_4 and C_5H_5), 3.99 (s, 2H, CH_2). ^{13}C NMR (gHSQC, gHMBC) 136.0 (C-7a), 134.3 (C-3a), 133.5 (C-1′), 128.8 (C-2′ and C-6′), 128.2 (C-3′ and C-5′), 127.7 (C-4′), 125.0 (C-2), 122.2 (C-6), 119.60 (C-4), 119.57 (C-5), 113.0 (C-3), 110.7 (C-7), 89.0 (C^1), 68.8 (C^2, C^5), 68.6 (C_5H_5), 66.9 (C^3, C^4), 24.6 (CH_2).

*4.1.2.2. 2-(4-Chlorophenyl)-3-ferrocenylmethyl-1H-indole (**9**).* Dark yellow solid, mp 179–181 °C. Yield 92%. Anal. Calc. For $C_{25}H_{20}ClFeN$: C, 70.52; H, 4.70; N, 3.29. Found: C, 70.16; H, 4.73; N, 3.30%. MS (ESI^+): $m/z = 425$ [M^+]. IR: 3540, 3413, 3397, 1483, 1455, 1435, 1335, 1311, 1105, 1089, 1010, 997, 832, 738, 495. ^1H NMR (gCOSY) 7.94 (b s, 1H, NH-indol), 7.63 (d, $J = 8$ Hz, 1H, H-4), 7.53 (d, $J = 8$ Hz, 2H, H-2′ and H-6′), 7.46 (d, $J = 8$ Hz, 2H, H-3′ and H-5′), 7.33 (d, $J = 7.6$ Hz, 1H, H-7), 7.19 (t, $J = 7.4$ Hz, 1H, H-6), 7.12 (dd, $J = 7.4$ and 8 Hz, 1H, H-5), 4.06 (s, 5 H, C_5H_5), 4.12 (s, 2H, H^2 and H^5, C_5H_4), 4.00 (s, 2H, H^3 and H^4, C_5H_4), 3.94 (s, 2H, CH_2). ^{13}C NMR (gHSQC, gHMBC) 135.9 (C-7a), 133.6 (C-4′), 133.0 (C-2), 131.7 (C-1′), 129.4 (C-2′ and C-6′), 129.0 (C-3′ and C-5′), 128.9 (C-3a), 122.5 (C-6), 119.8 (C-4), 119.6 (C-5), 113.6 (C-3), 110.8 (C-7), 88.9 (C^1), 68.8 (C^2 and C^5), 68.7 (C_5H_5), 67.0 (C^3 and C^4), 24.6 (CH_2).

*4.1.2.3. 3-Ferrocenylmethyl-2-(4-fluorophenyl)-1H-indole (**10**).* Yellow solid, mp 146–148 °C. Yield 94%. Anal. Calc. For $C_{25}H_{20}FFeN$: C, 73.37; H, 4.89; N, 3.42. Found: C, 73.28; H, 4.99; N, 3.50%. MS (ESI^+): $m/z = 409$ [M]+H.$^+$ IR: 3418, 1502, 1457, 1436, 1227, 1216, 1156, 1101, 841, 815, 735, 489. ^1H NMR (gCOSY) 7.94 (b s, 1H, NH-indol), 7.62 (d, $J = 8$ Hz, 1H, H-4), 7.54–7.60 (m, 2H, H-2′ and H-6′), 7.35 (d, $J = 8$ Hz, 1H, H-7), 7.15–7.22 (m, 3 H, H-6, H-3′ and H-5′), 7.12 (m, 1H, H-5), 4.12 (s, 2H, H^2 and H^5, C_5H_4), 4.04 (s, 5 H, C_5H_5), 4.00 (s, 2H, H^3 and H^4, C_5H_4), 3.93 (s, 2H, CH_2). ^{13}C NMR (gHSQC, gHMBC) 163.6, 161.2 (C-4′), 135.8 (C-7a), 133.3 (C-2), 130.0, 129.9 (C-2′ and C-6′), 129.4 (C-1′), 129.1 (C-3a), 122.3 (C-6), 119.7 (C-5), 119.6 (C-4), 115.9, 115.8 (C-3′ and C-5′), 113.1 (C-3), 110.7 (C-7), 88.9 (C^1), 68.8 (C^2 and C^5), 68.7 (C_5H_5), 67.1 (C^3 and C^4), 24.6 (CH_2). ^{19}F NMR -114.37.

*4.1.2.4. 3-Ferrocenylmethyl-5-methoxy-2-phenyl-1H-indole (**11**).* Grey solid, mp 141–143 °C. Yield 90%. Anal. Calc. For $C_{26}H_{22}FeNO$: C, 74.12; H, 5.50; N, 3.32. Found: C, 73.78; H, 5.67; N, 3.31%. MS (ESI^+): $m/z = 421$ [M]+H$^+$. IR: 3386, 1481, 1449, 1214, 1021, 828, 770, 698, 510, 496. ^1H NMR (gCOSY) 7.87 (b s, 1H, NH-indol), 7.60 (dd, $J = 7.8$ and 1.2 Hz, 2H, H-2′ and H-6′), 7.49 (t, $J = 7.8$ Hz, 2H, H-3′ and H-5′), 7.38 (tt, $J = 7.6$ and 1.2 Hz, 1H, H-4′), 7.24 (d, $J = 8.8$ Hz, 1H, H-7), 7.04 (d, $J = 2.6$ Hz, 1H, H-4), 6.84 (dd, $J = 8.6$ and 2.6 Hz, 1H, H-6), 4.16 (s, 2H, H^2 and H^5, C_5H_4), 4.05 (s, 5 H, C_5H_5), 4.02 (s, 2H, H^3 and H^4, C_5H_4), 3.94 (s, 2H, CH_2), 3.85 (s, 3 H, OCH_3). ^{13}C NMR (gHSQC, gHMBC) 154.2 (C-5), 135.2 (C-2), 133.3 (C-1′), 131.0 (C-7a) 129.6 (C-3a), 128.8 (C-3′ and C-5′), 128.1 (C-2′ and C-6′), 127.7 (C-4′), 112.7 (C-3), 112.2 (C-6), 111.4 (C-7), 101.7 (C-4), 90.0 (C^1), 69.4 (C^2, C^5 and C_5H_5), 67.7 (C^3 and C^4), 55.9 (OCH_3), 24.6 (CH_2).

*4.1.2.5. 3-Ferrocenylmethyl-5-nitro-2-phenyl-1H-indole (**12**).* Yellow-orange solid, mp 185 °C. Yield 93%. Anal. Calc. For $C_{25}H_{20}FeN_2O_2$: C, 68.82; H, 4.62; N, 6.42. Found: C, 68.94; H, 4.61; N, 6.37%. MS (ESI^+): $m/z = 436.4$ [M^+]. IR: 3470, 3450, 3382, 3325, 1515, 1473, 1328, 1300, 815, 737, 699, 480. ^1H NMR (gCOSY) 8.60 (d, $J = 2$ Hz, 1H, H-4), 8.34 (b s, 1H, NH-indol), 8.10 (dd, $J = 8.6$ and 2.2 Hz, 1H, H-6), 7.63 (m, 2H, H-2′ and H-6′), 7.55 (t, $J = 7.6$ Hz, 2H, H-3′ and H-5′), 7.47 (t, $J = 7.4$ Hz, 1H, H-4′), 7.37 (d, $J = 8.8$ Hz, 1H, H-7), 4.11 (t, $J = 1.6$ Hz, 2H, H^2 and H^5, C_5H_4), 4.07 (s, 5 H, C_5H_5), 4.03 (t, $J = 1.8$ Hz, 2H, H^3 and H^4, C_5H_4), 4.01 (s, 2H, CH_2). ^{13}C NMR (gHSQC, gHMBC) 141.7 (C-3a), 138.7 (C-7a), 133.3 (C-1′), 137.3 (C-2) 131.9 (C-1′), 129.1 (C-3′ and C-5′), 128.7 (C-5), 128.6 (C-4′), 128.3 (C-2′ and C-6′), 117.9 (C-6), 116.8 (C-4), 115.2 (C-3), 110.7 (C-7), 88.1 (C^1), 68.81 (C^2 and C^5), 68.80 (C_5H_5), 67.4 (C^3 and C^4), 24.5 (CH_2).

*4.1.2.6. 5-Chloro-3-ferrocenylmethyl-2-phenyl-1H-indole (**13**).* Orange solid, mp 140–143 °C. Yield 96%. Anal. Calc. For $C_{25}H_{20}FeClN$: C, 70.53; H, 4.74; N, 3.29. Found: C, 70.42; H, 4.97; N, 3.45%. MS (ESI^+): $m/z = 425.07$ [M^+]. IR: 3500, 3407, 1638, 1580, 1463, 1450, 1425, 1307, 1104, 1000, 815, 797, 763, 699, 484. ^1H NMR (gCOSY) 8.01 (b s,

1H, NH-indol), 7.62 (d, J = 7. 2 Hz, 2H, H-2′ and H-6′), 7.57 (d, J = 2 Hz, 1H, H-4), 7.51 (t, J = 7.2 Hz, 2H, H-3′ and H-5′), 7.42 (t, J = 7.2 Hz, 1H, H-4′), 7.26 (d, J = 8.4 Hz, 1H, H-7), 7.13 (dd, J = 8.6 and 2.2, 1H, H-6), 4.10 (t, J = 1.8 Hz, 2H, H^2 and H^5, C_5H_4), 4.03 (s, 5 H, C_5H_5), 4.00 (t, J = 2 Hz, 2H, H^3 and H^4, C_5H_4), 3.94 (s, 2H, CH_2). ^{13}C NMR (gHSQC, gHMBC) 135.7 (C-2), 134.1 (C-7a), 132.8 (C-1′), 130.3 (C-5), 128.9 (C-3′ and C-5′), 128.2 (C-2′ and C-6′), 128.1 (C-4′), 125.2 (C-3a), 122.4 (C-6), 119.0 (C-4), 112.7 (C-3), 111.7 (C-7), 88.6 (C^1), 68.7 (C^2 and C^5), 68.6 (C_5H_5), 67.1 (C^3 and C^4), 24.5 (CH_2).

4.1.2.7. 3-Ferrocenylmethyl-2-(2pyridyl)-1H-indole (***14***). Yellow solid, mp 133–136 °C. Yield 83%. Anal. Calc. For $C_{24}H_{20}FeN_2$: C, 73.48; H, 5.14; N, 7.14. Found: C, 73.10; H, 5.04; N, 6.83%. MS (ESI^+): m/z = 393.11{[M]+H}$^+$. IR: 3500, 3404, 3200, 3087, 2921, 1764, 1590, 1563, 1451, 1337, 1320, 1104, 999, 818, 742, 483. ^1H NMR (gCOSY) 9.55 (b s, 1H, NH-indol), 8.62 (dd, J = 3.2, 1.2 Hz, 1H, H-3′), 7.80 (d, J = 8 Hz, 1H, H-6′), 6.69–7.74 (m, 2H, H-4 and H-5′), 7.38 (d, J = 8 Hz, 1H, H-7), 7.23 (td, J = 7.6 and 1.6 Hz, 1H, H-6), 7.10–7.18 (m, 2H, H-5 and H-4′), 7.31 (td, J = 6.8 and 1.2 Hz, 1H, H-5), 4.18 (m, 4 H, CH_2, H^2 and H^5, C_5H_4), 4.09 (s, 5 H, C_5H_5), 4.01 (t, J = 2.4 Hz, 2H, H^3 and H^4, C_5H_4). ^{13}C NMR (gHSQ, gHMBC) 150.7 (C-1′), 149.3 (C-3′), 136.5 (C-5′), 135.4 (C-7a), 132.1 (C-2), 129.7 (C-3a), 123.3 (C-6), 121.6 (C-4′), 121.2 (C-6′), 119.7 (C-4), 119.4 (C-5), 114.4 (C-3), 111.2 (C-7), 88.5 (C^1), 68.7 (C_5H_5), 68.6 (C^2 and C^5), 67.1 (C^3 and C^4), 25.0 (CH_2).

4.2. Biology

4.2.1. Cell culture

Human lung carcinoma A549 cells (obtained from the American Type Culture Collection) were used in all the experiments. A549 cells were grown as a monolayer culture in minimum essential medium (DMEM with L-glutamine, without glucose and without sodium pyruvate) in the presence of 10% heat-inactivated fetal calf serum, 10 mM of D-glucose and 0.1% streptomycin/penicillin in standard culture conditions.

4.2.2. Cell proliferation assay

The assay was performed by a variation of the method described by Mosmann et al. [21] as specified by Matito and coworkers [22]. Briefly, 3×10^3 A549 cells/well were cultured in 96 well plates. Concentrations that inhibited cell growth by 50% (IC_{50}) after 72 h of treatment were calculated based on the survival rate compared with untreated cells. Relative cell viability was measured by the absorbance on an ELISA plate reader (Tecan Sunrise MR20-301, TECAN, Salzburg, Austria) at 550 nm.

4.2.3. Antiplasmodial assay

Eight parasite strains or isolates from a wide panel of countries (Africa (3D7), Cambodia (K2 and K14), Cameroon (FCM29), Comoros (IMT10500), Indochina (W2), Sierra Leone (D6), and Uganda (PA)) were maintained in culture in RPMI 1640 (Invitrogen, Paisley, United Kingdom), supplemented with 10% human serum (Abcys S.A. Paris, France) and buffered with 25 mM HEPES and 25 mM $NaHCO_3$. Parasites were grown in A-positive human blood under controlled atmospheric conditions that consisted of 10% O_2, 5% CO_2 and 85% N_2 at 37 °C with a humidity of 95%.

Chloroquine diphosphate (CQ) was purchased from Sigma (Saint Louis, MO). FQ base was obtained from Sanofi-Aventis (France). CQ was resuspended in water in concentrations ranging between 5 and 3200 nM. FQ and synthetic compounds were resuspended in DMSO and then diluted in RPMI-DMSO (99v/1v) to obtain final concentrations ranging from 0.125 to 500 nM and 0.1 μM–100 μM, respectively.

For *in vitro* isotopic microtests, 25 μL/well of antimalarial drug and 200 μL/well of the parasitized red blood cell suspension (final parasitemia, 0.5%; final hematocrit, 1.5%) were distributed into 96 well plates. Parasite growth was assessed by adding 1 μCi of tritiated hypoxanthine with a specific activity of 14.1 Ci/mmol (Perkin–Elmer, Courtaboeuf, France) to each well at time zero. The plates were then incubated for 48 h in controlled atmospheric conditions. Immediately after incubation, the plates were frozen and thawed to lyse erythrocytes. The contents of each well were collected on standard filter microplates (Unifilter GF/B; Perkin–Elmer) and washed using a cell harvester (Filter-Mate Cell Harvester; Perkin–Elmer). Filter microplates were dried, and 25 μL of scintillation cocktail (Microscint O; Perkin–Elmer) was placed in each well. Radioactivity incorporated by the parasites was measured with a scintillation counter (Top Count; Perkin–Elmer).

The IC_{50}, the drug concentration able to inhibit 50% of parasite growth, was assessed by identifying the drug concentration corresponding to 50% of the uptake of tritiated hypoxanthine by the parasite in the drug-free control wells. The IC_{50} value was determined by non-linear regression analysis of log-based dose-response curves (Riasmart™, Packard, Meriden, USA). IC_{50} are expressed as geometric means of 3–4 experiments.

Acknowledgment

The authors thank R. Amalvict, E. Baret and D. Travers for technical support. Financial support from the Ministry of Science and Innovation, Spain (Project CTQ2009-07021/BQU and CTQ2009-11501) and the AGAUR, Generalitat de Catalunya (Grant 2009-SGR-1111) is gratefully acknowledged. This study was funded by a grant from the Ministère de l'Enseignement Supérieur to F.D.

References

[1] R.D. Adams, J. Organomet. Chem. 694 (2009) 801–802.
[2] (a) A. Dorcier, P.J. Dyson, C. Gossens, U. Rothlisberger, R. Scopelliti, I. Tavernelli, Organometallics 24 (2005) 2114–2123;
(b) P.J. Dyson, G. Sava, Dalton Trans. 16 (2006) 1929–1933;
(c) B. Dutta, C. Scolaro, R. Scopelliti, P.J. Dyson, K. Severin, Organometallics 27 (2008) 1355–1357;
(d) A.K. Renfrew, A.D. Phillips, A.E. Egger, C.G. Hartinger, S.S. Bosquain, A.A. Nazarov, B.K. Keppler, L. Gonsalvi, M. Peruzzini, P.J. Dyson, Organometallics 28 (2009) 1165–1172.
[3] (a) D.S. Williams, G.E. Atilla, H. Bregman, A. Arzoumanian, P.S. Klein, E. Meggers, Angew. Chem. Int. Ed. 44 (2005) 1984–1987;
(b) H. Bregman, E. Meggers, Org. Lett. 8 (2006) 5465–5468;
(c) E. Meggers, Curr. Opin. Chem. Biol. 11 (2007) 287–292;
(d) E. Meggers, G.E. Atilla-Gokcumen, H. Bregman, J. Maksimoska, S.P. Mulcahy, N. Pagano, D.S. Williams, Synlett (2007) 1177–1189. doi:10.1055/s-2007-973893;
(e) K.S.M. Smalley, R. Contractor, N.K. Haass, A.N. Kulp, G.E. Atilla-Gokcumen, D.S. Williams, H. Bregman, K.T. Flaherty, M.S. Soengas, E. Meggers, M. Herlyn, Cancer Res. 67 (2007) 209–217.
[4] (a) H. Tamura, M. Miwa, Chem. Lett. (1997) 1177–1178;
(b) D. Osella, M. Ferrali, P. Zanello, F. Laschi, M. Fontani, C. Nervi, G. Cavigiolio, Inorg. Chim. Acta 306 (2000) 42–48;
(c) G. Tabbì, C. Cassino, G. Cavigiolio, D. Colangelo, A. Ghiglia, I. Viano, D. Osella, J. Med. Chem. 45 (2002) 5786–5796.
[5] (a) M.F.R. Fouda, M.M. Abd-Elzaher, R.A. Abdelsamaia, A.A. Labib, Appl. Organomet. Chem. 21 (2007) 613–625;
(b) D.R. van Staveren, N. Metzler-Nolte, Chem. Rev. 104 (2004) 5931–5985.
[6] (a) S. Top, A. Vessières, G. Leclercq, J. Quivy, J. Tang, J. Vaissermann, M. Huché, G. Jaouen, Chem. . A Eur. J. 9 (2003) 5223–5236;
(b) G. Jaouen, S. Top, A. Vessières, G. Leclercq, M.J. McGlinchey, Curr. Med. Chem. 11 (2004) 2505–2517;
(c) A. Vessières, S. Top, P. Pigeon, E. Hillard, L. Boubeker, D. Spera, G. Jaouen, J. Med. Chem. 48 (2005) 3937–3940;
(d) E. Hillard, A. Vessières, L. Thouin, G. Jaouen, C. Amatore, Angew. Chem. Int. Ed. 45 (2006) 285–290;
(e) A. Vessieres, S. Top, W. Beck, E. Hillard, G. Jaouen, Dalton Trans. 4 (2006) 529–541;
(f) A. Nguyen, E.A. Hillard, A. Vessières, S. Top, P. Pigeon, G. Jaouen, Chimia 61 (2007) 716–724;
(g) O. Buriez, J.M. Heldt, E. Labbé, A. Vessières, G. Jaouen, C. Amatore, Chem. A Eur. J. 14 (2008) 8195–8203;
(h) Q. Michard, G. Jaouen, A. Vessieres, B.A. Bernard, J. Inorg. Biochem. 102 (2008) 1980–1985;
(i) P. Pigeon, S. Top, O. Zekri, E.A. Hillard, A. Vessières, M.-A. Plamont, O. Buriez,

E. Labbé, M. Huché, S. Boutamine, C. Amatore, G. Jaouen, J. Organomet. Chem. 694 (2009) 895–901;
(j) M. Gormen, D. Plazuk, P. Pigeon, E.A. Hillard, M.-A. Plamont, S. Top, A. Vessières, G. Jaouen, Tetrahedron Lett. 51 (2010) 118–120.
[7] (a) F. Dubar, J. Khalife, J. Brocard, D. Dive, C. Biot, Molecules 13 (2008) 2900–2907;
(b) D. Dive, C. Biot, ChemMedChem 3 (2008) 383–391.
[8] N.I. Wenzel, N. Chavain, Y. Wang, W. Friebolin, L. Maes, B. Pradines, M. Lanzer, V. Yardley, R. Brun, C. Herold-Mende, C. Biot, K. Tóth, E. Davioud-Charvet, J. Med. Chem. 53 (2010) 3214–3226.
[9] (a) A. Nzila, J. Okombo, R.P. Becker, R. Chilengi, T. Lang, T. Niehues, Trends Parasitol. 26 (2010) 125–129;
(b) S. Kozlov, N.C. Waters, M. Chavchich, Infect. Disord. . Drug Targets 10 (2010) 165–190;
(c) P. Lawton, M. Sarciron, A. Pétavy, Drugs of the Future 31 (2006) 793–809;
(d) M. Klinkert, V. Heussler, Mini-Reviews Med. Chem. 6 (2006) 131–143;
(e) B. Kappes, P. Rohrbach, Future Microbiol. 2 (2007) 409–423;
(f) N. Kongkathip, N. Pradidphol, K. Hasitapan, R. Grigg, W.- Kao, C. Hunte, N. Fisher, A.J. Warman, G.A. Biagini, P. Kongsaeree, P. Chuawong, B. Kongkathip, J. Med. Chem. 53 (2010) 1211–1221.
[10] (a) C.S. Allardyce, A. Dorcier, C. Scolaro, P.J. Dyson, Appl. Organomet. Chem. 19 (2005) 1–10;
(b) C.G. Hartinger, P.J. Dyson, Chem. Soc. Rev. 38 (2009) 391–401;
(c) N. Chavain, C. Biot, Curr. Med. Chem. 17 (2010) 2729–2745.
[11] For a review see: A. Brancale, R. Silvestri Med. Res. Rev. 27 (2007) 209–238 and references cited herein.
[12] (a) R. Gastpar, M. Goldbrunner, D. Marko, E. von Angerer, J. Med. Chem. 41 (1998) 4965–4972;
(b) D. Kaufmann, M. Pojarová, S. Vogel, R. Liebl, R. Gastpar, D. Gross, T. Nishino, T. Pfaller, E. von Angerer, Bioorg. Med. Chem. 15 (2007) 5122–5136;
(c) M. Pojarová, D. Kaufmann, R. Gastpar, T. Nishino, P. Reszka, P.J. Bednarski, E. von Angerer, Bioorg. Med. Chem. 15 (2007) 7368–7379;
(d) S. Vogel, D. Kaufmann, M. Pojarová, C. Müller, T. Pfaller, S. Kühne, P.J. Bednarski, E. von Angerer, Bioorg. Med. Chem. 16 (2008) 6436–6447.
[13] A.K. Halder, N. Adhikari, T. Jha, Bioorg. Med. Chem. Lett. 19 (2009) 1737–1739.
[14] S.Y. Liao, L. Qian, T.F. Miao, H.L. Lu, K.C. Zheng, Eur. J. Med. Chem. 44 (2009) 2822–2827.
[15] Bischler indol synthesis (only selected articles): (a) V. Sridharan, S. Perumal, C. Avendaño, J.C. Menéndez, Synlett (2006) 91–95;
(b) J. Schmitt, C. Perrin, M. Langlois, M. Suquet, Bull. Soc. Chim. Fr. (1969) 1227–1236;
(c) R. Gastpar, M. Goldbrunner, D. Marko, E. von Angerer, J. Med. Chem. 41 (1998) 4965–4972;
(d) E. von Angerer, J. Prekajac, J. Strohmeier, J. Med. Chem. 27 (1984) 1439–1447;
(e) E. von Angerer, J.J. Strohmeier, Med. Chem. 30 (1987) 131–136.
[16] Fischer indol synthesis: (only selected articles): (a) W.E. Noland, K.R. Rush, L.R. Smith, J. Org. Chem. 31 (1966) 65–69 (see this article for 5-nitro-2-phenylindole, 5);
(b) R.P. Thummel, V. Hedge, J. Org. Chem. 54 (1989) 1720–1725 (see this article for the 2-pyridyl derivatives);
(c) Q. Liu, M.S. Mudadu, H. Schmider, R. Thummel, Y. Tao, S. Wang, Organometallics 21 (2002) 4743–4749 (see this article for several 2-phenylindoles).
[17] V.I. Boev, L.V. Snegur, V.N. Babin, Y.S. Nekrasov, Russ. Chem. Rev. 66 (1997) 613–636.
[18] M. Henry, S. Briolant, A. Zettor, S. Pelleau, M. Baragatti, E. Baret, J. Mosnier, R. Amalvict, T. Fusai, C. Rogier, B. Pradines, Antimicrob. Agents Chemother. 53 (2009) 1926–1930.
[19] Labelling of the atoms:

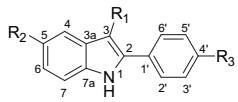

[20] For the preparation of the 2-(2-piridyl) derivative 14, the acidic aqueous phase was neutralized with saturated aqueous $NaHCO_3$ solution, prior extraction with dichloromethane.
[21] T. Mosmann, J. Immunol. Methods 65 (1983) 55–63.
[22] C. Matito, F. Mastorakou, J.J. Centelles, J.L. Torres, M. Cascante, Eur. J. Nutr. 42 (2003) 42–49.

CAPÍTULO 1E

COMPLEJOS DE PLATINO(II) DIASTEREOMÉRICAMENTE PUROS COMO AGENTES ANTITUMORALES. LA INFLUENCIA DEL MODO DE ENLACE {(N), (N,O)⁻ O (C,N)⁻} DE (1S,2R)-[(H^5-C^5H^5)FE{(H^5-C_5H_4)-CH=N-CH(ME)-CH(OH)-C_6H_5}] Y LA DISTRIBUCIÓN DE LOS LIGANDOS AUXILIARES.

Daniel Talancón [a], Concepción López [a*], Mercè Font-Bardía [b], Teresa Calvet [c], Josefina Quirante [d], Carme Calvis [e], Ramon Messeguer [e], Roldán Cortés [f], Marta Cascante [f], Laura Baldomà [g], Josefa Badia [g]

[a] Departament de Química Inorgànica, Facultat de Química, Universitat de Barcelona, Martí i Franquès 1–11, E-08028-Barcelona, España

[b] Unitat de Difracció de Raigs-X. Centre Científic i Tecnològic de la Universitat de Barcelona. Universitat de Barcelona, Solé i Sabaris 1–3, 08028-Barcelona, España

[c] Departament de Cristal·lografia, Mineralogia i Dipòsits Minerals. Facultat de Geologia. Universitat de Barcelona, Martí i Franquès s/n, E-08028-Barcelona, España

[d] Laboratori de Química Orgànica, Facultat de Farmàcia, Institut de Biomedicina, (IBUB), Universitat de Barcelona, Av. Joan XXIII, s/n, 08028-Barcelona, España

[e] Biomed Division, Leitat Tecnological Center, Parc Científic de Barcelona, Edifici Hèlix, C/ Baldiri Reixach, 15–21, 08028-Barcelona, España

[f] Departament de Bioquímica i Biologia Molecular, Facultat de Biologia, Institut de Biomedicina de la Universitat de Barcelona (IBUB) y IDIBAPS, Unidad Asociada al CSIC, Diagonal 643, 08028 Barcelona, España

[g] Departament de Bioquímica i Biología Molecular. Facultat de Farmàcia. Institut de Biomedicina de la Universitat de Barcelona (IBUB), Av. Joan XIII s/n 08028-Barcelona, España

Resumen

El estudio de la reactividad de (*1S,2R*)-[(η^5-C_5H_5)Fe{[(η^5-C_5H_4)-CH=N-CH(-Me)-CH(OH)-C_6H_5}] (**1a**) con *cis*-[$PtCl_2(DMSO)_2$] bajo diferentes condiciones experimentales ha permitido el aislamiento y caracterización de tres pares de complejos de platino(II) diastereoméricamente puros. Dos de los pares son isómeros *trans*- y *cis*- de (*1S,2R*)-[Pt(η^5-C_5H_5)Fe{[(η^5-C_5H_4)-CH=N-CH(Me)-CH(OH)-C_6H_5]}Cl_2(DMSO)] [*trans*-(**2a**) y *cis*-(**3a**), respectivamente], y de (*1S,2R*)-[Pt{(k^2-*N,O*)(η^5-C_5H_5)Fe[(η^5-C_5H_4)-CH=N-CH(Me)-CH(O)-C_6H_5]}, {*trans*-(Cl, N) en (**4a**)} o {*cis*-(Cl, N) en (**5a**)}; mientras que el tercer par está formado por cicloplatinados: [Pt{(k^2-C,N[(η^5-C_5H_3)]-CH=N-CH(Me)-CH(O-H)-C_6H_5]Fe(η^5-C_5H_5)}Cl(DMSO)] con distinta quiralidad planar [S_p (en **6a**) o R_p (en **7a**)]. También se incluyen las estructuras cristalinas de los compuestos **2a**, **3a**, **5a** y **6a**. Se ha realizado una evaluación de la capacidad antiproliferativa de los complejos **1a**-**7a** en líneas tumorales de pulmón (A549), mama (MDA-MB231) y colon (HCT116), que revela que la potencia de los compuestos depende del modo de enlace del iminoalcohol {(N) en **2a** and **3a**, $(N,O)^-$ en **4a** y **5a** o $(C,N)^-$ en **6a** y **7a**}, de la distribución relativa de los ligandos monodentados (en **2a**-**5a**) y de la quiralidad planar de la unidad 1,2-ferrocenilo (en **6a** y **7a**). Entre los productos de nueva síntesis (**2a**-**7a**), los compuestos **4a** y **5a** exhiben la mayor actividad antiproliferativa, con valores de IC_{50} inferiores a los del cisplatino en las tres líneas tumorales ensayadas. Se han realizado estudios electroforéticos de migración del ADN en presencia de los compuestos, para obtener información acerca de su posible mecanismo de acción. Se presenta también un estudio comparativo del comportamiento de todos los complejos en disolución en DMSO-d_6 o en DMSO-d_6:D_2O, a 298 K.

Journal of Inorganic Biochemistry 118 (2013) 1–12

Contents lists available at SciVerse ScienceDirect

Journal of Inorganic Biochemistry

journal homepage: www.elsevier.com/locate/jinorgbio

Diastereomerically pure platinum(II) complexes as antitumoral agents. The influence of the mode of binding {(N), (N,O)$^-$ or (C,N)}$^-$ of (*1S,2R*)–[(η^5-C_5H_5)Fe{(η^5-C_5H_4)–CH═N–CH(Me)–CH(OH)–C_6H_5}] and the arrangement of the auxiliary ligands

Daniel Talancón [a], Concepción López [a,*], Mercè Font-Bardía [b], Teresa Calvet [c], Josefina Quirante [d], Carme Calvis [e], Ramon Messeguer [e], Roldán Cortés [f], Marta Cascante [f], Laura Baldomà [g], Josefa Badia [g]

[a] Departament de Química Inorgànica, Facultat de Química, Universitat de Barcelona, Martí i Franquès 1–11, E-08028-Barcelona, Spain
[b] Unitat de Difracció de Raigs-X. Centre Científic i Tecnològic de la Universitat de Barcelona. Universitat de Barcelona, Solé i Sabaris 1–3, 08028-Barcelona, Spain
[c] Departament de Cristal·lografia Mineralogía i Dipòsits Minerals. Facultat de Geologia. Universitat de Barcelona, Martí i Franquès s/n, E-08028-Barcelona, Spain
[d] Laboratori de Química Orgànica, Facultat de Farmàcia, Institut de Biomedicina, (IBUB), Universitat de Barcelona, Av. Joan XXIII, s/n, 08028-Barcelona, Spain
[e] Biomed Division, Leitat Tecnological Center, Parc Científic de Barcelona, Edifici Hèlix, C/ Baldiri Reixach, 15–21, 08028-Barcelona, Spain
[f] Department of Biochemistry and Molecular Biology, Faculty of Biology, Institute of Biomedicine (IBUB), Universitat de Barcelona, Unit Associated with CSIC, Diagonal 645, 08028-Barcelona, Spain
[g] Departament de Bioquímica i Biología Molecular. Facultat de Farmàcia. Institut de Biomedicina de la Universitat de Barcelona (IBUB), Av. Joan XIII s/n 08028-Barcelona, Spain

ARTICLE INFO

Article history:
Received 30 April 2012
Received in revised form 3 September 2012
Accepted 3 September 2012
Available online 13 September 2012

Keywords:
Platinum(II) complexes
Ferrocene derivatives
Cancer
Chirality

ABSTRACT

The study of the reactivity of (*1S,2R*)–[(η^5-C_5H_5)Fe{[(η^5-C_5H_4)–CH═N–CH(Me)–CH(OH)–C_6H_5)] (**1a**) with *cis*-[$PtCl_2(DMSO)_2$] under different experimental conditions has allowed to isolate and characterize three pairs of isomeric and diastereomerically pure platinum(II) complexes. Two of the pairs are the *trans*- and *cis*- isomers of (*1S,2R*)–[Pt{(η^5-C_5H_5)Fe[(η^5-C_5H_4)–CH═N–CH(Me)–CH(OH)–C_6H_5]}Cl_2(DMSO)] [*trans*-(**2a**) and *cis*-(**3a**), respectively], and of (*1S,2R*)–[Pt{(κ^2-*N,O*)(η^5-C_5H_5)Fe[(η^5-C_5H_4)–CH═N–CH(Me)–CH(O)–C_6H_5]}Cl(DMSO)], {*trans*-(Cl, N) in (**4a**)} or a *cis*-(Cl, N) {in (**5a**)}; while the third one is formed by platinacycles: [Pt{(κ^2-*C,N*[(η^5-C_5H_3)]–CH═N-CH(Me)–CH(OH)–C_6H_5]Fe(η^5-C_5H_5)}Cl(DMSO)] with different planar chirality [S_p (in **6a**) or R_p (in **7a**)]. The crystal structures of compounds **2a**, **3a**, **5a** and **6a** are also reported. The cytotoxic assessment of **1a–7a** on lung (A549), breast (MDA-MB-231) and colon (HCT-116) cancer cell lines is also reported and reveals that the potency of the complexes is strongly dependent on the mode of binding of the iminoalcohol {(N) in **2a** and **3a**, (N,O)$^-$ in **4a** and **5a** or (C,N)$^-$ in **6a** and **7a**}, the relative arrangement of the monodentate ligands (in **2a–5a**), and the planar chirality of the 1,2-ferrocenylunit in (**6a** and **7a**). Among the new products (**2a**–**7a**), compounds **4a** and **5a** exhibit the highest potency with IC_{50} values smaller than cisplatin in the three cancer cell lines assayed. Electrophoretic DNA migration studies in the presence of **2a–7a** have been performed in order to get further insights into their mechanism of action. A comparative study of the solution behaviour of all the complexes in DMSO-d_6 or in DMSO-d_6:D_2O (1:1) mixtures at 298 K is also reported.

1. Introduction

The discovery of the cytotoxic properties of *cis*-[$PtCl_2(NH_3)_2$] (*cisplatin*, Fig. 1) and its clinical applications has marked the origin of fast and increasing interest in the chemistry of platinum(II) [1–13] in order to improve the antitumoral activity and to minimize the undesirable side-effects (i.e. nephrotoxicity, neurotoxicity, the increase of blood pressure, severe nausea, vomiting, or diarrhea) produced by *cisplatin* [1,14].

Most of the strategies used so far arise from the modification of the environment of the platinum(II) in *cisplatin* and are mainly centered on: a) the replacement of one NH_3 molecule by a monodentate N-donor ligand [such as in *Picoplatin* (Fig. 1)] or the two units by a bidentate (*N,N*) or (*N,N'*) ligands and b) the substitution of the Cl^- ligands by dicarboxylate units as in *carboplatin* (Fig. 1) and its derivatives [1–8]. The combined use of these two methodologies led to *oxaliplatin* (Fig. 1) [1,2,6].

More recently, other types of platinum(II) complexes, such as the *trans*- isomers of [$Pt(L)_2Cl_2$] and [Pt(L)(L')Cl_2] (L and L' = neutral monodentate ligands) [13–16] or the platinacycles [Pt(C,N)X(L)] or [Pt(C,N,N')X] [10,17–20] with greater activity than the corresponding *cis*- isomers [10,11] and *cisplatin* have been reported. Therefore, these

* Corresponding author. Tel.: +34 93 403 91 34; fax: +34 93 490 77 25.
E-mail address: conchi.lopez@qi.ub.es (C. López).

0162-0134/$ – see front matter © 2012 Elsevier Inc. All rights reserved.
http://dx.doi.org/10.1016/j.jinorgbio.2012.09.007

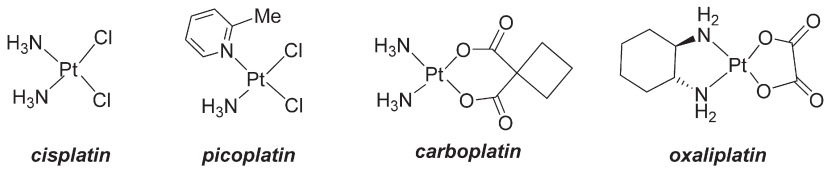

Fig. 1. Chemical formulae of some platinum(II) based anticancer agents.

families of complexes offer new possibilities and promising prospects for the development of new platinum(II) based anticancer drugs.

On the other hand, in the late decade novel ferrocene derivatives have become especially attractive due to their biological activity and biomedical applications [21–28]. A large amount of platinum(II) complexes arising from the replacement of the NH_3 ligands of *cisplatin* by a) a neutral N-donor ferrocenyl ligand and a dmso unit or b) a [C(sp^2, ferrocene),N)]$^-$ bidentate group have been published [29–32], but studies on their cytotoxic activity are extremely scarce [30].

Unfortunately, the use of ferrocene derivatives with different donor atoms able to: a) exhibit different binding modes {i.e. (N), (N, X)$^-$ (X═N′, O, S) or (C,N)$^-$} in front of platinum(II) and/or b) produce various isomers (i.e. geometrical or optical) has not been investigated so far and consequently the effects produced by the binding mode of this sort of products or the relative arrangement of the remaining ligands bound to the platinum(II) on their potential antitumoral activity still remain unknown.

We have recently reported the synthesis of the iminoalcohol [(η^5-C_5H_5)Fe{[(η^5-C_5H_4)−CH═NCH(Me)−CH(OH)C_6H_5)}] (**1a**) [32] that contains two heteroatoms (N and O) with good donor abilities and in addition the relative arrangement of the imine nitrogen and the σ[C(sp^2, ferrocene)-H] bonds on the ortho site are susceptible to metallate. In this case the formation of the σ[Pt-C(sp^2, ferrocene)] bond induces planar chirality and consequently two different diastereomers could form [33]. Besides that, **1a** coexists in solution with the closed forms (**1b**) (Scheme 1, step **A**) [34]. It its well-known that this type of ring–chain tautomerism between imines and 1,3-(N,O) heterocycles (i.e. oxazolines or oxazines) affects the reactivity of the species involved, and this property is important not only in view of their utility in organic synthesis but also in physical and medicinal chemistry [34–37]. Several platinum(II) complexes with oxazolidine or oxazine ligands have been reported [38–41] and some of them are specially interesting because of their cytotoxic properties [40,41].

In view of this, compound **1a** appeared an excellent candidate to study its coordination ability or that of its tautomer (**1b**) towards platinum(II) and to allow the elucidation of the effect induced by their coordination mode on the potential cytotoxic activity of the new complexes. On the other hand, **1a** and **1b** have the typical funtionalities commonly involved in hydrogen bonding interactions and this could enhance the solubility of the platinum derivatives in biological media [42–44]. In this paper we present the synthesis of three pairs of diastereomerically pure platinum(II) complexes derived from **1a**, their cytotoxic activity in three cancer cellular lines together with a study of their effect on the electrophoretic mobility of pBluescript SK$^+$ DNA tertiary structure and preliminary conclusions on their structure–activity relationship (SAR).

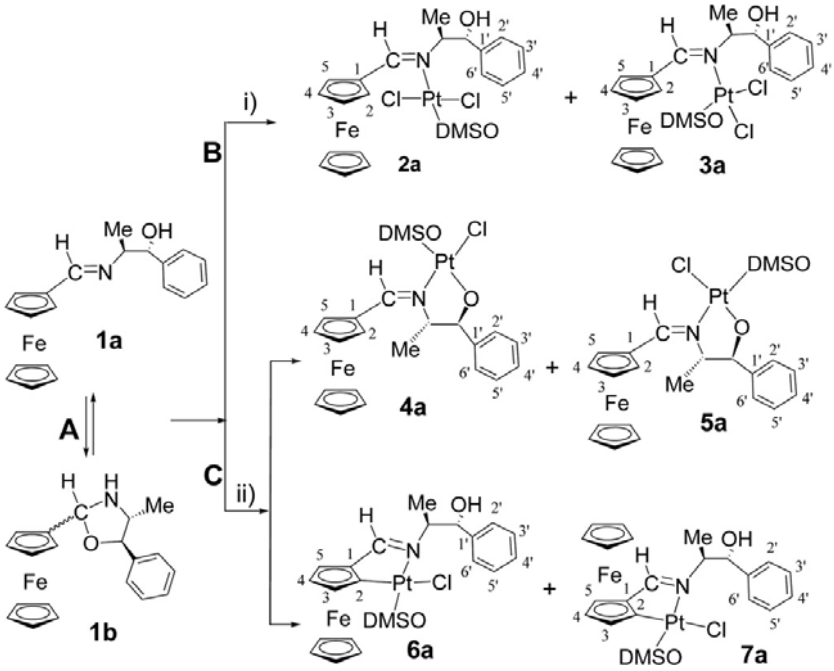

Scheme 1. i) *Cis*-[$PtCl_2(DMSO)_2$] in refluxing methanol (see text). ii) *Cis*-[$PtCl_2(DMSO)_2$] and NaOAc in molar ratios **1a**:Pt:OAc^- = (1:1:1) or (1:1:2) in a mixture toluene: methanol (4:1) under reflux (see text) followed by SiO_2 column chromatography.

2. Experimental

2.1. Chemistry

2.1.1. Materials and methods

Ligand **1a** and *cis*-[$PtCl_2(DMSO)_2$] were prepared as reported previously [32,45]. The remaining reagents were obtained from commercial sources and used as received. Except methanol (which was HPLC-grade), the remaining solvents were dried and distilled before use [46]. Elemental analyses were carried out at the Serveis de Cientifico-Tècnics (*Universitat Barcelona*). Mass spectra (ESI^+, positive-mode electrospray ionization) were performed at the Servei d'Espectrometria de Masses (*Universitat de Barcelona*). Infrared spectra of **2a-7a** were obtained with a Nicolet 400FTIR instrument using KBr pellets; while their far IR spectra (in the range 200–400 cm^{-1}) were registered with a Bomen DA3 instrument using polyethylene discs. UV-visisble (UV–vis) spectra of 1.0×10^{-4} M solutions of the compounds in CH_2Cl_2 were recorded with a Cary 100 scan Varian UV spectrometer at 298 K. The optical rotations were determined in CH_2Cl_2 at 293 K using a Perkin–Elmer 241 MC polarimeter and the concentration used is specified in the characterisation section of each compound. The R_f values were obtained using SiO_2 (Merck silica gel 60 F254) plates and the solvents specified in the characterization section of the corresponding product. High resolution ^{1}H-NMR spectra and the two-dimensional {^{1}H–^{1}H}-NOESY (nuclear Overhauser effect spectroscopy) and COSY (correlation spectroscopy) experiments were registered with a Varian VRX-500 or a Bruker Avance DMX-500 MHz instruments. ^{195}Pt{^{1}H} NMR spectra of **2a–7a** were obtained with a Bruker-250 MHz instrument. In all cases the solvent for the NMR experiments was $CDCl_3$ (99.9%) and the references were $SiMe_4$ [for ^{1}H and ^{13}C{^{1}H} NMR] and $H_2[PtCl_6]$ [δ^{195}Pt{$H_2[PtCl_6]$} = 0.0 ppm] for ^{195}Pt {^{1}H} NMR experiments. All these NMR studies were performed at 298 K. The chemical shifts (δ) are given in ppm and the coupling constants (*J*) in Hz. In the characterization section of each product the assignment of signals detected in the ^{1}H NMR spectra refer to the labelling patterns presented in Scheme 1.

2.1.2. Preparation of the compounds

For all the preparations described in this section the reaction flask was protected from the light with aluminium foil during the refluxing period and the work up of the column chromatographies should not be done in more than 8 h; for longer periods, the acidity of the SiO_2 produces the slow decomposition of the complexes, the amount of ferrocenecarboxaldehyde formed increased and the yields of the platinum(II) complexes decreased.

*2.1.2.1. Trans-(1S,2R)-(+)-[Pt{(η^5-C_5H_5)Fe[(η^5-C_5H_4)–CH═N–CH(Me)–CH(OH)–C_6H_5}]Cl_2(DMSO)] (**2a**).* *Cis*-[$PtCl_2(DMSO)_2$] (211 mg, 5.00×10^{-4} mol) was suspended in 35 mL of methanol. The reaction mixture was refluxed until complete dissolution of the Pt(II) complex. Afterwards the hot solution was filtered out and the filtrate was poured into an Erlenmeyer flask containing 174 mg (5.00×10^{-4} mol) of the ligand *(1S,2R)*-(+)-[(η^5-C_5H_5)Fe(η^5-C_5H_4)]–CH═N–CH(Me)–CH(OH)–C_6H_5 (**1a**). The mixture was heated at reflux temperature for 45 min. Then the undissolved materials were removed by filtration and discarded and the filtrate was concentrated on a rotary evaporator until ca. 5 mL and allowed to cool to 298 K. The solid formed, that contained traces of ferrocenecarboxaldehyde and a mixture of **2a** and **3a** (in a 1.00 : 0.11 molar ratio), was collected by filtration, washed with three (2 mL) portions of n-hexane, to remove the aldehyde, and air dried for 24 h. After this period the solid was dissolved in the minimum amount of CH_2Cl_2 (ca. 3 mL) and passed through a fast and short SiO_2 (15 mm×20 mm) column. Elution with CH_2Cl_2 produced the release of a wide red band, that was collected in ca. 25 mL portions. The first six collected portions gave after concentration **2a** (115 mg); while the remaining ones produced a solid that contained both isomers (**2a** and **3a**). An additional crop of **2a** (31 mg) could be obtained from the first portions eluted after an additional column chromatography of the mixture of isomers (yield: 146 mg, 42 %). *Characterization data.* Elemental analyses: calc. for $C_{22}H_{27}Cl_2FeNO_2PtS$ (FW = 691.3 g/mol): C, 38.22; H, 3.94; N, 2.03 and S, 4.64 %; found: C, 38.2; H, 3.9; N, 2.1 and S, 4.9 %. MS (ESI^+): *m/z* = 656.0 $\{[M]-Cl\}^+$. IR (in cm^{-1}): 3430 [br., vs, ν(O–H)], 3020 and 2993 [m, ν(C–H)], 1624 [s, ν(>C═N–)], 1449 (m), 1407 (m), 1249 (m), 1106 (s), 1023 (s), 990, (m), 756 (m), 702 (m), 481 (m), 437 (m) and 355(m) [ν(Pt–Cl)]. Solubility (in mg/mL): 22 (in $CDCl_3$); 14 (in DMSO-d_6) and 8 in a DMSO-d_6-D_2O (1:1) mixture. $[\alpha]_D$ (CH_2Cl_2 at 293 K, $c = 1.1\times10^{-1}$ g/100 mL) = +588º. UV–vis. data ($c = 1.7\times10^{-5}$ M in CH_2Cl_2 at 298 K): λ_{max} in nm (ε in M^{-1} cm^{-1}): 478 (3571), 348 (5299), 288 (41532) and 237 (59101). R_f [in CH_2Cl_2:MeOH (100:0.1) = 0.42]. ^{1}H NMR data: δ = 1.22 (d, 3 H, ^{3}J = 7.0, Me); 3.10 (d, 1 H, ^{3}J = 5.0, –OH); 3.43 [s, 3 H, $^3J_{Pt,H}$ = 22.0, Me(DMSO)]; 3.44 [s, 3 H, $^3J_{Pt,H}$ = 22.0, Me(DMSO)]; 4.45 [m, 1 H, –CH(Me)–]; 4.35 (s, 5 H, Cp); 4.70 (s, 1 H, H^3); 4.77 (s, 1 H, H^4); 5.23 (d, 1 H, ^{3}J = 1,0, H^2); 6.11 [s, 1 H, –CH(OH) –]; 6.21 (s, 1 H, H^5); 7.30 (t, 1 H, ^{3}J = 7.5, $H^{4'}$); 7.40 (t, 2 H, ^{3}J = 8.0, $H^{3'}$ and $H^{5'}$); 7.49 (d, 2 H, ^{3}J = 7.5, $H^{2'}$ and $H^{6'}$) and 8.20 (s, 1 H, $^3J_{Pt,H}$ = 84.0, –CH═N). ^{13}C{^{1}H} NMR data: δ = 13.1 (Me); 43.9 [Me(DMSO)]; 70.5 (Cp); 71.4 [–CH(Me)–]; 72.0 (C^2); 73.4 [–CH(OH)–]; 74.0 (C^3); 74.3 (C^4 and C^5); 74.8 (C^1); 125.9 ($C^{2'}$ and $C^{6'}$); 127.5 ($C^{4'}$); 128.5 ($C^{3'}$ and $C^{5'}$); 140.9 ($C^{1'}$) and 169.0 (–CH═N–). ^{195}Pt{^{1}H} NMR data: δ = −2991.

*2.1.2.2. Cis-(1S,2R)-(+)-[Pt{[(η^5-C_5H_5)Fe(η^5-C_5H_4)]–CH═N–CH(Me)–CH(OH)–C_6H_5}]Cl_2(DMSO) (**3a**).* This compound was isolated as by-product during the synthesis of **2a**; but the procedure described in this section allows its isolation in a higher yield. The method to achieve **3a** is practically identical to that of **2a**, except that the refluxing period was longer (3 h). Similarly, the solid isolated was later on passed through a SiO_2 (15 mm×20 mm) column chromatography using CH_2Cl_2 as eluant. The bands collected gave after concentration the aldehyde and a solution containing a mixture of the *trans*- and *cis*-isomers in a molar ratio (**2a**:**3a**) = (1.00:0.62). Further crystallization of this material in CH_2Cl_2 allowed to isolate **3a** (yield: 65 mg, 19%).

Characterization data: Elemental analyses: Calc. for $C_{22}H_{27}Cl_2FeNO_2PtS$ (FW = 691.3 g/mol): C, 38.22; H, 3.94; N, 2.03 and S, 4.64 %; found: C, 38.2; H, 3.9; N, 2.1 and S, 4.4 %. EM (ESI^+): *m/z* = 656.0 $\{[M]-Cl\}^+$. IR (in cm^{-1}): 3450 [br., vs, ν(O-H)], 3019 and 2993 [s, ν(C-H)], 1628 [s, ν(>C=N-)], 1451 (m), 1405 (s), 1251 (m), 1086 (s), 1043 (s), 995 (m), 820 (m), 752 (m), 690 (m), 468 (m), 440(m), 348(br.) and 338 [ν(Pt-Cl)]. Solubility (in mg/mL): 11 (in $CDCl_3$); 6 (in DMSO-d_6) and 3 [in a DMSO-d_6:D_2O (1:1) mixture]. $[\alpha]_D$ (CH_2Cl_2 at 293 K, $c = 2.6\times10^{-2}$ g/100 mL) = +1442º. UV–vis. data (CH_2Cl_2 at 298 K, $c = 4.6\times10^{-5}$ M): λ_{max} in nm (ε en M^{-1} cm^{-1}): 474 (2095), 357 (3240), 291 (22208) and 228 (34197). R_f [in CH_2Cl_2:MeOH (100:0.1) = 0.48]. ^{1}H NMR data: δ = 1.16 (d, 3 H, ^{3}J = 7.2, Me); 3,87 (d, 1 H, ^{3}J = 4.8, –OH); 3.20 [s, 3 H, Me(DMSO)]; 3,48 [s, 3 H, Me(DMSO)]; 4.41 (s, 5 H, Cp); 4.69 [m, 1 H, –CH(Me)–]; 4.71 (s, 2 H, H^3 and H^4); 4.86 (s, 1 H, H^2); 5.76 (s, 1 H, H^5) 7.17 [s, 1 H, –CH(OH)–]; 7.31 (t, 1 H, ^{3}J = 7.2, $H^{4'}$); 7.41 (t, 2 H, ^{3}J = 7.2, $H^{3'}$ and $H^{5'}$); 7.53 (d, 2 H, ^{3}J = 7.0, $H^{2'}$ and $H^{6'}$) and 8.26 (s, 1 H, $^3J_{Pt,H}$ = 120,0, –CH═N–). ^{13}C{^{1}H} NMR data: δ = 13,5 (Me); 44.4 and 44.8 [Me(DMSO)]; 65.0 [–CH(Me)–]; 72.3 (C^5); 73.9 (C^2); 76.4 (C^3 and C^4), 72.1 (Cp); 72.7 [–CH(OH)–]; 125.5 ($C^{2'}$ and $C^{6'}$); 127.4 ($C^{4'}$); 128.4 ($C^{3'}$ and $C^{5'}$); 139.8 ($C^{1'}$) and 168.5 (–CH═N–). ^{195}Pt{^{1}H} NMR data: δ = −2943.

*2.1.2.3. Preparation of a mixture of the two isomers {trans-(Cl, N) (**4a**) and cis-(Cl,N) (**5a**)}. of (1S,2R)-(+)-[Pt{(κ^2-N,O)(η^5-C_5H_5)Fe[(η^5-C_5H_4)–CH═N–CH(Me)–CH(O)–C_6H_5}]Cl(DMSO)].* Ligand **1a** (150 mg, 4.32×10^{-4} mol) and the equimolar amount of *cis*-[$PtCl_2(DMSO)_2$] (182 mg) were treated with 20 mL of toluene. Then a methanol solution (5 mL) of NaOAc (71 mg, 8.64×10^{-4} mol) was added. The resulting reaction mixture was stirred for 24 h and then filtered out. The hot filtrate was concentrated to dryness on a rotary evaporator and the residue was afterwards dissolved in the minimum amount of

CH_2Cl_2 and passed through a SiO_2 column (20 mm × 40 mm). Elution with CH_2Cl_2 produced a band containing small amount of the aldehyde. Once this band was collected, a CH_2Cl_2:MeOH (100:0.2) mixture was used as eluant. This produced the release of a purple one that contained a mixture of the platinacycles **6a** and **7a** [in a molar ratio (**6a**:**7a**) = 1.00:0.67]. Finally, the polarity of the eluant was increased by using a CH_2Cl_2:MeOH (100:0.4) mixture and this released an orange band. The solid isolated after its concentration, that contained **4a** and **5a** in a (1.00:0.93) molar ratio, was air-dried for two days (106 mg, yield: 38%).

*2.1.2.4. Separation of the trans- and cis-(Cl, N) isomers of (1S,2R)-(+)-[Pt{(η^5-C_5H_5)Fe[(η^5-C_5H_4)–CH═N–CH(Me)–CH(O)–C_6H_5]}Cl(DMSO)] (**4a** and **5a**, respectively).* These isomers were separated by SiO_2 column (20 mm × 40 mm) using a CH_2Cl_2:MeOH (100:0.2) mixture as eluent. The wide band released was collected in portions (of ca. 50 mL). The first 700 mL eluted gave, after concentration on a rotary evaporator, complex **5a**; the subsequent fractions eluted contained a nearly 1:1 mixture of both compounds; while the last ones (~400 mL) produced after work-up **4a** (yields: 58 mg, 54% for **4a** and 43 mg, 40% for **5a**).

2.1.2.4.1. Characterization data for **4a**. Elemental analyses: calc. for $C_{22}H_{26}ClFeNO_2PtS$ (FW = 654.9 g/mol): C, 40.35; H, 4.00; N, 2.14 and S, 4.90 %; found C, 40.2; H, 4.0; N, 2.0 and S, 4.1 %. EM (ESI^+): m/z = 656.0 $\{[M]+H\}^+$. IR (in cm^{-1}): IR (in cm^{-1}): 3008, 2955 and 2924 [s, ν(C–H)], 1616 [s, ν(>C═N–)], 1448 (m), 1383(m), 1124(m), 1086 (m), 1043 (s), 1004(m), 730 (m), 701 (m), 507 (m), 499 (m), 444 (m), 348 (br.) and 347 [m, ν(Pt-Cl)]. Solubility (in mg/mL): 35 (in $CDCl_3$); 19 (in DMSO-d_6) and 2 [in a DMSO-d_6:D_2O (1:1) mixture]. $[\alpha]_D$ (CH_2Cl_2 at 293 K, $c = 1.1\times10^{-1}$ g/100 mL) = +252º. UV–vis. data (CH_2Cl_2 at 298 K, $c = 4.3\times10^{-5}$ M): λ_{max} in nm (ε, in M^{-1} cm^{-1}): 469 (1171), 296 (14075) and 228 (25082). R_f [in CH_2Cl_2:MeOH (100:0.1) = 0.06]. H NMR data: δ = 1.21 (d, 3 H, ^{3}J = 6.4, Me); 3.52 [s, 6 H, $^3J_{Pt,H}$ = 26.4, Me(DMSO)]; 4.16 [m, 1 H, –CH(Me)–]; 4.32 (s, 5 H, Cp); 4.54 (s, 1 H, H^5); 4.65 (s, 1 H, H^3); 4.66 (s, 1 H, H^4); 4.69 (s, 1 H, H^2); 5,14 [d, 1 H, ^{3}J = 4,0, –CH(O)–]; 7.19 (t, 1 H, ^{3}J = 7.5, H$^{4'}$); 7.27 (this signal is partially overlapped with that due to the residual solvent, t, 2 H, ^{3}J = 7.0, H$^{3'}$ and H$^{5'}$); 7.42 (d, 2 H, ^{3}J = 7.5, H$^{2'}$ and H$^{6'}$) and 8.88 (s, 1 H, $^3J_{Pt,H}$ = 60.0, –CH═N–). $^{13}C\{^1H\}$ NMR data: δ = 13.7 (Me); 45.5 [Me(DMSO)]; 68.9 (C^5); 70.3 (Cp); 72.7 [–CH(Me)–]; 72.8 (C^1); 73.6 (C^3); 73.6 (C^4); 74.9 (C^2); 84.9 [–CH(O)–]; 126.7 (C$^{4'}$); 127.0 (C$^{2'}$ and C$^{6'}$); 127.6 (C$^{3'}$ and C$^{5'}$); 140.1 (C$^{1'}$) and 166.7 (–CH═N–). $^{195}Pt\{^1H\}$ NMR data: δ = −2911.

2.1.2.4.2. Characterization data for **5a**. Elemental analyses: calc. for $C_{22}H_{26}ClFeNO_2PtS$ (FW = 654.9 g/mol): C, 40.35; H, 4.00; N, 2.14 and S, 4.90 %; found C, 40.2; H, 4.1; N, 2.2 and S, 4.8 %. EM (ESI^+): m/z = 656.0 $\{[M]+H\}^+$. IR(in cm^{-1}): 2957 and 2924 [s, ν(C–H)], 1618 [s, ν(>C═N–)], 1447 (m), 1380 (m), 1125 (m), 1084 (m), 1025 (m), 1007 (m), 733 (m), 704 (m), 502 (m), 441 (m), 355 (br.) and 342 (m) [ν(Pt–Cl)]. Solubility (in mg/mL): 29 (in $CDCl_3$); 7 (in DMSO-d_6) and ca. 1 [in a DMSO-d_6: D_2O (1:1) mixture]. $[\alpha]_D$ (CH_2Cl_2 at 293 K, $c = 1.1\times10^{-1}$ g/100 mL) = +409°. UV–vis. data (CH_2Cl_2 at 298 K, $c = 3.7\times10^{-5}$ M): λ_{max} in nm (ε, in M^{-1} cm^{-1}): 472 (1311), 293 (16885) and 228 (22432). R_f [in CH_2Cl_2:MeOH (100:0.1) = 0.10]. ^{1}H NMR data: δ = 1.21 (d, 3 H, ^{3}J = 6.0, Me); 3.42 [s, 3 H, $^3J_{Pt-H}$ = 25, Me(DMSO)]; 3.43 [s, 3 H, $^3J_{Pt,H}$ = 27, Me(DMSO)]; 3.97 [m, 1 H, –CH(Me)–]; 4.34 (s, 5 H, Cp); 4.58 (s, 1 H, H^2); 4.67 (s, 1 H, H^3); 4.69 (s, 2 H, H^4, H^5); 5.04 [d, 1 H, ^{3}J = 3.5, –CH(O)–]; 7.22 (tt, 1 H, ^{3}J = 7.0, ^{4}J = 1.2, H$^{4'}$); 7.29 (t, 2 H, ^{3}J = 7.2, H$^{3'}$ and H$^{5'}$); 7.36 (d, 2 H, ^{3}J = 7.2, H$^{2'}$ and H$^{6'}$) and 8.77 (s, 1 H, $^3J_{Pt-H}$ = 45.0, -CH═N-). $^{13}C\{^1H\}$ NMR data: δ = 13.4 (Me); 43.1 and 43.5 [Me(DMSO)]; 69.7 (C^2); 70.6 (Cp); 70.8 [–CH(Me)–]; 71.9 (C^1); 74.1 (C^3); 75.1 (C^4); 86,0 [–CH(O)–]; 126,9 (C$^{2'}$ and C$^{6'}$); 127.0 (C$^{4'}$); 128.1 (C$^{3'}$ and C$^{5'}$); 140.4 (C$^{1'}$) and 167.4 (–CH═N–). $^{195}Pt\{^1H\}$ NMR data: δ = −2978.

*2.1.2.5. Preparation of the diastereomers {(S_p,1S,2R) and (R_p,1S,2R)} of the platinacycle [Pt{[(η^5-C_5H_3)]–CH═N–CH(Me) –CH(OH) –C_6H_5] Fe(η^5-C_5H_5)}Cl(DMSO)] (**6a** and **7a**, respectively).* The two products were isolated as minor components during the synthesis of **4a** and **5a** (Section 2.1.2.3) but the method presented here allows to isolate them in a higher yield.

Ligand **1a** (150 mg, 4.32×10^{-4} mol) and the equimolar amount of *cis*-[$PtCl_2(DMSO)_2$] (182 mg) were treated with 20 mL of toluene. Then a methanol solution (5 mL) of NaOAc (71 mg, 8.64×10^{-4} mol) was added. The resulting reaction mixture was heated under reflux for 190 h and then filtered out. The hot filtrate was concentrated to dryness on a rotary evaporator. The residue obtained afterwards was also passed through a fast and short SiO_2 column chromatography (20 mm × 40 mm) to remove the undesired ferrocenecarboxaldehyde formed as side product. After this stage, a CH_2Cl_2:MeOH (100:0.1) mixture was used as eluant and the purple band was collected in small portions (ca. 50 mL). The first 200 mL released produced, after concentration to dryness, complex **6a** and the subsequent 750 mL collected gave, after identical work-up, compound **7a** (yields: 40 mg, 14% for **6a** and 61 mg , 21% for **7a**)

2.1.2.5.1. Characterization data for **6a**. Elemental analyses: calc. for: $C_{22}H_{26}ClFeNO_2PtS$ (FW = 654.9 g/mol): C, 40.35; H, 4.00; N, 2.14 and S, 4.90 %; found: C, 40.5; H, 3.7; N 2.3 and S 5.2 %. EM (ESI^+): m/z = 619.1 $\{[M]-Cl\}^+$. IR (in cm^{-1}): 3448 [br., vs, ν(O–H)], 3022 and 2995 [s, ν(C–H)], 1634 [s, ν(>C═N–)], 1450 (m), 1384 (m), 1244 (m), 1127(w), 1020 (br. m), 818 (m), 747 (m), 703 (m), 509 (w), 465 (br. m) and 332 (m) [ν(Pt–Cl)]. Solubility (in mg/mL): 66 (in $CDCl_3$); 29 (in DMSO-d_6) and 12 [in a DMSO-d_6: D_2O (1:1) mixture]. $[\alpha]_D$ (CH_2Cl_2 at 293 K, $c = 1.1\times10^{-1}$ g/100 mL) = −3136. UV–vis. data (CH_2Cl_2 at 298 K, $c = 5.8\times10^{-5}$ M): λ_{max} in nm (ε, in M^{-1} cm^{-1}): 518 (1190), 368 (1190), 262 (13,845) and 228 (17,724). R_f [in CH_2Cl_2:MeOH (100:0.1) = 0.20]. ^{1}H NMR data: δ = 1.07 (d, 3 H, ^{3}J = 6.0, Me); 1.81 (s.a., 1 H, –OH); 3.52 [s, 3 H, $^3J_{Pt-H}$ = 20.8, Me(DMSO)]; 3.54 [s, 3 H, $^3J_{Pt,H}$ = 17.6, Me(DMSO)]; 4.48 (s, 5 H, Cp); 4.77 (s, 1 H, H^4); 4.78 (s, 1 H, H^3); 4.87 [m, 1 H, –CH(Me)–]; 5.33 (s, 1 H, H^5); 5.42 [s, 1 H, –CH(OH)–]; 7.25 (t, 1 H, ^{3}J = 7.0, H$^{4'}$); 7.34 (t, 2 H, ^{3}J = 7,5, H$^{3'}$ and H$^{5'}$); 7.61 (d, 2 H, ^{3}J = 7,5, H$^{2'}$ and H$^{6'}$) and 8.17 (s, 1 H, $^3J_{Pt,H}$ = 108.0, –CH═N–). $^{13}C\{^1H\}$ NMR data: δ = 12.5 (Me); 47.6 [Me(DMSO)]; 64.0 [–CH(Me) –]; 69.0 (C^4); 71.2 (Cp); 72.4 (C^3); 73.1 [–CH(OH) –]; 77.4 (C^5); 87.3 (C^1); 126.7 (C$^{2'}$ and C$^{6'}$); 128.2 (C$^{4'}$); 129.1 (C$^{3'}$ and C$^{5'}$); 142.6 (C$^{1'}$) and 177.0 (–CH═N–). $^{195}Pt\{^1H\}$ NMR data: δ = −3846.

2.1.2.5.2. Characterization data for **7a**. Elemental analyses: calc. for: $C_{22}H_{26}ClFeNO_2PtS$ (FW = 654.9 g/mol): C, 40.35; H, 4.00; N, 2.14 and S, 4.90 %; found: C, 40.5; H, 3.7; N, 2.3 and S, 5.2%. EM (ESI^+): m/z = 619.1 $\{[M]-Cl\}^+$. IR (in cm^{-1}): 3449 [br., vs, ν(O–H)], 3022 and 2995 [s, ν(C–H)], 1633 [s, ν(>C═N–)], 1466 (m), 1383 (m), 1244 (m), 1130 (w), 1020 (br. m), 817 (m), 745 (m), 703 (m), 506 (w), 461 (br. m), 442 (w) and 330 (m) [ν(Pt–Cl)]. Solubility (in mg/mL): 61 (in $CDCl_3$); 22 (in DMSO-d_6) and 9 [in a DMSO-d_6: D_2O (1:1) mixture]. $[\alpha]_D$ (CH_2Cl_2 at 293 K, $c = 1.1\times10^{-1}$ g/100 mL) = +2514. UV–vis. data (CH_2Cl_2 at 298 K, $c = 2.4\times10^{-5}$ M): λ_{max} in nm (ε, in M^{-1} cm^{-1}): 516 (1598), 257 (80,615) and 229 (72,541). R_f [in CH_2Cl_2:MeOH (100:0.1) = 0.24]. ^{1}H NMR data: δ = 1.16 (d, 3 H, ^{3}J = 7.0, Me); 2.25 (s.a., 1 H, –OH); 3.57 [s, 3 H, $^3J_{Pt,H}$ = 23.2, Me(DMSO)]; 3.60 [s, 3 H, $^3J_{Pt,H}$ = 20.8 Me(DMSO)]; 4.25 (s, 5 H, Cp); 4.53 (s, 1 H, H^4); 4.60 (s, 1 H, H^3); 4.96 [m, 1 H, –CH(Me)–]; 5.23 [br.s, 2 H, H^2 and –CH(OH)–]; 7.25 (t, 1 H, ^{3}J = 7,0, H$^{4'}$); 7.33 (t, 2 H, ^{3}J = 7.5, H$^{3'}$ and H$^{5'}$); 7.55 (d, 2 H, ^{3}J = 7.5, H$^{2'}$ and H$^{6'}$) and 8.09 (s, 1 H, $^3J_{Pt,H}$ = 110.0, –CH═N–). $^{13}C\{^1H\}$ NMR data: δ = 12.9 (Me); 47.0 [Me(DMSO)], 47.1 [Me(DMSO)]; 63.5 [–CH(Me) –]; 68.5 (C^4); 70.5 (Cp); 71.8 (C^3); 72.7 [–CH(OH)–]; 76.4 (C^5); 86.7 (C^1); 110.0 (C^2); 126.5 (C$^{2'}$ and C$^{6'}$); 127.5 (C$^{4'}$); 128.3 (C$^{3'}$ and C$^{5'}$); 141.2 (C$^{1'}$) and 176.1 (–CH═N–). $^{195}Pt\{^1H\}$ NMR data: δ = −3827.

2.2. Study of the stability of the platinum(II) complexes (**2a–7a**) in solution

In order to compare the solution behaviour of the new complexes **2a–7a**, the following methodology was used: the test compound was introduced in an NMR tube then 0.7 mL of DMSO-d_6 [or of a DMSO-d_6:D_2O (1:1) mixture] was added. The amount of **2a–7a** used was 5 mg. Due to the low solubility of **4a** and **5a** in the DMSO-d_6:D_2O mixture, in these cases the studies were carried out using only 1 mg (of **4a**) and 0.5 mg (of **5a**). In all cases, the mixtures were shaken at 298 K to complete dissolution of the complexes and afterwards the tubes were sealed and ^{1}H NMR spectra of these freshly prepared solutions were registered. Later on these solutions were kept at 298 K and they were studied by ^{1}H-NMR spectra after different periods of storage.

2.3. Crystallography

A prismatic crystal of **2a**, **3a**, **5a** or **6a** (sizes in Table 1) was selected and mounted on a MAR345 diffractometer with a image plate detector. Unit-cell parameters were determined from 3465 (for **2a**), 6011 (for **3a**), 561 (for **5a**) or 593 (for **6a**) reflections in the range $3°<\theta<31°$ and refined by least-squares method: intensities were collected with a graphite monochromatized Mo-Kα radiation. The number of reflections collected was 16182 (in the range $2.74°<\theta<25.61°$ for **2a**), 22592 (in the range $2.62°\leq\theta\leq32.61°$ for **3a**), 16145 ($2.68°\leq\theta\leq32.13°$ for **5a**) and 13284 ($1.53°\leq\theta\leq32.43°$ for **5a**); of which 4464, 6912, 5465 and 8048 reflections for **2a**, **3a**, **5a** and **6a**, respectively were not equivalent by symmetry {R(int on I) = 0.030 (for **2a**), 0.051 (for **3a**), 0.033 (for **5a**) and 0.055 (for **6a**)}. The number of reflections assumed as observed {applying the condition $I>2\sigma(I)$} was 4392, 6425, 5238 and 5231(for **2a**, **3a**, **5a** and **6a**). In all cases Lorentz-polarization corrections were made and for **2a**, **5a** and **6a** absorption corrections were also carried out.

The structures were solved by Patterson (for **2a**) or Direct methods (for **3a**, **5a** and **6a**) using SHELXS program [47] and refined by full-matrix least-squares method with SHELX97 computer program [48], using 16182 (for **2a**), 22592 (for **3a**), 14651 (for **5a**) and 13284 (for **6a**) reflections (very negative intensities were not assumed) The function minimized was $\Sigma w \mid |F_o|^2-|F_c|^2 \mid^2$, where $w=[\sigma^2(I)+(0.0203P)^2+0.6226P]^{-1}$ (for **2a**), $w=[\sigma^2(I)+(0.0608P)^2+9.6365\ P]^{-1}$(for **3a**), $w=[\sigma^2(I)+(0.0653P)^2+1.7198\ P]^{-1}$ (for **5a**) and $w=[\sigma^2(I)+(0.0799P)^2+1.7518P]^{-1}$ (for **6a**), with $P=(|F_o|^2\ 2\ |F_c|^2)/3$. f, f' and f'' were taken from the bibliography [49]. Hydrogen atoms were computed and refined using a riding model with an isotropic temperature factor equal to 1.2 times the equivalent temperature factor of the atom to which they are attached. The final R (on F) factors were 0.025 (for **2a**), 0.047 (for **3a**), 0.040 (for **5a**) and 0.075 (for **6a**) wR(on F^2) = 0.0721 (for **2a**), 0.122 (for **3a**), 0.114 (for **5a**) and 0.179 (for **6a**) The goodness of fit was 1.150 (for **2a**), 1.148 (for **3a**), 1.036 (for **5a**) and 1.061 (for **6a**) for all the observed reflections. The quality of the crystal of **6a** was poor, but all the attempts to grow better ones using different strategies failed and in this case, the displacement parameters of some bond lengths in the direction of the bond are restrained to be equal within an effective standard deviation (DELU sentences), 11 atoms closer are restrained to have the same U_{ij} components (SIMU sentences) and the bond distances of the solvation CH_2Cl_2 were also restrained (DIFX sentences). Further details concerning the resolution and refinement of the crystal structures of **2a**, **3a**, **5a** and **6a** are given in Table 1.

2.4. Biological studies

2.4.1. Cell culture

Human lung carcinoma A549 and colon adenocarcinoma HCT116 cells (from the *American Type Culture Collection*), and MBA-MD-231 breast cancer cells (from the *European Collection of Cell Cultures – ECACC*) were used in all the experiments. Cells were grown as a monolayer culture in Dulbecco's minimum essential medium (DMEM) with L-glutamine, without glucose and without sodium pyruvate in the presence of 10 % heat-inactivated fetal calf serum, 10 mM of D-glucose and 0.1% streptomycin/penicillin in standard culture conditions.

2.4.2. A549 cell viability assay

The compounds were disolved in DMSO at 20 mM as stock solution. To obtain final assay concentratios, they were diluted in DMEM (final concentration of DMSO was always lower than 1%). The assay was performed by a variation of the method described by Mosmann et al. [50] as specified by Matito and coworkers [51]. In brief, 3×10^3 A549 cells/well were cultured in 96 well plates. Concentrations that inhibited cell growth by 50 % (IC_{50}) after 72 h of treatment were

Table 1
Crystal data and details of the refinement of the crystal structures of **2a**, **3a**, **5a** and **6a**·$2CH_2Cl_2$.

	2a	**3a**	**5a**	**6a**·$2CH_2Cl_2$
Empirical formula	$C_{22}H_{27}Cl_2FeNO_2PtS$	$C_{22}H_{27}Cl_2FeNO_2PtS$	$C_{22}H_{26}ClFeNO_2PtS$	$C_{22}H_{26}Cl_5FeNO_2PtS$
Formula weight	691.35	691.35	654.89	824.74
Temperature (K)	293(2)	293(2)	293(2)	105(2)
λ(Å)	0.71073	0.71073	0.71069	0.71073
Crystal size (mm×mm×mm)	0.2×0.1×0.1	0.15×0.15×0.13	0.2×0.1×0.1	0.2×0.08×0.08
Crystal system	Orthorhombic	Orthorhombic	Orthorhombic	Monoclinic
Space group	$P2_12_12_1$	$P2_12_12_1$	$P2_12_12_1$	$P2_1$
a (Å)	10.544(7)	9.780(4)	9.810(4)	12.360(7)
b (Å)	13.091(6)	12.869(4)	10.439(3)	8.727(4)
c (Å)	17.469(8)	19.920(5)	22.217(6)	14.292(4)
$\alpha=\gamma$ (°)	90.0	90.0	90.0	90.0
β (°)	90.0	90.0	90.0	111.41(2)
Volume (Å^3)	2411(2)	2427.8(14)	2275.2(13)	1435.2(11)
Z	4	4	4	2
D_{calc} (mg×m^{-3})	1.904	1.891	1.912	1.908
μ (mm^{-1})	6.724	6.679	7.007	5.935
F(000)	1344	1344	1272	804
Θ range for data collection (°)	from 2.74 to 25.61	from 2.62 to 32.41	from 2.68 to 32.13	from 1.53 to 32.43
N. of reflections collected	16,182	22,592	16,451	13,284
N. of unique reflections, {R(int)}	4446 {0.0301}	6912{0.519}	5465 {0.0335}	8048 {0.0548}
N. of parameters	271	272	263	316
Goodness of fit on F^2	1.150	1.148	1.036	1.061
Absolute structure parameter	−0.002(7)	−0.042(11)	−0.023(5)	−0.017(14)
Final R indices $I>2\sigma(I)$	$R_1=0.0252$, $wR_2=0.0721$	$R_1=0.0472$, $wR_2=0.1216$	$R_1=0.0399$, $wR_2=0.1139$	$R_1=0.0746$, $wR_2=0.1794$
R indices (all data)	$R_1=0.0255$, $wR_2=0.0723$	$R_1=0.0542$, $wR_2=0.1378$	$R_1=0.0412$, $wR_2=0.1149$	$R_1=0.1079$, $wR_2=0.1950$

calculated based on the survival rate compared with untreated cells. Relative cell viability was measured by the absorbance on an ELISA (enzyme-linked immunosorbent assay) plate reader (Tecan Sunrise MR20-301, TECAN, Salzburg, Austria) at 550 nm.

2.4.3. MDA-MB-231 and HCT116 cell viability assay

The compounds were dissolved in 100% DMSO at 50 mM as stock solution; then, serial dilutions have been done in DMSO (1:1) (in this way dmso concentration in cell media was always the same); finally, 1:500 dilutions of the serial dilutions of compounds on cell media were done. The assay was performed as described by Givens et al. [52]. In brief, HCT116 and MDA-MB-231 cells were plated at 5000 cells/well, respectively, in 100 μL media in tissue culture 96 well plates (Cultek). After 24 h, media was replaced by 100 μL/well of serial dilution of drugs. Control wells did not contain compounds. Each point concentration was run in triplicate. Reagent blanks, containing media plus colorimetric reagent without cells were run on each plate. Blank values were subtracted from test values and were routinely 5–10% of uninhibited control values. Plates were incubated 72 h. Hexosaminidase activity was measured according to the following protocol: the media containing was removed and cells were washed once with PBS 60 μL of substrate solution (*p*-nitrophenol-*N*-acetyl-β-*D*-glucosamide 7.5 mM [Sigma N-9376], sodium citrate 0.1 M, pH = 5.0, 0.25 % Triton X-100) was added to each well and incubated at 37 °C for 1–2 h; after this incubation time, a bright yellow appears; then, plates could be developed by adding 90 μL of developer solution (glycine 50 mM, pH 10.4; EDTA 5 mM), and absorbance was recorded at 410 nm.

2.4.4. DNA migration studies

Plasmid pBluescript SK^+ was obtained using QIAGEN plasmid midikit as described by the manufacturer. Interaction of drugs with pBluescript SK^+ plasmid DNA (Stargene) was analyzed by agarose gel electrophoresis following a modification of the method described by Abdullah et al. [53]. In brief plasmid DNA aliquots (40 μg/mL) were incubated with different concentrations of the compounds (from 5 μM to 100 μM) at 37 °C for 24 h. For comparison, cisplatin was used as positive control. Aliquots of 20 μL of compounds:DNA complexes containing 0.8 μg of DNA were subject to 1% agarose gel lectrophoresis in TAE buffer (40 mM tris-acetate, 2 mM EDTA, pH = 8.0). The gel was stained in the same buffer containing ethidiumbromide (0.5 mg /mL) and visualized and photographed under UV light.

3. Results and discussion

3.1. Synthesis and characterization of the complexes

Treatment of **1a** with the equimolar amount of *cis*-$[PtCl_2(DMSO)_2]$ [45] in refluxing methanol for 45 min, gave after work up, traces of ferrocenecarbaldehyde and the *trans*- and *cis*-isomers of (*1S,2R*)-[Pt{(η^5-C_5H_5)Fe[(η^5-C_5H_4)–CH═N-CH(Me)–CH(OH)–C_6H_5]}Cl_2(DMSO)] (**2a** and **3a**, respectively) (Scheme 1, step **B**). Longer reaction periods (*t*)

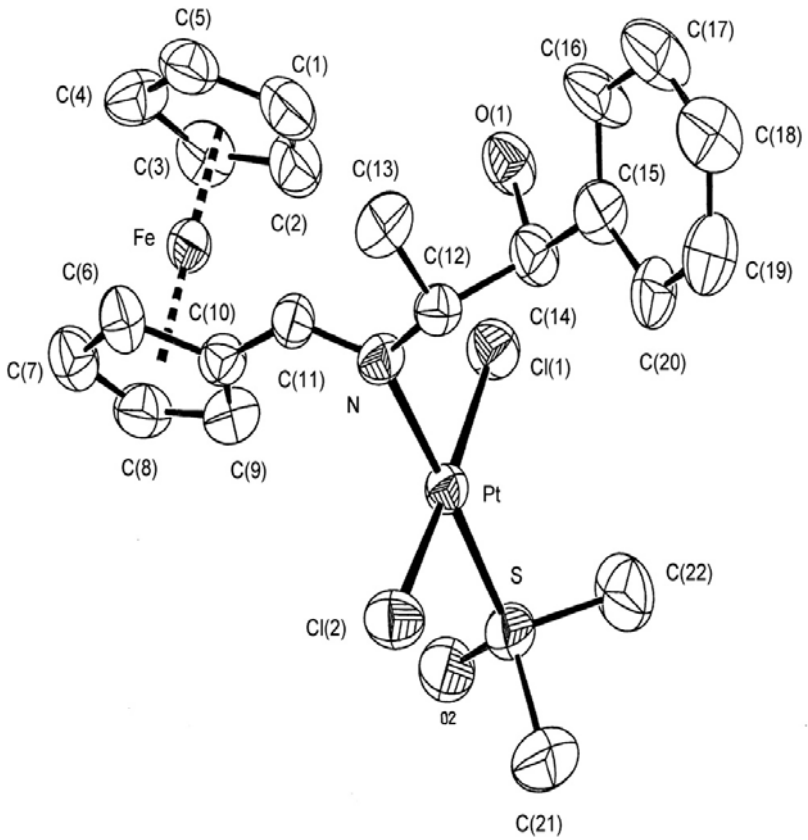

Fig. 2. ORTEP plot of **2a**. Hydrogen atoms have been omitted for clarity. Selected bond lengths (in Å) and angles (in deg.) for **2a:** Pt–N, 2.068(4); Pt–S, 2.395(16); Pt–Cl(1), 2.3244(16); Pt–Cl(2), 2.2969(17); C(10)–C(11), 1.427(8); C(11)–N, 1.296(7); C(12)–N, 1.480(7); Cl(1)–Pt–Cl(2), 176.63(4); S–Pt–Cl(2), 93.06(7); Cl(1)–Pt–S, 90.05(6); N–Pt–Cl(1), 90.19(13) and N–Pt–Cl(2), 86.63(14).

produced the same products but the molar ratio **2a**:**3a**, decreased substantially {from 9.1 (t = 45 min) to 1.6 (t = 3 h)}. Characterization data of **2a** and **3a** agreed with the proposed formulae and their absolute configuration was established unambiguously by X-ray diffraction. The crystal structures of **2a** and **3a** (Figs. 2 and 3, respectively) revealed that: a) **1a** adopted the *anti*-(*E*) form [torsion angle C(10)-C(11)-N-C(12) = 178.10° (in **2a**) and 178.56° (in **3a**)] and acted as a neutral N-donor ligand, b) the "$PtCl_2S_{(DMSO)}$" moiety was nearly orthogonal to the imine group, c) the values of the bond angles angles Cl(1)-Pt-Cl(2) {176.63(4)° (in **2a**) and 91.62(10)° (in **3a**)} confirmed the *trans*- (in **2a**) and *cis*- (in **3a**) arrangement of the two Cl^- ligands and d) bond lengths and angles around the platinum(II) were similar to those reported for related *trans*- and *cis*-isomers of [Pt(N-donor ligand)Cl_2(DMSO)] complexes [54].

When the reaction was performed in the presence of a two-fold excess of NaOAc and using a toluene:methanol (4 :1) mixture as solvent, four different platinum(II) complexes (hereinafter referred to as **4a**-**7a**) were isolated (Scheme 1, step **C**). The molar ratios **4a**:**5a**:**6a**:**7a** were time (t) dependent and varied from 0.96:1.00:0.66:0.70 (for t = 24 h) to 0.80:0.82:1.00:0.95 (for t = 190 h).

Two of these products were identified as the *trans*- (**4a**) or *cis*- (**5a**) (*Cl, N*) isomers of [Pt{(κ^2-*N,O*)(η^5-C_5H_5)Fe[(η^5-C_5H_4) – CH═N – CH(Me) – CH(O) – C_6H_5]}Cl(DMSO)]. Mono and two-dimensional NMR studies of **4a** and **5a** suggested a *syn*- (Z) form of the imine ligand and the existence of a five-membered chelate formed by the coordination of the nitrogen atom and the deprotonated oxygen of the –OH moiety of the imine **1a**. The X-ray crystal structure of **5a** (Fig. 4), confirmed these results and a *cis*- arrangement between the Cl^- and the nitrogen [bond angle Cl(1) – Pt – N(1) = 92.26(17)°], thus indicating that **5a** was the *cis*- (*Cl,N*) isomer of [Pt{(κ^2-*N,O*)(η^5-C_5H_5)Fe[(η^5-C_5H_4) – CH═N – CH(Me) – CH(O) – C_6H_5]}Cl(DMSO)]. In view of this, we assumed that **4a** was the *trans*- *(Cl,N)* isomer. The existence of a NOE peak between the imine proton and those of the DMSO ligand in the {^{1}H–^{1}H}-NOESY spectrum of **4a** supported this hypothesis.

Characterization data of the remaining two products (**6a** and **7a**) agreed with those expected for the cyclometallated complex [Pt{(κ^2-*C,N*[(η^5-C_5H_3)] – CH═N – CH(Me) – CH(OH) – C_6H_5]Fe(η^5-C_5H_5)}Cl(DMSO)] that arise from the coordination of the imine nitrogen and the activation of the σ(C – H) bonds in the ortho sites of the C_5H_4 ring. NMR studies indicated that in both cases the imine ligand adopted the *anti-(E)* form, a *cis*- disposition between the sulphur atom of the DMSO ligand and the metallated carbon and the existence of a σ[Pt-Csp^2(ferrocene)] bond. Due to the symmetry of the ferrocenyl unit the formation of this bond induces planar chirality [31,33]. Therefore, compounds **6a** and **7a** should differ in the planar chirality of ferrocenyl unit.

Several techniques were used to obtain monocrystals of **6a** or **7a** suitable for X-ray analyses. Unfortunately most of the attempts failed and only small and poor quality crystals of **6a** could be isolated. Despite of this, the X-ray analyses confirmed the nature and mode of binding of the ligands attached to the platinum(II) atom (Fig. 5) and a *cis*-disposition between the metallated carbon and the DMSO ligand, in good agreement with the results obtained from NMR studies and the *transphobia effect* [55]. These studies also showed that the

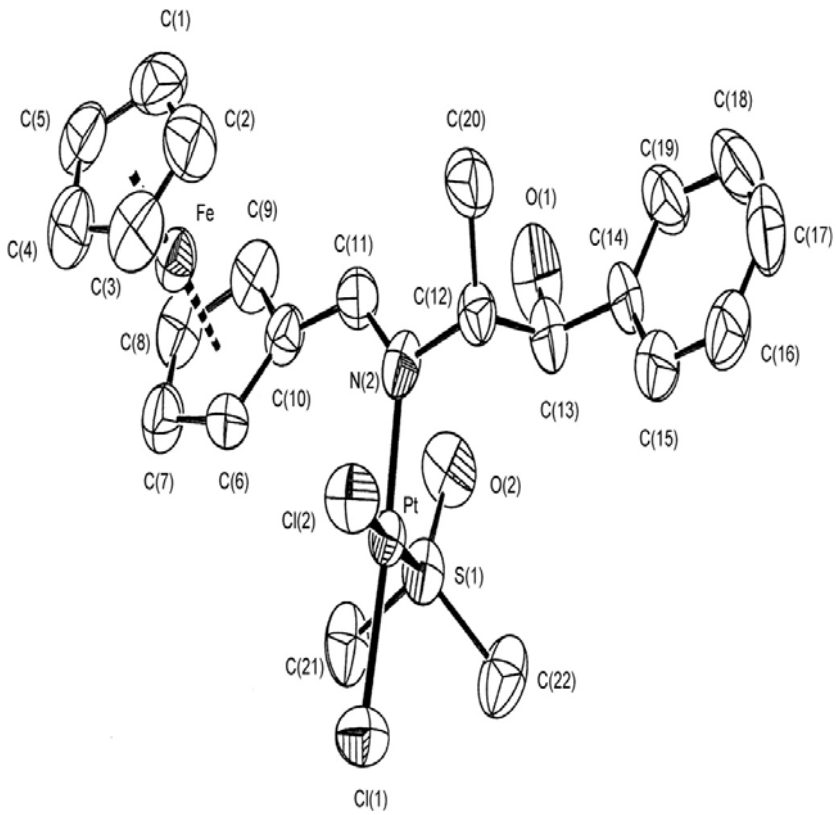

Fig. 3. ORTEP plot of **3a**. Hydrogen atoms have been omitted for clarity. Selected bond lengths (in Å) and angles (in deg.) for **3a**: Pt – Cl(1), 2.314(3); Pt – Cl(2), 2.319(2); Pt – S(1), 2.206(2); Pt – N, 1.997(9); C(10) – C(11), 1.447(13); N(2) – C(11), 1.274(11); N(2) – C(12), 1.513(11); Cl(1) – Pt – Cl(2), 91.62(10); N(2) – Pt – Cl(2), 86.7(2); S(1) – Pt – Cl(1), 89.75(10); N(2) – Pt – S(1), 92.0(2); C(10) – C(11) – N(2), 124.6(9); C(11) – N(2) – C(12), 118.4(8) and N – C(12) – C(13), 109.6.

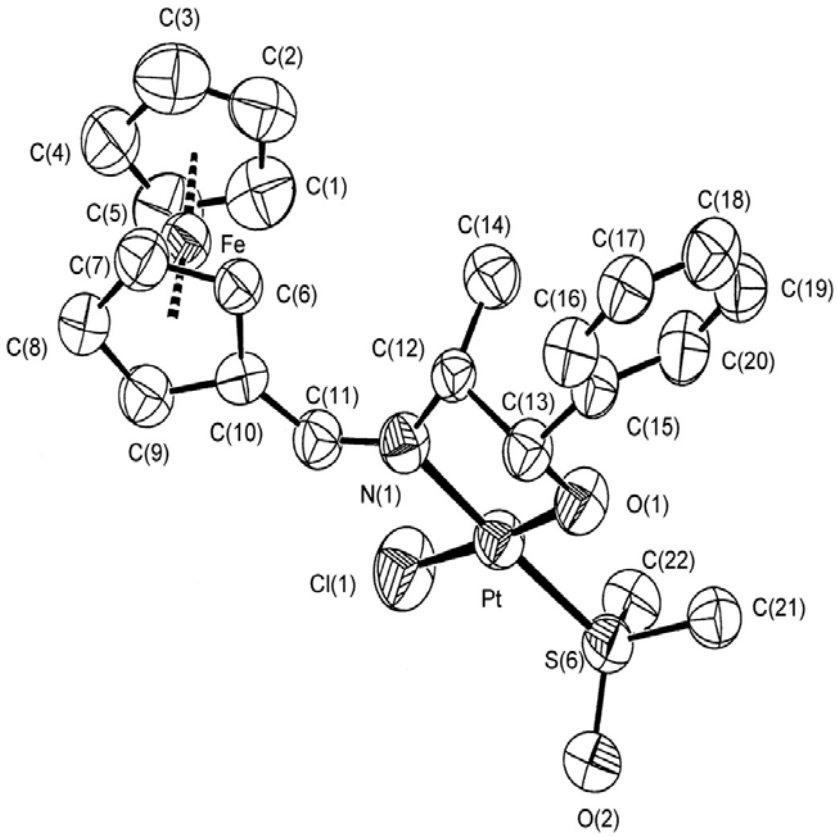

Fig. 4. ORTEP plot of **5a**. Hydrogen atoms have been omitted for clarity. Selected bond lengths (in Å) and angles (in deg.): Pt–Cl(1), 2.322(2); Pt–S(6), 2.2023(19); Pt–O(1), 2.005(5); Pt–N(1), 2.057(6); C(10)–C(11), 1.454(10); C(11)–N(1), 1.256(9), N(1)–C(12), 1.48(8); S(6)–Pt–Cl(1), 90.06(8); Cl(1)–Pt–N(1), 92.26(17), O(1)–Pt–S(6), 91.49(16) and N(1)–Pt–O(1), 83.7(2).

atoms involved in the bicyclic [5.5] system formed by the five-membered platinacycle and the metallated C_5H_3 ring were practically coplanar. Besides that, the relative arrangement of the "Fe(η^5-C_5H_5)" moiety with regard to the substituents of the C_5H_3 unit indicated that in **6a** the planar chirality of the ferrocenyl unit is S_p and consequently, in **7a** it should be R_p.

Finally, it should be noted that no evidences of the formation of platinum(II) complexes containing the oxazolidines (**1b**) as ligands were detected by ^{1}H NMR studies of the crude of any of the reactions studied. Thus suggesting that the imine form (**1a**) is more prone to bind to the platinum(II) than its tautomeric forms (**1b**).

3.2. Biological studies

Human lung carcinoma, breast and colon cancer cell lines (A549, MDA-MB-231 and HCT-116, respectively) were used to test the cytotoxic activity of the free ligand **1a** and the new platinum(II) complexes **2a–7a** including *cisplatin* as a positive control.

Data presented in Table 2 reveal that the iminoalcohol **1a** exhibits a moderate activity in front of the A549 cell line (IC_{50} = 33.5 μM), and no activity in the other two cell lines. However, the new platinum(II) compounds **2a–7a** are highly cytotoxic, showing most of them IC_{50} values lower than *cisplatin* in the three cellular lines (Fig. 6). In spite of having a considerably potency (IC_{50} value in the range 14 − 21.7 μM), compound **3a**, the *cis*- isomer of (*1S,2R*)-[Pt{(η^5-C_5H_5)Fe[(η^5-C_5H_4)–CH═N–CH(Me)–CH(OH)–C_6H_5]}Cl_2(DMSO)] turned out to be the less potent of the series with cytotoxic effectiveness, smaller than that of its *trans*- configured isomer **2a**. In the three cellular lines, **2a** (*trans*-) is approximately four times more potent than **3a** (*cis*-). *Trans*-isomers of several platinum(II) complexes [9,13,15,16] with greater activity than their corresponding *cis*- isomers and *cisplatin* have been reported and some of them also exhibit strong cytotoxic activity against *cisplatin* resistant tumour cells [13].

Compounds **4a–7a** can be envisaged as conformationally restricted analogues of **2a** and **3a**, in which the ferrocenyliminoalcohol **1a** behaves as an N-donor ligand with an open-like structure. In the pair **4a**, **5a**, the ligand acts as a bidentate $(N,O)^-$ group forming a five-membered chelate ring and in the couple **6a**, **7a**, the formation of the σ(Pt-C) bond generates a [5.5] bicyclic system.

The two isomers of [Pt{(κ^2-*N,O*)(η^5-C_5H_5)Fe[(η^5-C_5H_4)–CH═N–CH(Me)–CH(O)–C_6H_5]}Cl(DMSO)] {*cis*- and *trans*-(Cl, N), **4a** and **5a**, respectively}, are more potent [IC_{50} values in the range (1.3 μM–4.2 μM)] than the open forms **2a** and **3a**, thus indicating that the variation of the mode of binding of ligand **1a** from N-donor (in **2a** and **3a**) to $(N,O)^-$ (in **4a** and **5a**) produces a significant improvement on the cytotoxic activity of these two pairs of complexes. However, compounds **4a** and **5a** [that differ exclusively in the relative arrangement of the Cl^- ligand and the imine nitrogen {*trans*- (in **4a**) or *cis*- (in **5a**)] show a similar and remarkable activity against the three cellular lines assayed. This finding suggests that the interchange of the monodentate Cl^- and DMSO ligands does not discriminate in their biological activity. Another interesting feature of **4a** and **5a** arises from

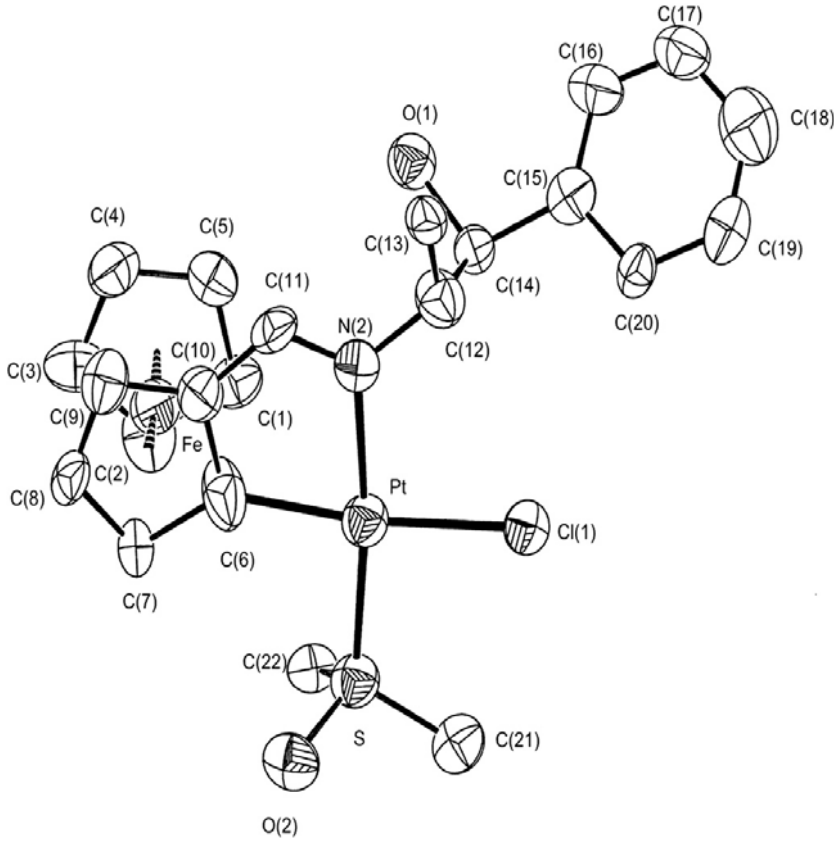

Fig. 5. ORTEP plot of **6a**. Hydrogen atoms have been omitted for clarity. Selected bond lengths (in Å) and angles (in deg.): Pt–C(6), 2.083(14); Pt–N(2), 2.088(11); Pt–Cl(1), 2.402(4); Pt–S, 2.199(4); C(10)–C(11), 1.412(19); C(11)–N(2), 1.304(18); N(2)–C(12), 1.538(17); C(6)–Pt–N(2), 79.1(6); N(2)–Pt–Cl(1), 94.0(3); Cl(1)–Pt–S, 93.40(10); S–Pt–C(6), 93.4(5); Pt–C(6)–C(10), 111.5(106); C(6)–C(10)–C(11), 115.7(12) and C(11)–N(2)–Pt, 114.9(8).

the existence of the Pt–O(alcoxo) bond. It is well-known that hypoxia and acidity of tumours have important consequences for antitumor therapy [55–57]. The potential proclivity of **4a** and **5a** to react in moderate acidic media by protonation of this bond may also favour the selectivity of this complex for tumor cells in front of healthy ones.

Platinacycles **6a** and **7a**, are also conformationally rigid, but rotation around the single bonds of the "=N–CH(Me)–CH–O–" moiety is free as happens for **2a** and **3a**. Compounds **6a** and **7a** show also a great cytoxicity ($IC_{50} \leq 10$ μM), but their potency are smaller than those of **4a** and **5a**. In particular, complex **7a** is approximately four, five and six times less potent than **5a** in front of the A549, MDA-MB-231 and the HCT 116 cell lines respectively.

For HCT116 and the MDA-MB-231 cell lines, **7a** is four and three times more cytotoxic than **6a**, thus pointing out that the chiral planarity of the ferrocenyl unit in **6a** (S_p) and **7a** (R_p) and the different orientation of the "Fe(η^5-C_5H_5) moiety in relation to the environment of the platinum(II) may have some influence in their cytotoxic activity. Furthermore, since it is well known that the variations detected in the ^{195}Pt NMR spectra of platinum(II) complexes can be taken as a measure of the strength of the interaction between the platinum(II) and the ligands bound to it. The comparison of the ^{195}Pt chemical shifts of these diastereomers [$\delta = -3846$ ppm (for **6a**) and -3827 (for **7a**)], suggests that the electronic environment of the platinum(II) is not identical in both cases, and consequently these small electronic effects may also be important to discriminate the cytotoxic activity of the two diastereomers in front of the HCT116 and the MDA-MB-231 cell lines.

The Pt-Cl(1) bond of **6a** [2.402(4) Å] is clearly longer than any of the two Pt-Cl bonds of **2a** [Pt–Cl(1), 2.3244(10) Å, Pt–Cl(2), 2.2969(17) Å] and **3a** [Pt–Cl(1), 2.314(3)Å] and Pt–Cl(2), 2.319(2) Å], thus suggesting that in **6a** the Pt–Cl(1) bond is more labile and more prone to cleave or hydrolise. That is in concordance with the greater potency of **6a** in front of the open structures **2a** and **3a**. Unfortunately, structural data for **4a** are not available at present and in **5a** the Pt–Cl(1) bond length [2.322 (2)Å] is similar to that of **2a** and consequently the greater potency of **5a** when compared with that of **2a** cannot be ascribed exclusively to the strength of the Pt–Cl bond. Therefore, other factors should be considered in order to understand the cytotoxicity of these complexes and their mechanism of action. For instances, the form adopted by the imine ligand [*anti*-(*E*) (in **2a**-**3a** and **6a**-**7a**) and *syn*-(Z) (in **4a**-**5a**)], the capability to establish hydrogen bonding interaction due to the presence of the –OH group (in **2a**, **3a**, **6a** and **7a**) or its deprotonated form (in **4a** and **5a**), etc.

The IC_{50} values for the three lines increase according to the sequences:

5a ≤ **4a** < **2a** < **6a** ≤ ***cisplatin*** ≤ **7a** < **3a** (for A549 cell line) [I]

5a ~ **4a** < **6a** < ***cisplatin*** < **2a** ≤ **7a** < **3a** (for MDA-MB-231 cell line) [II]

5a ~ **4a** < **6a** < **2a** ≤ **7a** < **3a** < ***cisplatin*** (for HCT116 cell line) [III]

Table 2
Cytotoxic activities on A549 human lung carcinoma, MDA-MB-231 breast and HCT116 colon cancer lines of **1a**, complexes **2a**-**7a** and *cisplatin* under identical experimental conditions.

			IC_{50} (μM) for the cell lines[a]		
Product	Mode of Binding	Isomer	A549	MDA-MB-231	HCT116
1a	–	–	33.5 ± 0.2	>100	>100
2a	N	*trans*-	5.7 ± 0.4	3.9 ± 0.62	4.4 ± 2.8
3a	N	*cis*-	21.7 ± 6.5	14 ± 4.0	14 ± 2.3
4a	$(N,O)^-$	*trans*-[b]	4.1 ± 0.8	1.4 ± 0.05	1.4 ± 2.8
5a	$(N,O)^-$	*cis*-[b]	2.8 ± 0.6	1.4 ± 0.45	1.4 ± 0.20
6a	$(C,N)^-$	S_p	8.8 ± 1.8	2.7 ± 0.21	2.0 ± 0.18
7a	$(C,N)^-$	R_p	10.0 ± 0.7	9.5 ± 0.53	8.1 ± 0.60
Cisplatin	–	–	9.3 ± 3.0	6.5 ± 2.4	40 ± 4.40

[a] Data are shown as mean values obtained of two or more experiments performed in triplicate with the corresponding standard deviation.
[b] This refers to the arrangement of the Cl^- and N atoms.

Comparison of sequences I-III shows that most of the new complexes are more potent than *cisplatin* under identical experimental conditions in breast and lung cancer cell lines, and all of them (**2a–7a**) are more potent than *cisplatin* in colon cancer cell line HCT-116. Furthermore, for the three cell lines compounds **4a** or **5a** with a bidentate $(N,O)^-$ ligand, were the most potent ones; the *cis*- isomer of (*1S,2R*)-[Pt{(η^5-C_5H_5)Fe[(η^5-C_5H_4)–CH═N-CH(Me)–CH(OH)–C_6H_5]}Cl_2(DMSO)] (**3a**) was the less active and the cycloplatinated complexes (**6a** and **7a**) and the *trans*-isomer **2a** fell in between the two ends of the sequences.

We also investigated the ability of compounds **1a–7a** to modify the electrophoretic mobility of supercoiled closed circular (ccc) and open circular (oc) forms of pBluescript plasmid DNA. In this experiment, plasmid DNA was mainly in super coiled form, so it showed only one band in gel. When the test compounds were incubated with plasmid DNA at 37 °C, they could bind to the DNA molecule, As a result, the plasmid DNA coordinated to platinum complexes was cleaved into fragments, and the brightness of band was diminished in gel.

Fig. 7 shows the electrophoretic mobility of native pBluescript DNA incubated with the synthesized compounds (**1a–7a**) at different concentrations, (from 10 μM to 200 μM) and for comparison purposes a parallel study with *cisplatin* was also performed. As expected, *cisplatin* greatly altered the electrophoretic mobility of pBluescript DNA at all concentrations tested. For the free ligand **1a**, no shift in DNA mobility was observed at any concentration tested.

At low concentrations (≤25 μM) none of the assayed compounds produced any significant effect on the electrophoretic mobility of native pBluescript DNA. In spite of their great antiproliferative activity, all the compounds were less efficient than *cisplatin* in removing the supercoils from DNA. These results could be related to the shorter incubation time of the electrophoretic DNA-migration experiment (24 h) when compared with those used for the cell viability assays (72 h), that may not allow hydrolysis of the platinum complex.

Compounds **3a** and **4a** alter the electrophoretic mobility of plasmid DNA at concentration up to 50 μM. Complexes **2a**, **6a** and **7a** at concentration up to 100 μM. For all these compounds the rate of migration of supercoiled band (ccc) decreased and tend to approach to that of the nicked relaxed band (oc) at 200 μM.

Considering the five membered chelates (**4a** and **5a**), compound **4a** exhibited a great effect on plasmid DNA mobility, while compound **5a** had no significant effect on that, although the two compounds showed similar and the smallest IC_{50} values in the three cancer cell lines (A549, MDA-MB-231 and HTC116) studied. Hence, the DNA cleavage ability of complexes suggests that different cytotoxicities of complexes might be due not only to cleavage ability but also to diversity of DNA affinity or

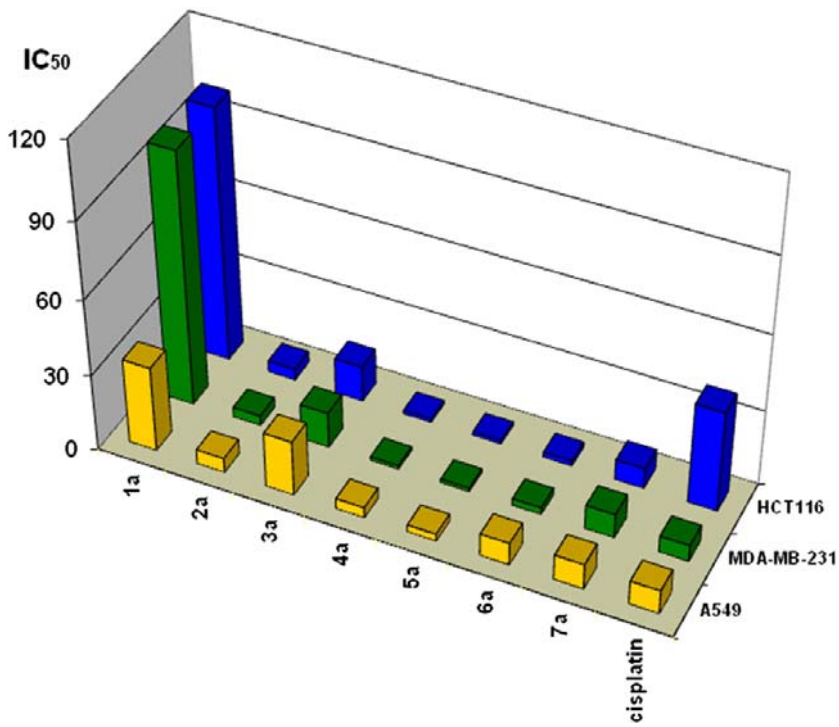

Fig. 6. IC_{50} (μM) values for ligand **1a,** the new platinum(II) complexes (**2a–7a**) and *cisplatin* for A549 (in yellow), MDA-MB-213(in green) and HCT116 (in blue) cell lines.

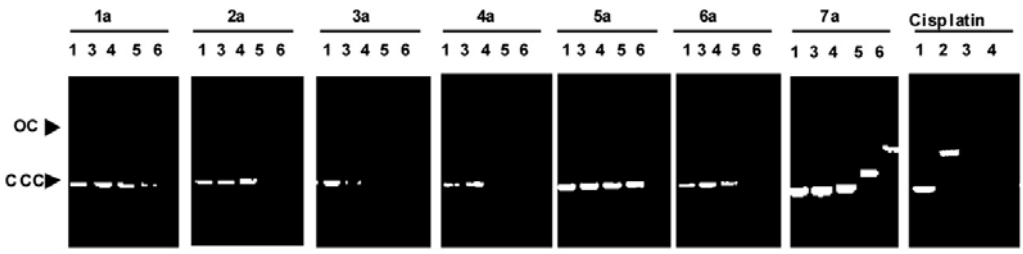

Fig. 7. DNA unwinding assay of supercoiled pBluescript SK$^+$ (40 μg/mL) by the free ligand (**1a**) and the platinum(II) complexes (**2a–7a**) at different concentration Lanes 1, DNA only; lanes 2, 10 μM; lanes 3, 25 μM, lanes 4, 50 μM; lanes 5, 100 μM; and lane 6, 200 μM. Unwinding assay with cisplatin was performed for comparison. ccc, supercoiled closed circular DNA form; oc, open circular DNA form.

other important factors in predicting anticancer activity. In complexes **4a** and **5a** the presence of two different atoms [N_{imine} (in **4a**) or O_{alcoxo} (in **5a**)] in a *trans*- arrangement to the Cl^- ligand could modify the proclivity of the Pt-Cl bond to hydrolise.

As mentioned above, all the new products (**2a–7a**), showed high stability in $CDCl_3$ at 298 K. However, for the biological assays, the complexes were dissolved in DMSO and subject to dilutions with water. Dimethylsulfoxide and water are more polar solvents with greater coordination abilities than the $CDCl_3$, and they could be involved or promote specific chemical processes, such as formation of solvato-complexes, hydrolises of the Pt-Cl bond, changes in the form adopted by the ligand [*anti*-(E) or *syn*-(Z)] in the complexes, *cis*- / *trans*- isomerizations of the complexes, etc.

In view of this, and in order to get further information about the stability of the complexes **2a–7a** in solution, we compared the ^{1}H NMR spectra of freshly prepared solutions with those obtained after different periods of storage (t) at 298 K. In a first stage, these studies were carried out in DMSO-d_6 (see Supporting information, Figs. S1–S6) to find out if the complexes remained unchanged at least during the time needed to do the dilutions required for the biological assays. In a second step, a parallel study using a DMSO-d_6: D_2O (1:1) mixture as solvent (see Supporting information, Figs. S6–S12) was also performed.

The study of the solution behavior of **1a** in DMSO-d_6, under identical experimental conditions, has been reported [31] and revealed that the tautomeric equilibrium between **1a** and the closed forms (**1b**) is strongly displaced to the imine form (no evidences of the presence of **1b** were detected by NMR). In order to ease the understanding of the solution behavior of the Pt(II) complexes, it should be noted that one of the most relevant features of the ^{1}H NMR of the freshly prepared solutions is the presence of a singlet {in the range 7.8 ppm$<\delta<$9.0 ppm}, due to the imine proton. It is well-known that the position of this signal is indicative of the *anti*-(*E*) or *syn*-(*Z*) form adopted by the ligand in the complexes and it is sensitive to the nature and arrangement of the remaining ligands bound to the Pt(II) centre. [31] This is why it is commonly used to monitor the solution behavior of Pt(II) complexes containing imine ligands. Close to this signal all the spectra showed a doublet due to the protons on the ortho site of the phenyl ring.

Comparison of the variations detected in the ^{1}H NMR spectra of the *trans*- and *cis*-isomers of *(1S,2R)*-(+)-[Pt{(η^5-C_5H_5)Fe[(η^5-C_5H_4)–CH═N–CH(Me)–CH(OH)–C_6H_5]}Cl_2(DMSO)] (**2a** and **3a**, respectively) in DMSO-d_6 (Figs. S1 and S2) and in DMSO-d_6: D_2O mixtures (Figs. S7 and S8) revealed that the *trans*- isomer (**2a**) degradated faster than **3a**. This agrees with previous studies on related *trans*- dichloro(or chloro-aquo)platinum(II) complexes. [2] These NMR studies also suggested that the degradation process of the *cis*-isomer **3a**: a) was more complex than that of **2a**, b) it involved the formation of new platinum(II) containing species and later on ferrocenecarbaldehyde (Fig. S2) and c) in the presence of D_2O the degradation is faster.

The pair of isomers **4a** and **5a** also exhibited different solution behavior and stability in DMSO-d_6 (Figs. S3 and S4). Degradation of **4a** is slower than that of **5a** and involves the presence of a new intermediate specie that coexists in a nearly 1:1 ratio with **4a** after 18 h, but for longer storage periods the intensities of the two singlets at $\delta = 8.82$ and 8.91 ppm decreased and new and additional singlets appeared between 7.8 and 8.4 ppm. When this study was performed with **5a** (Fig. S4) the spectra suggested the also the coexistence of other Pt(II) complexes, but all of them were less abundant than those detected for **4a**.

Due to the scarce solubility of compounds **4a** and **5a** in the DMSO-d_6:D_2O (1:1) (see Experimental section), the study of their stability in this medium was more complex, longer acquisition periods were required to register the spectra and their resolution was low (Figs. S9 and S10). However, these studies revealed that complexes **4a** and **5a**: a) degradated faster than when the solvent was DMSO-d_6 and b) exhibited different behaviors in both media. This could be attributed to the different trans- influence of the two donor atoms of the chelating ligand.

In contrast with the results obtained for the pairs of compounds (**2a, 3a**) and (**4a, 5a**), the ^{1} H-NMR spectra of platinacycles (**6a** and **7a**) in DMSO-d_6 and even in the mixtures DMSO-d_6:D_2O did not vary with time and those obtained after several days of storage were practically identical to those of the freshly prepared solutions (Figs. S5, S6, S11 and S12 in the supporting information). This observation confirms the expected greater stability of the cyclometallated complexes versus that of pair **4a** and **5a** where ligand **1a** acts as a $(N,O)^-$ bidentate group. Therefore the platinacycles (**6a** and **7a**) would be more likely to reach their biological target intact [58,59]. The comparison of the solution behavior of the new platinum(II) complexes in solution reveals that their stability in DMSO-d_6 and in the mixtures DMSO-d_6:D_2O decreases according to the sequence: **6a≈7a > > 4a > 5a > 3a > 2a.**

4. Conclusions

Three pairs of diastereomerically pure platinum(II) complexes [(**2a**, **3a**), (**4a**, **5a**) and (**6a**, **7a**)} have been prepared and characterized. The results reveal that the iminoalcohol **1a**, can adopt three different binding modes in front of Pt(II) acting as a neutral (N)-donor as a monoanionic and bidentate ligand {$(N,O)^-$ (in **4a** and **5a**)} or $(C,N)^-$ (in **6a** and **7a**)}. The two products of each pair differ in the relative arrangement of the Cl^- ligands (in **2a** and **3a**), of the imine nitrogen and the Cl^- (in **4a** and **5a**) or on the planar chirality of the 1,2-disubstituted ferrrocenyl unit in the platinacycles **6a** and **7a**. Moreover, we have also demonstrated that an accurate control of the experimental conditions permits the formation of one of the three pairs of complexes preferentially.

All platinum(II) complexes (**2a–7a**) exhibited cytotoxic activity in front of the A549 human lung carcinoma, colon (HCT116) and breast (MDA-MB-231) cancer cell lines and most of them are even more potent than *cisplatin*, specially in HCT116. The comparison of their IC_{50} values provides conclusive evidences of: a) the influence of the mode of binding of the ligand **1a** in the complexes, b) the importance of the shape and conformational restriction of the new complexes **2a–7a**, c) relative arrangement of the auxiliary ligands (Cl^- and DMSO) bound

to the platinum(II) and d) the planar chirality of the 1,2-disubstituted ferrocenyl unit on their cytotoxic activity. In particular, the pair of complexes with the bidentate $(N,O)^-$ ligand (**4a** and **5a**) are more potent than the platinacycles (**6a** and **7a**) or the pair **2a** and **3a,** in which the iminalcohol **1a** is bound to the Pt(II) through the imine nitrogen exclusively.

The platinum complexes, produced (in a greater or lesser extent) changes in the tertiary structure of DNA. However, none of them had an effect on DNA electrophoretic mobility as strong as cisplatin, despite most of them showed IC_{50} values lower than that of the reference drug. These results underscore the importance of additional factors in predicting anticancer activity. Solution studies have proved that in DMSO-d_6 as well as in DMSO-d_6:D_2O (1:1) mixtures, the platinacycles (**6a**–**7a**) are more stable and robust than the five membered chelates (**4a-5a**) and the open like structures (**2a**–**3a**), for which the presence of D_2O produced a faster degradation than in DMSO-d_6.

The results presented here constitute the first stage of current work centered on: a) the synthesis of related complexes with different central chirality and/or arising from the replacement of the DMSO ligands in **4a–7a** by other neutral ligands and b) mechanistic studies for elucidating the mode of action of **4a–7a** (cell cycle arrest, induction of apoptosis, etc.). These may provide additional and valuable information for the development of other and more potent platinum(II) complexes containing related (N), $(N,O)^-$ or $(C,N)^-$ donor ligands.

Acknowledgement

This work was supported by the *Ministerio de Ciencia e Innovación* of Spain {grant numbers CTQ2009-11501, CTQ2009-07021 (both within the subprogram BQU) and (SAF2011-25726)}, FEDER Funds, the *Instituto de Salud Carlos III* and *European Regional Development Fund* (ISCIII-RTICC, RD06/0020/0046), the *Generalitat de Catalunya* (2009SGR1308, 2009SGR-1111), 2009 CTP 00026 and Icrea Academia award 2010 granted to M. Cascante).

Appendix A. Supplementary data

Figures containing partial views of the ^{1}H-NMR spectra of freshly prepared solutions of **2a-7a** in: a) DMSO-d_6 and b) 1:1 mixtures of DMSO-d_6 and D_2O and after different periods of storage at 298 K (Figs. S1-S12) together with full details of crystallographic analyses of **2a**, **3a**, **5a** and **6a** in CIF format. Crystallographic information files of the structures included in this manuscript have been deposited at the *Cambridge Crystallographic Data Centre* (reference codes: 837310–837313). Supplementary data to this article can be found online at http://dx.doi.org/10.1016/j.jinorgbio.2012.09.007.

References

[1] In: B. Lippert (Ed.), Cisplatin: Chemistry and Biochemistry of a Leading Anticancer Drug, Verlag, Zurich, Switzerland, 1999.
[2] F. Arnesano, G. Natile, Coord. Chem. Rev. 253 (2009) 2070–2081.
[3] A.-M. Florea, D. Buesselberg, Cancers 3 (2011) 351–1371.
[4] U. Olszewski, G. Hamilton, Anti Cancer Agents Med. Chem. 10 (2010) 293–301.
[5] L. Dvorak, I. Popa, P. Starha, Z. Travnicek, Eur. J. Inorg. Chem. (2010) 3441–3448.
[6] A.M. Montaña, C. Batalla, Curr. Med. Chem. 16 (2009) 2235–2260.
[7] I. Kostova, R.K. Soni, Int. J. Curr. Chem. 1 (2010) 81–88.
[8] S.J. Berners-Price, Angew. Chem. Int. Ed. 50 (2011) 804–805.
[9] C. Marzano, S.S. Mazzega, V. Gandin, D. Colavito, E. del Giudice, R.A. Michelin, A. Venzo, R. Seraglia, F. Benetollo, M. Schiavon, R. Bertani, J. Med. Chem. 53 (2010) 6210–6227.
[10] J. Liu, C.-H. Leung, A.L.-F. Chow, R.W.-Y. Sun, S.-C. Yan, C.-M. Che, Chem. Commun. 47 (2011) 719–721.
[11] J. Ruiz, C. Vicente, C. de Haro, A. Espinosa, Inorg. Chem. 50 (2011) 2151–2158.
[12] X. Wang, Anti Cancer Agents Med. Chem. 10 (2010) 396–411.
[13] U. Kalinowska-Lis, J. Ochocki, K. Matlawska-Wasowska, Coord. Chem. Rev. 252 (2008) 1322–1345.
[14] R.Y. Tang, T. Al-Fayea, H.-J. Au, Drug Saf. 32 (2009) 1109–1122.
[15] Y.Y. Scaffidi-Domianello, K. Meelich, M.A. Jakupec, V.B. Arion, V.Y. Kukushkin, M. Galanski, B.K. Keppler, Inorg. Chem. 49 (2010) 5669–5678.
[16] C.-Y. Shi, E.-J. Gao, S. Ma, M.-L. Wang, Q.-T. Liu, Bioorg. Med. Chem. Lett. 20 (2010) 7250–7254.
[17] X. Riera, V. Moreno, C.J. Ciudad, V. Noe, M. Font-Bardía, X. Solans, Bioinorg. Chem. Appl. 15 (2007) 1–15.
[18] J. Ruíz, J. Lorenzo, C. Vicente, G. López, J.M. López-de-Luzuriaga, M. Monge, F.X. Aviles, D. Bautista, V. Moreno, A. Laguna, Inorg. Chem. 47 (2008) 6990–7001.
[19] E. López-Torres, M.A. Mendiola, Inorg. Chim. Acta 363 (2010) 1735–1740.
[20] R. Cortés, M. Crespo, L. Davin, R. Martín, J. Quirante, D. Ruiz, R. Messeguer, C. Calvis, L. Baldomà, J. Badía, M. Font-Bardía, T. Calvet, M. Cascante, Eur. J. Med. Chem. 54 (2012) 557–566.
[21] Ferrocene, in: P. Stepnicka (Ed.), Ligands, Materials and Biomolecules, Wiley, Weinheim (Germany), 2008.
[22] G. Jaouen, Bioorganometallics. Biomolecules. Labelling, Medicine, Wiley-VCH, Weinheim (Germany), 2006.
[23] R. van Stavaren, N. Metzler-Nolte, Chem. Rev. 104 (2004) 5931–5986.
[24] E.A. Hillard, A. Vessieres, G. Jaouen, Top. Organomet. Chem. 32 (2010) 81–117.
[25] A. Mooney, A.J. Corry, C.N. Ruairc, T. Mahgoub, D. O'Sullivan, N. O'Donovan, J. Crown, S. Varughese, S.M. Draper, D.K. Rai, P.T.M. Kenny, Dalton (2010) 8228–8239.
[26] O. Buriez, J.M. Heldt, E. Labbe, A. Vessieres, G. Jaouen, C. Amatore, Chem. Eur. J. 14 (2008) 8195–8203.
[27] Y.L.K. Tan, P. Pigeon, E.A. Hillard, S. Top, M.-A. Plamont, A. Vessieres, M.J. McGlinchey, H. Muller-Bunz, G. Jaouen, Dalton (2009) 10871–10881.
[28] J. Quirante, F. Dubar, A. González, C. López, M. Cascante, R. Cortes, I. Forfar, B. Pradines, C. Biot, J. Organomet. Chem. 696 (2011) 1011–1017.
[29] Y. Wu, S. Huo, J. Gong, X. Cui, L. Ding, K. Ding, C. Du, Y. Liu, M. Song, J. Organomet. Chem. 637–639 (2001) 27–46 (and references therein).
[30] R.W. Mason, K. McGrouther, P.R.R. Ranatunge-Bandarage, B.H. Robinson, J. Simpson, Appl. Organomet. Chem. 13 (1999) 163–173.
[31] S. Pérez, C. López, A. Caubet, X. Solans, M. Font-Bardía, New J. Chem. 27 (2003) 975–982.
[32] D. Talancón, C. López, R. Bosque, J. Org. Chem. 75 (2010) 3294–3300.
[33] A. Togni, T. Hayashi, Ferrocenes, in: Homogeneous Catalysis, Organic Synthesis, Materials Science, Wiley-VCH, Weinheim (Germany), 1995.
[34] R. Valters, W. Flitch, Ring-Chain Tautomerism, Plenum Press, New York (USA), 1985.
[35] N.A. Keiko, N.V. Vchisio, L.G. Stepanova, L.I. Larina, Y.A. Chuvashev, E.A. Funtikova, Chem. Heterocycl. Comp. 44 (2008) 1466–1471.
[36] K. Pilahja, M. Juhasz, H. Kivela, F. Fülöp, Rapid Commun. Mass Spectrom. 22 (2008) 1510–1518.
[37] M. Juhash, L. Lazar, F. Fülöp, J. Heterocycl. Chem. 44 (2007) 1465–1473.
[38] E.T.J. Strong, S.A. Cardile, A.L. Brazeau, M.C. Jennings, R. McDonald, N.D. Jones, Inorg. Chem. 47 (2008) 10575–15086.
[39] C.A. Caputo, N.D. Jones, Dalton Trans. (2007) 4627–4640.
[40] P.N. Yadav, R.E. Beveridge, J. Blay, A.R. Boyd, M.W. Chojnacka, A. Decken, A.A. Deshpande, M.G. Gardiner, T.W. Hambley, M.J. Hughes, L. Jolly, J.A. Lavangie, T.D. MacInnis, S.A. McFarland, E.J. New, R.A. Gossage, Med. Chem. Commun. 2 (2011) 274–277.
[41] D.W. Dodd, H.E. Toews, E. Heather, M.J. Trevail, M.C. Jennings, R.H.E. Hudson, N.D. Jones, Can. J. Chem. 87 (2009) 321–327.
[42] F.J. Ramos-Lima, O. Vrána, A.G. Quiroga, C. Navarro-Ranninger, A. Halámiková, H. Rybnícková, L. Hejmalová, V. Brabec, J. Med. Chem. 49 (2006) 2640–2651.
[43] A.G. Quiroga, L. Cubo, E. de Blas, P. Aller, C. Navarro-Ranninger, J. Inorg. Biochem. 101 (2007) 104–110.
[44] D.-L. Ma, C.-M. Che, Chem. Eur. J. 9 (2003) 6133–6144.
[45] J.H. Price, A.N. Williamson, R.F. Schramm, B.B. Wayland, Inorg. Chem. 11 (1972) 1280–1284.
[46] D.D. Perrin, W.L.F. Armarego, D.L. Perrin, Purification of Laboratory Chemicals, in: 3rd ed., Butterworth-Heinemann, Oxford (UK), 1988.
[47] G.M. Sheldrick, SHELXS, A program for automatic solution of crystal structure refinement, Univ. Goettingen, Germany, 1997.
[48] G.M. Sheldrick, SHELX97, A program for crystal structure refinement, Univ. Goettingen, Germany, 1997.
[49] International Tables of X-Ray Crystallography Ed. Kynoch press, (1974) Vol. *IV*, (pp 99–100 and 149) Birmirgham (UK).
[50] T. Mosmann, J. Immunol. Methods 65 (1983) 55–63.
[51] C. Matito, F. Mastorakou, J.J. Centelles, J.L. Torres, M. Cascante, Eur. J. Nutr. 42 (2003) 42–49.
[52] K.T. Givens, S. Kitada, A.K. Chemn, J. Rothschiller, D.A. Lee, Invest. Ophthalmol. Vis. Sci. 31 (1990) 1856–1862.
[53] A. Abdullah, F. Hug, A. Chowdhury, H. Tayyem, P. Beale, K. Fisher, BMC Chem. Biol. 6 (2006) 3.
[54] F.H. Allen, Acta Crystallogr. B B58 (2002) 380–388.
[55] J. Vicente, J.A. Abad, A.D. Frankland, M.C. Ramírez de Arellano, Chem. Eur. J. 5 (1999) 3066–3075.
[56] J. Jiang, Y.-L. Tang, X.-H. Liang, Cancer Biol. Ther. 11 (2011) 714–723.
[57] W.R. Wilson, M.P. Hay, Nat. Rev. Cancer 11 (2011) 393–410.
[58] P. Rouhi, L.D. Jensen, Z. Cao, K. Hosaka, T. Laenne, E. Wahlberg, J.F. Steffensen, Y.-H. Cao, Nat. Protoc. 5 (2010) 1911–1918.
[59] G.L. Edwards, D.S.C. Black, G.B. Deacon, L.P.G. Wakelin, Can. J. Chem. 83 (2005) 969–979.

CAPÍTULO 02

UN NUEVO COMPLEJO CICLOMETALADO DE PT(II) DERIVADO DEL FERROCENO INDUCE LOCALIZACIÓN NUCLEAR DE FOXO3A Y APOPTOSIS, Y PRESENTA SINERGIA CON CISPLATINO EN LA INHIBICIÓN DE LA PROLIFERACIÓN DE CÉLULAS DE CÁNCER DE PULMÓN.

CAPÍTULO 02

UN NUEVO COMPLEJO CICLOMETALADO DE PT(II) DERIVADO DEL FERROCENO INDUCE LOCALIZACIÓN NUCLEAR DE FOXO3A Y APOPTOSIS, Y PRESENTA SINERGIA CON CISPLATINO EN LA INHIBICIÓN DE LA PROLIFERACIÓN DE CÉLULAS DE CÁNCER DE PULMÓN.

Roldán Cortés,[a] Míriam Tarrado-Castellarnau,[a] Daniel Talancón,[b] Concepción López,*[b] Wolfgang Link,[cd] Daniel Ruiz,[e] Josep Joan Centelles,[a] Josefina Quirante[e] y Marta Cascante*[af]

[a] Departament de Bioquímica i Biologia Molecular, Facultat de Biologia, Unidad Asociada al CSIC, Diagonal 643, 08028 Barcelona, España. E-mail: martacascante@ub.edu

[b] Departament de Química Inorgànica, Facultat de Química, Universitat de Barcelona, Martí i Franquès 1-11. E-08028-Barcelona, España. E-mail: conchi.lopez@qi.ub.es

[c] Regenerative Medicine Program, Departamento de Ciencias Biomédicas e Medicina, Universidade do Algarve, Portugal. E-mail: walink@ualg.pt

[d] IBB-Institute for Biotechnology and Bioengineering, Centro de Biomedicina Molecular e Estrutural, Universidade do Algarve, Campus de Gambelas, Faro, Portugal

[e] Laboratori de Química Orgànica, Facultat de Farmàcia, Institut de Biomedicina, (IBUB), Universitat de Barcelona, Av. Joan XXIII, s/n, E-08028-Barcelona, España

[f] Institut d'Investigacions Biomèdiques August Pi i Sunyer (IDIBAPS), Barcelona, España

Resumen

El cisplatino es un compuesto basado en el platino que actúa como un agente alquilante y que es utilizado en el tratamiento de una gran variedad de tumores malignos, incluyendo los de cáncer de pulmón. Dado que el cisplatino presenta limitaciones significativas en la práctica clínica, otro tipo de compuestos de platino, como complejos cicloplatinados, han sido considerados interesantes agentes antitumorales alternativos. Aquí presentamos la actividad antiproliferativa sobre la línea de adenocarcinoma pulmonar A549 del nuevo compuesto cicloplatinado diastereoméricamente puro (S_p,1*S*,2*R*)-[Pt{(k^2-*C*,*N*)[(η^5-C_5H_3)–CH=N–CH(-Me)–CH(OH)–C_6H_5]Fe(η^5-C_5H_5)}Cl(DMSO)] **6a**. Estudios acerca de su mecanismo de acción revelaron que el compuesto **6a** induce la translocación nuclear tanto de una proteína marcadora de FOXO3a como del FOXO3a endógeno en células U2OS y A549. El tratamiento de las células A549 con **6a** activa la vía intrínseca de las caspasas provocando un gran aumento en el porcentaje de células apoptóticas. Además, **6a** exhibe un efecto antiproliferativo sinérgico con el cisplatino sobre la proliferación celular. El compuesto **6a** también es activo sobre la línea de cáncer de pulmón NCIH460. Finalmente, la actividad del cicloplatinado **6a** sobre la línea celular no tumoral y no proliferante 3T3-L1 es significativamente más débil que en el resto de líneas celulares de cáncer ensayadas.

Metallomics

PAPER

View Article Online
View Journal | View Issue

Cite this: *Metallomics*, 2014, **6**, 622

A novel cyclometallated Pt(II)–ferrocene complex induces nuclear FOXO3a localization and apoptosis and synergizes with cisplatin to inhibit lung cancer cell proliferation

Roldán Cortés,[a] Míriam Tarrado-Castellarnau,[a] Daniel Talancón,[b] Concepción López,*[b] Wolfgang Link,[cd] Daniel Ruiz,[e] Josep Joan Centelles,[a] Josefina Quirante[e] and Marta Cascante*[af]

Received 11th July 2013,
Accepted 17th January 2014

DOI: 10.1039/c3mt00194f

www.rsc.org/metallomics

Cisplatin is a platinum-based compound that acts as an alkylating agent and is used to treat a variety of malignant tumors including lung cancer. As cisplatin has significant limitations in the clinic, alternative platinum compounds such as cycloplatinated complexes have been considered as attractive anti-tumor agents. Here, we report the antiproliferative activity of a novel diastereomerically pure cycloplatinated complex (S_p,1*S*,2*R*)-[Pt{(κ^2-*C*,*N*)[(η^5-C_5H_3)–CH=N–CH(Me)–CH(OH)–C_6H_5]Fe(η^5-C_5H_5)}Cl(DMSO)] **6a**, against A549 non-small cell lung cancer. Mechanistic studies revealed that compound **6a** induces nuclear translocation of a FOXO3a reporter protein as well as endogenous FOXO3a in U2OS and A549 cells, respectively. Accordingly, treatment of A549 cells with compound **6a** activates the intrinsic caspase pathway and dramatically increases the percentage of apoptotic cells. Furthermore, **6a** displays a synergistic antiproliferative effect when applied together with cisplatin. Compound **6a** is also active in other cancer cell lines including NCI-H460 large cell lung cancer cells. Importantly, antiproliferative activity of the platinacycle **6a** on the non-tumor and non-proliferating 3T3-L1 cell line is weaker than in all cancer cell lines tested.

Introduction

Lung cancer is today the leading cause of cancer-related deaths worldwide.[1] The disease is commonly classified into two large groups: small cell lung cancer (SCLC) and non-small cell lung cancer (NSCLC). NSCLC accounts for approximately 85% of all lung cancer cases, and the overall 5-year survival rate for it is only 15%.[2] Since it is usually diagnosed at an advanced stage, the dominant clinical strategy is chemotherapy-based treatment, but currently its outcome is still far from satisfactory. In combined therapy[3–9] platinum drugs such as cisplatin and carboplatin are used in combination with different anti-cancer agents including docetaxel, bevacizumab and gemcitabine in most of the NSCLC treatment protocols. However the efficacy of these drug combinations has encountered a plateau due to their side effects and drug resistance.[10–13] Hence, great efforts are being made in the design of new metal drugs[14–17] that can be part of novel, more effective combined therapies in the treatment of NSCLC.

Two of the main strategies which are used to improve metal drugs are:[18–42] (a) the stabilization of the Pt(II) ion in the complexes, using bi-{(*N*,*N*), (*N*,*N*′), (N,O)$^-$, (C,N)$^-$} or terdentate (C,*N*,*N*′) ligands[14–21,28,32,34–42] or (b) the incorporation of ferrocenyl units into the backbones of representative drugs.[43–52] However, and despite the potential synergistic biological effects that may arise from the presence of the Pt(II) centre and ferrocenyl units, studies on the antitumor activity of Pt(II)–ferrocene compounds are not too common[47–58] and reports on complexes with N, (*N*,*N*) or (C,N)$^-$ ferrocenyl ligands bound to Pt(II) are even more rare (Fig. 1).[55–58] A representative example is complex **C** (Fig. 1), with a different mechanism of action and greater potency than cisplatin in the resistant WiDr colon cancer cell line.[56]

[a] *Department of Biochemistry and Molecular Biology, Faculty of Biology, and IBUB, Universitat de Barcelona, Unit Associated with CSIC Diagonal 645, E-08028-Barcelona, Spain. E-mail: martacascante@ub.edu*
[b] *Departament de Química Inorgànica, Facultat de Química, Universitat de Barcelona, Martí i Franquès 1-11. E-08028-Barcelona, Spain. E-mail: conchi.lopez@qi.ub.es*
[c] *Regenerative Medicine Program, Departamento de Ciências Biomédicas e Medicina, Universidade do Algarve, Portugal. E-mail: walink@ualg.pt*
[d] *IBB-Institute for Biotechnology and Bioengineering, Centro de Biomedicina Molecular e Estrutural, Universidade do Algarve, Campus de Gambelas, Faro, Portugal*
[e] *Laboratori de Química Orgànica, Facultat de Farmàcia, Institut de Biomedicina, (IBUB), Universitat de Barcelona, Av. Joan XXIII, s/n, E-08028-Barcelona, Spain*
[f] *Institut d'Investigacions Biomèdiques August Pi i Sunyer (IDIBAPS), Barcelona, Spain*

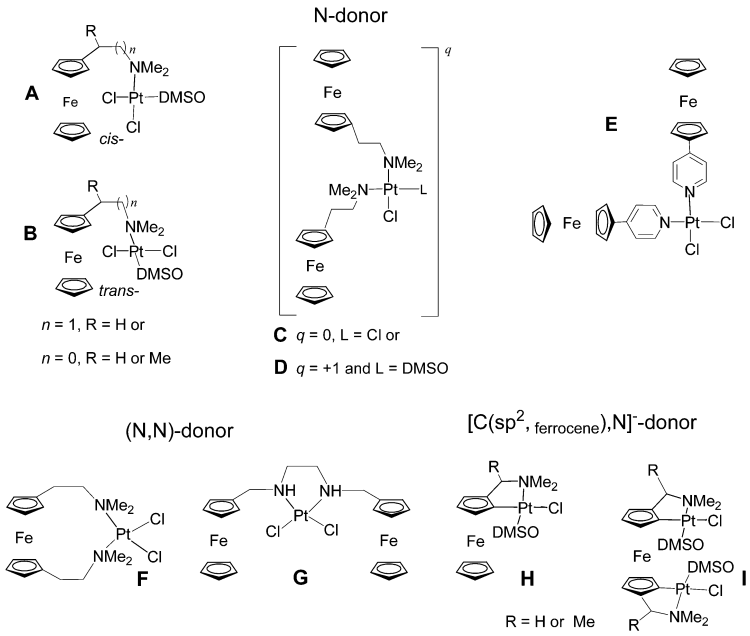

Fig. 1 Representative examples of Pt(II) complexes containing mono- or polyfucntional ferrocenyl-amines and diamines with cytotoxic activity reported so far.[55–58]

More recently, we have reported the Pt(II) complexes (**2a–7a**) shown in Fig. 2 with remarkable cytotoxic activity against colon (HCT116), breast (MDA-MB-231) and lung (A549) human adenocarcinoma cell lines.[59] DNA mobility shift assay showed that all of them induce changes in the tertiary structure of DNA, but their effect over DNA mobility was not as strong as that of cisplatin, pointing to other mechanisms of action or biomolecular targets.

Cycloplatinated complexes have attracted increasing interest as new antitumor agents in the last decade.[42,48,59,60] This is due to their higher stability in physiological media and their lower toxicity to normal cells than cisplatin and derivatives. In order to identify stable and efficient anti-cancer agents we synthesized several platinacycles and, based on their cytotoxic properties against lung cancer cells, selected compound **6a** as the candidate for further biological studies.

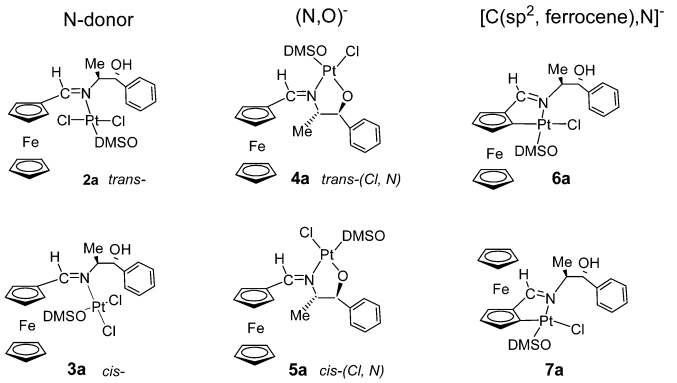

Fig. 2 Chemical formulae of the six pairs of diastereomerically pure platinum(II) complexes described recently.[59] These products differ in the mode of binding of the ligand, the relative arrangement of the ancillary groups or the planar chirality of the 1,2-disubstituted ferrocenyl moieties.

It has been reported that Forkhead Box O3a (FOXO3a) is a key mediator of the cytotoxic effects of cisplatin in colon cancer cells.[61,62] The FOXO family of transcription factors have received much attention in recent years due to their involvement in multiple signaling pathways[63] playing an important role in physiological and pathological processes related to cell proliferation and survival.[64] Increasing evidence shows that members of the FOXO family exhibit a tumor suppressor activity, maintaining tissue homeostasis and being frequently dysregulated in cancer.[65,66]

FOXO transcription factors are susceptible to regulation by many different post-translational modifications.[67] Nevertheless, phosphorylation *via* AKT is commonly recognized as one of the key regulators of FOXO activity. Phosphorylation of FOXO by AKT enables the docking to 14-3-3 protein, inducing the translocation of the resulting complex from the cell nucleus to the cytoplasm, where FOXO cannot execute its transcriptional functions. Dephosphorylation of FOXO, in turn, mediates the dissociation of the complex, allowing FOXO to relocate to the nucleus where it can exhibit its tumor suppressor activity.[68]

In cancer, therefore, FOXO factors are commonly accumulated in the cytoplasm, resulting in their degradation and the general suppression of their transcriptional activity.[69] The relocation of FOXO to the cell nucleus, which would imply the activation of its regulatory functions over apoptosis, cell cycle and stress protection, is therefore an appealing target for new cancer treatments, and a rising strategy to combat the dysregulation of cell proliferation in different tumors.

To get further information on the mechanism of action of the Pt(II)–ferrocene cyclometallated complex **6a** we report herein: (1) antiproliferative activity in additional non-small lung cancer cell lines (NCI-H460), besides A549, (2) induction of cell cycle arrest and apoptosis in both lung cancer cell lines, (3) FOXO nuclear translocation and its effect on the mechanism involved in the apoptotic cell death, and (4) the synergistic effect with cisplatin and reduced toxicity *versus* non-tumor and non-proliferant 3T3-L1 cells.

Results and discussion

Nuclear GFP-FOXO3a translocation in U2foxRELOC cells induced by complex 6a

As FOXO proteins have been reported to mediate the action of several anticancer agents, in particular cisplatin, we investigated if complex **6a** had any effect on the subcellular localization of FOXO. We used U2foxRELOC cells, which stably express GFP-FOXO3a reporter protein. The U2foxRELOC cell system is based on human U2OS osteosarcoma cells, and has been previously used to study the FOXO nuclear-cytoplasmic shuttling using image-based cell screening.[70–72]

In order to determine the active concentration of complex **6a**, first we evaluated the dose-dependent sensitivity of U2foxRELOC cells. For this purpose, we performed the MTT (3-[4,5-dimethylthiazol-2-yl]-2,5 diphenyl tetrazolium bromide) colorimetric viability assay incubating U2foxRELOC cells for 72 h using 8 different concentrations of compound **6a**. The results shown in Fig. 3 indicate that the IC_{50} value for **6a** in U2foxRELOC is in the lowest micromolar range, even lower than the IC_{50} value obtained with A549 cells (which was 8.8 μM).[59]

We then incubated U2foxRELOC cells with 10 μM **6a** for 6 h, and after fixing the cells we observed the intracellular location of GFP-FOXO3a using confocal microscopy. As a positive control, we used LY294002, a PI3K inhibitor widely used to inhibit P3K/AKT signaling. Fig. 3 shows that incubation with complex **6a** rises the proportion of FOXO3a in the nuclei of U2foxRELOC cells (the cells in which GFP-FOXO3a intensity is at least 2.5 times higher in the nucleus than in the cytoplasm are less than 25% for the control conditions, but almost 60% after incubation with **6a**). In order to elucidate if the effect produced by platinacycle **6a** on FOXO translocation could be driven by (a) the presence of the ferrocenyl unit and/or (b) the environment of the Pt(II) center, we undertook a structure activity relationship (SAR) study using *cis*-[Pt{κ^2,(*N*,*N*′)[η^5-(C_5H_4)CH=N–(CH_2)$_2$ NMe_2]}Cl_2] (**8**)[73] (Fig. 3).

Complex **8** also contains a ferrocenylimine moiety but the environment of the Pt(II) is different from that of compound **6a** and more similar to that of cisplatin. Unlike palladacycle **6a**, complex **8** exhibits a poor antiproliferative activity with higher IC_{50} values than that of compound **6a** in both A549 (IC_{50} > 100 μM)[60] and U2FoxRELOC cells (Fig. 3).

Incubation of U2foxRELOC cells with complex **8** at a concentration which was enough for platinacycle **6a** to induce FOXO3a translocation but too small for compound **8** to affect viability does not seem to induce any significant effects on FOXO3a translocation, since there is no significant difference in the cellular localization of FOXO3a-GFP after incubation with complex **8** from the one observed under control conditions. This result reveals that the platinacycle **6a** has a greater capability to relocate FOXO3a to the cell nucleus and exhibits a higher antiproliferative activity than that of complex **8**, thus suggesting a relationship between both phenomena.

Platinacycle 6a induces GFP-FOXO3a nuclear translocation and an increase in nuclear FOXO3a in A549 cells

As the effect of platinacycle **6a** on the viability of U2foxRELOC and A549 cells was very similar we hypothesized that it might also induce the translocation of FOXO3a to the nucleus of A459 cells. To test this hypothesis, we transfected A459 cells with the GFP-FOXO3a plasmid and then we incubated them with the same concentrations of LY294002 and **6a** used in U2foxRELOC cells for 6 h. As shown in Fig. 4, platinacycle **6a** also induces FOXO translocation from the cytoplasm to the cell nucleus in A549 cells. It is worth noting that under control conditions the proportion of nuclear FOXO3a in A549 cells is much lower when compared to that found in U2foxRELOC cells. The vast majority of A549 cells showed higher FOXO3a-GFP intensity in the cytoplasm than in the nucleus, as is usually the case for tumor cells.

To determine if complex **6a** also induced an increase in the nuclear concentration of endogenous FOXO3a in A549 cells, we performed Western Blot analysis of cell lysates after incubating the cells for 6 h with the same products (LY294002 and **6a**) at the same concentrations tested previously. The results show

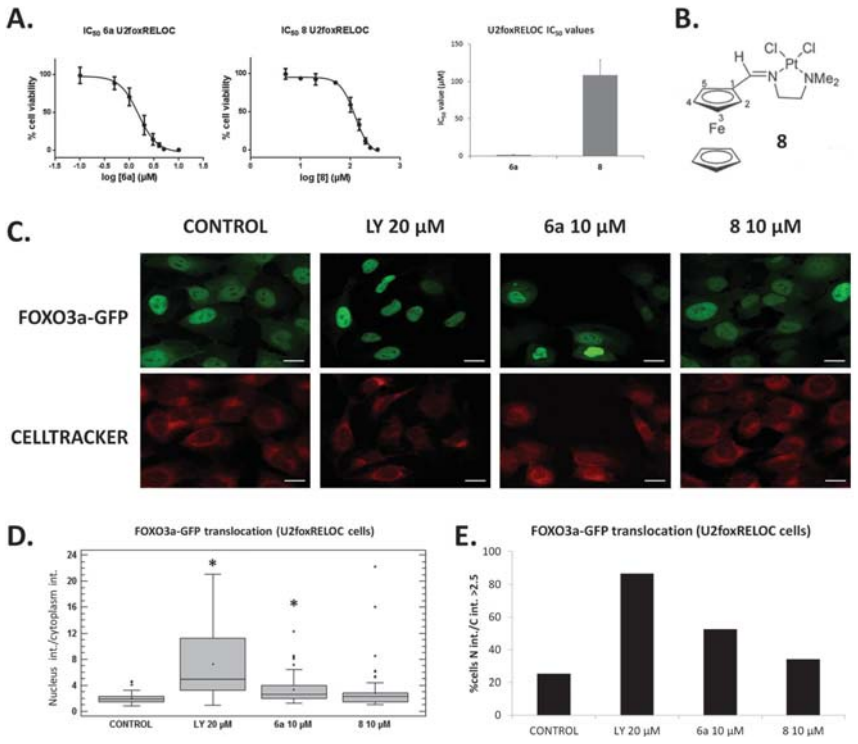

Fig. 3 (A) Two representative examples of the viability assays in U2foxRELOC cells with products **6a** and **8**, and the comparison between the IC_{50} values for both products. The IC_{50} concentration is two orders of magnitude higher when treating the cells with product **8** (p = 0.0003). (B) Structure of compound **8**, used in this study for comparative purposes. (C) Representative confocal microscopy images for the U2foxRELOC cells under different conditions. The upper row (green) indicates the location of FOXO3a-GFP in the cells. The lower row (red) indicates the location of celltracker, a cytoplasm marker that does not mark nuclei. Scale bar, 5 μm. (D) The box and whiskers plot for the relationship of the intensities of the green fluorescence (Foxo3a-GFP) between the nucleus and the cytoplasm. LY was used as a positive control. Higher values indicate a higher FOXO3a-GFP presence in the nucleus compared to the cytoplasm. Only the conditions marked with an asterisk (LY 20 μM and **6a** 10 μM) show statistically significant differences with the control condition according to a multiple rang test with a 95% confidence. (E) Percentage of cells in which FOXO3a-GFP intensity in the nucleus/FOXO3a-GFP intensity in the cytoplasm is higher than 2.5.

how product **6a** induces an increase in the concentration of active FOXO3a in the nucleus, with a concomitant decrease of phosphorylated FOXO3a in the cytoplasm, validating the observations with the GFP-FOXO3a plasmid described above.

Regulation of FOXO3a localization by platinacycle 6a *via* the AKT pathway

Phosphorylation of FOXO *via* AKT is considered as the most important key regulator of FOXO cellular localization (and therefore of FOXO activity as a transcriptional regulator). Interestingly, it has been reported[61] that the cytotoxic effect of cisplatin occurs through cisplatin-induced dephosphorylation of AKT sites within the FOXO3a proteins and their subsequent nuclear re-localization. To assess whether complex **6a** mediated its effect on FOXO nuclear concentration by affecting the AKT pathway, we incubated the cells for 6 h with **6a** and analyzed the phosphorylation of AKT on Ser473 by Western Blot. In addition, we monitored the AKT activity by analyzing the phosphorylation status of the AKT substrate PRAS-40.

As shown in Fig. 4, compound **6a** decreases the concentration of both phospho-AKT and phospho-PRAS-40, suggesting that the platinacycle affects the AKT activity, resulting in a decreased phosphorylation of AKT-downstream substrates like PRAS-40 and FOXO. Dephosphorylation of FOXO would allow it to relocate to the cell nucleus, where it should be able to exercise its antiproliferative functions.

Effect of platinacycle 6a on cell cycle distribution in A549 cells

The cell cycle is typically divided into different phases: quiescent and gap 1 (G0/G1 phase), synthesis (S phase) and gap 2 and mitosis (G2 phase). One of the main hallmarks of cancer is cell cycle dysregulation, and it has been proposed that one of the mechanisms used by FOXO3a to exercise its tumor suppressor activity is the regulation of the cell cycle.[74–76] Therefore we

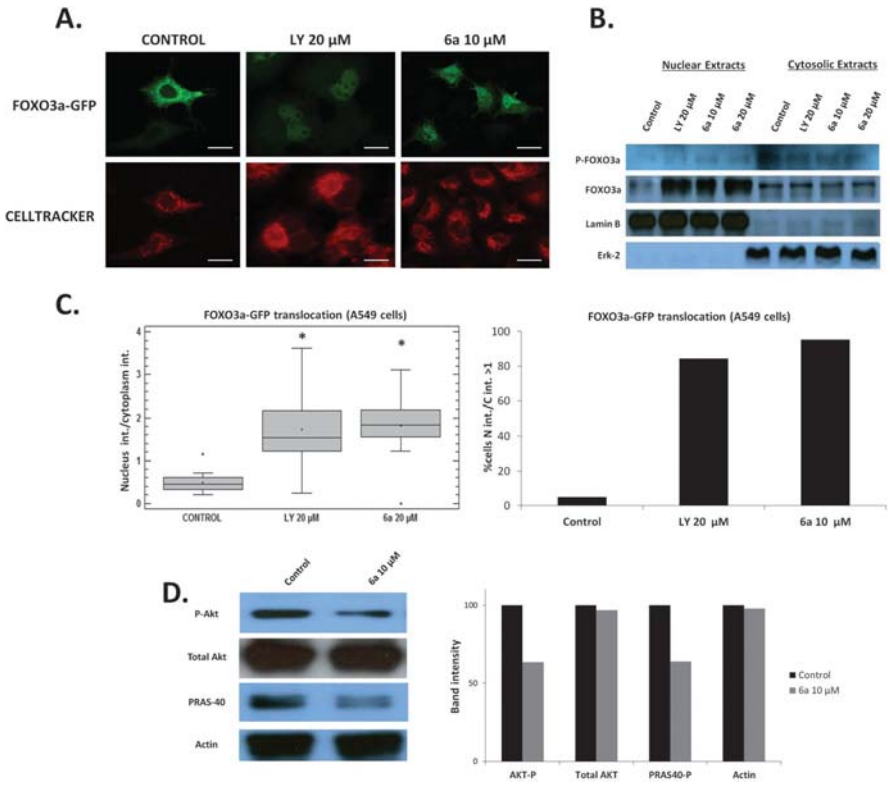

Fig. 4 (A) Representative confocal microscopy images for A549 cells transfected with a FOXO3a-GFP reporter plasmid under different conditions. Upper row (green) indicates the location of FOXO3a-GFP in the cells. Lower row (red) indicates the location of celltracker, a cytoplasm marker that does not mark nuclei. Scale bar, 5 μm. (B) Western Blots for the nuclear and cytoplasm fractions of A549 cells. Endogenous fosforilated FOXO3a cytosolic levels decrease after 6 h incubation with **6a**, while unfosforilated FOXO3a nuclear levels rise. Lamin B (a nuclear marker) and Erk-2 (a cytoplasm marker) antibodies were used to assess the quality of the separation of the nuclear and cytoplasmic fractions. (C) The box and whiskers plot for the relationship of the intensities of the green fluorescence (Foxo3a-GFP) between the nucleus and the cytoplasm. LY was used as a positive control. Higher values indicate a higher FOXO3a-GFP presence in the nucleus compared to the cytoplasm. Conditions marked with an asterisk (LY 20 μM and **6a** 10 μM) show statistically significant differences with the control condition according to a multiple rang test with a 95% confidence. Percentage of cells in which FOXO3a-GFP intensity in the nucleus/FOXO3a-GFP intensity in the cytoplasm is higher than 1 is also shown. (D) Western Blots for the total fractions of A549 cells. Akt-P and PRAS40-P levels decrease after 6 hour incubation with 10 μM **6a**, while total AKT levels remain stable.

studied if complex **6a**-induced nuclear FOXO3a translocation could affect cell cycle distribution of A549 cells. We incubated the cells with 10 μM **6a** or a vehicle for 24, 48 and 72 h and analyzed cell cycle progression by FACS analysis. As shown in Fig. 5, incubation of A549 cells with platinacycle **6a** for 24 h provokes a slight redistribution of the percentage of cells in each of the cell cycle phases. In particular, there is a 25% decrease in the percentage of cells in the S phase with a concomitant 50% increase of the cells in the G2 phase. This result suggests the appearance of a block in cell cycle progression, but the redistribution of the cells in these cell cycle phases is not retained for longer than 24 hours. After 48 and 72 hours of incubation with compound **6a**, the percentage of cells in G0/G1, S and G2/M phases returns to levels which cannot be considered statistically different from the ones under control conditions. Thus, cell cycle arrest may not be the main mechanism by which complex **6a** affects A549 cells viability.

Nevertheless, treatment of A549 cells with **6a** results in the appearance of a sub-G1 peak that becomes bigger with longer incubation times until it gets to encompass the main cell population. The presence of a sub-G1 peak points to DNA degradation associated with apoptotic or necrotic processes.

Complex 6a induces apoptosis in A549 cells *via* intrinsic caspase pathway activation

The presence of the **6a**-induced sub-G1 peak and the known role of FOXO3a in apoptosis[66,77,78] suggest that this compound promotes programmed cell death in A549 cells. In the earlier events of the apoptotic process, plasma membrane asymmetry is lost, and that causes phosphatidylserine (PS) to be translocated

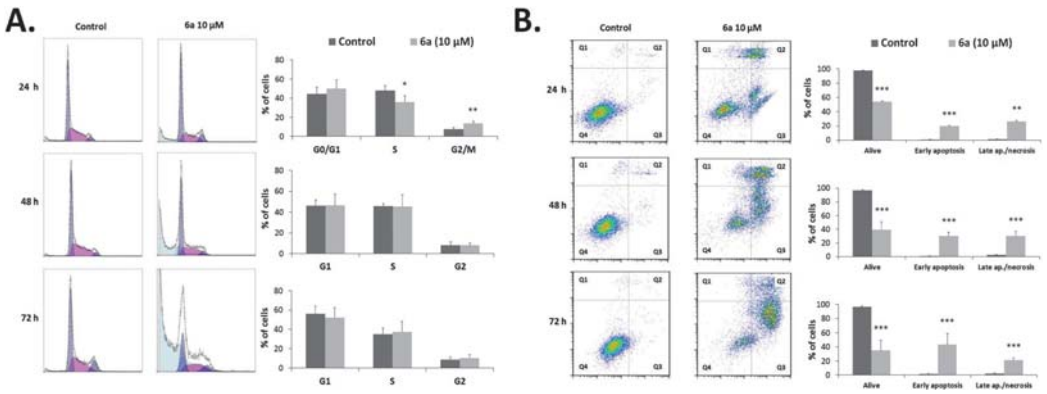

Fig. 5 (A) Representative histograms for the cell cycle analysis of A549 cells untreated (Control) or treated with **6a** at a concentration equal to 10 μM for 24, 48 and 72 h. The harvested cells were stained with PI and their DNA content analyzed by flow cytometry. *X*-axis represents DNA content, and the *Y*-axis represents the cell count. Plots depict the variation of the percentage of cells in each phase of the cell cycle. (B) Representative flow cytometric plots for the quantification of apoptosis in A549 cells untreated (Control) or treated with **6a** at a concentration equal to 10 μM for 24, 48 and 72 h. Quadrant 4 (annexin V^- and PI^-) represents non-apoptotic cells, quadrant 3 (annexin V^+ and PI^-) represents early apoptotic cells and quadrants 1 and 2 (PI^+) represent late apoptotic/necrotic cells. Plots depict the variation of the percentage of cells in early apoptosis and late apoptosis/necrosis. Data are given as the mean ± standard deviation (SD) for a minimum of three independent experiments. After a Student's *t*-test, differences between treated and control groups were considered significant when $p < 0.05$(*), $p < 0.01$(**) or $p < 0.001$(***).

from the inner to the outer membrane.[79] Once exposed to the external part of the cell, PS is able to bind to an annexin V-FITC conjugate, to which PS has a high affinity.[79,80] In the later stages of the apoptotic process, as well as in necrotic processes, the loss of integrity of cell membranes allows PI to access the nucleus, where it intercalates between the DNA bases. FACS analysis using both annexin V-FITC staining and PI accumulation was used to differentiate nonapoptotic cells (annexin V^- and PI^-) from early apoptotic (annexin V^+ and PI^-) and necrotic or late apoptotic (PI^+) cells.

We incubated A549 cells with platinacycle **6a** at 10 μM concentration for 24, 48 and 72 h. As shown in Fig. 5, treatment with compound **6a** for 24 h generated around 20% of apoptotic cells, as opposed to the 1% apoptotic cells under control conditions, with the percentage of necrotic cells rising similarly. In this case, the apoptotic effect is not only maintained but enhanced with longer incubation times. After 48 and 72 h of incubation with complex **6a**, the percentage of cells in early apoptosis raised to 30 and 40%, respectively. Fig. 5 shows how, as the incubation time with platinacycle **6a** raises, the intensity of the IP label on the Annexin V/FITC labeled population increases. This is indicative of progress in the apoptotic process as time goes on.

Apoptosis eventually entails DNA damage providing another experimental endpoint to validate the existence of apoptotic processes in the cells. Hence, in order to asses DNA integrity we performed the modified single-cell gel electrophoresis assay known as Comet Assay. Fig. 6 shows that 24 h treatment with complex **6a** produced a significant increase in the tail length values of A549 cells genetic material. These clastogenic effects also concur with the compound **6a**-mediated induction of apoptosis in A549 cells.

One of the most important mechanisms involved in apoptotic cell death in many cell systems is the activation of the caspase pathway. In the intrinsic activation of this pathway, cytochrome c is released from the mitochondria and forms a complex with the cytosolic protein apaf-1 and ATP. This apoptosome complex then recruits pro-caspase 9, activating it by proteolysis. The resultant active caspase 9 is then able to recruit pro-caspase 3 and activate it in turn, also by proteolysis. Active caspase 3 is involved in the cleavage of poly(ADP-ribose) polymerase (PARP), and the resulting 89 kDa PARP fragment is considered a biomarker of apoptosis.

To assess the apoptotic pathway activated by complex **6a**, we performed western blot analysis to test the levels of procaspase 9, procaspase 3 and the 89 kDa PARP fragment after 24 h incubation with compound **6a**. As shown in Fig. 6, incubation of A549 cells with complex **6a** decreased the levels of procaspase 9 and procaspase 3, suggesting their cleavage. Furthermore, PARP-1 levels increase under the same conditions. Taken together, our data suggest that treatment of A549 cells with platinacycle **6a** does not only mediate FOXO3a nuclear relocalization, but also leads to apoptosis by activating the intrinsic caspase pathway.

Platinacycle 6a as a new potential antitumor drug

For many years, cisplatin has been one of the cornerstone products in chemotherapy treatment of many cancers, including non-small cell lung cancer. But even when the initial responsiveness to cisplatin treatment is high, acquired resistances and dose-limiting side effects limit its clinical efficacy. Therefore, combined therapies are often needed to achieve better results. We decided to test whether compound **6a** could exhibit synergistic effects with cisplatin to inhibit the growth of A549 cells. As seen in Table 1, combined incubation of A549 cells with complex

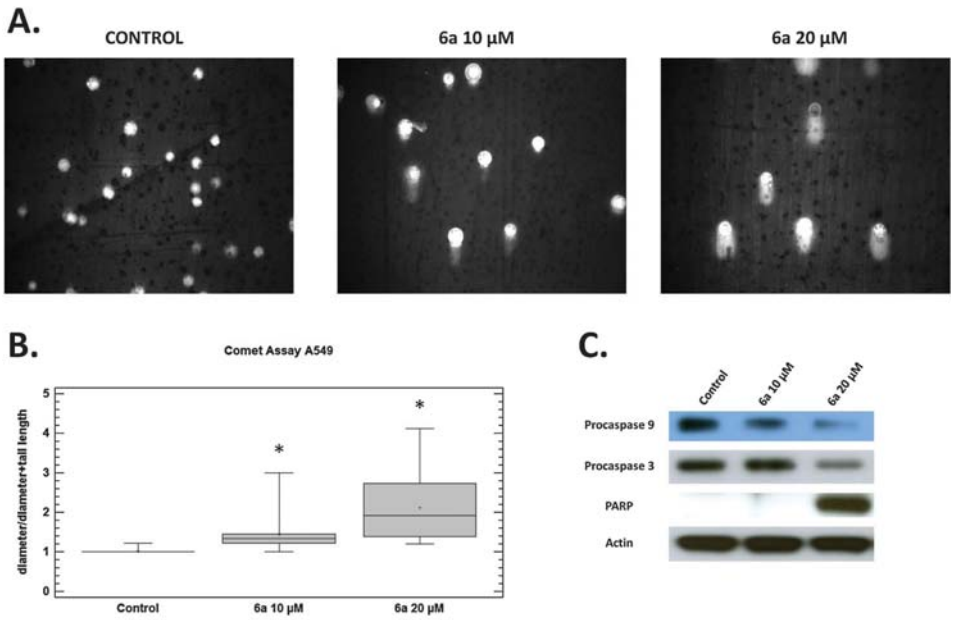

Fig. 6 (A) A549 cells DNA stained with EtBr after electrophoresis in an agarose gel (Comet Assay). Control cells have undergone no DNA fragmentation, so the genetic material appears as a regular sphere (DNA circular head). Treated cells have suffered DNA damage, and after electrophoresis the DNA fragments appear as a comet tail of variable length dependant on the magnitude of the fragmentation. (B) The box and whiskers plot for the relationship of the diameter of the DNA circular head and the total length of the head plus the DNA tail. Conditions marked with an asterisk (**6a** 10 μM and **6a** 20 μM) show statistically significant differences with the control condition according to a multiple rang test with a 95% confidence. (C) Western Blots for total extracts of A549 cells. After 24 h incubation with 10 μM **6a**, PARP levels raise while levels of procaspases 3 and 9 decrease, which indicates intrinsic caspase pathway activation of apoptosis.

Table 1 Calcusyn software results for the study of the synergistic effects of a combined incubation of A549 cells with **6a** and cisplatin for 72 hours. Rows italicized have CI values below 1, which indicates a synergy in the antiproliferative effects of both products

6a (μM)	Cisplatin (μM)	1-Viability	CI
1	3	1.00×10^{-10}	12.946
3	*9*	*0.478*	*0.525*
5	*15*	*0.759*	*0.658*
15	45	0.911	1.581
30	90	0.993	1.933

6a and cisplatin for 72 h revealed a synergy between them. Hence, our data suggest that co-treatment with compound **6a** may enable a decrease of the cisplatin concentration needed in therapy, thus reducing its associated side effects.

6a has a higher biological activity over U2foxRELOC cells than cisplatin, as can be seen in Fig. 3 and 7 (the IC_{50} value for that cell line is significantly higher for cisplatin than for **6a**). We previously assessed the IC_{50} value of cisplatin in A549 cells, and found it to be similar to the IC_{50} value of compound **6a**.[59] However, and although cisplatin has been shown to dephosphorylate AKT in colon cancer cells,[61] when we decided to test the effects of cisplatin on AKT activity we found no effect over the phosphorylation of AKT or PRAS-40 in A549 cells (Fig. 7) at the concentrations used with **6a**. This suggests a difference in the mechanism of action of **6a** and cisplatin in A549 cells, which could also explain the synergy between both products.

Furthermore, we previously demonstrated how HCT116 cells were significantly more resistant to cisplatin than A549 cells (IC_{50} values of 40.0 μM *vs.* 9.3 μM), but more sensitive to **6a** (IC_{50} values of 2.0 μM *vs.*8.8 μM).[59] This also suggests that **6a** acts in a fashion distinct from cisplatin, which enhances interest in it as a potential new antitumor product.

In order to determine if platinacycle **6a** was also biologically active against other lung cancer cell lines, we studied its effect on cell viability, cell cycle phase distribution and apoptosis activation in NCI-H460 cells. As shown in Fig. 7, the IC_{50} value of complex **6a** after 72 h of incubation is even lower in NCI-H460 cells than it was in A549 cells, highlighting its antiproliferative potential in different lung cancer cells. The effect of compound **6a** on the cell cycle and apoptosis in NCI-H460 cells is similar to the one observed in A549 cells, which also suggests similar mechanisms of action in both cell lines (Fig. 7).

To evaluate the selectivity of platinacycle **6a** against a non-tumor, non-proliferating cell line, we conducted a viability assay using differentiated 3T3-L1 adipocytes. Cells were incubated for 72 h with 7 different concentrations of complex **6a**, and its effect on cell proliferation was evaluated using the MTT assay. As shown in

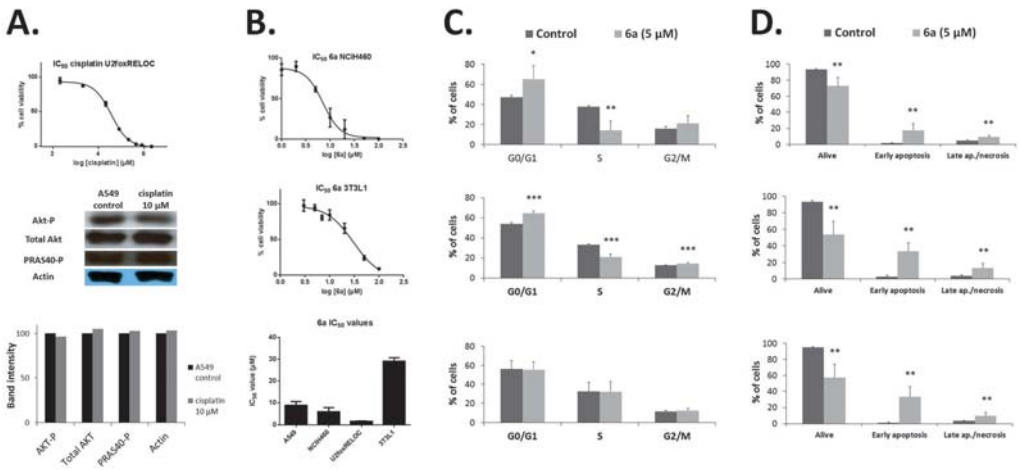

Fig. 7 (A) Representative example of a viability assay with product **6a** in the U2foxRELOC cell line, and Western Blots for the total fractions of A549 cells. Levels of phosphorylated AKT and PRAS-40 do not change significantly after treatment with 10 μM cisplatin. (B) Two representative examples of viability assays with product **6a** in NCI-H460 and differentiated 3T3-L1 cells, and comparison between the IC_{50} values for the tested cell lines. The IC_{50} concentration for the 3T3-L1 non-tumor cell line is between three and fifteen times higher than in the tested tumor cell lines. (C) Plots depicting the variation of the percentage of NCI-H460 cells in each phase of the cell cycle after treatment with **6a** at a concentration equal to 5 μM for 24, 48 and 72 h. (D) Plots depicting the variation of the percentage of non-apoptotic NCI-H460 cells, in early apoptosis and in late apoptosis/necrosis after treatment with **6a** at a concentration equal to 5 μM for 24, 48 and 72 h. Data are given as the mean ± standard deviation (SD) for a minimum of three independent experiments. After a Student's *t*-test, differences between treated and control groups were considered significant when $p < 0.05$(*), $p < 0.01$(**) or $p < 0.001$(***).

Fig. 7, the antiproliferative effects of **6a** are selective to proliferating tumor cells. IC_{50} values for compound **6a** in 3T3-L1 cells are more than one to three times higher than in all other tumor cell lines that have been tested.

Conclusions

The present study reveals that the cycloplatinated complex **6a** induces the nuclear translocation of the tumor suppressor FOXO3a. This effect is mediated by the phosphorylation of FOXO3a, which happens concurrently with the inhibition of upstream AKT phosphorylation. Accordingly, compound **6a** caused apoptosis in A549 cells by activating the intrinsic caspase pathway. Moreover, its remarkable activity against non-small A549 and large NCI-H460 lung cancer cell lines, its low toxicity against non-tumor and non-proliferative cells (3T3-L1) and its synergy with cisplatin inhibiting the viability of A549 cells make this product an excellent candidate for further studies to evaluate its potential against other types of cancer lines alone or in combination with other Pt(II) based drugs.

Experimental

Chemistry

The platinum(II) complexes **6a** and **8** were prepared as described previously.[59,73]

Cell culture

Human osteosarcoma stably transfected U2foxRELOC cells, human lung adenocarcinoma A549 cells, human lung large cell carcinoma NCI-H460 cells and adipocyte-like differentiated 3T3-L1 cells were grown as a monolayer culture in minimum essential medium (DMEM with L-glutamine and 4500 mg L^{-1} D-glucose) in the presence of 10% heat-inactivated fetal bovine serum and 0.5% streptomycin/penicillin, under standard culture conditions (humidified air with 5% CO_2 at 37 °C). Mouse embryo 3T3-L1 pre-adipocyte cells were grown as a monolayer culture in the same DMEM medium in the presence of 0% FBS, 10% NCS and 0.5% streptomycin/penicillin, also under standard culture conditions.

3T3-L1 differentiation

Pre-adipocyte 3T3-L1 cells were seeded in 96 well plates. 48 hours after they reached confluence, their growth medium was replaced with DMEM containing 0% NCS, 10% FBS and an induction cocktail (250 μM isobutylmethylxanthine, 1 μM Dexamethasone and 0.98 μM insulin). After two more days, the medium was replaced again with 10% FBS DMEM containing 0.98 μM insulin. 48 h later the medium was replaced with 10% FBS only DMEM, and two days after that the cells were fully differentiated into adipocytes and the cell viability assay was performed on them.

Cell viability assays

For all cell viability assays, tested compounds were suspended in 20 mM dimethyl sulfoxide (DMSO) as stock solutions. To obtain final assay concentrations, the stock solutions were diluted in DMEM (final concentration of DMSO was constant under all conditions, and always lower than 0.5%). The assay

was performed by a variation of the MTT assay described by Mosmann[81] as specified by Matito and coworkers,[82] which is based on the ability of live cells to cleave the tetrazolium ring of the MTT thus producing formazan, which absorbs at 550 nm. In brief, 3×10^3 cells per well were cultured in 96 well plates for 24 h prior to the addition of the different compounds at different concentrations, in triplicate (in the case of differentiated 3T3-L1 cells the compounds were added once the differentiation process was completed). After incubation for 72 h more, the supernatant was aspirated and 100 μL of filtered MTT (0.5 mg mL^{-1}) was added to each well. Following 1 h of incubation with the MTT, the supernatant was removed and the precipitated formazan was dissolved in 100 μL of DMSO. Relative cell viability, compared to the viability of untreated cells, was measured by absorbance at 550 nm on an ELISA plate reader (Tecan Sunrise MR20-301, TECAN, Salzburg, Austria). Concentrations that inhibited cell growth by 50% (IC_{50}) after 72 h of treatment were subsequently calculated using Graphpad Prism 6 software.

A549 transfection with the FOXO3a-GFP reporter plasmid

A549 cells were seeded in 6 well plates containing cover slips (so that the cells would grow on the surface of the cover slips). When confluence reached 80%, a mix containing 200 μL media, 2 μg of the GFP-FOXO3a reporter plasmid and 2 μL of X-tremeGENE HP (Roche) was incubated for 30 minutes and added to each well. 6 hours later media was changed in all the wells and replaced with media containing the products of interest at the specified concentrations, and after 6 hours of incubation the FOXO translocation assay was performed.

FOXO translocation assay

24 hours after seeding U2foxRELOC cells in 6 well plates containing cover slips (30 h after transfection in the case of A549 cells) the medium was changed in all the wells and replaced with a medium containing the products of interest at the specified concentrations. After 6 hours of incubation, the medium was again replaced with a fresh medium containing 1 μM CellTracker Red (Invitrogen). After 10 minutes, all the medium was removed and the cover slides containing the cells were washed 3×5 min with PBS, fixed with paraformaldehyde for 15 minutes and washed again 3×5 min with phosphate buffered saline (PBS) containing 20 mM glycine. The cover slips were then mounted on slides using 20 μL of ProLong Gold (Invitrogen). After 16 h, the slides were analyzed using a TCS SPE Leica confocal microscope and the intensity of the GFP fluorescence in nuclei and the cytoplasm for a minimum of 50 random cells per condition was measured using ImageJ software.

Preparation of total protein extracts

A549 cells (3×10^5 cells) were cultured in 6-well plates and, 24 h after seeding, were treated for 6 h (for AKT-P and PRAS40-P analysis) or 24 h (for cytochrome C, procaspase 9, procaspase 3 and PARP analysis) with the products of interest at the specified concentrations. After treatment the cells were washed twice with ice-cold PBS and then scrapped and resuspended in lysis buffer containing 20 mM Trizma Base (pH 7.5), 1 mM dithriothreitol, 1 mM EDTA, 0.0002% triton X-110 (SIGMA), 0.5 mM sodium deoxycholate, 0.4 mM PMSF, 1% protease inhibitor cocktail (SIGMA) and 1% phosphatase inhibitor cocktail (Thermo Scientific). The samples were sonicated, incubated on ice for 20 min and centrifuged at 16 000*g* for 10 min at 4 °C. The pellets were discarded, and the supernatants containing the protein extracts were assayed for protein concentration using a BCA kit (Pierce Biotechnology, Rockford).

Preparation of cytosolic protein extracts

A549 cells (3×10^5 cells) were cultured in 6-well plates and, 24 h after seeding, were treated for 6 h with the products of interest at the specified concentrations. After treatment, A549 cells were washed twice with ice-cold PBS and lysed in ice-cold hypotonic buffer containing 20 mM HEPES (pH 7.6), 10 mM NaCl, 1.5 mM $MgCl_2$, 0.2 mM EDTA, 20% (v/v) glycerol, 0.1% (v/v) triton X-100 (SIGMA), 1% protease inhibitor cocktail (SIGMA) and 1% phosphatase inhibitor cocktail (Thermo Scientific). After incubation on ice for 10 min, cells were scrapped and pipetted into a cold eppendorf tube and then centrifuged at 1000 rpm at 4 °C. The resulting supernatant was the cytoplasmic extract, which was assayed for protein concentration using a BCA kit (Pierce Biotechnology, Rockford). The pellet contained the nuclei.

Preparation of nuclear protein extracts

The nuclei pellet obtained after centrifugation was resuspended in five times its volume of hypertonic buffer (hypotonic buffer plus 500 mM NaCl), rocked for one hour at 4 °C and then spinned at maximum speed (13 000 rpm) at 4 °C for 5 min. The resulting supernatant was the nuclear extract, which was assayed for protein concentration using a BCA kit (Pierce Biotechnology, Rockford).

Western blot analysis

For the western-blot analysis, 20 μg of protein were loaded on a 10% SDS-polyacrylamide gel and transferred to a polyvinyl nitrocellulose transfer membrane (Bio-Rad Laboratories). The membranes were blocked by incubation in TBS buffer (20 mM Tris (pH 7.5) and 132 mM NaCl) containing 0.1% of Tween and 5% dry milk for 1 h, at room temperature, and washed three times with TBS–0.1% Tween. Then, membranes were blotted with the primary antibodies overnight at 4 °C. After primary antibody incubation, the blots were washed three times with TBS–0.1% Tween and incubated with the appropriate secondary antibody for 1 h at room temperature. After secondary antibody incubation, membranes were washed again three times with TBS–0.1% Tween before protein detection. All blots were treated with the Immobilon ECL Western Blotting Detection Kit Reagent (Millipore) and developed after exposure to an autoradiography film in a film cassette. The primary antibodies used were Akt-P, procaspase 3 and procaspase 9 (from Cell Signalling), FOXO3a (from Upstate), Erk-2 and Lamin B (from Santa Cruz), PRAS40-P (from Biosource), PARP (from Pharmingen) and actin (from MP Biomedicals).

Cell cycle analysis

The cell cycle was assessed by flow cytometry using a fluorescence-activated cell sorter (FACS). 3×10^4 A549 cells or 2×10^4 NCI-H460 cells per well were seeded in 6 well plates with 2 mL of medium. After 24 h, the products were added at their respective concentrations. Following 24, 48 and 72 h of incubation, cells were harvested by mild trypsinization, collected by centrifugation and resuspended in Tris-buffered saline (TBS) containing 50 mg mL^{-1} PI, 10 mg mL^{-1} DNase-free RNase and 0.1% Igepal CA-630 (SIGMA). The cell suspension was incubated for 1 h at room temperature to allow for the staining of the cells with the PI, and afterwards FACS analysis was carried out at 488 nm in an Epics XL flow cytometer (Coulter Corporation, Hialeah, FL). Data from 1×10^4 cells were collected and analyzed using the Multicycle software (Phoenix Flow Systems, San Diego, CA).

Apoptosis assay

Apoptosis was assessed evaluating the annexin-V binding to phosphatidylserine (PS), which is externalized early in the apoptotic process. 3×10^4 A549 cells or 2×10^4 NCI-H460 cells per well were seeded in 6 well plates with 2 mL of medium and treated as described above for the cell cycle analysis assay. After cell collection and centrifugation, cells were resuspended in 95 μL binding buffer containing 10 mM HEPES/NaOH (pH 7.4) 140 mM NaCl, and 2.5 mM $CaCl_2$. 3 μL of Annexin-V FITC conjugate (1 mg mL^{-1}) were then added and the suspension was incubated in darkness for 30 min, at room temperature. Just before FACS analysis, the cell suspension was added to a vial containing 500 μL of binding buffer, and then stained with 20 μL of 1 mg mL^{-1} PI solution. Data from 1×10^4 cells were collected and analyzed.

Comet assay

For this assay, 3×10^4 A549 cells per well were seeded in 6 well plates with 2 mL of medium. After 24 h, the medium was replaced with a medium containing the products at their respective concentrations. Following 24 h of incubation, cells were harvested by mild tripsinization, collected by centrifugation and resuspended in PBS before the comet assay was carried out. The technique described by Singh *et al.*[83] and Tice *et al.*[84] was followed with some modifications. 70 μL of 0.5% agarose-LMP containing around 5×10^4 cells were distributed quickly on 1% agarose-coated slides. A cover slip was added and the agarose was allowed to set for 10 min on ice before the cover slip was removed. The cells were then lysed immediately by immersion of the slide in a cold solution (pH 10.5) of 2.5 M NaCl, 100 mM Na_2EDTA, 10 mM Trizma-HCl and 1% triton X-100 for 1 h. After that, the slides were placed on a horizontal gel electrophoresis platform and covered with an alkaline solution made up of 300 mM NaOH and 1 mM Na_2EDTA. The slides were left in the solution for 20 min to allow unwinding of the DNA and expression of alkali-labile sites. The power supply was then set at 0.7 V cm^{-1} (300 mA), the DNA was electrophoresed for 15 min and the slides were rinsed gently three times with 400 mM Trizma (pH 7.5) to neutralize the excess alkali. Each slide was stained with 20 μL of GelGreen (Biotium), covered with a cover slip and coded before microscopic analysis. A minimum of 100 random GelGreen-stained nuclei per condition were evaluated using a Leica DMIRB fluorescence microscope. The diameter of each DNA circular head and the total length of the comet (including the tail when DNA damage had occurred) were measured using ImageJ software.

Synergy study

A549 cells were treated with both compounds (cisplatin and **6a**) at the same time, following the same procedure as in the cell viability assays. The compounds were added at different concentrations, but the relationship between the concentrations of both products was kept constant (in this case, cisplatin concentration was always 3 times higher than **6a** concentration). After evaluating the effect of the combined treatment over A549 cells' viability using the MTT assay, results were introduced in Calcusyn software, which was used to calculate the CI (Combination Index) for each treatment. A CI value below 1 indicates a synergy in the measured effect of both products at the related concentrations.

Acknowledgements

This work was supported by the *Ministerio de Ciencia e Innovación* of Spain {grant numbers CTQ2009-11501, CTQ2009-07021 (both within the subprogram BQU) and SAF2011-25726}, FEDER Funds, the *Instituto de Salud Carlos III* and *European Regional Development Fund* (ISCIII-RTICC, RD06/0020/0046), the *Generalitat de Catalunya* (2009SGR-1308, 2009SGR-1111), 2009 CTP 00026, the European Commission (FP7) grants METAFLUX (PITN-GA-2010-264780), SYNERGY (no. FP7-ICT-2009-270086) and COSMOS research infrastructures grant (no. 312941), and the Icrea Academia award 2010 (granted to M. Cascante).

The authors would like to thank Dr Atanasio Pandiella, of the *Centro de Investigación del Cáncer* (CIC), Salamanca, Spain.

Notes and references

1 A. Jemal, R. Siegel, E. Ward, Y. Hao, J. Xu and M. J. Thun, *Ca-Cancer J. Clin.*, 2009, **59**, 225–249.
2 J. R. Molina, P. Yang, S. D. Cassivi, S. E. Schild and A. A. Adjei, *Mayo Clin. Proc.*, 2008, **83**, 584–594.
3 C. P. Belani, G. Goss and G. Blumenschein, *Cancer Treat. Rev.*, 2012, **38**, 173–184.
4 A. Custodio and J. de Castro, *Crit. Rev. Oncol. Hematol.*, 2012, **82**, 338–360.
5 G. Des Guetz, B. Uzzan, P. Nicolas, D. Valeyre, G. Sebbane and J.-F. Morere, *Crit. Rev. Oncol. Hematol.*, 2012, **84**, 340–349.
6 P. K. Koh, C. Faivre-Finn, F. H. Blackhall and D. De Ruysscher, *Cancer Treat. Rev.*, 2012, **38**, 626–640.
7 A. G. Pallis and K. Syrigos, *Cancer Treat. Rev.*, 2012, **38**, 861–867.

8 E. Quoix, *Ther. Adv. Med. Oncol.*, 2012, **4**, 247–254.
9 N. Saijo, *Cancer Treat. Rev.*, 2012, **38**, 194–202.
10 A. M. Thayer, *Chem. Eng. News*, 2010, **88**, 24–28.
11 D. W. Shen, L. M. Hall and M. Gottesman, *Pharmacol. Rev.*, 2012, **64**, 706–721.
12 R. Kaushal, N. Kumar, R. Kaushal and P. Awasthi, *Int. J. Curr. Res. Rev.*, 2011, **3**, 15–23.
13 Y. Wang, L. V. Juan, X. Ma, D. Wang, H. Ma, Y. Chang, G. Nie, L. Jia, X. Duan and X.-J. Liang, *Curr. Drug Metab.*, 2010, **11**, 507–515.
14 G. Sava, A. Bergamo and P. J. Dyson, *Dalton Trans.*, 2011, **40**, 9069–9075.
15 S. H. van Rijt and P. J. Sadler, *Drug Discovery Today*, 2009, **14**, 1089–1097.
16 S. J. Berners-Price, *Angew. Chem., Int. Ed.*, 2011, **50**, 804–805.
17 N. J. Farrer, J. A. Woods, L. Salassa, Y. Zhao, K. S. Robinson, G. Clarkson, F. S. Mackay and P. J. Sadler, *Angew. Chem., Int. Ed.*, 2010, **49**, 8905–8908.
18 S. Dhar and S. J. Lippard, in *Current Status and Mechanism of Action of Platinum-Based Drugs in Bioinorganic Medicinal Chemistry*, ed. E. Alessio, Wiley-VCH, 2011, ch. 3, pp. 79–95.
19 X. Wang and Z. Guo, *New Trends and Future Developments of Platinum-Based Antitumor Drugs in Bioinorganic Medicinal Chemistry*, ed. E. Alessio, Wiley-VCH, 2011, ch. 4, pp. 97–149.
20 U. Olszewski and G. Hamilton, *Anti-Cancer Agents Med. Chem.*, 2010, **10**, 320–332 and references therein.
21 A. L. Noffke, A. Habtemariam, A. M. Pizarro and P. J. Sadler, *Chem. Commun.*, 2012, **48**, 5219–5246, and references therein.
22 J. Alemán, V. del Solar, A. Alvarez-Valdés, C. Ríos-Luci, J. M. Padrón and C. Navarro-Ranninguer, *MedChemComm*, 2011, **2**, 789–793, and references therein.
23 L. Cubo, M. Groessl, P. J. Dyson, A. G. Quiroga, C. Navarro-Ranninguer and A. Casini, *ChemMedChem*, 2010, **5**, 1335–1343.
24 E. I. Montero, J. Zhang, J. J. Moniodis, S. J. Berners-Price and N. Farrell, *Chem.–Eur. J.*, 2010, **16**, 9175–9185.
25 E. Wexselblatt and D. Gibson, *J. Inorg. Biochem.*, 2012, **117**, 320–329.
26 C. S. Matos, A. L. M. B de Carvalho, R. P. Lopes and M. P. M. Marques, *Curr. Med. Chem.*, 2012, **19**, 4678–4687.
27 P. Zhang, Y. Yang and Z. Shen, *Mini-Rev. Med. Chem.*, 2013, **13**, 265–272.
28 I. Kostova, *Front. Anti-Cancer Drug Discovery*, 2010, **1**, 298–339.
29 B. N. Chaudhari, P. S. Gide, R. S. Kankate, Z. J. Jain and R. D. Kakad, *Int. J. Pharm. Chem.*, 2012, **2**, 27–35.
30 L. Trynda-Lemiesz and U. Sliwinska-Hill, *J. Oncol.*, 2011, **61**, 465–474.
31 E. Wexselblatt, E. Yavin and D. Gibson, *J. Inorg. Biochem.*, 2012, **117**, 220–229.
32 A. G. Quiroga, *Curr. Top. Med. Chem.*, 2011, **11**, 2613–2622.
33 M. Galanski and B. K. Keppler, *Drug Delivery Oncol.*, 2012, **3**, 1605–1629.
34 J. Ruíz, V. Rodríguez, C. de Haro, A. Espinosa, J. Pérez and C. Janiak, *Dalton Trans.*, 2010, **39**, 3290–3301.
35 I. M. El-Mehasseb, M. Kodaka, T. Okada, T. Tomohiro, K. Okamoto and H. Okuno, *J. Inorg. Biochem.*, 2001, **84**, 157–158.
36 T. Okada, I. M. El-Mehasseb, M. Kodaka, T. Tomohiro, K. Okamoto and H. Okuno, *J. Med. Chem.*, 2001, **44**, 4661–4667.
37 J. Ruiz, V. Rodríguez, N. Cutillas, A. Espinosa and M. J. Hannon, *J. Inorg. Biochem.*, 2011, **105**, 525–531.
38 G. L. Edwards, D. S. C. Black, G. B. Deacon and L. P. G. Wakelin, *Can. J. Chem.*, 2005, **83**, 980–989.
39 H. Samouei, M. Rashidi and F. W. Heinemann, *J. Organomet. Chem.*, 2011, **696**, 3764–3771.
40 P. Wang, C.-H. Leung, D.-L. Ma, R. W.-Y. Sun, S.-C. Yan, Q.-S. Chen and C.-M. Che, *Angew. Chem., Int. Ed.*, 2011, **50**, 2554–2558.
41 D.-L. Ma and C.-M. Che, *Chem.–Eur. J.*, 2003, **9**, 6133–6144.
42 R. Cortés, M. Crespo, L. Davin, R. Martín, J. Quirante, D. Ruiz, R. Messeguer, C. Calvis, L. Baldomà, J. Badia, M. Font-Bardía, T. Calvet and M. Cascante, *Eur. J. Med. Chem.*, 2012, **54**, 557–566.
43 *Ferrocene Ligands, Materials and Biomolecules*, ed. P. Stepnicka, Wiley-VCH, Weinheim (Germany), 2008.
44 G. Jaouen, *Bioorganometallics. Biomolecules. Labelling, Medicine*, Wiley-VCH, Weinheim (Germany), 2006.
45 R. van Stavaren and N. Metzler-Nolte, *Chem. Rev.*, 2004, **104**, 5931–5986.
46 D. Dive and C. Biot, *ChemMedChem*, 2008, 3383–3391.
47 E. A. Hillard, A. Vessieres, G. Jaouen and S. Top, *Organometallics*, 2010, **32**, 81–117.
48 J. Quirante, F. Dubar, A. González, C. López, M. Cascante, R. Cortes, I. Forfar, B. Pradines and C. Biot, *J. Organomet. Chem.*, 2011, **696**, 1011–1017.
49 Y. L. K. Tan, P. Pigeon, S. Top, E. Labbé, O. Buriez, E. A. Hillard, A. Vessières, C. Amatore, W. K. Leong and G. Jaouen, *Dalton Trans.*, 2012, **41**, 7537–7549.
50 A. Mooney, A. J. Corry, C. N. Ruairc, T. Mahgoub, D. O'Sullivan, N. O'Donovan, J. Crown, S. Varughese, S. M. Draper, D. K. Rai and P. T. M. Kenny, *Dalton Trans.*, 2010, **39**, 8228–8239.
51 S. J. Harland, I. E. Smith, N. Smith and D. L. Alison, in: *Platinum Coordination Complexes in Cancer Chemotherapy*, ed. M. P. Hacker, E. B. Douple and I. H. Krakoff, Martinus Nihoff, Boston, 1984.
52 V. Scarcia, A. Fulrani, B. Longato, B. Corain and G. Pilloni, *Inorg Chim. Acta*, 1988, **153**, 67–70.
53 E. Fourie, E. Erasmus, J. C. Swarts, A. Jakob, H. Lang, G. Joone and C. E. J. van Rensburg, *Anticancer Res.*, 2011, **31**, 825–830.
54 J. Schulza, A. K. Renfrewb, I. Císařová, P. J. Dyson and P. Štěpnička, *Appl. Organomet. Chem.*, 2010, **24**, 392–397.
55 R. W. Mason, K. McGrouther, P. R. R. Ranatunge-Bandarage, B. H. Robinson and J. Simpson, *Appl. Organomet. Chem.*, 1999, **13**, 163–173.
56 D. Nieto, A. M. González-Vadillo, S. Bruña, C. J. Pastor, C. Ríos-Lucia, L. G. León, J. M. Padrón, C. Navarro-Ranninger and I. Cuadrado, *Dalton Trans.*, 2012, **41**, 432–441.
57 E. W. Neuse, M. G. Meirim and N. F. Bloom, *Organometallics*, 1988, **7**, 2562–2565.

58 J. Rajput, J. R. Moss, A. T. Hutton, D. T. Hendricks, C. E. Arendse and C. Imrie, *J. Organomet. Chem.*, 2004, **689**, 1553–1568.
59 D. Talancón, C. López, M. Font-Bardía, T. Calvet, J. Quirante, C. Calvis, R. Messeguer, R. Cortés, M. Cascante, L. Baldomà and J. Badia, *J. Inorg. Biochem.*, 2013, **118**, 1–12.
60 J. Albert, R. Bosque, M. Crespo, J. Granell, C. López, R. Cortés, A. Gonzalez, J. Quirante, C. Calvis, R. Messeguer, L. Baldomà, J. Badia and M. Cascante, *Bioorg. Med. Chem.*, 2013, **21**, 4210–4217.
61 S. F. De Mattos, P. Villalonga, J. Clardy and E. W.-F. Lam, *Mol. Cancer Ther.*, 2008, **7**, 3237–3246.
62 Y. Koo, K. W. Muir and E. W.-F. Lam, *Biochim. Biophys. Acta, Gene Regul. Mech.*, 2012, **1819**, 28–37.
63 H. Tran, A. Brunet, E. C. Griffith and M. E. Greenberg, *Sci. STKE*, 2003, re5.
64 Y. Zhang, B. Gan, D. Liu and J. H. Paik, *Cancer Biol. Ther.*, 2011, **12**, 253–259.
65 T. B. Dansen and B. M. Burgering, *Trends Cell Biol.*, 2008, **18**, 421–429.
66 X. Zhang, N. Tang, T. J. Hadden and A. K. Rishi, *Biochim. Biophys. Acta*, 2011, **1813**, 1978–1986.
67 H. Daitoku, J. Sakamaki and A. Fukamizu, *Biochim. Biophys. Acta*, 2011, **1813**, 1954–1960.
68 G. Tzivion, M. Dobson and G. Ramakrishnan, *Biochim. Biophys. Acta*, 2011, **1813**, 1938–1945.
69 J. Y. Yang and M. C. Hung, *Clin. Cancer Res.*, 2009, **15**, 752–757.
70 F. Zanella, A. Rosado, B. Garcia, A. Carnero and W. Link, *ChemBioChem*, 2008, **9**, 2229–2237.
71 W. Link, J. Oyarzabal, B. G. Serelde, M. I. Albarran, O. Rabal, A. Cebria, P. Alfonso, J. Fominaya, O. Renner, S. Peregrina, D. Soilan, P. A. Ceballos, A. I. Hernandez, M. Lorenzo, P. Pevarello, T. G. Granda, G. Kurz, A. Carnero and J. R. Bischoff, *J. Biol. Chem.*, 2009, **284**, 28392–28400.
72 F. Zanella, A. Rosado, B. Garcia, A. Carnero and W. Link, *BMC Cell Biol.*, 2009, **10**, 14.
73 S. Pérez, C. López, A. Caubet, X. Solans and M. Font-Bardía, *New J. Chem.*, 2003, **27**, 975–982.
74 A. Eijkelenboom and B. M. Burgering, *Nat. Rev. Mol. Cell Biol.*, 2013, **14**, 83–97.
75 P. F. Dijkers, R. H. Medema, C. Pals, L. Banerji, N. S. Thomas, E. W. Lam, B. M. Burgering, J. A. Raaijmakers, J. W. Lammers, L. Koenderman and P. J. Coffer, *Mol. Cell. Biol.*, 2000, **20**, 9138–9148.
76 M. Schmidt, S. Fernandez de Mattos, A. van der Horst, R. Klompmaker, G. J. Kops, E. W. Lam, B. M. Burgering and R. H. Medema, *Mol. Cell. Biol.*, 2002, **22**, 7842–7852.
77 T. T. Tang, D. Dowbenko, A. Jackson, L. Toney, D. A. Lewin, A. L. Dent and L. A. Lasky, *J. Biol. Chem.*, 2002, **277**, 14255–14265.
78 P. F. Dijkers, R. H. Medema, J. W. Lammers, L. Koenderman and P. J. Coffer, *Curr. Biol.*, 2000, **10**, 1201–1204.
79 D. L. Bratton, E. Dreyer, J. M. Kailey, V. A. Fadok, K. L. Clay and P. M. Henson, *J. Immunol.*, 1992, **148**, 514–523.
80 A. K. Hammill, J. W. Uhr and R. H. Scheuermann, *Exp. Cell Res.*, 1999, **251**, 16–21.
81 T. Mosmann, *J. Immunol. Methods*, 1983, **65**, 55–63.
82 C. Matito, F. Mastorakou, J. J. Centelles, J. L Torres and M. Cascante, *Eur. J. Nutr.*, 2003, **42**, 42–49.
83 N. P. Singh, M. T. McCoy, R. R. Tice and E. L. Schneider, *Exp. Cell Res.*, 1988, **175**, 184–191.
84 R. R. Tice, E. Agurell, D. Anderson, B. Burlinson, A. Hartmann, H. Kobayashi, Y. Miyamae, E. Rojas, J. C. Ryu and Y. F. Sasaki, *Environ. Mol. Mutagen.*, 2000, **35**, 206–221.

CAPÍTULO 03

EL ESTUDIO DE LA REPROGRAMACIÓN METABÓLICA DE CÉLULAS DE CÁNCER DE PULMÓN REVELA UNA DEPENDENCIA DE LA GLUTAMINA QUE PUEDE SER EXPLOTADA EN EL DISEÑO DE NUEVAS TERAPIAS ANTITUMORALES

CAPÍTULO 03

EL ESTUDIO DE LA REPROGRAMACIÓN METABÓLICA DE CÉLULAS DE CÁNCER DE PULMÓN REVELA UNA DEPENDENCIA DE LA GLUTAMINA QUE PUEDE SER EXPLOTADA EN EL DISEÑO DE NUEVAS TERAPIAS ANTITUMORALES

Roldán Cortés[1], Enric Milà[1], Concepción López[2], Josefina Quirante[3], Vitaly Selivanov[1], Silvia Marín[1], Marta Cascante[1, 4].

[1] Departament de Bioquímica i Biologia Molecular, Facultat de Biologia, Unidad Asociada al CSIC, Diagonal 643, 08028 Barcelona, España

[2] Departament de Química Inorgànica, IBUB, Universitat de Barcelona, Diagonal 645, 08028 Barcelona, España

[3] Departament de Farmacologia I Química Terapèutica, Facultat de Farmàcia, IBUB, Universitat de Barcelona, Av. Joan XXIII s/n, 08028 Barcelona, España.

[4] Institut d'Investigacions Biomediques August Pi i Sunyer (IDIBAPS), Barcelona, España

Resumen

El bajo índice de supervivencia a cinco años del cáncer de pulmón lo convierte en la causa más común de muerte por cáncer a nivel mundial. Los tratamientos actuales, muchos de los cuales utilizan quimioterapia basada en compuestos de platino, se caracterizan por una gran heterogeneicidad tanto en términos de eficacia como de toxicidad, y en general su efectividad a largo plazo es muy limitada. El estudio de la reprogramación metabólica del cáncer de pulmón puede constituir una herramienta eficaz para detectar dianas enzimáticas sobre las que intervenir para bloquear las vías metabólicas que las células de cáncer necesitan para mantener una proliferación acelerada. En este estudio hemos combinados medidas bioquímicas clásicas con técnicas metabolómicas basadas en el uso de trazadores usando los sustratos marcados con ^{13}C [1,2-^{13}C]-glucosa y [3-^{13}C]-glutamina, con la intención de estudiar las diferencias en el metabolismo central entre las líneas de cáncer de pulmón mutadas en KRAS A549 y NCIH460 y la línea de pulmón no tumoral BEAS2B. Los resultados señalaron la existencia de una dependencia de la glutamina en ambas líneas tumorales, que fue confirmada por el efecto antiproliferativo selectivo del inhibidor de la glutaminasa BPTES. 1 μM de BPTEs fue suficiente para inhibir en un 50% la viabilidad de las células tumorales A549 y NCIH460, mientras que no se observaron efectos apreciables sobre la viabilidad de la línea no tumoral BEAS2B. Así, el estudio de la reprogramación metabólica tumoral nos ha permitido identificar una diana metabólica que puede ser explotada para inhibir la proliferación celular.

STUDY OF LUNG CANCER CELLS METABOLLIC REPROGRAMMING REVEALS A GLUTAMINE DEPENDANCE THAT CAN BE EXPLOITED IN THE DESIGN OF NEW THERAPIES

Roldán Cortés[1], , Enric Milà[1], Concepción López[2], Josefina Quirante[3], Vitaly Selivanov[1], Silvia Marín[1], Marta Cascante[1, 4].

[1] Departament de Bioquímica i Biologia Molecular, Facultat de Biologia, IBUB, University of Barcelona, Diagonal 643, 08028 Barcelona, Spain.

[2] Departament de Química Inorgànica, IBUB, Universitat de Barcelona, Diagonal 645, 08028 Barcelona, Spain

[3] Departament de Farmacologia I Química Terapèutica, Facultat de Farmàcia, IBUB, Universitat de Barcelona, Av. Joan XXIII s/n, 08028 Barcelona, Spain.

[4] Institut d'Investigacions Biomediques August Pi i Sunyer (IDIBAPS), Barcelona, Spain

KEYWORDS: Lung cancer, metabolic reprogramming, glutaminase, tracer-based metabolomics.

Abstract

Lung cancer's very low 5-year survival rate makes it the most common cause of cancer death worldwide. Current treatments, many of which use platinum-based chemotherapies, are characterized by great heterogeneity both in terms of efficacy and toxicity, and their long-term effectiveness is generally very limited. The study of lung cancer metabolic reprogramming can be an effective tool to detect enzymes to be targeted in order to block the metabolic pathways that cancer cells need to sustain their accelerated proliferation rates. In this study we have combined classical biochemical measurements and tracer-based metabolomics measurements using the ^{13}C labelled substrates [1,2-^{13}C]-glucose and [3-^{13}C]-glutamine, in order to study the differences in central metabolism between the KRAS-mutated lung cancer cell lines A549 and NCIH460, and the non-tumor lung cell line BEAS2B. Results indicated a strong glutamine dependence in both tumor cell lines, which was confirmed by the selective antiproliferative effect of the glutaminase inhibitor BPTES. 1 mM BPTES was enough to inhibit 50% of viability in A549 and NCIH460 tumor cell lines, with

no effect observed on the viability of the non-tumorl cell line BEAS2B. Thus, the study of lung cancer metabolic reprogramming has allowed us not only to identify a metabolic target to be exploited to impair tumor proliferation.

Introduction

Lung cancer is the most diagnosed cancer in males worldwide, and has risen to be the fourth most diagnosed cancer in women, too. The low survival rate associated with this disease, which is lower than 20%, make it the most common cause of cancer death worldwide, with almost 1.4 million casualties in 2008 alone (Jemal, Bray et al. 2011; Bray, Jemal et al. 2012).

The lower survival rate is associated with two main factors. First, most lung cancers are diagnosed at the symptomatic stage, in which the disease is already spread. At that point, most patients are already past their optimal therapy window and surgical treatment is no longer a viable option. Second, platinum-based chemotherapy, which remains the main option for more than 80% of patients diagnosed with advanced NSCLC, is characterized by great heterogeneity both in terms of efficacy and toxicity, and its long-term effectiveness is generally very limited, with platinum-treated patients exhibiting a median progression-free survival of three to seven months, and a median overall survival of less than one year (Bonanno, Favaretto et al. 2014). All these problems highlight the need to find new therapeutical targets that can be exploited in new treatments against lung cancer.. Cancer cell energy metabolism is significantly different from that of normal cells, and therefore the study of cancer cells metabolic reprogramming can help overcome this need identifying targets that can be exploited to inhibit cancer metabolic adaptations.

Lung cancer cells need to acquire a particular metabolic phenotype able to maintain the tumor cells' accelerated proliferation, which needs both energy and a constant supply of new biomolecules. Therefore, the metabolic differences found in tumor cells are not a passive consequence of the genomic, transcriptomic and proteomic changes that take place in cancer development, but rather an essential step that is required to acquire and maintain the tumor phenotype. One of the main hallmarks of cancer metabolic reprogramming is the activation of glycolysis, which is used instead of oxidative phosphorylation to produce energy even in normoxic conditions where the supply of oxygen is high enough. Besides this phenomenon, which receives the name of Warburg effect, more cancer metabolic alterations have been described through the years, including increased uptake and consumption of glucose and glutamine (McCracken and

Edinger 2013), increased glutaminolysis (Daye and Wellen 2012), and altered fatty acid metabolism (Biswas, Lunec et al. 2012).

Activating mutations of KRAS constitute the most common oncogenic alteration in lung cancer, specially between males, smokers and western hemisphere inhabitants (Cooper, Lam et al. 2013). KRAS is involved in different downstream signaling cascades, including the RAF/MEK/ERK and PI3K/AKT/mTOR pathways, and therefore plays a crucial role regulating proliferation, survival, and apoptosis, while also affecting metabolism predominantly through the upregulation of hypoxia-inducible factor 1α (HIF1α) (Chun, Johnson et al. 2010; Mucaj, Shay et al. 2012; Semenza 2013). Specifically, KRAS has been described to promote an increased expression of glucose transporters, upregulate the levels of glycolytic enzymes, promote the cells' glutamine dependence, promote the cells' folate metabolism dependence and regulate autophagy (Pylayeva-Gupta, Grabocka et al. 2011; Bryant, Mancias et al. 2014; Moran, Trusk et al. 2014). Besides, mutations in KRAS are a potential negative predictive marker for efficacy of epidermal growth factor receptor tyrosine kinase inhibitors (EGFR TKIs) like *erlotinib*, one of the standard treatments used in patients with non-small cell lung cancer (NSCLC) (Riely, Marks et al. 2009; Suda, Tomizawa et al. 2010; Koudelakova, Kneblova et al. 2013). Since EFGR is upstream of KRAS, its inactivation will not affect cells where mutated KRAS is constitutively activated regardless of EGFR signaling. Other agents targeting KRAS or its downstream pathways have been tested, and although some of them are in clinical trials so far none of them has been successful enough to be used in cancer therapy (Cardarella and Johnson 2013).Tracer-based metabolomics is a very effective tool to study the metabolic state of a biological system (Alcarraz-Vizan, Boren et al. 2010; Paul Lee, Wahjudi et al. 2010; Rodriguez-Prados, Traves et al. 2010). By adding a ^{13}C labeled substrate to the cells' growth medium, and by analyzing the ^{13}C label incorporation in different metabolites derived from that substrate, it is possible to infer the activity of the metabolic pathways and to establish maps for the metabolic fluxes. The ^{13}C-based metabolic flux maps are characteristic of each cancer cell line, and comparisons can be made between them. From these metabolic flux-fingerprint comparisons, the key players in the specific metabolic reprogramming of each cancer cell line can be identified.. Although there are metabolomics studies on the alterations associated with NSCLC metabolism, using very different techniques on biological fluids (Carrola, Rocha et al. 2011; Hori, Nishiumi et al. 2011; Rocha, Carrola et al. 2011; Niu, Jiang et al. 2012; Wen, Gao et al. 2013), tissues (Kami, Fujimori et al. 2013), animal models (Fan, Lane et al. 2011), or cell line models (Pirman, Efuet et al. 2013), to our knowledge there are no studies that focus on a thorough tracer-based metabolomics study of the differences in the metabolic fluxes of central metabolism between non-tumor and KRAS-mutated lung cancer cells.

Here we present a study on the specific differences between the metabolic pathways of two lung cancer KRAS-mutated cell lines (A549 and NCIH460) and a non-tumor lung cell line (BEAS2B). Using [1,2-^{13}C]-glucose and [3-^{13}C]-glutamine and Mass Isotopomer Distribution Analysis (MIDA), we characterized the metabolic flux reprogramming associated with KRAS mutated lung cancer, which allowed us to identify metabolic targets to be exploited in new therapeutic approaches.

Results and discussion

Differences in proliferation rates between A549, NCIH460 and BEAS2B cells

Since cancer metabolic reprogramming is related to the energetic and biosynthetic needs that are required for maintaining an improved proliferation rate, we first conducted a proliferation assay to see what was the growth speed of the tumor cell lines in comparison to the non-tumor one. As seen in **Figure 1A**, both A549 and NCIH460 tumor cell lines exhibit a faster proliferation rate compared to BEAS2B cell line. Between the tumor cells, NCIH460 cells (which are derived from large cell carcinoma, often characterized by its high growth speed) duplicate faster than A549 cells (derived from adenocarcinoma).

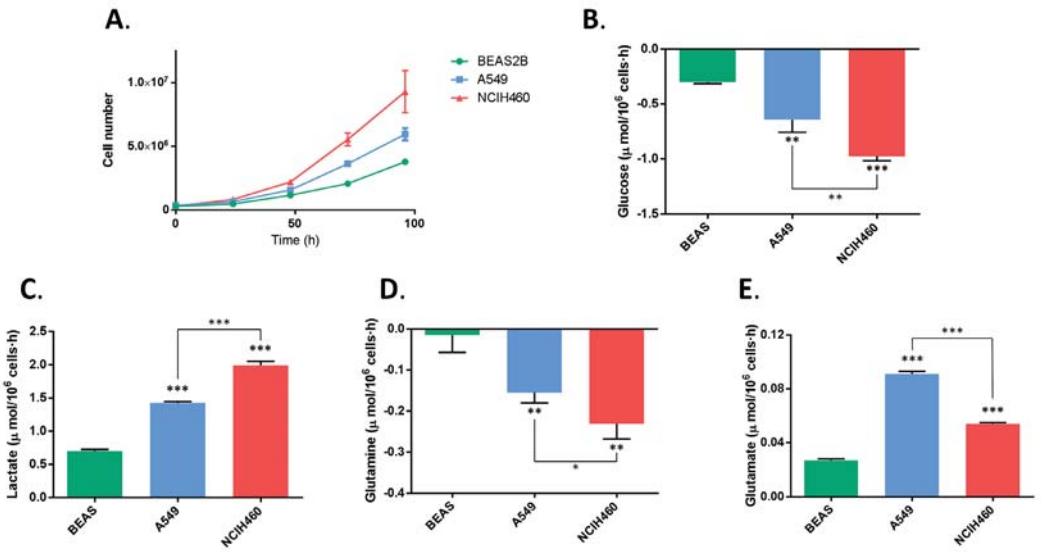

FIGURE 1. Proliferation (A), Glucose consumption (B), lactate production (C), glutamine consumption (D), and glutamate production (E) measurements for BEAS2B, A549 and NCIH460 cell lines. Biochemical measurements are from culture media after 24 h incubation, and their values are expressed as micromoles consumed/produced by one million cells per hour. Asterisks indicate where changes in production/consumption with regards to BEAS2B cells are statistically significant according to an unpaired t test (differences were considered significant when $p < 0.05$[*], $p < 0.01$ [**], or $p < 0.001$[***]).

Differences in nutrient consumption patterns and production of metabolites between A549, NCIH460 and BEAS2B cells

Glucose and glutamine consumption and lactate and glutamate production were measured in A549, NCIH460 and BEAS2B cell lines in order to evaluate if their rates were different in the KRAS-mutated lung tumor cell lines (A549 and NCIH460) in comparison to the non-tumor lung cell line BEAS2B.

As shown on **Figure 1B-C**, both tumor cell lines consume more glucose and produce more lactate than BEAS2B cells. This fact indicates that glycolyisis is enhanced in both cancer cell lines with regards to non-tumor BEAS2B cells. Furtermore, glutamine consumption (Figure 1D) and glutamate production (Figure 1E) are also strongly increased in KRAS-mutated tumor cells. The changes are always more dramatic for NCIH460 cells, with the exception of glutamate production which is higher for A549 cells. The glutamine consumption of the non-tumor lung cells (BEAS2B) is, like their glutamate production, very low. This suggests that the metabolism of non-tumor BEAS2B cells may be less dependant on glutamine than the metabolism of both KRAS mutated tumor cells.

^{13}C assisted metabolomics using [1,2-^{13}C]-glucose

Given the clear differences in the metabolism of glucose detected between the tumor and non-tumor cell lines, we sought to explore the fate of the carbons of glucose substrate, which have the potential to point out which are the main differences in the metabolic pathways preferently used in each cell line. To this end, we cultured BEAS2B, A549 and NCIH460 cells in the presence of 50% [1,2-^{13}C]-glucose, and the mass isotopomer distribution of several metabolites was analyzed by GC-MS (see raw data in **Appendix 1**) .The amount of lactate produced from glucose can be estimated from the concentrations and the mass isotopomer distribution of lactate in cell culture media, assuming that during the incubation period with labeled glucose cells only produce (and do not consume) lactate. Mass isotopomer distribution of lactate *LacTot(m0,m1,m2,m3)* was multiplied by the final concentration of lactate *[Lac]* to obtain the absolute mass isotopomer distribution of total lactate in mM *[LacTot(m0,m1,m2,m3)] (mM)*. Lactate present in the cell culture media at the beginning of the incubation period does not contain ^{13}C, but it will contribute to the m0 pool of total lactate at the end of the incubation. Therefore, initial lactate concentration *[Lac]t=i* was subtracted from the concentration of total lactate m0 *[LacTot(m0)] (mM)* to obtain the produced lactate in mM that does not contain ^{13}C *[LacProd(m0)] (mM)*. The value of produced lactate that contains ^{13}C atoms *[LacProd(m1,m2,m3)] (mM)* coincides with the calculated

values *[LacTot(m1,m2,m3)] (mM)*. After subtracting initial lactate concentration from the concentration of total lactate m0, relative mass isotopomer distribution of produced lactate *LacProd(m0,m1,m2,m3) (%)* was recalculated.

From the obtained LacProd isotopomer distribution, the percentage of produced lactate that comes from glucose through direct glycolysis (glycolytic tax or GT), was calculated as follows:

$$GT = LacProd(m2)\ (\%) * 2 / Glc(m2)t{=}i\ (\%)$$

where *Glc(m2)t=i* is the percentage of [1,2-^{13}C]-glucose in the cell culture media at the beginning of the experiment. Next, the amount of lactate obtained from glucose $[Lac_{GLC}]$ was obtained by multiplying the GT by the produced lactate *[LacProd]* (obtained by substracting initial lactate concentration *[Lac]t=i* from final concentration of lactate *[Lac]*). $[Lac_{GLC}]/2$ indicates the amount of glucose that has been used to produce lactate $[Glc_{LAC}]$, and we can obtain the ratio of glucose that was used to produce lactate by dividing $[Glc_{LAC}]$ between the total amount of consumed glucose.

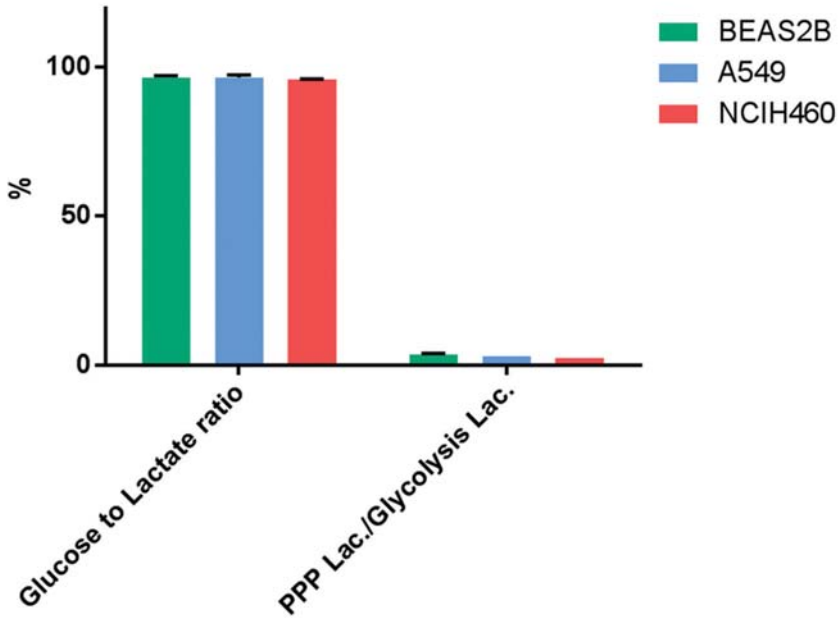

FIGURE 2. The % of glucose that is used to produce lactate (glucose to lactate ratio) is depicted for all three cell lines. The % of glucose-derived lactate that is produced through PPP related to the lactate that is produced through direct glycolisis (PPP Lac./Glycolisis Lac.) is also represented.

Results, shown in **Figure 2**, indicate that all three cell lines use the vast majority of glucose to produce lactate, suggesting that even the non-tumor cell line BEAS2B has high aerobic glycolysis rates. Initially this came as a surprise, but taking into account that BEAS2B is an inmortalyzed cell line (Reddel, Ke et al. 1988), the preferential use of glucose for aerobic glycolisis can be explained as a necessary metabolic adaptation associated to cell proliferation both in tumor and non-tumor cells.The relative amount of lactate metabolized through glycolysis related to the amount of lactate metabolized through the pentose phosphate pathway (PC-parameter) was calculated from the mass isotopomer distribution of total lactate, as follows:

$$PC = [LacTot(m1) / LacTot(m2)] / [3 + LacTot(m1) / LacTot(m2)]$$

The PC-parameter values obtained for each cell line are depicted in **Figure 2**. From the obtained results we can conclude that almost all lactate produced from glucose is metabolized through direct glycolysis in all three cell lines. A detailed description of the mathematical expression used to compute the PC-parameter from lactate isotopomer distributions can be found in Lee et al. 1998 (Lee et al., 1998).

The relatively low amount of glucose that is not used to produce lactate can enter into the TCA cycle through two major enzymes: pyruvate dehydrogenase (PDH), which converts pyruvate into acetyl-CoA, or pyruvate carboxylase (PC), which transforms pyruvate into oxaloacetate. Acetyl-CoA and oxaloacetate are combined in a reaction catalyzed by the enzyme citrate synthase that yields citrate, which is subsequently transformed into α-ketoglutarate, which is in equilibrium with glutamate. If a molecule of [1,2-$^{13}C_2$]-glucose enters into TCA cycle through PDH enzyme, it will yield [1,2-^{13}C]-acetyl-CoA, which will be eventually transformed into [4,5-$^{13}C_2$]-glutamate. On the other hand, if a molecule of [1,2-$^{13}C_2$]-glucose enters into TCA cycle through PC, it will yield [2,3-$^{13}C_2$]-glutamate. The relative contribution (%) of each pathway employed to enter glucose into TCA cycle can be assessed by analyzing the mass isotopomer distribution of glutamate molecule fragments C2-C4 and C2-C5 from cells cultured in the presence of [1,2-$^{13}C_2$]-glucose, using the following equations (Sanchez-Tena, Alcarraz-Vizan et al. 2013):

$$\%\ PC = Glu_{C2\text{-}C4}(m2) / Glu_{C2\text{-}C5}(m2)$$

$$\%\ PDH = (Glu_{C2\text{-}C5}(m2) - Glu_{C2\text{-}C4}(m2)) / Glu_{C2\text{-}C5}(m2)$$

Results, as shown in **Figure 3**, indicate that even if all cell lines prioritize the entrance into the TCA via PDH enzyme, in the lung cancer cell line A549 the entrance through PC is enhanced in comparison to BEAS2B non tumor cell line. PC activity is required

for glutamine-independent growth of tumor cells (Cheng, Sudderth et al. 2011), and therefore the reduced activity of PC in A549 cells with regards to BEAS2B cells could imply that A549 cells are more dependent on glutamine than BEAS2B cells.

The fraction of glucose that is not used in the production of lactate can be used to synthesize ribose. The need for ribose phosphate is enhanced in proliferating cells to sustain the synthesis of nucleic acids associated with cell duplication. Ribose phosphate is synthesized through the pentose phosphate pathway (PPP), which has two different branches: the oxidative branch and the non-oxidative one. When ribose is synthesized from [1,2-^{13}C]-glucose, it will incorporate one ^{13}C atom (in position 1) if it has been synthesized through the oxidative branch On the contrary, if ribose has been obtained through the non-oxidative branch in will incorporate two ^{13}C atoms in positions 1 and 2. Therefore, by comparing the relationship between the ribose m2 and m1 mass isotopomers distributions after incubation with [1,2-^{13}C]-glucose, we can study the relationship between the two branches (oxidative/non-oxidative) in each cell line.

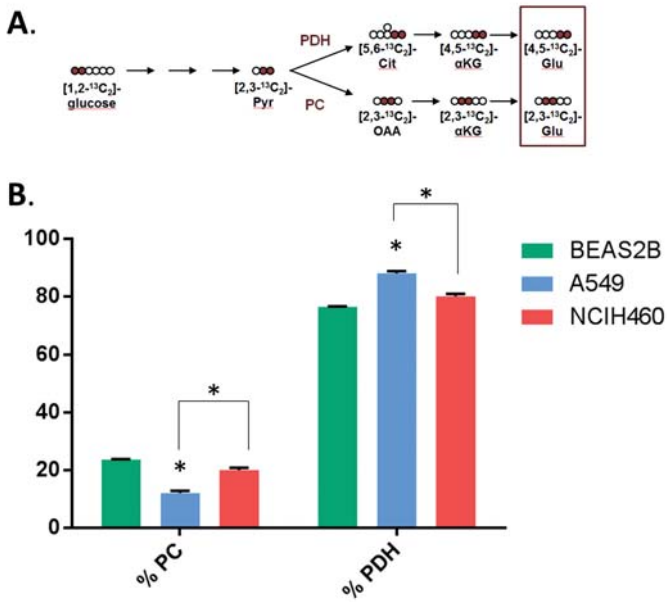

FIGURE 3. (A) Model depicting the ^{13}C label distribution after incubation with [1,2-$^{13}C_2$]-glucose. Pyr: pyruvate, Cit: citrate, αKG: α-ketoglutarate, Glu: glutamate, PDH: pyruvate dehydrogenase, PC: pyruvate carboxylase. (B) % PC indicates the % of glucose-derived glutamate that has been synthesized through the TCA cycle via pyruvate carboxylase. % PDH indicates the % of glucose-derived glutamate that has been synthesized through the TCA cycle via pyruvate dehydrogenase. Asterisks indicate where changes with regards to BEAS2B cells are statistically significant according to a unpaired t test (differences were considered significant when $p < 0.05$[*]).

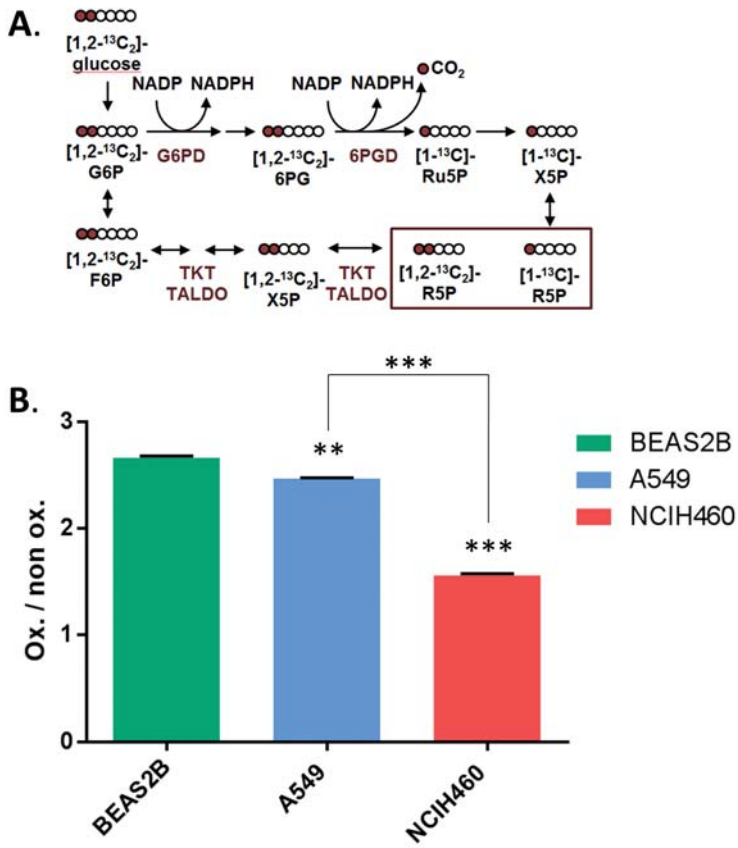

FIGURE 4. (A) Model depicting the ^{13}C label distribution after incubation with [1,2-$^{13}C_2$]-glucose. G6P: glucose-6-phosphate, 6PG: 6-phosphogluconate, Ru5P: ribulose-5-phosphate, X5P: xylulose-5-phosphate, F6P: fructose-6-phosphate, R5P: ribose-5-phosphate, G6PD: glucose-6-phosphate dehydrogenase, 6PGD: 6-phosphogluconate dehydrogenase, TKT: transketolase, TALDO: transaldolase. (B) Graphic depicting the ratio between the oxidative and the non-oxidative branches of the PPP. Asterisks indicate where changes with regards to BEAS2B cells are statistically significant according to a unpaired t test (differences were considered significant when $p < 0.01$ [**] or $p < 0.001$[***]).

A diagram on the ribose-label distribution expected when either oxidative or non-oxidative branches of PPP are followed is depicted in **Figure 4A**, and the results of the oxidative/ non-oxidative ratios obtained for each cell line are shown in **Figure 4B**. Results show that all three cell lines use mainly the oxidative branch of the pentose phosphate pathway to produce ribose from glucose. However, tumor cell lines A549 and especially NCIH460 give more preference to the non-oxidative branch, in comparison to the oxidative one. The non-oxidative branch of the PPP has been previously described as the main source for the gen-

eration of ribose for nucleotide synthesis within cancer cells (Boros, Puigjaner et al. 1997; Cascante, Centelles et al. 2000; Comin-Anduix, Boren et al. 2001). Transketolase and transketolase-like 1 enzymes (TKT and TKTL1) play a central role in this branch of the PPP. While TKT has been found to be increased in some tumor cells (Frederiks, Vizan et al. 2008) and decreased in some others (de Atauri, Benito et al. 2011), TKTL1 has been found to be overexpressed in a variety of tumors and correlates with aggressiveness in different carcinomas (Langbein, Zerilli et al. 2006; Staiger, Coy et al. 2006; Foldi, Stickeler et al. 2007; Krockenberger, Honig et al. 2007; Diaz-Moralli, Tarrado-Castellarnau et al. 2011). TKTL1 overexpression confers a moderate proliferative advantage to non-transformed cells (Hartmannsberger, Mack et al. 2011), while its silencing inhibits cell proliferation (Zhang, Yang et al. 2007). Our findings suggest that the non-oxidative branch of the pentose phosphate pathway also confers proliferative advantages to KRAS-mutated lung tumor cells.

^{13}C assisted metabolomics using [3-^{13}C]-glutamine

Given the clear differences detected between the cell lines in the metabolism of glutamine (with more glutamine consumed and glutamate produced in the tumor cell lines in comparison with BEAs2B), we sought to explore the fate of the carbons of glutamine substrate, which have the potential to point out which are the relationships between the main glutamine metabolic pathways in the studied cell lines. To this end, we cultured BEAS2B, A549 and NCIH460 cells in the presence of 100% [3-^{13}C]-glutamine, and the mass isotopomer distribution of several metabolites was also analyzed by GC-MS (see raw data in **Appendix 2**).After 24 hours incubation with [3-^{13}C]-glutamine almost all intracellular glutamate detected in BEAS2B cells is in the form of its m1 mass isotopomer, while the percentage of intracellular m1 glutamate is lower in both A549 and NCIH460 lung tumor cell lines (see **Figure 5A**). This points out that a certain intracellular accumulation of glutamate produced from glutamine exists in BEAS2B cells, while in both tumor cell lines the glutamate synthesized from glutamine (which is the one labelled with ^{13}C) could be diluted with glutamate produced from other sources, like α-ketoglutarate. Both tumor cell lines can use the glutamine to glutamate transformation to produce NH_3, which is needed in the synthesis of nitrogenous bases and therefore is very important in proliferating cells (Meng, Chen et al. 2010), and then expel the glutamine-derived glutamate from the cells, thus diminishing the percentage of glutamate m1 isotopomer. This would imply a higher glutamate concentration in the extracellular media, which is in accordance to the higher levels of glutamate found in the

media of both tumor cell lines.The percentage of aspartate and malate m1 mass isotopomers can provide us with information about the glutamine entrance in the TCA. As seen in **Figure 5B-C**, the percentage of m1 isotopomers for both molecules is fairly similar in all cell lines tested. Around 75-80% of aspartate and malate have one ^{13}C atom, which indicates that they have been generated from labelled glutamine. This points out how glutamine is the main source of carbons in the TCA cycle, which is consistent with our results showing how in all three lines tested glucose is mainly used to produce lactate. The percentage of the m1 mass isotopomers of aspartate and malate in A549 and NCIH460 cell lines is slightly lower than in BEAS2B cell line, indicating that a certain "dilution" of the label exists in the tumor cells. This result, which can also be observed for citrate (**Figure 5D**), suggests that a non-labelled carbon source is entering the TCA with a higher relative flux in tumor cells.

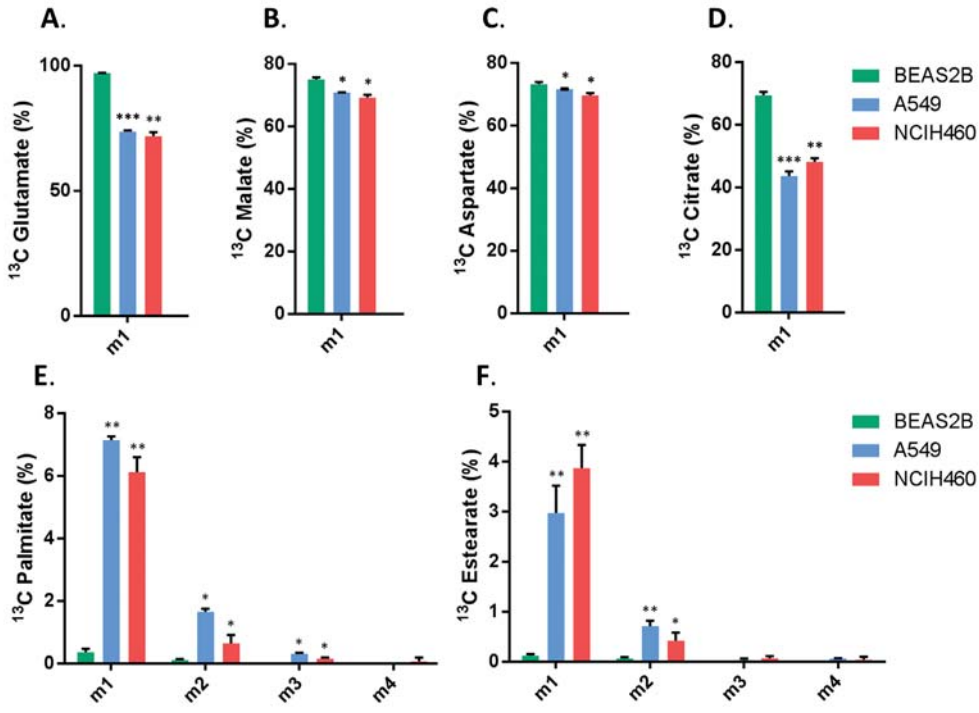

FIGURE 5. The % of m1 isotopomers (which indicate the presence of one ^{13}C atom in the molecule) after incubation of the cells with 100% [3-^{13}C]-glutamine is showed for (A) glutamate, (B) malate, (C) aspartate, and (D) citrate in all cell lines. E and F depict the % of the m1, m2, m3 and m4 mass isotopomers of palmitate and estearate, respectively. Asterisks indicate where changes with regards to BEAS2B cells are statistically significant according to a unpaired t test (differences were considered significant when $p < 0.05$[*], $p < 0.01$ [**], or $p < 0.001$ [***]).

Fatty acids like palmitate and stearate are needed to build the lipid membranes that surround cells and organelles. As **Figure 5E-F** shows, virtually no label from [3-^{13}C]-glutamine is found in BEAS2B cells' palmitate and stearate, but there is a significant amount of ^{13}C label in those fatty acids for both A549 and NCIH460 cells. Those mass isotopomer distributions indicate that in the tumor cell lines, glutamine is used as a carbon source to synthesize fatty acids. In order to be incorporated into newly synthesized fatty acids, the ^{13}C atom from the position 3 of the glutamine has to follow a specific pathway from glutamine to pyruvate, via ME (malic enzyme, see **Figure 6**)

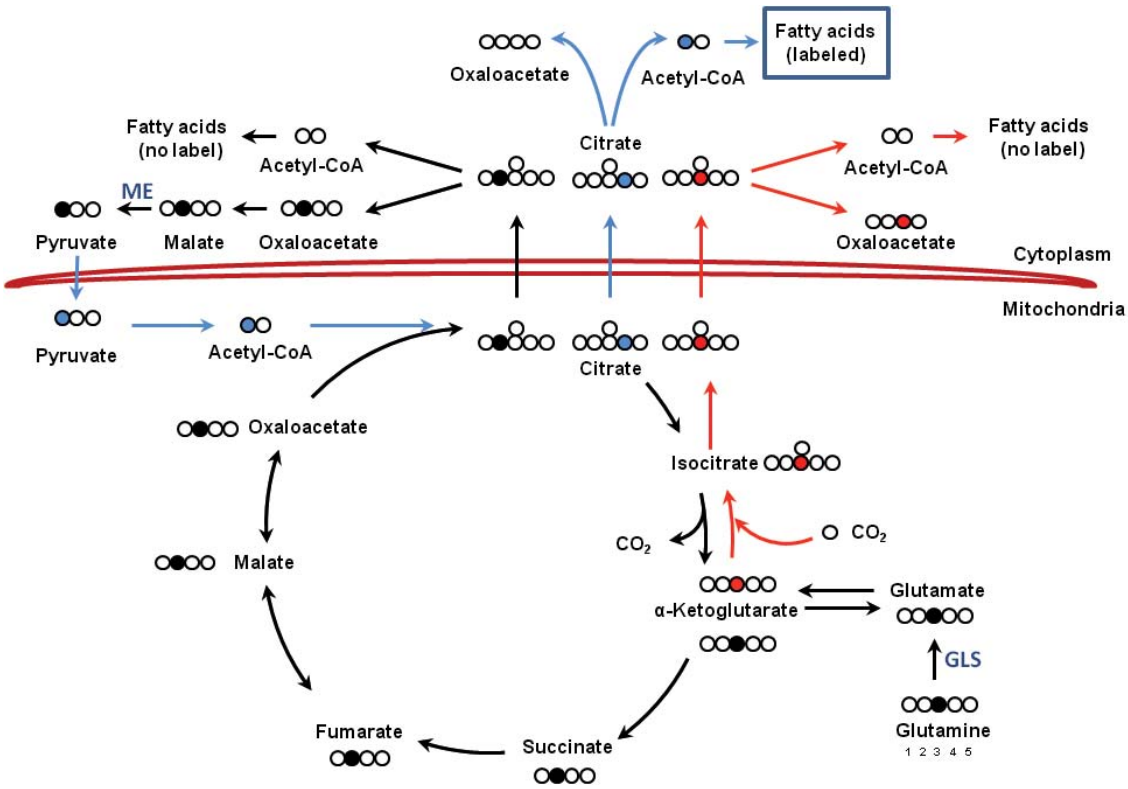

FIGURE 06. Graphic depicting the ^{13}C label distributon through central metabolism after incubation with [3-^{13}C]-glutamine. The ^{13}C label is not transferred from citrate to acetyl-CoA neither when it follows oxidative metabolism (black arrows and label) nor when it follows reductive metabolism (red arrows and label). If the citrate shuttle is active, oxaloacetate produced from citrate in the cytoplasm by the action of citrate lyase does incorporate the ^{13}C label, which can be transferred to malate and then to pyruvate in a reaction catalyzed by the malic enzyme (ME). This labelled pyruvate can reenter the TCA cycle (blue arrows and label) forming citrate, which via citrate lyase can now generate ^{13}C labelled acetyl-CoA and, through it, ^{13}C labelled fatty acids.

This glutaminolytic pathway implies the activation of the citrate shuttle, which exports citrate from the mitochondria to the cytoplasm, where it can be converted first to malate and then to pyruvate in a reaction catalyzed by malic enzyme (ME). In this reaction, ME also uses $NADP^+$ to generate NADPH, which is necessary to maintain the redox state of the cell and to synthesize fatty acids. Pyruvate generated from [3-^{13}C]-glutamine through this pathway can reenter the TCA cycle and be used to generate fatty acids enriched in ^{13}C from citrate. The activation of the citrate shuttle in conjunction with the malic enzyme forms a cycle in which pyruvate is converted to citrate in the mitochondria and citrate is converted to piruvate in the cytoplasm. This cycle eventually transfers the ^{13}C label from citrate to acetyl-coA, which explains the reduction of the m1 isotopomers of all TCA cycle intermediates, and especially of citrate, that was observed in both tumor cell lines. In pancreatic cancer cells, glutamine has been reported to follow a similar KRAS-mediated pathway in which glutamine-derived aspartate is transported to the cytoplasm and converted into pyruvate via oxalacetate and malate, increasing the NADPH/$NADP^+$ ratio (Son, Lyssiotis et al. 2013). Furthermore, our results showed how both A549 and NCIH460 cells make less use than BEAS2B cells of the oxidative-branch of the PPP, which is also used to generate NADPH. Therefore, it makes sense that ME activity in A549 and NCIH460 cells contributes to compensate this loss of PPP NADPH production through glutamine conversion into piruvate, especially when considering that both A549 and NCIH460 cells have higher proliferation rates than BEAS2B, and therefore demand a higher production of fatty acids. Using glutamine as a source for this production is also consistent with the tumor cell lines' increased glutamine consumption rate.Glutaminase inhibition as a new strategy to selectively impair KRAS-mutated lung cancer cells proliferation

The consumption of glutamine and the production of glutamate are remarkably higher in KRAS-mutated tumor cell lines A549 and NCIH460 than in non tumor cell line BEAS2B, and the ^{13}C assisted metabolomics experiments using [3-^{13}C]-glutamine hint at the existence of a fatty acid synthesis that relies on glutamine not only to generate NADPH, but also as a carbon source to synthesize palmitate and estearate. In sum, our results point out that the tumor cell lines A549 and BEAS2B exhibit a strong glutamine dependance with regards to the non-tumor cell line BEAS2B. This dependence on glutamine that KRAS-mutated cells exhibit seems a promising strategy to be exploited in therapy, and the fact that the increase in glutamate production observed in tumor cells correlates with an increase in glutamine consumption, point to glutaminase as a putative drug-target which could be specific for KRAS-mutated lung tumor cells. Having this in mind, we decided to check if the use of a glutaminase inhibitor, like bis-2-(5-phenylacetamido-1,3,4-thiadiazol-2-yl)ethyl sulfide (BPTES), could

selectively affect tumor cells proliferation. We incubated the three cell lines with different concentrations of BPTES for 72 hours, and then performed a cell viability assay with a HO33342 staining assay to see how the different concentrations of BPTES affected cell proliferation.

As shown in **Figure 7,** BPTES treatment clearly affects both A549 and NCIH460 tumor cell lines' viability, while the tested concentrations don't have a clear impact on non-tumor BEAS2B proliferation. IC_{50} values, which indicate the concentrations that inhibit cell viability by 50% with regards to the control condition, are in the low micromolar range for A549 and NCIH460, but the maximum concentration tested (50 µM) didn't affect BEAS viability enough to define an IC_{50} value.

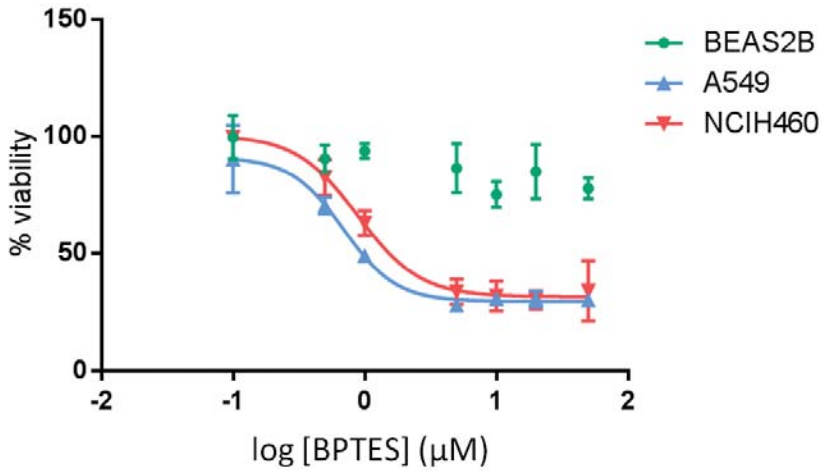

FIGURE 7. Representative examples of viability assay with glutaminase inhibitor BPTES in BEAS2B, A549 and NCI-H460 cells. IC_{50} values are 1.05 µM for A549 and 1.20 µM for NCIH460 cells. Tested concentrations didn't get to inhibit 50% of BEAS2B cells viability.

Conclusions

Study of cancer metabolic reprogramming can be an effective tool to detect enzymes to be targeted in order to block the metabolic pathways that cancer cells need to sustain their accelerated proliferation rates. In this study, we have combined metabolite concentration measurements in cell culture media and isotopomer distributions in several internal metabolite pools (obtained

with tracer-based metabolomics methods using the ^{13}C labelled substrates [1,2-^{13}C]-glucose and [3-^{13}C]-glutamine), in order to study the differences in central metabolism between the KRAS-mutated lung cancer cell lines A549 and NCIH460, and the non-tumor lung cell line BEAS2B.

Our results show that both tumor cell lines, and especially NCIH460, consume more glucose and glutamine than BEAS2B cells, while producing more lactate. Both tumor cell lines also produce more glutamate, being A549 cells those with the highest glutamate production rate. Tracer-based metabolomics experiments indicate that the relative weight of the non-oxidative branch of the PPP is higher in tumor cell lines, and especially in NCIH460. Besides, only tumor cells use glutamine to synthesize fatty acids, which implies the activation of malic enzyme in a pathway that could also be used to generate reductive NADPH.

Results indicated the possible existence of a glutamine dependence in both tumor cells. The antiproliferative effect of BPTES glutaminase inhibitor, which was observed only in A549 and NCIH460 cells, confirmed that hypothesis. Thus, the study of lung cancer metabolic reprogramming has allowed us to identify a metabolic target to be exploited to impair tumor proliferation.

Materials and methods.

Chemistry

The platinum(II) complex **6a** was prepared as described previously (Talancon, Lopez et al. 2013).

Cell culture

Human lung adenocarcinoma A549 cells and human lung large cell carcinoma NCI-H460 cells were grown as a monolayer culture in minimum essential medium (DMEM with L-glutamine and 4500 mg L1 D-glucose) in the presence of 10% heat-inactivated fetal bovine serum and 0.5% streptomycin/penicillin, under standard culture conditions (humidified air with 5% CO_2 at 37 °C).

Biochemical assays

Consumption of glucose and glutamate and production of lactate and glutamate were determined by spectrophotometry (COBAS Mira Plus, Horiba

ABX) from cell culture media by monitoring the 340 nm wavelength absorbance of the NAD(P)H produced or consumed in specific reactions for each metabolite (de Atauri et al., 2011). Glucose concentration was measured using HK and G6PD coupled enzymatic reactions (commercial enzymatic kit). Lactate concentration was determined by LDH reaction, which was carried out at 37 °C by adding media sample to a cuvette containing 1.55 mg/mL NAD and 87.7 U/mL LDH in pH 9 0.2M hydrazine 12 mM EDTA buffer. Determination of glutamate concentration was done by its conversion to α-ketoglutarate through glutamate dehydrogenase (GLDH) reaction in the presence of ADP. This reaction was performed at 37 °C by adding media sample to a cuvette containing 2.41 mM ADP, 3.9 mM NAD and 39 U/mL of GLDH in pH 9 0.5M glycine/0.5M hydrazine buffer. Determination of glutamine required its previous conversion into glutamate through glutaminase (GLS) reaction and subsequent quantification of glutamate concentration as described above. GLS reaction was performed by adding media sample to a cuvette containing a mixture of 90 mU/mL GLS in pH 5 111 mM acetate buffer. Reaction was carried out for 45 min at 37 °C in agitation.

In order to calculate the consumption/production rates of each metabolite, media samples at were taken at 0 h and 24 h incubation times, and frozen for subsequent analysis. From the same plates, or parallel plates when required, cell numbers were counted both at 0 h and 24 h for normalization purposes.

Tracer-based fluxomics

At the beginning of the experiment culture media was replaced by fresh media containing either 50% [1,2-$^{13}C_2$]-glucose (Sigma-Aldrich) or 100% [3-$^{13}C_1$]-glutamine (Sigma-Aldrich), and after 24 hours incubation media, pellets, and cultured plates were collected. Media samples were frozen at -20 °C for ulterior determination of mass isotopomer distributions of glucose, lactate and glutamate, and also to evaluate glucose, lactate, glutamate and glutamine concentrations as described above. Pellets were obtained by trypsinization and kept at -20 °C until used for analysis of mass isotopomer distribution of ribose and fatty acids. Cultured plates were frozen in liquid nitrogen and stored at -80 °C for mass isotopomer distribution analysis of TCA cycle intermediates. Cell number was determined at the beggining of the experiment and after the incubation period (0 h and 24 h, respectively).

Analysis of ^{13}C-labeled intracellular and extracellular metabolites for mass isotopomer distribution analysis was done by gas chromatography coupled to mass spectrometry (GC-MS). GC-MS was performed using an Agilent 7890A GC

equipped with a HP5 capillary column connected to an Agilent 5975C MS. Fatty acids GC-MS analysis was performed employing a GCMS-QP 2012 Shimadzu equipped with a bpx70 (SGE) column. In all cases, one microliter of sample was injected at 250 °C using helium as a carrier gas at a flow rate of 1 ml/min. Different procedures for metabolite isolation, derivatization and detection were used for each metabolite as described below.

Glucose

Glucose was isolated from cell culture media using a tandem set of Dowex-1X8/ Dowex-50WX8 ion-exchange columns, through which glucose eluded with water. After water evaporation under airflow, isolated glucose was held at 100 °C for 30 min with 2% (v/v) hydroxylamine hydrochloride in pyridine and then for 60 minutes more with acetic anhydride for derivatization. Excess of reagent and solvent was removed by evaporation with a N_2 flow, and glucose derivative was dissolved in ethyl acetate for GC-MS analysis under chemical ionization mode.

Lactate

Culture media was acidified by addition of HCl and the lactic acid formed was extracted with ethyl acetate and evaporated to dryness under a flow of N_2. Dry lactate was incubated at 75 °C for 1 h in presence of dimethoxypropane and dichloromethane. Next, n-propilamine was added to the reaction mixture, which was held at 100 °C for 1 h and then evaporated to dryness under a N_2 flow. The precipitate was then resuspended in dichloromethane and heptafluorobutyric anhydride at room temperature for 10 min, after which the mixture was evaporated to dryness under N_2 and resuspended again in CH_2Cl_2 for GC-MS analysis under chemical ionization mode.

Aminoacids from the culture media

Sample media was passed through a 3-mL Dowex-50WX8 (H+) column. Aminoacids were eluted from the column with 2N NH_4OH, and the solution was evaporated to dryness by airflow. Dried samples were then held at 100 °C for 1h in butanolic HCl, before removing reagents in excess under N_2. Precipitate was then dissolved in methylene chloride, and derivatization reaction was completed with the addition of trifluoroacetic anhydride. Samples were finally dried under N_2, and the derivative was dissolved in dichloromethane for injection into GC-MS equipment, where it was analyzed under electron impact mode.

Ribose

RNA was isolated from cultured cells after addition of Trizol® (Invitrogen) and extraction of the aqueous phase. Purified RNA was hydrolyzed in 2N HCl for 2h at 100 °C and solvent was evaporated to dryness under airflow. RNA ribose was derivatized as previously described for glucose, and GC-MS analysis was performed under chemical ionization mode.

Palmitate and estearate

Fatty acids from cultured cells were extracted after addition of Trizol® (Invitrogen) and extraction of the intermediate and lower phases after addition of 100% ethanol and 30% KOH. Samples were then incubated at 70 °C overnight, and afterwards free fatty acids were extracted with petroleum ether, which was subsequently evaporated to dryness under a flow of N_2. Fatty acids were then derivatized adding 0.5N methanolic-HCl and held at 70 °C for 1h. GC-MS analysis was subsequently performed under chemical ionization mode.

TCA cycle intermediates from cell extracts

TCA cycle intermediates were extracted from liquid nitrogen frozen cultured plates by adding a 100% methanol:H_2O (1:1) mixture and scrapping on ice. Cell extracts were then sonicated using a titanium probe (VibraCell, Sonics & Materials Inc., Tune: 50, Output: 30) and vortexed for 30 min at 4 °C. After that, samples were centrifuged and the upper aqueous phase was separated and evaporated to dryness under airflow at room temperature. TCA cycle intermediates were derivatized by addition of 2% (v/v) methoxyamine in pyridine and held at 37 °C for 90 min. Next, MBTSTFA + 1% TBDMCS was added to the samples, which were incubated for 1 more hour at 55 °C and transferred to GC-MS vials. GC-MS analysis was performed under electron impact ionization.

GC-MS data reduction

Spectral data obtained from a mass spectrometer simply represent the distribution of ions of a compound (or its fragments) with different molecular weights. The value for each observed *m/z* is affected not only by experimental isotope incorporation, but also by the presence of natural abundance of ^{13}C in the background, and, when corresponds, by the ^{12}C isotope impurity in the ^{13}C-labeled precursor used as a tracer. Furthermore, the derivatizing reagents often contain isotopes which also contribute to the mass isotopomer distribution of the derivatized compound. Therefore, correction for all such contributions is necessary

before the amount of isotope incorporation and its distribution in the compound of interest can be determined. This correction was performed by using regression analysis employing in-house developed software, which corrects all those contributions over the observed spectral intensities of each ion cluster, giving us the distribution of mass isotopomers in the metabolite of study due only to the incorporation of ^{13}C atoms from the tracer precursor. Results of the mass isotopomers in any of the ion clusters were reported as fractional enrichments of molecule isotopomers, defined as the fraction of molecules having a certain number of isotope substitutions. They are designated as m0, m1, m2, etc., where the number indicates the number of labeled carbons in the molecule already corrected for the reasons described above. Note that the sum of all mass isotopomers of the ion clusters is equal to 1 (or 100 %).

Viability assays

For all cell viability assays, tested compounds were suspended in 20 mM dimethyl sulfoxide (DMSO) as stock solutions. To obtain final assay concentrations, the stock solutions were diluted in DMEM (final concentration of DMSO was constant under all conditions, and always lower than 0.5%). In brief, 3 x 10^3 cells per well were cultured in 96 well plates for

24 h prior to the addition of different compounds at different concentrations, in triplicate. After incubation for 72 h more, the supernatant was aspirated and 100 mL of 0.01% SDS was added to each well. Plates were then frozen at -20 °C until analyzed. To analyze the samples, plates were thawed at 37 °C until fully liquid and 100 µl of HO3343 were added to each well, minimizing light exposure. Plates were then placed on a shaker and incubated at 37 °C for 1 h in the dark. Finally, well fluorescence, which is proportional to cell number, was measured in a fluorescence plate reader (Ex:355 nm, Em: 460 nm), and relative cell viability, compared to the viability of untreated cells, was defined for each condition. Concentrations that inhibited cell growth by 50% (IC_{50}) after 72 h of treatment were subsequently calculated using Graphpad Prism 6 software.

Acknowledgements

This work was supported by the Ministerio de Ciencia e Innovación of Spain (SAF2011-25726), the Generalitat de Catalunya (2009-SGR-1308, 2009-SGR-1111), the European Commission (FP7) grant METAFLUX (PITN-GA-2010-264780), and the Icrea Academia award 2010 (granted to M. Cascante).

References

Alcarraz-Vizan, G., J. Boren, et al. (2010). "Histone deacetylase inhibition results in a common metabolic profile associated with HT29 differentiation." Metabolomics **6**(2): 229-237.

Biswas, S., J. Lunec, et al. (2012). "Non-glucose metabolism in cancer cells--is it all in the fat?" Cancer Metastasis Rev **31**(3-4): 689-698.

Bonanno, L., A. Favaretto, et al. (2014). "Platinum drugs and DNA repair mechanisms in lung cancer." Anticancer Res **34**(1): 493-501.

Boros, L. G., J. Puigjaner, et al. (1997). "Oxythiamine and dehydroepiandrosterone inhibit the nonoxidative synthesis of ribose and tumor cell proliferation." Cancer Res **57**(19): 4242-4248.

Bray, F., A. Jemal, et al. (2012). "Global cancer transitions according to the Human Development Index (2008-2030): a population-based study." Lancet Oncol **13**(8): 790-801.

Bryant, K. L., J. D. Mancias, et al. (2014). "KRAS: feeding pancreatic cancer proliferation." Trends Biochem Sci **39**(2): 91-100.

Cardarella, S. and B. E. Johnson (2013). "The impact of genomic changes on treatment of lung cancer." Am J Respir Crit Care Med **188**(7): 770-775.

Carrola, J., C. M. Rocha, et al. (2011). "Metabolic signatures of lung cancer in biofluids: NMR-based metabonomics of urine." J Proteome Res **10**(1): 221-230.

Cascante, M., J. J. Centelles, et al. (2000). "Role of thiamin (vitamin B-1) and transketolase in tumor cell proliferation." Nutr Cancer **36**(2): 150-154.

Comin-Anduix, B., J. Boren, et al. (2001). "The effect of thiamine supplementation on tumour proliferation. A metabolic control analysis study." Eur J Biochem **268**(15): 4177-4182.

Cooper, W. A., D. C. Lam, et al. (2013). "Molecular biology of lung cancer." J Thorac Dis **5**(Suppl 5): S479-S490.

Cheng, T., J. Sudderth, et al. (2011). "Pyruvate carboxylase is required for glutamine-independent growth of tumor cells." Proc Natl Acad Sci U S A **108**(21): 8674-8679.

Chun, S. Y., C. Johnson, et al. (2010). "Oncogenic KRAS modulates mitochondrial metabolism in human colon cancer cells by inducing HIF-1alpha and HIF-2alpha target genes." Mol Cancer **9**: 293.

Daye, D. and K. E. Wellen (2012). "Metabolic reprogramming in cancer: unraveling the role of glutamine in tumorigenesis." Semin Cell Dev Biol **23**(4): 362-369.

de Atauri, P., A. Benito, et al. (2011). "Carbon metabolism and the sign of control coefficients in metabolic adaptations underlying K-ras transformation." Biochim Biophys Acta **1807**(6): 746-754.

Diaz-Moralli, S., M. Tarrado-Castellarnau, et al. (2011). “Transketolase-like 1 expression is modulated during colorectal cancer progression and metastasis formation.” PLoS One **6**(9): e25323.

Fan, T. W., A. N. Lane, et al. (2011). “Stable isotope resolved metabolomics of lung cancer in a SCID mouse model.” Metabolomics **7**(2): 257-269.

Foldi, M., E. Stickeler, et al. (2007). “Transketolase protein TKTL1 overexpression: A potential biomarker and therapeutic target in breast cancer.” Oncol Rep **17**(4): 841-845.

Frederiks, W. M., P. Vizan, et al. (2008). “Elevated activity of the oxidative and non-oxidative pentose phosphate pathway in (pre)neoplastic lesions in rat liver.” Int J Exp Pathol **89**(4): 232-240.

Hartmannsberger, D., B. Mack, et al. (2011). “Transketolase-like protein 1 confers resistance to serum withdrawal in vitro.” Cancer Lett **300**(1): 20-29.

Hori, S., S. Nishiumi, et al. (2011). “A metabolomic approach to lung cancer.” Lung Cancer **74**(2): 284-292.

Jemal, A., F. Bray, et al. (2011). “Global cancer statistics.” CA Cancer J Clin **61**(2): 69-90.

Kami, K., T. Fujimori, et al. (2013). “Metabolomic profiling of lung and prostate tumor tissues by capillary electrophoresis time-of-flight mass spectrometry.” Metabolomics **9**(2): 444-453.

Koudelakova, V., M. Kneblova, et al. (2013). “Non-small cell lung cancer--genetic predictors.” Biomed Pap Med Fac Univ Palacky Olomouc Czech Repub **157**(2): 125-136.

Krockenberger, M., A. Honig, et al. (2007). “Transketolase-like 1 expression correlates with subtypes of ovarian cancer and the presence of distant metastases.” Int J Gynecol Cancer **17**(1): 101-106.

Langbein, S., M. Zerilli, et al. (2006). “Expression of transketolase TKTL1 predicts colon and urothelial cancer patient survival: Warburg effect reinterpreted.” Br J Cancer **94**(4): 578-585.

McCracken, A. N. and A. L. Edinger (2013). “Nutrient transporters: the Achilles’ heel of anabolism.” Trends Endocrinol Metab **24**(4): 200-208.

Meng, M., S. Chen, et al. (2010). “Nitrogen anabolism underlies the importance of glutaminolysis in proliferating cells.” Cell Cycle **9**(19): 3921-3932.

Moran, D. M., P. B. Trusk, et al. (2014). “KRAS mutation status is associated with enhanced dependency on folate metabolism pathways in Non Small Cell Lung Cancer cells.” Mol Cancer Ther.

Mucaj, V., J. E. Shay, et al. (2012). “Effects of hypoxia and HIFs on cancer metabolism.” Int J Hematol **95**(5): 464-470.

Niu, Y., Y. Jiang, et al. (2012). “[Preliminary results of metabolite in serum and urine of lung cancer patients detected by metabolomics].” Zhongguo Fei Ai Za Zhi **15**(4): 195-201.

Paul Lee, W. N., P. N. Wahjudi, et al. (2010). "Tracer-based metabolomics: concepts and practices." Clin Biochem **43**(16-17): 1269-1277.

Pirman, D. A., E. Efuet, et al. (2013). "Changes in cancer cell metabolism revealed by direct sample analysis with MALDI mass spectrometry." PLoS One **8**(4): e61379.

Pylayeva-Gupta, Y., E. Grabocka, et al. (2011). "RAS oncogenes: weaving a tumorigenic web." Nat Rev Cancer **11**(11): 761-774.

Reddel, R. R., Y. Ke, et al. (1988). "Transformation of human bronchial epithelial cells by infection with SV40 or adenovirus-12 SV40 hybrid virus, or transfection via strontium phosphate coprecipitation with a plasmid containing SV40 early region genes." Cancer Res **48**(7): 1904-1909.

Riely, G. J., J. Marks, et al. (2009). "KRAS mutations in non-small cell lung cancer." Proc Am Thorac Soc **6**(2): 201-205.

Rocha, C. M., J. Carrola, et al. (2011). "Metabolic signatures of lung cancer in biofluids: NMR-based metabonomics of blood plasma." J Proteome Res **10**(9): 4314-4324.

Rodriguez-Prados, J. C., P. G. Traves, et al. (2010). "Substrate fate in activated macrophages: a comparison between innate, classic, and alternative activation." J Immunol **185**(1): 605-614.

Sanchez-Tena, S., G. Alcarraz-Vizan, et al. (2013). "Epicatechin gallate impairs colon cancer cell metabolic productivity." J Agric Food Chem **61**(18): 4310-4317.

Santidrian, A. F., A. Matsuno-Yagi, et al. (2013). "Mitochondrial complex I activity and NAD+/NADH balance regulate breast cancer progression." J Clin Invest **123**(3): 1068-1081.

Semenza, G. L. (2013). "HIF-1 mediates metabolic responses to intratumoral hypoxia and oncogenic mutations." J Clin Invest **123**(9): 3664-3671.

Son, J., C. A. Lyssiotis, et al. (2013). "Glutamine supports pancreatic cancer growth through a KRAS-regulated metabolic pathway." Nature **496**(7443): 101-105.

Staiger, W. I., J. F. Coy, et al. (2006). "Expression of the mutated transketolase TKTL1, a molecular marker in gastric cancer." Oncol Rep **16**(4): 657-661.

Suda, K., K. Tomizawa, et al. (2010). "Biological and clinical significance of KRAS mutations in lung cancer: an oncogenic driver that contrasts with EGFR mutation." Cancer Metastasis Rev **29**(1): 49-60.

Wen, T., L. Gao, et al. (2013). "Exploratory investigation of plasma metabolomics in human lung adenocarcinoma." Mol Biosyst **9**(9): 2370-2378.

Zhang, S., J. H. Yang, et al. (2007). "Gene silencing of TKTL1 by RNAi inhibits cell proliferation in human hepatoma cells." Cancer Lett **253**(1): 108-114.

Metabolite	Cell line	Tracer	Incubation Time (h)	m0 (%)		m1 (%)		m2 (%)		m3 (%)		m4 (%)		m5 (%)		m6 (%)	
				mean	SD	mean	SD	mean	SD	mean	SD	mean	SD	mean	SD	mean	SD
Glucose	BEAS-2B	[1,2-^{13}C]-glucose	0	50,8817	0,0945	0,0000	0,0000	48,1111	0,0938	0,1469	0,0591	0,7965	0,0018	0,0440	0,0177	0,0198	0,0068
			24	50,8040	0,1100	0,0000	0,0000	48,1339	0,0285	0,1616	0,0515	0,8024	0,0082	0,0822	0,0419	0,0159	0,0056
	A549		0	56,5257	0,1302	0,0092	0,0130	42,7150	0,1485	0,0000	0,0000	0,7104	0,0015	0,0212	0,0055	0,0185	0,0013
			24	57,4011	0,0294	0,0227	0,0234	41,8378	0,0460	0,0004	0,0006	0,6948	0,0042	0,0285	0,0136	0,0148	0,0055
	NCIH460		0	55,0235	0,0194	0,0000	0,0000	44,0783	0,0212	0,1187	0,0103	0,7434	0,0050	0,0186	0,0017	0,0175	0,0017
			24	57,2399	0,4884	0,0000	0,0000	41,9100	0,5089	0,0739	0,0259	0,7248	0,0050	0,0291	0,0009	0,0222	0,0045
Lactate	BEAS-2B	[1,2-^{13}C]-glucose	24	76,4649	0,1610	2,3920	0,1659	20,9083	0,0161	0,2347	0,0111						
	A549		24	80,5049	0,1601	1,6472	0,0083	17,7222	0,1617	0,1257	0,0055						
	NCIH460		24	79,5559	0,0235	1,3521	0,0067	18,8922	0,0150	0,1998	0,0024						
Glutamate (C2-C4 fragment)	BEAS-2B	[1,2-^{13}C]-glucose	24	99,4217	0,0408	0,4585	0,0230	0,1105	0,0120	0,0093	0,0058						
	A549		24	97,0707	0,0663	2,6042	0,0596	0,2925	0,0139	0,0327	0,0277						
	NCIH460		24	95,6775	0,2892	3,4904	0,2312	0,7429	0,0582	0,0891	0,0077						
Glutamate (C2-C5 fragment)	BEAS-2B	[1,2-^{13}C]-glucose	24	99,2823	0,0448	0,1834	0,0182	0,4800	0,0229	0,0472	0,0028						
	A549		24	96,5753	0,0305	0,8496	0,0076	2,4352	0,0399	0,1061	0,0093						
	NCIH460		24	95,1028	0,1854	0,8830	0,0363	3,7146	0,1439	0,2081	0,0110						
Ribose	BEAS-2B	[1,2-^{13}C]-glucose	24	72,3773	0,2345	17,5066	0,1153	6,5750	0,0799	2,5053	0,0192	0,9694	0,0224	0,0663	0,0066		
	A549		24	74,1487	0,1790	15,8222	0,1350	6,4159	0,0510	2,6397	0,0125	0,8622	0,0132	0,1113	0,0116		
	NCIH460		24	70,4859	0,5756	15,5668	0,2414	9,9669	0,2338	2,2720	0,0553	1,6278	0,0507	0,0806	0,0051		

APPENDIX 1. Mass isotoper distribution of analyzed metabolites in BEAS2B, A549 and NCIH460 cells, after incubation with 50% [1,2-13C]-glucose. Values are expressed as percentage of each mass isotopomer and denote mean ± SD of n=3.

Metabolite	Cells	Tracer	Incubation Time (h)	m0 (%)		m1 (%)		m2 (%)		m3 (%)		m4 (%)		m5 (%)		m6 (%)	
				mean	SD	mean	SD	mean	SD	mean	SD	mean	SD	mean	SD	mean	SD
Glutamate (C2-C5 fragment)	BEAS-2B	[3-^{13}C]-glutamine	24	2,3661	0,1134	96,9700	0,1253	0,0369	0,0106	0,6270	0,0021						
	A549		24	25,3225	0,5169	73,5956	0,5230	0,6189	0,0201	0,4630	0,0063						
	NCIH460		24	27,4965	1,5571	71,7678	1,5731	0,2823	0,0281	0,4534	0,0107						
Malate	BEAS-2B	[3-^{13}C]-glutamine	24	24,3869	0,7362	74,9488	0,7473	0,0374	0,0159	0,6044	0,0140	0,0226	0,0109				
	A549		24	28,6862	0,1046	70,7801	0,1130	0,0000	0,0000	0,4693	0,0179	0,0644	0,0237				
	NCIH460		24	30,2824	0,8587	69,2157	0,8642	0,0000	0,0000	0,4969	0,0172	0,0049	0,0062				
Aspartate	BEAS-2B	[3-^{13}C]-glutamine	24	25,8841	0,5984	73,2600	0,6155	0,2394	0,0178	0,6165	0,0147						
	A549		24	27,7469	0,1389	71,5467	0,1286	0,1989	0,0322	0,5075	0,0286						
	NCIH460		24	29,8653	0,7243	69,6478	0,7163	0,0040	0,0069	0,4829	0,0094						
Citrate	BEAS-2B	[3-^{13}C]-glutamine	24	26,1186	0,3611	69,4509	1,0513	2,8330	0,6560	1,3560	0,0895	0,2416	0,0933	0,0461	0,0235	0,0327	0,0317
	A549		24	53,9059	1,8023	43,5693	1,5500	1,9837	0,2548	0,5064	0,0446	0,0289	0,0435	0,0051	0,0088	0,0007	0,0012
	NCIH460		24	50,0710	1,3306	48,1219	1,1720	1,2649	0,1635	0,5422	0,0156	0,0000	0,0000	0,0000	0,0000	0,0000	0,0000
Palmitate	BEAS-2B	[3-^{13}C]-glutamine	24	99,5244	0,1235	0,3587	0,1133	0,1109	0,0258	0,0003	0,0005	0,0005	0,0004	0,0001	0,0001	0,0002	0,0004
	A549		24	90,8901	0,1888	7,1435	0,1188	1,6493	0,1043	0,3135	0,0324	0,0010	0,0015	0,0003	0,0005	0,0000	0,0000
	NCIH460		24	92,9263	0,8344	6,1158	0,4768	0,4840	0,0171	0,1518	0,0389	0,0692	0,1198	0,0217	0,0124	0,0338	0,0405
Estearate	BEAS-2B	[3-^{13}C]-glutamine	24	99,7860	0,0544	0,1157	0,0334	0,0646	0,0256	0,0006	0,0010	0,0015	0,0004	0,0006	0,0010	0,0003	0,0001
	A549		24	96,2114	0,6727	2,9682	0,5457	0,7105	0,1082	0,0263	0,0314	0,0560	0,0082	0,0000	0,0000	0,0179	0,0017
	NCIH460		24	95,3302	0,2297	3,8741	0,4605	0,4175	0,1589	0,0669	0,0417	0,0406	0,0578	0,0131	0,0207	0,0022	0,0028

APPENDIX 2. Mass isotoper distribution of analyzed metabolites in BEAS2B, A549 and NCIH460 cells, after incubation with 100% [3-13C]-glutamine. Values are expressed as percentage of each mass isotopomer and denote mean ± SD of n=3.

CAPÍTULO 04

ANÁLISIS DEL AIRE EXHALADO MEDIANTE CROMATOGRAFÍA DE GASES-ESPECTROMETRÍA DE MASAS EN LA DETECCIÓN DEL CÁNCER DE PULMÓN Y LA ENFERMEDAD PULMONAR OBSTRUCTIVA CRÓNICA.

CAPÍTULO 04

ANÁLISIS DEL AIRE EXHALADO MEDIANTE CROMATOGRAFÍA DE GASES-ESPECTROMETRÍA DE MASAS EN LA DETECCIÓN DEL CÁNCER DE PULMÓN Y LA ENFERMEDAD PULMONAR OBSTRUCTIVA CRÓNICA.

Roldán Cortés[1] , Ana Guaman[2] , Idoya Agudo[2] , Daniel Calvo[3] , Antonio Pardo[3] , Santiago Marco[2,3] , Yolanda Torralba[4], Josep Roca[4, 5] , Joan Albert Barberà[4, 5] , Marta Cascante[1, 5].

[1] Departament de Bioquímica i Biologia Molecular, Facultat de Biologia, Unidad Asociada al CSIC, Diagonal 643, 08028 Barcelona, España

[2] Artificial Olfaction Group, Institut de Bioenginyeria de Catalunya (IBEC), 08028 Barcelona, España

[3] Intelligent Signal Processing (ISP), Department d'Electrònica, Universitat de Barcelona, 08028 Barcelona, España

[4] Department de Medicina Pulmonar, Hospital Clínic, CIBERES, IDIBAPS, Barcelona, España

[5] Centro de Investigación en Red de Enfermedades Respiratorias (CibeRes), Palma de Mallorca, Spain

Resumen

El cáncer de pulmón es la causa más común de muerte por cáncer a nivel mundial, con un índice de supervivencia a 5 años de únicamente el 16%. Esta elevada mortalidad está íntimamente asociada a la tardía aparición de síntomas, que hacen que la enfermedad sea diagnosticada cuando los tratamientos disponibles ya no son efectivos o viables. Esto hace que el desarrollo de métodos para la diagnosis temprana del cáncer de pulmón sea una necesidad imperiosa que aún no ha podido ser satisfecha. Existe un interés creciente en el análisis de aire exhalado como método para el diagnóstico temprano y no invasivo de diferentes enfermedades, pero distintas limitaciones metodológicas previenen la recomendación de su uso en la práctica clínica. El estudio que aquí se presenta ha utilizado cromatografía de gases acoplada a espectrometría de masas (GC-MS) para analizar muestras de aire exhalado de 83 sujetos pertenecientes a cuatro categorías diagnósticas diferentes: sanos (23), cáncer de pulmón (12), enfermedad pulmonar obstructiva crónica (29) y cáncer de pulmón y EPOC (19). Previamente se llevó a cabo un estudio piloto con un grupo distinto de 29 sujetos (17 sanos y 12 EPOC) para identificar las limitaciones metodológicas relevantes de la técnica. Los resultados indican que los patrones de compuestos orgánicos volátiles (VOCs) de muestras de aire exhalado pueden ser utilizados para distinguir entre distintas categorías diagnósticas, aunque la variabilidad dentro de cada grupo sigue siendo un obstáculo para el uso rutinario de la técnica en la práctica clínica.

BREATH ANALYSIS BY GAS CHROMATOGRAPHY-MASS SPECTROMETRY FOR DETECTION OF LUNG CANCER AND COPD

Roldán Cortés[1], Ana Guaman[2], Idoya Agudo[2], Daniel Calvo[3], Antonio Pardo[3], Santiago Marco[2, 3], Yolanda Torralba[4], Federico Gómez[4], Josep Roca[4, 5], Joan Albert Barberà[4, 5], Marta Cascante[1, 5].

[1] Department of Biochemistry and Molecular Biology, IBUB, University of Barcelona, Barcelona, Spain.

[2] Artificial Olfaction Group, Institute for Bioengineering of Catalonia (IBEC), Barcelona, Spain.

[3] Intelligent Signal Processing (ISP), Department of Electronics, University of Barcelona, Barcelona, Spain.

[4] Department of Pulmonary Medicine, Hospital Clínic, CIBERES, IDIBAPS, Barcelona, Spain

[5] Centro de Investigación en Red de Enfermedades Respiratorias (CibeRes), Palma de Mallorca, Spain

KEY WORDS: lung cancer, chronic obstructive pulmonary disease, breath analysis, random forest.

Abstract

Lung cancer is the most common cause of cancer death worldwide with a 5-year survival rate of only 16%. This high mortality is strongly associated with late symptoms appearance when available treatments are no longer effective or viable. The phenomenon makes the search for methods for early diagnosis of lung cancer an urgent unmet need. There is an increasing interest in exhaled breath analysis for early non-invasive diagnosis of several diseases, but different methodological limitations preclude recommendation of its use in the clinical scenario. The current research used Gas Chromatography-Mass Spectroscopy (GC-MS) to analyze breath samples of 83 subjects allocated in four diagnostic categories: 23 healthy, 12 lung cancer, 29 chronic obstructive pulmonary disease (COPD); and, 19 with lung cancer and COPD. A pilot study with an different additional group of 29 subjects: 17 healthy and 12 COPD was performed

to identify relevant methodological limitations of the technique. The results indicate that patterns of volatile organic compounds (VOCs) in human breath samples can be used to distinguish between diagnostic categories, but inter-group variability still remains an obstacle for a routine use of the technique in the clinical practice.

Introduction

Lung cancer is the most common cause of cancer death worldwide. It is the most diagnosed cancer type in males and the fourth most diagnosed in females, and it accounted for more than 1.3 million deaths in 2008 alone (Bray, Jemal et al. 2012). Despite decades of research to improve diagnostic and therapeutic strategies, lung cancer 5-year survival rate remains at a very low 16% (Chan, Lewis et al. 2010).

One of the main reasons for the low survival rate in lung cancer is that its symptoms, which include shortness of breath, coughing and weight loss, are non-specific and diffcult to discriminate from other lung diseases. Because of this, lung cancer is often diagnosed at a late stage when available therapeutic strategies are no longer effective (Dent, Sutedja et al. 2013; Wen, Gao et al. 2013). There is consequently a great need of new diagnostic methods that can be used in screenings for early detection of the disease in high risk populations of asymptomatic individuals. Diagnostic techniques for the detection of lung cancer include chest radiography, lung CT scan magnetic resonance imaging (MRI), and analysis of tissue biopsies, but none of them is fully accepted for early screening due to their high costs, invasiveness, or potential risks (Kanne 2014).

Current understanding of the physio-pathological mechanisms of lung cancer suggests that oxidative stress plays a key role in the development of the disease, and it is known that cigarette smoke, which is widely considered as the main risk factor for the development of lung cancer, confers a significant amount of oxidative stress upon lung cells (Faux, Tai et al. 2009; Valavanidis, Vlachogianni et al. 2013). One of the most relevant consequences of oxidative stress is DNA damage, which is caused via different mechanisms like oxidation, nitration, methylation, lipid peroxidation, deamination, and depurination (Chan, Lewis et al. 2010), and can affect many different processes related to cell survival and proliferation and provoke mutations of both proto-oncogenes and tumor suppressor genes. All these alterations can induce a neoplastic process, which in turn also induces a pro-inflamatory state that further contributes to the oxidative burden of the tumor. Hence, the detection of oxidative stress arises as a promising method in the early detection of lung cancer, even before it causes detectable symptoms.

Many volatile organic compounds (VOCs) are derived from reactions involving different reactive oxygen species (ROS), and therefore are produced in situations of oxidative stress. Those VOCs, which are initially found in the blood, are transferred to the exhaled breath thanks to the gaseous exchange that takes place in the alveoli. It has been proven that, merely by smelling the subject's breath, dogs can be trained to detect the presence of different diseases (including lung cancer) with impressive accuracy (Lippi and Cervellin 2012; Bijland, Bomers et al. 2013). This suggests that the pattern of VOCs in exhaled breath can differ between healthy subjects and patients with lung cancer, and therefore exhaled breath analysis can be a promising and completely non-invasive approach for the detection of biomarkers associated with the disease.

There has been an increased interest in the use of exhaled breath analysis for the diagnosis of several diseases, and there are studies in the literature indicating that the analysis of exhaled gas using various techniques can be useful in the detection of biomarkers of many different disorders (Gordon, Szidon et al. 1985; Phillips, Gleeson et al. 1999; Machado, Laskowski et al. 2005; Mazzone, Hammel et al. 2007; Bajtarevic, Ager et al. 2009; Dragonieri, Annema et al. 2009; D'Amico, Pennazza et al. 2010; Peng, Hakim et al. 2010). Nevertheless, after 20 years of research it is not yet possible to accurately identify individuals with lung cancer in large screenings by breath analysis alone, due to many different methodological limitations and the existence of different factors with the potential to confound the VOC analysis results.

It is of note that the main limitation in exhaled breath analysis nowadays is probably the lack of standardized recommended guidelines for the sampling of the exhaled gas, which also happens to be the most critical process in the whole analytical procedure. Many different sampling approaches have been used, varying in concepts like: collection technique, use of room air collection for normalization or filtering of exhaled gas prior to sampling for analysis. All these different approaches may affect results generating high variability among research groups. Therefore, the development of a standardized method enhancing factors associated with sampling reproducibility of exhaled breath can pave the way for the use of breath analysis-based early diagnosis of lung cancer.

Collected samples can be analyzed using many different techniques, including ion mobility spectrometry (IMS), electronic noses, liquid phase analysis of the breath condensate and gas chromatography-mass spectrometry (GC-MS). Although gas chromatographers and mass spectrometers are expensive and require highly experienced analysts to operate them and interpret the results, the high accuracy and sensitivity of these systems make them ideal for the analysis of

VOCs, whose concentration in exhaled breath is often in the range of parts per billion (Machado, Laskowski et al. 2005; Barker, Hengst et al. 2006). The prior separation step carried out with GC facilitates the MS analysis of the different VOCs separately, and introduces a new factor, the retention time of each compound in the chromatographic column, that can be very helpful in the identification of the VOCs. The high sensitivity and accuracy of coupled GC-MS enhances analytical information, makes this technique one of the best choices for the analysis of the VOCs contained in exhaled gas.

We acknowledge, however, that variables like: age, diet, gender, smoking status or environmental factors have been shown to induce differences in the pattern of VOCs found in exhaled breath, constituting additional sources of variability to be taken into account in the interpretation of the results. In particular, in studies in which the number of samples is limited (Phillips, Cataneo et al. 2000; Gordon, Wallace et al. 2002; Calusic, Varnai et al. 2011; Das, Bishwal et al. 2014; Tarnoki, Bikov et al. 2014). Many studies compare the pattern of exhaled VOCs between health and lung cancer without taking into account that patients may often present airway inflammation and oxidative stress due to frequent co-morbid conditions like COPD, which shares tobacco smoking as common risk factor of lung cancer. It is currently under debate if COPD itself can be an independent risk factor for lung cancer (Turner, Chen et al. 2007) or the two diseases, COPD and lung cancer, are merely different consequences of the exposure to the same inhaled irritant (Petty 2005; Prevot, Plat et al. 2012). In any case, it would be interesting to see if the pattern of VOCs in samples of exhaled breath analyzed via GC-MS can be used to distinguish between healthy subjects, patients with COPD and patients with lung cancer. The ultimate aim is the search for new non-invasive diagnostic tools that can be used for early detection of lung cancer, and not just non-specific changes associated to airway inflammation and/or oxidative stress. It can be reasonably hypothesized that early diagnosis of lung cancer will be strongly associated to higher health efficiencies and improved survival rate.

The main objectives of our research are: *i)* to conduct a pilot study aiming at developing a method able to detect VOCs contained in exhaled gas for analysis via GC-MS; *ii)* to apply the expertise acquired in the pilot study in the design of a more thorough assessment of the patterns of VOCs in breath samples in: healthy subjects and patients with lung cancer, COPD and both lung cancer and COPD; and, *iii)* to explore if the differences among the VOC patterns of the four groups can be used to predict the group to which each sample belongs, which would confirm the diagnostic potential of the technique in the non-invasive detection of both lung cancer and COPD.

Results

Pilot Study

The aim was to explore the feasibility of using GC-MS to detect the patterns of VOCs in samples of exhaled gas in COPD patients and in healthy volunteers. A volume of 1 liter of exhaled air was sampled in Tedlar Bags and, after solid phase microextraction (SPME) with a carboxen/PDMS fiber, the VOCs contained in the breath sample were analyzed via GC-MS (see **materials and methods**).

VOCs from the sample were separated in the GC and then ionized and fragmented in the MS. The analysis gave us information about the presence of each fragment in the sample, specifically their m/z values, intensities and retention times. We used MZmine software to identify the related peaks in every sample and align the spectra accordingly, obtaining a total of over 2.000 detected fragments. We then normalized each peak intensity to the total intensity of the spectrum in which each peak was contained, in order to compare the relative weight of every fragment in their respective spectra instead of comparing their absolute intensity.

The impact of COPD on the patterns of VOCs from the exhaled gas samples was explored using a principal component analysis (PCA) with all the fragment intensities detected in all the samples, in order to reduce the huge amount of variables (2029, corresponding to the number of detected fragment intensities) into just two. The two principal components depicted in **Figure 1** were obtained by combining different fragment intensities and they explained the highest possible amount of variability in the analyzed samples (Jolliffe 2005). **Figure 1** shows that the two dimensions of PCA were not able to separate the patterns of VOCs between health and COPD which indicates the presence of sources of variability other than presence or absence of COPD. Consequently, we decided to explore the sources of this non-COPD related variability in order to assess potential actions to enhance reproducibility of the technique that could facilitate the detection of disease-associated changes.

A first step was to enhance sampling procedures by assessing the impact of reused bags for sampling. While the first breath samples were taken using brand new Tedlar bags, after some time sampling was done with reused bags after a cleansing procedure that consisted on filling them with N_2 and then subsequently emptying them several times. We acknowledge that there was a possibility that some VOCs remained attached to the walls of the Tedlar bag, which could be released in subsequent samplings or change the adsorption properties of the bag's internal surface.

To assess if sampling with recycled Tedlar bags induced changes in the pattern of VOCs from the analyzed samples, we decided to repeat the PCA grouping the samples in a different way, depending on whether they were taken with brand new or reused bags. Results, which can be seen in **figure 1**, seem to indicate that the reuse of Tedlar bags does generate a variability that is big enough to cause a separation using the first two principal components of PCA. These results indicate that the variability introduced in the samples by the recycling of the Tedlar bags is bigger than the variability introduced by the presence of COPD, thus distorting the analysis results and complicating the separation of the healthy and COPD groups.

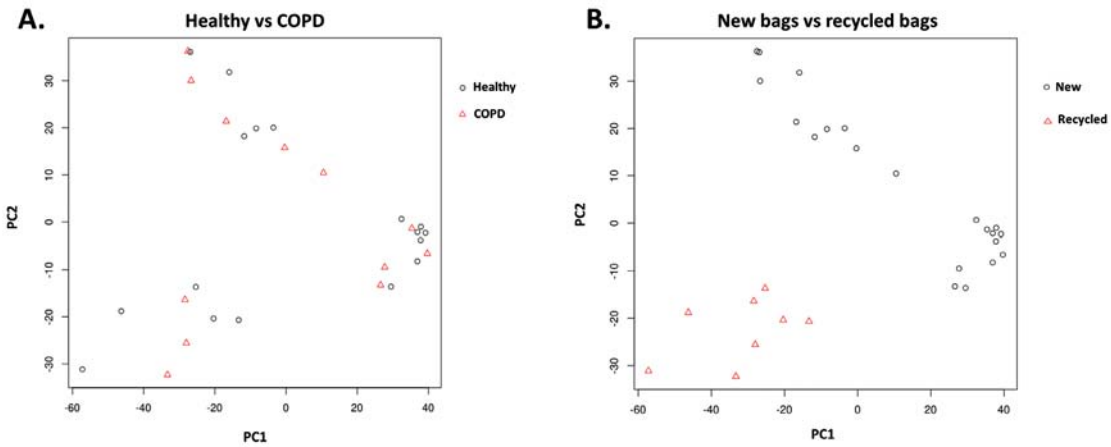

FIGURE 01. PCA analysis of the VOC pattern in breath samples of healthy volunteers and COPD patients. Grouping is made according to the presence or absence of the disease (A) or to the use of brand new or recycled Tedlar Bags (B). Principal component 1 and principal component 2 (PC1 and PC2) account for 44% of the total variance between all samples included in the analysis. Using PC1 and PC2, there is not a clear separation between Healthy and COPD samples, but there is one between samples taken using brand new and recycled Tedlar bags.

Figure 2, generated after removal of all results taken with reused bags, indicates that even when using only new Tedlar bags the two principal components are not related to the healthy-COPD separation, indicating persistence of factors introducing variability in the breath samples that precluded identification of COPD.

In a second step, we explored the impact of VOCs composition in the room air inhaled by the subject on the VOC composition of the exhaled air, to assess potential contamination of inhaled gas by VOCs of exhaled gas. It is

acknowledged that while part of the VOCs from the inhaled air is metabolized or otherwise retained in the organism of the subject, another part is exhaled and therefore can contaminate subsequent breath sampling. If the composition of VOCs in the room air where samples are taken is constant, and barring differences in inhaled VOCs absorption between different subjects, this effect should be similar in all cases and therefore should not induce important variability in the VOCs composition of exhaled air. All samples were taken in the same room at equal conditions of pressure and temperature, but while the first period of sampling was carried out in the month of February, a second period of sampling took part in November.

The effect of the sampling calendar on the VOC patterns of the breath samples was explored by grouping sampling by months. The resulting PCA shown in **Figure 2** indicates that a significant variability was introduced by sampling calendar. To assess the potential effects of contamination by the VOCs of the inhaled room air, we analyzed the room air samples from the days in which the breath samples were taken (room air samples were taken and analyzed in a similar manner to breath samples, as we explain in the **materials and methods** section). After PCA analysis of the room air samples, we obtained a clear separation between air room samples taken in different months. This separation is very similar to the separation obtained for the breath samples, which suggests that the shift in the room air VOCs composition between different months affects the patterns of VOCs in exhaled air, introducing a variability that has the potential to disguise the differences induced by the presence of the disease.

Since we were unable to eliminate this kind variability from our breath samples, we decided to use a different approach in the VOCs pattern analysis between breath samples from COPD patients and healthy volunteers. In order to maximize the separation between the two groups, a principal component discriminant analysis (PCDA) was used. PCDA starts as a regular PCA, but instead of keeping and representing only the first two resulting principal components (PC1 and PC2), it selects the first 14 components (which explain more than 95% of the total variability across all the samples) and uses them as new variables to conduct a linear discriminant analysis, in which the maximum separation between the healthy and COPD groups is searched for.

As seen in **Figure 3**, PCDA is able to separate the breath samples from COPD patients and healthy volunteers in a clear way. The characteristics of the subjects included in this final analysis can be seen in **Table 1**. After internal cross-validation, 58% sensitivity and 72% specificity were achieved in the correct assignment of the samples to their corresponding groups, with a global

accuracy of 66%. Considering the limited number of samples of the pilot study and the great sources of variability found in our sampling procedure, the results were promising about the possibilities of using the pattern of VOCs in exhaled breath detected by GCMS in the separation of healthy volunteers and patients with a lung disease, which encouraged us to conduct a more thorough, bigger study in which we would adopt a different sampling system in order to avoid the variability-inducing issues we had detected in our pilot study.

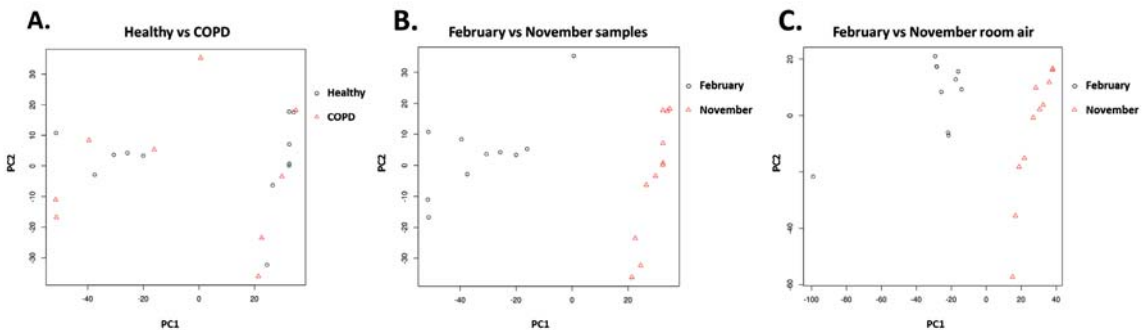

FIGURE 02. PCA analysis of the VOC pattern in breath samples of healthy volunteers and COPD patients, using only samples taken with new Tedlar Bags. Grouping is made according to the presence or absence of the disease (A) or to the month in which the samples were taken (B). Principal component 1 and principal component 2 (PC1 and PC2) account for 48% of the total variance between all samples included in the analysis. Using PC1 and PC2, there is not a clear separation between Healthy and COPD samples. However, a clear separation arises when the samples are grouped according to the month in which they were taken. (C) shows room air samples taken on the same days as breath samples. The separation between room air samples is very similar to the separation between breath samples, indicating the big influence that the variability of room air VOCs can exert over exhaled air VOCs.

From what we learnt in the pilot study, we made test subjects to breath medical air during the sample procedure. Room air composition is different in different times of the year, so we hoped to diminish its influence on exhaled VOCs using the same source of medical air (22% O_2, 78% N_2) in all samples.

The impossibility of recycling Tedlar bags highlighted the need to implement a different system to be used in a larger study. Sorbent-based sampling systems called sorbent tubes provided us with a suitable alternative, since most sorbents are able to endure very high temperatures (over 350 ºC). This makes a thorough cleansing of all VOCs that may remain in the sorbent after analysis with a gas current at very high temperature an easy possibility, thus making it possible to recycle the tubes while avoiding cross-contamination

between samples. Since the VOCs contained in exhaled air exhibit a big range in volatility and hydrophobicity, we decided to use a mixture of two different sorbents, Tenax and Unicarb, both inert and able to endure high temperatures, but with different hydrophobicites in order to adsorb the maximum possible range of VOCs.

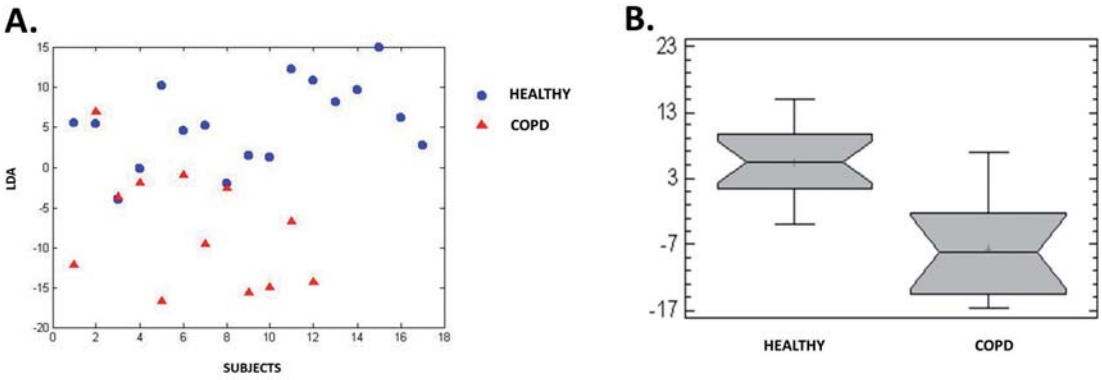

FIGURE 03. (A) After PCDA, the samples can be separated using one dimension, as shown in the figure. (B) Dispersion of healthy and COPD samples according to the PCDA separation. An internal cross-validation method (leave one out) was used to test the robustness of the separation, after which we obtained a 58% sensitivity and 72% specificity, with 66% of the samples correctly assigned to their corresponding groups.

In order to avoid any intermediate sampling steps like the use of a Bio-VOC sampler, which may also contribute to cross-contamination, we designed a system that collects the breath's VOCs directly from the subject's exhaled air without the need for any additional steps. Exhaled air goes through a tube made of glass, a material chosen because of its inertness, and an air pump collects the gas from the first part of the glass tube through the metal tube containing the sorbent, which adsorbs the VOCs from the breath sample. The presence of Unicarb in the sorbent mixture ensures the gathering of the less hydrophobic VOCs, but it also entails the disadvantage of retaining breath humidity, which has the potential to seriously distort the MS spectra. To address this problem, a humidity-adsorbing silica gel filter was attached to the sampling system just before the sorbent trap with the Tenax/Unicarb sorbent tube. The whole glass tube was also kept warm with a heating system in order to avoid condensation, which could cause the loss of the more hydrophilic VOCs (see **materials and methods** for a description of the whole sampling system).

	Healthy	COPD
N	17	12
Males/Females	10/7	12/0
Age (years)	40 ± 10	72 ± 7
FEV1%	99 ± 7	51 ± 12

TABLE 01. Characteristics of the subjects whose breath samples were finally included in the pilot study. FEV1%, the ratio between forced expiratory value in one second and forced vital capacity, represents the proportion of a person's vital capacity that they are able to expire in the first second of expiration.

Extended study

	CONTROL	COPD	LC	COPDLC
N	23	29	12	19
Males/Females	14/9	24/5	10/2	13/6
Age (years)	60 ± 13	65 ± 7	68 ± 9	68 ± 8
FEV1%	99 ± 15	45 ± 14	80 ± 12	64 ± 14

TABLE 02. Characteristics of the subjects whose exhaled air samples were included in the final study.

The study entailed a total of 83 breath samples which, as shown in **Table 2**, were divided in four different groups: control healthy subjects (23 samples), patients with lung cancer (12 samples), patients with COPD (29 samples) and patients with both lung cancer and COPD (19 samples). After sampling, the VOCs in the sorbent tubes were automatically desorbed and carried to the GC-MS system using a UNITY thermal desorption unit (Markes). After analysis of the samples, spectra were processed with MZmine software, and we obtained a total of 3049 different fragments identified by their peak area, m/z relationship and the retention time at which they eluted from the chromatographic column. Peaks with the same retention time and which co-varied in all samples were considered part of the same original compound, and therefore were clustered. At the end, the data had a dimension of n samples by 1679 fragments/compounds, whose peak areas were normalized against the total area of the specter in which the each peak was contained. Therefore, we didn't compare the absolute area of each compound between samples, but rather the relative importance of every compound in their corresponding spectra.

The data obtained was arranged according to the four initial groups: healthy subjects (CONTROL), patients with COPD (COPD), patients with lung cancer (LC) and patients with lung cancer and COPD (COPDLC). Then, 6 binary models were established: CONTROL vs. LC, CONTROL vs COPD, Control vs COPDLC, COPD vs LC, COPD vs COPDLC and COPDLC vs LC. A more robust strategy than PCA was proposed in this study with a proper validation methodology. In this sense, random forest, which is an ensemble classifier that consists of many decision trees (see matherials and methods), was built in each binary problem. The different trees provide a variable importance that indicates which variables are relevant in the classification of the samples in their corresponding groups, and ultimately classify the samples by averaging class membership of each individual tree.

		INTERNAL VALIDATION DATA				EXTERNAL VALIDATION DATA			
MODELS	K-FOLD	CONTROL	COPD	LC	COPDLC	CONTROL	COPD	LC	COPDLC
CONTROL vs LC	8	19		9		4		3	
CONTROL vs COPD	7	19	25			4	4		
CONTROL vs COPDLC	8	19			16	4			3
COPD vs LC	8		25		16		4	3	3
COPD vs COPDLC	8		25	9			4	3	
COPDLC vs LC	10			9	16				3

TABLE 03. Samples included in the training and validation sets for each binary model.

The samples were split in external validation and internal validation data using a double-cross validation strategy, in which K-fold cross validation was implemented: each K model had a subset of internal validation data and external validation data (see Table 3). The internal validation data was used for setting up internal parameters of random forest, while external validation, also known as blind data set, tested the robustness of the classifier models. A permutation test was also applied to each model, in order to test if the classification was caused by chance. When the models passed the null-hypothesis, the outputs of each binary problem were combined, and the final combined model predicted the group to which any sample most likely belonged. All binary models passed the permutation test with p-values of ≤ 0.001, with the exception of the binary model that tried to separate the CONTROL and COPDLC groups and the binary model that tried to separate the COPDLC and LC groups. The external validation data were used to test the accuracy of the binary models that passed the permutation test. The results, as shown in Table 4, indicate that after external validation the models were able to predict the separations between COPD and LC groups, and between CONTROL and COPD groups. The separation between CONTROL and LC groups was less successful, especially regarding the sensitivity of the model, which is also reflected in the ROC curves (see Figure 4).

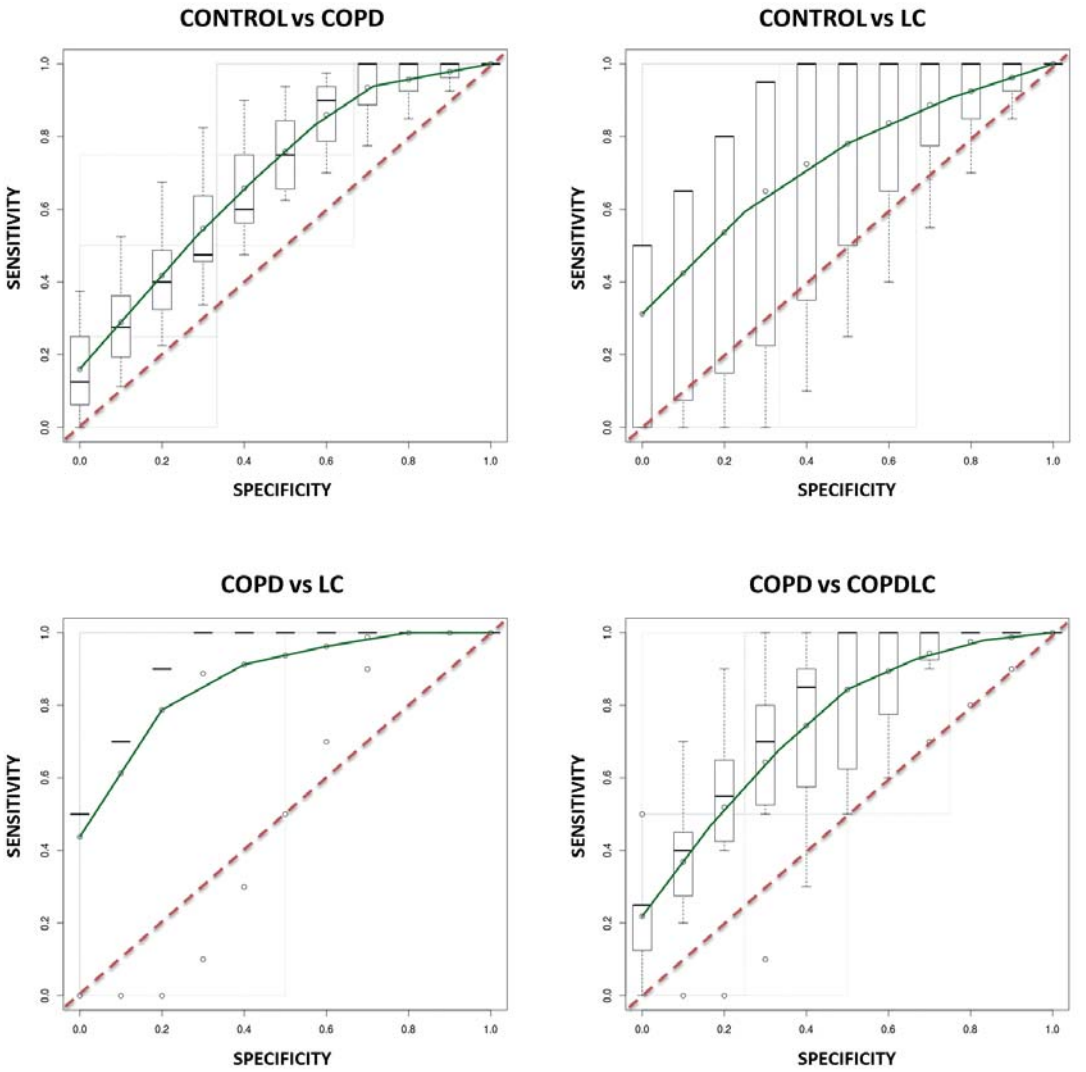

FIGURE 04. ROC curves of the four binary models that passed the permutation test (red-dashed line depicts a random classification).

All binary models passed the permutation test with p-values of 0.001 and lower, with the exception of the binary model that tried to separate the CONTROL and COPDLC groups, and the binary model that tried to separate the COPDLC and LC groups. An external validation (using multiple samples that took no part in the building of each model) was used to test the accuracy of the binary models that passed the permutation test. The results, as shown in **Table 4**, indicate that after external validation the models were able to predict the separations between COPD

and LC groups, and between CONTROL and COPD groups. The separation between CONTROL and LC groups was less successful, especially regarding the sensitivity of the model, which is also reflected in the ROC curves (see **Figure 4**).

MODELS	Permutation test p-value	AUC	ACC	Sensitivity	Specificity
CONTROL vs LC	0,001	0,71 ± 0,24	0,55 ± 0,13	0,36 ± 0,17	0,86 ± 0,18
CONTROL vs COPD	0,001	0,73 ± 0,15	0,67 ± 0,14	0,68 ± 0,23	0,73 ± 0,23
CONTROL vs COPDLC	0,3	0,53	-	-	-
COPD vs LC	0,0009	0,86 ± 0,22	0,7 ± 0,12	0,68 ± 0,12	0,81 ± ,37
COPD vs COPDLC	0,0009	0,76 ± 0,16	0,7 ± 0,13	0,69 ± 0,13	0,71 ± 0,31
COPDLC vs LC	0,33	0,52	-	-	-

TABLE 04. Area under the ROC curve (AUC), accuracy (ACC), sensitivity and specificity for each binary model that passed the permutation test using external validation data.

External validation was also used to test the accuracy of the combined models. Results, as shown in **Table 5**, indicate that the COPD samples are the ones best placed in their corresponding group. Global accuracy was 52%, being the expected accuracy of a random classification in all four groups of a mere 26%.

	Predicted group			
Actual group	CONTROL	COPD	LC	COPDLC
CONTROL	*13 (57%)*	4 (17%)	1 (9%)	4 (17%)
COPD	2 (7%)	*21 (72%)*	3 (10%)	3 (10%)
LC	1 (8%)	2 (17%)	*3 (25%)*	6 (50%)
COPDLC	2 (11%)	5 (26%)	6 (32%)	*6 (32%)*

TABLE 05. Sample classifications made by the combined model. Global accuracy is 52% (expected random accuracy is 26%).

Discussion

Although the use of breath analysis in the early detection of multifactorial diseases is a promising field of research, there is still much work to be done to develop a standardized methodology able to produce consistent and reliable results to be applied and clinically validated in different hospitals. We have conducted this study to evaluate the main complications presented in this research field, from the sampling step to the analysis of the results, and to evaluate the usefulness of GC-MS analysis of exhaled gas in the assessment of lung cancer and COPD.

Our results with a pilot study comprised of breath samples from healthy subjects and COPD patients showed that the reuse of Tedlar bags is not a viable option for the sampling of exhaled air, since it introduces a big variability in the sample that surpasses the one provoked by the presence or absence of COPD. It is also apparent that a big variability emerged between breath samples taken in February and samples taken in November. A very similar variability existed between the room air samples, suggesting that the changeable pattern of VOCs in the environmental air also induces changes in the VOC pattern of the exhaled air. Nevertheless, even if a simple non-discriminant PCA was not enough to separate the samples of the healthy and COPD groups, after PCDA both groups were separated, and the accuracy, sensitivity and specificity results after internal cross-validation showed promising potential in the utility of breath analysis to differentiate COPD from healthy subjects.

To address the problems detected in the pilot study and try to control the aforementioned variability sources, we conducted an extended study in which we developed a new sampling system. Patients inhaled medical air during all the sampling procedure, and samples were taken in sorbent tubes: metal tubes containing a VOC-adsorbent fiber. A simple non-discriminant PCA was still not enough to separate the study groups, so we conducted a thorough statistical analysis using a random forest approach to try to select the VOCs patterns associated with each set of samples.

There were two binary models that did not pass the permutation test: CONTROL vs COPDLC and COPDLC vs LC. COPDLC includes patients with both diseases, which could potentially display a predominantly COPD-like phenotype, a predominantly lung cancer-like phenotype, or any degree of combinations between both phenotypes, depending on the particularities of each subject included in the group. Besides, the phase and type of lung cancer in the COPDLC group was also heterogeneous, further adding to its variability and thus making the detection of a specific group-defining VOC pattern more difficult. From the binary models that passed the permutation test, CONTROL vs LC was the one with the lowest classification accuracy after external validation. The

patterns from the CONTROL group displayed a high dispersion, indicative of the marked variability between the breath samples of the subjects. Furthermore, not only was LC the group with the smallest number of samples (only 12), but it also included patients with different types of lung cancer (adenocarcinoma, squamous cell carcinoma, leimyosarcoma…) and different stages of the disease, which also were under different combinations of treatments.

Classification according to the CONTROL vs COPD model showed higher sensitivity, specificity and global accuracy than in the pilot study, even when the validation procedure was much more strict (external validation vs the internal cross-validation used in the pilot study), which suggests the advantages of the sampling system we developed with regards to the one used in the pilot study. The accuracy of the classification according to the COPD vs LC binary model proves that the patterns of VOCs can be used to separate both diseases, and do not simply indicate the existence of non-specific changes associated to airway inflammation and/or oxidative stress.

The results of the combined model were promising when considering that the samples could be initially classified in any of the four groups. The biggest number of mistakes came from the COPDLC group, since many samples from patients with both diseases were classified in COPD or LC groups, and many samples from patients with lung cancer were classified in COPDLC group. Very few samples from subjects with a disease were erroneously classified in the CONTROL group.

All in all, our results show that the sampling of exhaled air in Sorbent Traps and their subsequent analysis by GC-MS shows promising potential in the detection of LC and COPD using the patterns of VOCs they contain. We present a new standardized sampling system method that can be easily used to collect tidal exhaled air reducing variability and cross-minimizing cross-contamination. Although variability between samples in the same group still constitutes the main difficulty for accurate classification, we present a novel pattern analysis method based on *random forest* which shows promising results even in combined models with four different classification groups. The existence of a COPDLC group, whose subjects may potentially express any phenotype between lung cancer and COPD, can be confounding factor, especially when using combined models with new samples. Lung cancer patients usually present different kinds of tumors in different stages, and therefore are under different treatments. A more homogenous classification, or alternatively a larger amount of samples, would facilitate a correct classification in that particular group. In general, steps to reduce inter-group variability should be taken when conducting studies on the diagnostic potential of breath analysis.

Future steps include the validation of the observed results in parallel studies conducted in different research centers, the thorough exploration of the effect that potential confounding factors in patients' metadata may exert in the samples classification and the continued research to further improve both sampling systems and pattern analysis methods.

Materials and Methods

Pilot study: sampling

Samples were taken using a 200ml Bio-VOC breath sampler (from Markes International) and Tedlar Bags (from SKC). The Bio-VOC breath sampler contains an air entrance, through which the subject breathes, and an air exit which is used afterwards to inject the sampled air into the Tedlar Bag. The air from the first seconds of the exhalation comes mainly from the dead space, which is defined as the volume of exhaled air which did not take part in the gas exchange because it remained in the mouth and the conducting airways. The dead space air does not contain any VOCs transferred from the blood to the exhaled air in the alveoli, and therefore it is of no interest for us. Consequently, in the first seconds of the exhalation the air exit of the Bio-VOC was kept open, and the air flowed freely through the sampler without being collected. After a few seconds, when all the air being exhaled by the subject was alveolar and therefore containing the VOCs transferred to it in the gas exchange process, both Bio-VOC ends (air entrance and air exit) were closed and the subject stopped exhaling into the sampler. Once the sample was collected in the Bio-VOC sample, its exit end was connected to the fitting of the Tedlar Bag, and a plunger was added to its entrance end. Pushing the plunger in discharged the air sample into the Tedlar bag. The process was repeated 5 times until we obtained a final sample of 1 liter of exhaled tidal end breath in a Tedlar bag. Room air samples were taken similarly, but instead of breathing into the Bio-VOC the room air was sampled using a plunger to fill the Bio-VOC with air from the room environment.

Pilot study: sample pre-concentration

The concentration of many VOCs in exhaled air can be considered very low, in the range of ppbs. To sort this problem, we went through a concentration step before injecting the sample in the GC-MS, using a process called solid-phase micro-extraction (SPME) in which we injected a fiber-containing needle through the septum of the Tedlar bag. Once injected, pressing the needle plunger exposed

a thin fiber to the air inside the Tedlar bag. The fiber, composed of a mixture of carboxen and polidimethylsiloxane (PDMS), was kept in contact with the air inside the bag for 30 minutes, during which the VOCs contained in the sample adhered to the fiber's surface by adsorption. After those 30 minutes, the VOCs were already concentrated in the surface of the carboxen/PDMS, so the fiber was withdrawn and the needle extracted from the Tedlar bag.

Pilot study: sample injection and GC-MS analysis

Once the VOCs were preconcentrated in the carboxen/PDMS fiber, the latter was injected via a septum into the GC. There, the fiber was subjected to high temperatures that provoked the desorption of the VOCs from the carboxen/PDMS mixture, after which they were carried by a carrier gas current to the gas chromatographer (FocusGC, from Thermo Scientific). The chromatographic column used was a 60 m DB-624 capillary column with 0.32 mm of internal diameter and a stationary phase thickness of 1.8 µm. The temperature ramp used to optimize the separation and sensitivity of the chromatographic process was: 40ºC (5 minutes) – 10 ºC (1 minute) – 180 ºC (1 minute) – 15 ºC (1 minute) – 230 ºC (10 minutes). Once eluded from the column at different retention times, the separated compounds were injected into the MS (DSQII MS, from ThermoScientific), where they were ionized via electron impact and subsequently fragmented. The mass/charge (m/z) relations of the resulting fragments, along with their intensities, were detected by the MS and used to generate a spectra which also included the retention time at which each of the compounds were eluted from the chromatographic column.

Pilot study: data preprocessing

RAW data obtained from the GC-MS was processed with mz-mine software. MZ-mine was used to detect peaks in the spectra and conduct algorithms of mass recognition, spectra alignment and peak deconvolution. After MZ-mine processing, we obtained thousands of peaks, each with its associated intensity, corresponding to the fragments in which the different VOCs were broken in the mass spectrometer. The parameters used to identify each peak were their m/z relationship and retention time.

Pilot study: data normalization

The non-targeted approach of the analysis and the particular nature of the samples make the use of both external and internal standards non-viable, greatly

complicating direct quantitative analysis of the different fragments obtained. We conducted a normalization step in which the intensity of each fragment was relativized against the total intensity of the spectra that contains it. Therefore, we didn't directly compare intensities of fragments between different samples, but rather the relative importance of each fragment in the whole sample in which it is contained.

Pilot study: PCA statistical analysis

Principal component analysis (PCA), a statistical procedure that uses orthogonal transformation to convert a set of observations of possibly correlated variables into a smaller set of values of linearly uncorrelated variables called principal components (Jolliffe 2005), was first used to evaluate if it could separate the samples from each of the study groups. It is a non-discriminant analysis, and the first principal component it creates has the largest possible variance (that is, accounts for as much of the variability in the data as possible), while each succeeding component in turn has the highest variance possible under the constraint that it is orthogonal to (i.e., uncorrelated with) the preceding components. Normally only the first two dimensions (each one being one of the two orthogonal principal components that describe the highest variability of the data) are represented. Lack of separation between the groups in PCA does not mean the groups are equal, but rather that the highest variability between the samples does not depend on the differences between groups.
Linear discriminant analysis followed by principal component analysis (PCDA) was also used to classify the different sample groups. Linear discriminant analysis (LDA) is used to find a linear combination of features which characterizes or separates the classes under study (Belhumeur, Hespanha et al. 1997). PCLDA reduces the dimensionality of the sample with a previous PCA analysis, and it is a discriminant procedure in the sense that it explicitly attempts to model the difference between the classes of data that are being analyzed (it searches, for example, for the specific fragments that are different in healthy and COPD breath samples).

Extended study: sampling system

Exhaled air was collected using a breath sampler developed by our research group and called tidal breath sampler (TDS). It consists on a glass tube (material chosen because of its chemical inertness) with a particular geometry that is designed to allow the collection of tidal exhaled air. An air pump (FLEC Air

Pump 1001) extracts the air from the first section of the glass tube through a Sorbent Trap filled with a fiber composed of 200 mg Tenax and 200 mg Unicarb. Between the glass tube and the fiber, a filter made of silica gel is also attached in order to remove the humidity from the breath sample, which provokes important distorsions in the MS spectra. A unidirectional Rudolph Valve (also called Two-Way Non-Rebreathing Valve) connects a Douglas Bag with the air entrance end of the glass tube. The Douglass bag is kept filled with medicinal air (22% O_2, 78% N_2), and when the subject breathes into the Rudolph Valve, its unidirectionality ensures that he inhales medical air from the Douglass bag and exhales into the glass tube (**see Figure 5**).

To avoid the formation of breath condensation in the walls of the crystal tube, a home developed heating system, consisting on a long warmed filament, was wrapped along the glass tube to keep its temperature high. This prevented the appearance of condensed humidity in the sampling system, which has the potential to dilute the hydrophilic VOCs from the breath sample, thus diminishing their concentration and altering final results.

Extended study: sampling protocol

First, the heating system was activated at a temperature of 80 ºC, and a source of medical air at a pressure of 1 bar is directly attached to the air entrance of the glass tube. The silica gel filter and the air pump are connected to the short end of the glass tube, and the pump is turned on at a flow rate of 1000 ml/minute, thus sucking part of the hot medical air through the silica gel filter. The current of heated medical air through the glass tube and the filter is kept for 30 minutes, to remove the room air from within the system and to avoid any contamination. After half an hour, the source of medical air is connected to a Douglas bag, and a Rudolph unidirectional valve is adjusted between the bag and the air entrance end of the glass tube. The heating system temperature is reduced to 60ºC, and the subject starts breathing in the Rudolph Valve, inhaling from the Douglas bag filled with medical air and exhaling into the glass tube. During 10 minutes, the subject keeps breathing into the system without any sampling (the short end exit of the glass tube, which connects it to the air pump, is kept closed during this process) to homogenize his breathing with the medical air. The flow of medical air into the Douglas bag is controlled to assure an adequate air pressure in the latter at all times. After 10 minutes, the sorbent trap with the tenax/unicarb fiber is connected between the silica gel filter and the air pump, the short end air exit of the glass tube is opened and the air pump is turned on at a flow rate of 200

ml/min, so that part of the exhaled air that is being breathed into the glass tube flows through the silica gel filter and the sorbent trap, in that order.

The sampling process is maintained for 5 more minutes, after which the sorbent trap (whose fiber now contains the adsorbed VOCs of 1 liter of exhaled air that has flown through it) was disconnected from the system and the subject stopped breathing into the glass tube. Once the sampling procedure is finished, and if there are any more samples to be taken, the medical air source is again connected directly to the glass tube at a pressure of 1 bar, a new silica gel filter is connected between the glass tube and the air pump, and the heating is turned up to 80ºC. The heated air is kept flowing through the system for another 30 minutes, to purge the new filler and to remove the VOCs from the previous sample that may remain in the system, thus avoiding cross-contamination. The silica gel used in the previous sample is discarded until thoroughly dried in a heater, and the glass tube is cleaned with water and medical soap after all the samples have been taken.

Extended study: sample transportation

Samples were taken in the *Hospital Clínic de Barcelona* and analyzed in the *Universitat de Barcelona*. To avoid fiber contamination and loss of VOCs, between sampling and analysis all sorbent traps were kept hermetically closed and stored in a container in void conditions. Samples were analyzed on the same day they were taken.

Extended study: sample injection

Samples were injected in the GC-MS system using a UNITY thermal desorption unit for sorbent tubes (MARKES). This unit applies a flow of hot carrier gas through the fibers contained in the sorbent traps, desorbing the VOCs in its surface and carrying them to the GC-MS system. Once desorbed, fibers in the sorbent traps were further cleaned of any possible remaining VOCs with a flow of N_2 at 320 ºC for two hours, before being closed and stored in vacuum again in order to be reused.

Extended study: data preprocessing and normalization

RAW data obtained from the GC-MS was processed with MZ-mine software, just like in the pilot study. Peaks with the same retention time and which co-varied in all samples were considered part of the same original compound, and therefore were clustered before normalizing their area against the total area of

the specter in which the cluster is contained.

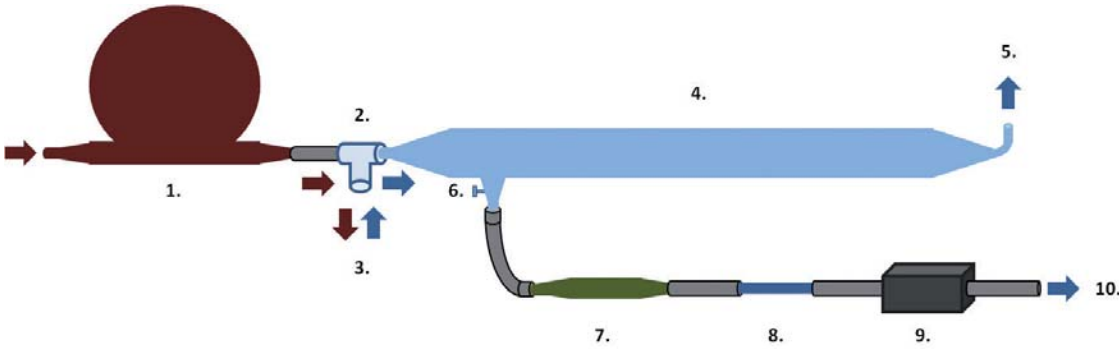

FIGURE 05. Tidal Breath Sampler. Representation of the sampling system used to collect the volatile organic compounds in the samples of exhaled breath. 1: Douglas bag that was kept filled with a stream of medical air (maroon arrows). 2: unidirectional Rudolph Valve that prevented exhaled air (blue arrows) to access the Douglas while impeding air from the glass tube to be inhaled by the subject. 3: subject breathes in the Rudolph Valve, inhaling medical air from the Douglas bag and exhaling VOCs-containing breath into the glass tube. 4: Glass tube that is kept at high temperature by a heating system. 5: the biggest part of the air from each exhalation is not collected, and instead flows out of the system by this exit. 6: second air exit in the glass tube, which can be opened and closed with a manual valve and whose proximity to the air entrance ensures that most of the air collected from this end will belong to the final part of the subject's exhalation, and therefore will be tidal air containing the VOCs from the gas exchange. 7: silica gel filter that removes the humidity from the exhaled air sample. 8: tube containing a fiber made of tenax/unicarb, which will concentrate the VOCs of the exhaled breath sample that flows through it. 9: pump that sucks the air from the glass tube at a flow rate of 200 ml/min. 10: the breath air that comes from the pump, and which is now deprived (at least partly) of VOCs, is discarded.

Extended study: statistical analysis

Random forest was selected as classifier, and an extremely robust validation procedure was planned in order to avoid any overfitting result. Random forest (Breiman 2001), which is currently the state of the art in proteomics, metabolomics and genomics (Svetnik, Liaw et al. 2003; Strobl, Boulesteix et al. 2007), is based on the building many decision trees (Safavian and Landgrebe 1991) which splits the original space in different decision spaces that maximize the separation between classes. Each decision tree was built using a random subset of features and samples, and the output of the algorithm indicated both a probability of membership to each class and the variable importance of each selection feature. In this study, a first model was generated using the whole feature space, and the variable importance output was used together with rank products (Breitling, Armengaud et al. 2004) to select the most significant features in the classification.

Despite the robustness of the random forest method, double-cross validation (Marco,2014) was also used to validate our results. The data was split in two sets: external validation data and internal validation data. External validation data tested the discriminatory power of the model with data that was not used in its generation. Internal validation data was used to set up the internal parameters of the model (the number of features of each decision tree).

A permutation test (Hsing, Attoor et al. 2003; Ojala and Garriga 2010) was used to test each binary problem using the classification given by external validation data. Permutation tests asses if the classification figure of merit (e.g. Area Under the Curve (AUC) in a ROC analysis) can be obtained by chance. To this und a number of classification experiments are carried out where the sample labels are assigned in a random manner, producing in such a way an estimation of the probability density function of the null hypothesis. Finally, when models have passed the permutation test, the final classification of each binary problem is combined. In this case, a partial least squares model (Barker and Rayens 2003) together with a kNN classifier in the reduced space (Bezdek, Chuah et al. 1986) was implemted for the final label prediction.

Acknowledgements

This work was supported by the Ministerio de Ciencia e Innovación of Spain (SAF2011-25726), the Generalitat de Catalunya (2009SGR-1308), the European Commission (FP7) grant SYNERGY (no. FP7-ICT-2009-270086), the Instituto de Salud Carlos III (PI080283) and the ICREA Academia award 2010 (granted to M. Cascante)

References

Bajtarevic, A., C. Ager, et al. (2009). "Noninvasive detection of lung cancer by analysis of exhaled breath." BMC Cancer **9**: 348.

Barker, M., M. Hengst, et al. (2006). "Volatile organic compounds in the exhaled breath of young patients with cystic fibrosis." Eur Respir J **27**(5): 929-936.

Bijland, L. R., M. K. Bomers, et al. (2013). "Smelling the diagnosis: a review on the use of scent in diagnosing disease." Neth J Med **71**(6): 300-307.

Bray, F., A. Jemal, et al. (2012). "Global cancer transitions according to the Human Development Index (2008-2030): a population-based study." Lancet Oncol **13**(8): 790-801.

Calusic, A. L., V. M. Varnai, et al. (2011). "Acute effects of smoking and food consumption on breath condensate pH in healthy adults." Exp Lung Res **37**(2): 92-100.

Chan, H. P., C. Lewis, et al. (2010). "Oxidative stress and exhaled breath analysis: a promising tool for detection of lung cancer." Cancers (Basel) **2**(1): 32-42.

D'Amico, A., G. Pennazza, et al. (2010). "An investigation on electronic nose diagnosis of lung cancer." Lung Cancer **68**(2): 170-176.

Das, M. K., S. C. Bishwal, et al. (2014). "Investigation of gender-specific exhaled breath volatome in humans by GCxGC-TOF-MS." Anal Chem **86**(2): 1229-1237.

Dent, A. G., T. G. Sutedja, et al. (2013). "Exhaled breath analysis for lung cancer." J Thorac Dis **5**(Suppl 5): S540-S550.

Dragonieri, S., J. T. Annema, et al. (2009). "An electronic nose in the discrimination of patients with non-small cell lung cancer and COPD." Lung Cancer **64**(2): 166-170.

Faux, S. P., T. Tai, et al. (2009). "The role of oxidative stress in the biological responses of lung epithelial cells to cigarette smoke." Biomarkers **14 Suppl 1**: 90-96.

Gordon, S. M., J. P. Szidon, et al. (1985). "Volatile organic compounds in exhaled air from patients with lung cancer." Clin Chem **31**(8): 1278-1282.

Gordon, S. M., L. A. Wallace, et al. (2002). "Volatile organic compounds as breath biomarkers for active and passive smoking." Environ Health Perspect **110**(7): 689-698.

Jolliffe, I. (2005). Principal Component Analysis. Encyclopedia of Statistics in Behavioral Science, John Wiley & Sons, Ltd.

Kanne, J. P. (2014). "Screening for lung cancer: what have we learned?" AJR Am J Roentgenol **202**(3): 530-535.

Lippi, G. and G. Cervellin (2012). "Canine olfactory detection of cancer versus laboratory testing: myth or opportunity?" Clin Chem Lab Med **50**(3): 435-439.

Machado, R. F., D. Laskowski, et al. (2005). "Detection of lung cancer by sensor array analyses of exhaled breath." Am J Respir Crit Care Med **171**(11): 1286-1291.

Mazzone, P. J., J. Hammel, et al. (2007). "Diagnosis of lung cancer by the analysis of exhaled breath with a colorimetric sensor array." Thorax **62**(7): 565-568.

Peng, G., M. Hakim, et al. (2010). "Detection of lung, breast, colorectal, and prostate cancers from exhaled breath using a single array of nanosensors." Br J Cancer **103**(4): 542-551.

Petty, T. L. (2005). "Are COPD and lung cancer two manifestations of the same disease?" Chest **128**(4): 1895-1897.

Phillips, M., R. N. Cataneo, et al. (2000). "Effect of age on the breath methylated alkane contour, a display of apparent new markers of oxidative stress." J Lab Clin Med **136**(3): 243-249.

Phillips, M., K. Gleeson, et al. (1999). "Volatile organic compounds in breath as markers of lung cancer: a cross-sectional study." Lancet **353**(9168): 1930-1933.

Prevot, G., G. Plat, et al. (2012). "[COPD and lung cancer: epidemiological and biological links]." Rev Mal Respir **29**(4): 545-556.

Tarnoki, D. L., A. Bikov, et al. (2014). "Lack of heritability of exhaled volatile compound pattern: an electronic nose twin study." J Breath Res **8**(1): 016001.

Turner, M. C., Y. Chen, et al. (2007). "Chronic obstructive pulmonary disease is associated with lung cancer mortality in a prospective study of never smokers." Am J Respir Crit Care Med **176**(3): 285-290.

Valavanidis, A., T. Vlachogianni, et al. (2013). "Pulmonary oxidative stress, inflammation and cancer: respirable particulate matter, fibrous dusts and ozone as major causes of lung carcinogenesis through reactive oxygen species mechanisms." Int J Environ Res Public Health **10**(9): 3886-3907.

Wen, T., L. Gao, et al. (2013). "Exploratory investigation of plasma metabolomics in human lung adenocarcinoma." Mol Biosyst **9**(9): 2370-2378.